

AD-A196 738

MTL TR 88-12

DTIC FILE COPY

AD

2

HYDROGEN ASSISTED CRACKING OF HIGH STRENGTH STEEL WELDS

STEVEN A. GEDEON

MATERIALS PRODUCIBILITY BRANCH

MAY 1988

Approved for public release; distribution unlimited.

DTIC
EXCERPT
JUN 14 1988
S H D



US ARMY
LABORATORY COMMAND
MATERIALS TECHNOLOGY LABORATORY



U.S. ARMY MATERIALS TECHNOLOGY LABORATORY
Watertown, Massachusetts 02172-0001

88 6 13 147

UNCLASSIFIED

SECURITY CLASSIFICATION OF THIS PAGE (When Data Entered)

REPORT DOCUMENTATION PAGE		READ INSTRUCTIONS BEFORE COMPLETING FORM
1. REPORT NUMBER MTL TR 88-12	2. GOVT ACCESSION NO.	3. RECIPIENT'S CATALOG NUMBER
4. TITLE (and Subtitle) HYDROGEN ASSISTED CRACKING OF HIGH STRENGTH STEEL WELDS		5. TYPE OF REPORT & PERIOD COVERED Final Report
		6. PERFORMING ORG. REPORT NUMBER
7. AUTHOR(s) Steven A. Gedeon		8. CONTRACT OR GRANT NUMBER(s)
9. PERFORMING ORGANIZATION NAME AND ADDRESS U.S. Army Materials Technology Laboratory Watertown, Massachusetts 02172-0001 ATTN: SLCMT-MEM		10. PROGRAM ELEMENT, PROJECT, TASK AREA & WORK UNIT NUMBERS AMCMS Code: 612015.H84 D/A Project: 1L162105.AH84
11. CONTROLLING OFFICE NAME AND ADDRESS U.S. Army Laboratory Command 2800 Powder Mill Road Adelphi, Maryland 20783-1145		12. REPORT DATE May 1988
		13. NUMBER OF PAGES 363
14. MONITORING AGENCY NAME & ADDRESS (if different from Controlling Office)		15. SECURITY CLASS. (of this report) Unclassified
		15a. DECLASSIFICATION/DOWNGRADING SCHEDULE
16. DISTRIBUTION STATEMENT (of this Report) Approved for public release; distribution unlimited.		
17. DISTRIBUTION STATEMENT (of the abstract entered in Block 20, if different from Report)		
18. SUPPLEMENTARY NOTES Submitted to the Department of Materials Science and Engineering, MIT, on May 1, 1987 in partial fulfillment of the requirements for the degree of Doctor of Philosophy.		
19. KEY WORDS (Continue on reverse side if necessary and identify by block number) High strength steels , Hydrogen measurement, Hydrogen embrittlement. Gas metal arc welds : Absorption , Welds Cracking (fracturing)		
20. ABSTRACT (Continue on reverse side if necessary and identify by block number) (SEE REVERSE SIDE)		

DD FORM 1 JAN 73 1473

EDITION OF 1 NOV 65 IS OBSOLETE

UNCLASSIFIED

SECURITY CLASSIFICATION OF THIS PAGE (When Data Entered)

Block No. 20

ABSTRACT

Methods of measuring the hydrogen content of Gas Metal Arc Welds (GMAW) are evaluated. The recently developed American Welding Society standard A4.3-86 using gas chromatography was found to measure the relevant content with reasonable reproducibility, whereas the IIW specification does not. The amount of hydrogen absorbed by Gas Metal Arc Welds as a function of percent H_2 , O_2 , and CO_2 added to the argon weld shielding gas is quantified. }

Sievert's law is shown to be invalid for modeling the amount of hydrogen initially absorbed by the molten weld pool. A new model is postulated based on the hypothesis that diatomic hydrogen will dissociate in the cathode boundary layer at a different reaction temperature than the hydrogen absorption reaction which occurs at the temperature of the weld pool surface. Using this hypothesis, it is shown that hydrogen absorption will be controlled by monatomic hydrogen absorption into the cooler outer region of the weld pool rather than diatomic hydrogen absorption into the hotter central portion as was previously believed.

When oxygen is added to the shielding gas, the amount of hydrogen absorbed by the weld pool increases. It is shown that the hydrogen will be bound to the more thermodynamically stable H_2O . It is believed that the water molecule is more strongly absorbed than the H_2 molecule. The resulting effect on hydrogen solubility is explained by a consideration of the FE-H-O phase diagram which was calculated in this study. The effect of CO_2 on hydrogen absorption is explained by its effect on the stability of H_2O and H_2 at high temperatures.

Implant testing is used to quantify the effect of hydrogen on cracking of high strength steel welds. The microplasticity theory originally proposed by Beachem is used to explain the effect of hydrogen on the various fracture modes observed.

Accession For	
NTIS GRA&I	<input checked="" type="checkbox"/>
DTIC TAB	<input type="checkbox"/>
Unannounced	<input type="checkbox"/>
Justification	
By	
Distribution/	
Availability Codes	
Dist	Avail and/or Special
A-1	

HYDROGEN ASSISTED CRACKING OF HIGH STRENGTH STEEL WELDS

	Page
Report Documentation Page	1
Abstract	2
Table of Contents	3
List of Figures	6
List of Tables	15
List of Abbreviations	16
Acknowledgements	17
Preface	19
Chapter 1 Literature Review of Hydrogen Embrittlement of High Strength Steel Welds	21
1.1 Introduction	21
1.2 Sources of Hydrogen During Welding	24
1.3 Hydrogen Absorption into the Weld Pool	27
1.4 Diffusion of Hydrogen	35
1.5 Methods of Measuring Hydrogen Content	39
1.6 Measured Values of Diffusible Weld Hydrogen Contents	44
1.7 Effect of Hardness and Composition on Cracking	46
1.8 Mechanisms of Hydrogen Embrittlement	48
1.9 Methods of Determining Weld Hydrogen Crack Susceptibility	51
1.10 Methods of Predicting and Preventing Hydrogen Embrittlement	54
1.11 Conclusions	57
Chapter 2 Measurement of Hydrogen in Welds	77
2.0 Abstract	77
2.1 Introduction	79
2.2 Fundamentals of Analytical Chemistry	81
2.3 Experimental Outline	86
2.4 Results of Hydrogen Measurement Technique Variations	89
2.4.1 Calibration Procedure of the Gas Chromatograph	89
2.4.2 Specimen Size	90
2.4.3 Surface Condition	91
2.4.4 Outgassing Temperature and Time	92
2.4.5 Time Delay Between Weld Completion and Quench	94
2.5 Discussion of Hydrogen Measurement Technique Variations	94
2.5.1 Calibration Procedure	94
2.5.2 Specimen Size	96
2.5.3 Surface Condition	98
2.5.4 Outgassing Temperature and Time	99
2.5.5 Time Delay Between Weld Completion and Quench (Methods for Determining Initially Absorbed Hydrogen Content and Hydrogen Remaining in the Cracking Zone)	102
2.6 Results of Weld Process Variations on Hydrogen Content	106
2.6.1 Effect of Shielding Gas Composition	106

2.6.2	Effect of Droplet Transfer Mode	109
2.6.3	Effect of Base Metal Composition	110
2.6.4	Effect of Preheat	111
2.7	Discussion of the Effect of Weld Process	111
	Variations on the Diffusible Hydrogen Content	
2.7.1	Effect of Shielding Gas Composition	111
2.7.2	Effect of Droplet Transfer Mode	114
2.7.3	Effect of Base Metal Composition	115
2.7.4	Effect of Preheat	116
2.8	Conclusions	117
Appendix2A	Effect of Shielding Gas Variations on Diffusible Hydrogen Content	154
Chapter 3	Thermochemical Analysis of Hydrogen Absorption in Welding	168
3.0	Abstract	168
3.1	Calculation of Hydrogen Absorption Reaction Temperature Using Sievert's Law Neglecting Dissociation	169
3.2	Absorption of Monatomic Hydrogen into the Weld Pool	177
3.3	Hydrogen Dissociation in the Welding Arc	180
3.4	The Effect of Dissociation on the Amount of Hydrogen Absorbed into the Weld Pool	184
3.5	The Effect of Non-Equilibrium Dissociation in the Welding Arc on the Amount of Hydrogen Absorbed into the Weld Pool	185
3.6	The Effect of Radial Temperature Distribution and a Moving Weld Pool	188
3.7	Fundamentals of the Sievert Relationship	192
3.8	Summary	195
Chapter 4	The Effect of Fe-C-H-O Phase Relationships on Hydrogen Absorption in Weld Pools	222
4.0	Abstract	222
4.1	General Phase Equilibria	223
4.2	Thermodynamic Data	223
4.3	Equilibrium Phase Relationships During Solidification	225
4.3.1	The Fe-H-O Ternary System	225
4.3.2	The Fe-C-H Ternary System	230
4.3.3	The Fe-C-O Ternary System	232
4.3.4	The Fe-C-H-O Quaternary System	233
4.4	The Effect of Oxygen and Carbon Dioxide in GMAW Shielding Gases on Hydrogen Absorption in Weld Pools	234
Chapter 5	Assessing Hydrogen Assisted Cracking of High Strength Steel Weldments Using the Implant Test Method	265
5.0	Abstract	265
5.1	Introduction and Experimental Procedure	266
5.2	Experimental Results	268
5.3	Fractographic Analysis of Implant Specimens	271

5.4	Hydrogen Embrittlement Mechanisms	276
5.5	Comparison of Current Results with the Predictions of Other Researchers	282
Appendix5A		314
Chapter 6	Summary	321
References for all Chapters		324
Biographical Note		360

LIST OF FIGURES

Figure		page
1.1	Typical hydrogen content of various electrode wires. The curve height indicates the relative frequency of test results for each type of consumable. (Ref C.15)	59
1.2	Typical moisture content of various fluxes and coatings. The curve height indicates the relative frequency of test results for each type of consumable. (Ref C.15)	60
1.3	Effect of temperature and humidity on moisture levels of a low moisture E7018 electrode. (Redrawn from Ref N.1)	61
1.4	Relationship between potential hydrogen and weld hydrogen. (Ref C.15)	62
1.5	Iron-Hydrogen phase diagram. (Ref H.1)	63
1.6	Measured hydrogen content of weld metal as a function of the square root of hydrogen partial pressure. (Ref C.7)	64
1.7	Hydrogen solubility versus temperature curves. The low temperature part of the curves is derived from known experimental data; the high temperature portion is obtained by extrapolating these data and then applying a correction for metal vapor. (Ref H.18)	65
1.8	Variation in overall diffusivity coefficient, D , as a function of temperature. (Ref C.15)	66
1.9	Approximate times for removing 75% of the original hydrogen: (a) butt welds, (b) fillet welds. (Ref C.15)	67
1.10	Variation in weld current and voltage as a function of hydrogen in the shielding gas. (Ref F.5)	68
1.11	Variation in the diffusible hydrogen content as a function of heat input. (Ref F.5)	69
1.12	Diffusible hydrogen content of GTA welds as a function of hydrogen in the shielding gas. (Ref F.5)	70
1.13	Comparison between experimental and theoretical results of retained diffusible hydrogen content. H_R/H_0 is the ratio of retained hydrogen to originally absorbed hydrogen. h_v is the bead width, and h is the specimen thickness. (Ref T.4)	71
1.14	Hydrogen embrittlement as a function of HAZ hardness for three different steels. (Ref C.15)	72

1.15	Demonstration of the effect of carbon equivalent and cooling rate on hardness. (Ref C.15)	73
1.16	Schematic plot of a "static fatigue" curve from constant load rupture tests.	74
1.17	General diagram of the implant test. (Ref S.13)	75
1.18	Prediction nomograph using material composition (carbon equivalent) and plate thickness to select preheat and arc energy to avoid cracking. (Ref C.15)	76
2.1	Schematic of a typical Gas Chromatograph. (Ref E.11)	128
2.2	Electrical circuit of a thermal conductivity detector. R_1 and R_2 are temperature sensitive elements, R_3 and R_4 are ratio arms, R_5 is a zero adjustment, and R_6 is a current limiter. In practice the galvanometer G is replaced by a voltmeter. (Ref E.11)	129
2.3	Schematic of an elution chromatographic separation of a two-component mixture. (Ref S.22)	130
2.4	Diagram of the specimen holding chamber for the Yanaco gas chromatography unit.	131
2.5	Diffusible hydrogen in an IIW size specimen as a function of percent hydrogen added to Ar/2% O_2 shielding gas.	132
2.6	Diffusible hydrogen in an AWS size specimen as a function of percent hydrogen added to Ar/2% O_2 shielding gas.	133
2.7	Diffusible hydrogen measurement versus time for an out-gassing temperature of 45 C. (A36, AWS, Ar/.5%H ₂ /2% O_2)	134
2.8	Effect of the delay between weld completion and quench on the measured hydrogen content. (A36, AWS, Ar/1% O_2 /2%H ₂)	135
2.9	Average diffusible hydrogen content after "complete" evolution as a function of sample cleaning method and electrode re-drying conditions. (Ref B.18)	136
2.10	Thermal analysis peaks of hydrogen in pure iron, 0.49% carbon steel, and AISI 4340 steel furnace cooled at 850 C. (Ref L.4)	137
2.11	Dependence of the hydrogen peak height as a function of the amount of cold work. (Ref L.4)	138
2.12	Dependence of the hydrogen peak height as a function of the amount of ferrite-carbide interface. (Ref L.4)	139

2.13	Comparison between experimental and theoretical hydrogen evolution curve. (Ref T.2)	140
2.14	Comparison between experimental and theoretical results of retained diffusible hydrogen content. H_R/H_0 is the ratio of retained hydrogen to originally absorbed hydrogen. h_w is the bead width, and h is the specimen thickness used in the theoretical calculation. (Ref T.4)	141
2.15	Hydrogen distribution as a function of distance in the weld for $r = 0.011, 0.044, 0.10, 0.20, \text{ and } 0.50$. (Ref C.13)	142
2.16	Hydrogen concentration as a function of r for different locations in the weld. C_0 is the amount of hydrogen initially in the weld, and Q is the total amount in the weld region.	143
2.17	Diffusible hydrogen as a function of hydrogen in the GMAW shielding gas. Curves depict Ar with 0%, 2%, and 5% oxygen. (A36, AWS)	144
2.18	Diffusible hydrogen as a function of percent hydrogen in a shielding gas with different amounts of carbon dioxide in argon. (A36, AWS)	145
2.19	Comparison of the effect of 2% oxygen and 2% carbon dioxide in the shielding gas. (A36, AWS)	146
2.20	Metal transfer mode regions as a function of voltage and wire feed rate (wire feed determines the current) for 3/4" and 1-1/4" tip-to-work distances. (A36)	147
2.21	Metal transfer mode regions as a function of voltage and wire feed rate for various shielding gases.	148
2.22	Effect of voltage on diffusible hydrogen content. The transition voltage from globular to spray is 28 volts.	149
2.23	Diffusible hydrogen versus hydrogen in pure argon shielding gas for A36 and 46100 steel.	150
2.24	Diffusible hydrogen versus hydrogen in Ar/2% O_2 shielding gas for A36 and 46100 steel.	151
2.25	Diffusible hydrogen content of 46100 versus hydrogen in the shielding gas for Ar/2% O_2 and Ar/2% CO_2 .	152
2.26	Diffusible hydrogen content as a function of the carbon content of the steels tested. Each curve represents a different amount of hydrogen in the Ar/2% O_2 shielding gas.	153

3.1	Equilibrium hydrogen solubility as a function of diatomic hydrogen partial pressure for various assumed absorption temperatures.	200
3.2	Equilibrium hydrogen solubility as a function of the absorption temperature for various diatomic hydrogen partial pressures.	201
3.3	Ratio of retained hydrogen to initially absorbed hydrogen as a function of the "thermal factor". (Ref T.4)	202
3.4	Ratio of deposited metal to fused metal as a function of hydrogen in the shielding gas for pure argon and Ar/2% O ₂ .	203
3.5	Initially absorbed hydrogen as a function of hydrogen in pure argon shielding gas. (A36)	204
3.6	Initially absorbed hydrogen as a function of hydrogen in Ar/2% O ₂ shielding gas. (A36)	205
3.7	Initially absorbed hydrogen as a function of hydrogen in Ar/2% CO ₂ shielding gas. (A36)	206
3.8	Measured hydrogen content of GTA weld metal as a function of the square root of hydrogen partial pressure. (Ref C.7)	207
3.9	Variation in weld current, voltage, and heat input as a function of hydrogen in the shield gas. (Ref F.5)	208
3.10	Diffusible weld hydrogen content as a function of GMAW shield gas hydrogen content. (Ref W.8)	209
3.11	Diffusible hydrogen content of pulsed GMAW welds on a fusion zone basis with moisture additions to the shield gas. (Ref S.6)	210
3.12	Variation of hydrogen content with hydrogen partial pressure at different currents for: (a) Armco iron; (b) nickel; (c) copper; (d) aluminum. (Ref H.18)	211
3.13	Results of a series of determinations of hydrogen absorption by iron containing oxide (numbers give the order of testing). (Ref H.18)	212
3.14	Free energy of dissociation of diatomic gases.	213
3.15	Equilibrium hydrogen solubility as a function of the partial pressure of monatomic hydrogen gas for	214

various assumed absorption temperatures.

3.16	Equilibrium hydrogen solubility as a function of the absorption temperature for various partial pressures of monatomic hydrogen.	215
3.17	Percent hydrogen dissociation as a function of temperature, 1 atm pressure. (Ref C.9)	216
3.18	Percent hydrogen dissociation as a function of both pressure and temperature. Curves are from right: 1 atm, .1 atm, .01 atm, .001 atm, .0001 atm, and .00001 atm hydrogen partial pressure.	217
3.19	Percent hydrogen dissociation as a function of both pressure and temperature. Curves are from right: 10^0 atm, 10^{-2} atm, 10^{-4} atm, and 10^{-6} atm hydrogen partial pressure.	218
3.20	Theoretical hydrogen solubility as a function of assumed hydrogen dissociation and absorption temperature.	219
3.21	Temperature distribution on the surface of arc-melted iron. Shielding gas argon and various additions of nitrogen; current 80A. (Erokin 1978)	220
3.22	Theoretical hydrogen absorption due to monatomic and diatomic hydrogen as a function of weld pool location. Calculation assumes a dissociation temperature of 2500 C, an absorption temperature as given above, and .01 atm hydrogen.	221
4.1	Iron - Carbon phase diagram. (ref H.1)	241
4.2	Iron - Hydrogen phase diagram. (ref H.1)	242
4.3	Iron - Oxygen phase diagram. (ref H.1)	243
4.4	Iron - Oxygen phase diagram showing the partial pressure of oxygen gas. (Muan and Osborn)	244
4.5	Isotherm of Fe-H-O at 1538 C. Each line shows the solubility of hydrogen and oxygen in liquid iron at a specified H_2O partial pressure.	245
4.6	Isotherm of Fe-H-O at 1537 C and a moisture pressure of .01 atmospheres.	246
4.7	Isotherm of Fe-H-O at 1533 C and .01 atm moisture. The three phase region touches the H-O binary at a ratio of $P_{H_2O} / P_{H_2} = .299$	247

- 4.8 Isotherm of Fe-H-O at 1528 C and .01 atm moisture. 248
The three phase region touches the H-O binary at a ratio of $P_{H_2O} / P_{H_2} = .692$
- 4.9 Isotherm of Fe-H-O at 1520 C and .01 atm moisture. 249
The liquid phase is replaced with an FeO slag. The three phase region touches the H-O binary at a ratio of $P_{H_2O} / P_{H_2} = .60$
- 4.10 Isotherm of Fe-H-O at 1533 C and .05 atm moisture. 250
The three phase region touches the H-O binary at a ratio of $P_{H_2O} / P_{H_2} = .237$
- 4.11 Isotherm of Fe-H-O at 1528 C and .05 atm moisture. 251
The three phase region touches the H-O binary at a ratio of $P_{H_2O} / P_{H_2} = .64$
- 4.12 Isotherm of Fe-H-O at 1533 C and .001 atm moisture. 252
The three phase region touches the H-O binary at a ratio of $P_{H_2O} / P_{H_2} = .28$
- 4.13 Isotherm of Fe-C-H at 1538 C. Each line shows the 253
solubility of carbon and hydrogen in liquid iron at a specified pressure of methane.
- 4.14 Isotherm of Fe-C-H at 1533 C and a pressure of 254
 10^{-7} methane. The three phase region touches the C-H binary very close to the hydrogen corner.
- 4.15 Isotherm of Fe-C-H at 1520 C and 10^{-7} atm 255
methane. The three phase region still touches the C-H binary near the hydrogen corner.
- 4.16 Isotherm of Fe-C-H at 1490 C and 10^{-7} atm 256
methane. γ iron is now in equilibrium with the liquid phase which is off the diagram. The maximum solubility in this liquid is 6 ppm hydrogen and .56% carbon.
- 4.17 Isotherm of Fe-C-O at 1528 C and 1 atm CO. 257
(Ref W.10)
- 4.18 Isotherm of Fe-C-O at 1520 C and 1 atm CO. 257
(Ref W.10)
- 4.19 Isotherm of Fe-C-O at 1490 C and 1 atm CO. 258
(Ref W.10)
- 4.20 Slice through the Fe-C-O-H quaternary at 259
1528 C and .4% carbon.
- 4.21 Slice through the Fe-C-H-O quaternary at 260
1490 C and .4% carbon.

4.22	Slice through the Fe-C-H-O quaternary at 1528 C and .1% carbon.	261
4.23	Diffusible hydrogen content in pulsed GMAW welds on metal added basis, hydrogen additions to the shielding gas. (Ref S.6)	262
4.24	Diffusible hydrogen content in pulsed GMAW welds on metal added basis, moisture additions to the shielding gas. (Ref S.6)	263
5.1	Implant specimen geometry.	289
5.2	Microstructure of as-recieved MIL-A-46100 high strength steel alloy. 100X, Nital etch.	290
5.3	Microstructure of as-recieved MIL-A-46100 500X, Nital etch.	291
5.4	Microstructure of MIL-A-46100 after heat treament procedure and machining. 50X, Nital etch.	292
5.5	Microstructure of MIL-A-46100 after heat treatment procedure. 500X, Nital etch.	293
5.6	Implant test results for GMA welds made with 0% H ₂ / 2% O ₂ / Ar and loaded 5 minutes after ² welding. Curves depict welds made with 250 F, 150 F, and no preheat.	294
5.7	Implant test results for GMA welds made with 0% H ₂ / 2% O ₂ / Ar and loaded 5 minutes after welding and 24 hours after welding.	295
5.8	Implant test results for GMA welds made with 2% O ₂ and loaded after 5 minutes. Curves depict ² 0%, .5%, and 2% H ₂ added to the shielding gas.	296
5.9	Implant test results for GMA welds made with .5% H ₂ / 2% O ₂ / Ar and loaded at 5 minutes and ² 24 hours.	297
5.10	Lower Critical Stress for welds loaded at 5 minutes after welding versus the initially absorbed hydrogen content.	298
5.11	Lower Critical Stress for welds loaded at 24 hours after welding versus the amount of hydrogen remaining 24 hours after welding.	299

5.12	Lower Critical Stress for welds loaded at 24 hours after welding versus the amount of hydrogen present in the cracking zone after 24 hours.	300
5.13	Overall SEM view of a fractured implant specimen surface. 20X	301
5.14	Schematic showing the regions from which the magnified photos were taken.	301
5.15	Region of intergranular fracture characteristic of hydrogen embrittlement. 2000X	302
5.16	Region of microvoid coalescence showing ductile dimples. 2000X	302
5.17	Transition region where both intergranular fracture and microvoid coalescence are evidenced. 200X	303
5.18	Region of fast fracture in the shear lip bordered by microvoid coalescence. 2000X	303
5.19	Quantitative fracture map showing the regions of fracture types.	304
5.20	Area of quasi-cleavage fracture. 200X	305
5.21	Magnified area of quasi-cleavage fracture. 1000X	305
5.22	Area of "fisheyes" evidenced in implant specimens with low hydrogen content. 200X	306
5.23	Magnified area of "fisheyes". 500X	306
5.24	Magnification of one "fisheye" showing the inclusion at the bottom of the embrittled region. 2000X	307
5.25	Strain energy release rates for a circular-arc fronted edge crack and a straight fronted edge crack in a round bar in tension. (Ref D.2)	308
5.26	Crack geometry for a single straight fronted edge cracked round bar in tension. (Ref D.1)	309
5.27	Crack geometry for a circular-arc fronted edge crack in a round bar in axial tension. (Ref D.2)	310
5.28	Suggested interrelationship by Beachem between stress intensity factor, dissolved hydrogen	311

- content, and HAC deformation mode of
microscopically small volumes of crack-tip
material. (Ref B.7)
- 5.29 Interrelationship developed in this study 312
between the stress intensity factor and
hydrogen content in the cracking zone for
initiation of microvoid coalescence.
- 5.30 A method of predicting the LCS developed by 313
Ito, et al. (Ref I.11)

LIST OF TABLES

Table		Page
2.1	Calibration values for Janaco GC	119
2.2	Effect of surface condition on measured diffusible hydrogen	120
2.3	Diffusible hydrogen remaining in AWS specimen after 24 hours	121
2.4	Temperature where maximum hydrogen release occurs for various trapping sites (Ref. L.4)	122
2.5	Welding parameters used throughout this study unless otherwise stated	123
2.6	Composition of the steels used in this study	124
2.7	GMAW electrode composition	125
2.8	Diffusible hydrogen content determined on different steels	126
2.9	Diffusible hydrogen remaining in AWS specimen after 24 hours as a function of preheat	127
3.1	Thermodynamic data used in this study	196
3.2	Table of values for hydrogen dissociation calculation	197
3.3	Hydrogen absorption as a function of assumed reaction temperature and percent hydrogen	198
3.4	Hydrogen absorption as a function of assumed dissociation and absorption reaction temperatures	199
4.1	Thermodynamic data used in this study	239
4.2	Freezing point depression data	240
4.3	Distribution coefficient data	240
5.1	Composition of the steel used in this study	285
5.2	Heat treatment procedure for implant specimens	286
5.3	Summary of experimental results	287
5.4	Tabulation of fracture toughness estimates	288

LIST OF ABBREVIATIONS

AWS	American Welding Society
CE	Carbon Equivalent
CERL	U.S. Army Construction Engineering Research Laboratory
CTS	Controlled Thermal Severity
DCRP	Direct Current Reverse Polarity (Electrode Positive)
ESW	Electroslag Welding
EDX	Energy Dispersive X-ray Analysis
FCAW	Flux Cored Arc Welding
GC	Gas Chromatograph
GMAW	Gas Metal Arc Welding
GTAW	Gas Tungsten Arc Welding
HAZ	Heat Affected Zone
IIW	International Institute of Welding
LTE	Local Thermodynamic Equilibrium
LCS	Lower Critical Stress
MTL	U.S. Army Materials Technology Laboratory
NIS	Notch Tensile Stress
SEM	Scanning Electron Microscope
SMAW	Shielded Metal Arc Welding
STP	Standard Temperature and Pressure
SAW	Submerged Arc Welding
TC	Thermal Conductivity
TGA	Thermogravimetric Analysis

ACKNOWLEDGEMENTS

Just as no man is an island, no dissertation can be completed without the help of many others. Special thanks go to my wife, Maryanne, whose love and encouragement kept my personal life happy while allowing me time to complete this document. I also owe much of the grammatical exactitude to her diligent proofreading.

Professor Tom Eagar was, of course, his usual stellar self. His insightful questions, theoretical comments, and extensive knowledge of the field helped build this thesis tremendously. My desire to emulate his scientific thought processes dramatically altered the shape of this thesis. His cheerful giving of his time also made me feel that the research was important and worthwhile.

The majority of this research was performed while I was an employee at the U.S. Army Materials Technology Laboratory (formerly the Army Materials and Mechanics Research Center). Even though my duties encompassed a large number of research projects and technical assistance to others, I was allowed to set my own research priorities. For this I profoundly thank all of my supervisors. Special credit needs to be given to the technicians who helped tremendously on all of the projects going on in the lab, as well as help with the experiments in this thesis: Attilio Santoro and Jim Catalano.

Others who helped give advice or make my life enjoyable are too numerous to mention by name. Fellow students, employees, researchers in the field, friends, and relatives all were willing to help in whatever way they could. Thank you all.

PREFACE

Despite the many research efforts on the effect of hydrogen in steel, hydrogen assisted cracking continues to be a problem, especially when welding very strong, hard, or thick steels. This is of particular concern to the U.S. Army since the majority of their vehicles utilize armor steels which are chosen for their high hardness. Since ballistic protection versus penetration increases with increasing hardness, alloy developers strive to make the hardest steel possible. Unfortunately, protection versus shock of the entire structure decreases if this hard material is embrittled due to hydrogen introduced during welding. In some cases, the welded material is so embrittled that cracking occurs due to the residual stresses alone with no externally applied load.

In order to alleviate the problem of hydrogen assisted cracking of welded high strength steel, a research program was initiated at the U.S. Army Materials and Mechanics Research Center (now renamed the Materials Technology Laboratory) in 1985 (G3, G7, G8). This dissertation is the result of a portion of that program which was performed in conjunction with the Massachusetts Institute of Technology. A portion of the diffusible hydrogen measurements was performed at the U.S. Army Construction Engineering Research Laboratory. This work plan was supervised by Steven Gadeon under MTL contract AW-6-MD0045 (G5).

This dissertation is formatted as a compilation of original papers

on the subject of hydrogen assisted cracking of high strength steel welds. The papers follow a logical progression from previous work, to testing method determination, to results, modeling, and discussion. The set of papers is then followed with a summary chapter to help tie them into a cohesive thesis document. To provide a rationale for this research program, hydrogen embrittlement is reviewed to determine which aspects require further investigation and also to set the groundwork for the analyses to be presented in later sections. Special emphasis is paid to Gas Metal Arc Welding (GMAW) due to the low hydrogen potential of the process. Low hydrogen levels are studied since the high strength steels of interest are so crack susceptible.

1.0 LITERATURE REVIEW OF HYDROGEN ASSISTED CRACKING OF HIGH STRENGTH STEEL WELDS

1.1 INTRODUCTION

Hydrogen embrittlement refers to the loss of ductility and enhanced crack susceptibility resulting from the presence of hydrogen in a material near room temperature. This form of cracking in steel weldments is also called cold cracking, delayed cracking, underbead cracking, or hydrogen assisted cracking. Hydrogen embrittlement is especially dangerous because it can occur hours, days, or even weeks after welding has been completed and is difficult to detect even though the amount of cracking may be quite extensive. Catastrophic failures of weldments have occurred without a load even after performing satisfactorily in service for some time (L6).

In Britain alone, the estimated annual cost of repairing hydrogen-induced cracks amounts to over 40 million pounds. Service failures of welded components cost an additional 140 million pounds annually (C15). Several famous disasters have occurred as a direct result of hydrogen embrittlement, such as the Morgantown molasses pressure vessel in 1944, the Liberty Ships and T-2 tankers during and after World War II, the Alexander Kielland drilling rig in 1980, several bridges in Europe, as well as numerous pipelines and aircraft (E2, H16, P4, R5).

As a result of these unexpected failures, hydrogen-induced cracking has received a tremendous amount of attention as a topic of research and thousands of papers have been written on the subject (J4). Unfortunately, much remains to be understood regarding the mechanisms of embrittlement, the influence of various welding procedures, the specific sources of hydrogen, interpretation of test results, and means for predicting safe welding practices. Even though fabricators pay close attention to avoiding hydrogen embrittlement, the incidence of failures suggests that they have not always been successful. The importance of the behavior of hydrogen in a weldment cannot be overemphasised.

Hydrogen adversely affects most metals. The effect on nickel, palladium, and electrolytically charged materials has been investigated extensively (B9, C2, I3, P6), as has the effect on most types of ferrous alloys. Even though these results are not all directly applicable to the welding of high strength steel, a number of the results can be used to shed light on some of the problems peculiar to welding.

Fontana and Green (F6) have postulated four different categories of hydrogen damage: hydrogen blistering, decarburization, hydrogen attack, and hydrogen embrittlement. A fifth category which could be added is hydride formation. Metal hydrides tend to be very susceptible to embrittlement, and Birnbaum (B10) has shown cinematography of hydride formation and fracture. However, since no iron hydrides are known to exist, this topic has little to offer the current investigation.

Hydrogen blistering, otherwise known as flaking, occurs due to an interaction of dissolved hydrogen and internal stresses. This phenomenon occurs chiefly in forged or wrought steels, but has also been evidenced in cast steels (B6). Ni-Cr and Ni-Cr-Mo steels are particularly susceptible to this form of failure, whereas austenitic steels are virtually immune (B6). Weldments do not generally suffer from flaking, but a phenomenon known as fish-eyes, which resembles flakes, can appear when a weldment is stressed in excess of the yield point (V1).

Decarburization and hydrogen attack are high temperature processes. Hydrogen diffuses to voids or crack tips and combines with the carbon in steel to form methane. The resulting loss of strength at these areas of high stress can result in failure.

The fourth, and by far the most prevalent, form of hydrogen damage in welds is hydrogen embrittlement. It is generally recognized that hydrogen embrittlement will occur to some extent whenever sufficient hydrogen and sufficient stress are present in a hard microstructure at a temperature between 150°C and -100°C . Since a weldment must usually withstand specified service stresses and temperatures, methods of avoiding cracking are generally restricted to controlling the amount of hydrogen, the type of microstructure, or both. These areas, as they relate to welding of steel, are discussed in more detail below.

1.2 SOURCES OF HYDROGEN DURING WELDING

Hydrogen can be present in the welding arc atmosphere from a variety of sources such as:

- 1) moisture in the flux and coating of SMAW electrodes, or the flux used in SAW, FCAW, or ESW;
- 2) moisture in the shielding gas of GMAW, GTAW, or FCAW;
- 3) any hydrogenous compounds on the base material such as oil, rust, or degreasing fluids;
- 4) lubricating oils used for drawing of the electrode or wire. Also other oil, dirt, or grease trapped on the welding wire such as in the seam of a FCAW wire;
- 5) entrainment of the ambient atmosphere into the arc region, or contact between the atmosphere and the solidifying weld bead.

The potential hydrogen level available for each different welding process can vary dramatically. Coe (C15) has quantified the amount of hydrogen available from a number of different types of welding electrodes as shown in figure 1.1. This histogram shows the relative frequency of measurements over the total range. It can be seen that GMAW electrodes have less hydrogen than the SAW electrodes or other filler metals despite the fact that the smaller diameter GMAW wires have a higher surface-to-volume ratio.

Coe has also compiled values for the moisture content of various fluxes and SMAW electrode coatings as is reproduced in figure 1.2. Since

the silicate binders typically used in the coating of SMAW electrodes require some moisture to keep them sound and free from cracks, the total elimination of hydrogen from this welding process can be difficult if not impossible. These types of binders are also hygroscopic and can pick up substantial amounts of moisture from a humid atmosphere, as is demonstrated in figure 1.3 (N1). Thus they must be carefully stored, packaged, and dried. Baking will reduce the amount of moisture, but not below a certain level. Typical moisture levels in two types of SAW fluxes are also shown in figure 1.2; the overall level of potential hydrogen in this process is a combination of the wire and flux contents.

The welding community has attempted to reduce the hydrogen potential of SMAW electrodes for quite some time. There has been some success through the addition of carbonates, etc., but the hydrogen levels are still not low enough to be used for some applications. A sol-gel technique has been patented at MIT which promises to provide a non-hygroscopic SMAW coating (B3, R4). However, until a sol-gel coating has been fully developed, the lowest hydrogen welding processes which can be used for welding high hardenable steel are still GTAW and GMAW.

Hydrogen can also enter the arc atmosphere directly from the shielding gas. This is normally a small fraction of the overall hydrogen potential, but long lengths of tubing from the gas cylinder to the torch may increase moisture levels (G15), or an almost empty cylinder may have abnormally high amounts (K7). Standard welding grade cylinders have a dewpoint of -76 C which amounts to about 10ppm water vapor. Little or no

data has been generated on the effect of this amount of potential hydrogen on extremely crack sensitive steels.

Since we are interested in very crack sensitive steels which require only minute quantities of hydrogen to promote cracking, the literature will now be reviewed to provide a better understanding of the actual mechanisms of hydrogen absorption into the weld pool.

1.3 HYDROGEN ABSORPTION INTO THE WELD POOL

Coe has shown how the potential hydrogen level and resulting weld hydrogen content are related for various weld processes. This relationship is reprinted in figure 1.4. The potential hydrogen level and coating moisture content axes are superimposed onto the same axis by assuming that all the water in the coating breaks down directly into available hydrogen. This assumption establishes the conversion factor:

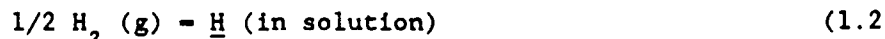
$$1\text{g H}_2\text{O} = 1245\text{ ml H}_2 \quad (1.1)$$

It is not clear if this relationship always holds, however, especially when various gas forming compounds are added to the flux coating. Many researchers have shown (C5, E1, N1, V3) that the relationship between coating moisture and hydrogen content can vary significantly with the type of SMAW electrode. Moisture absorption is heavily influenced by the flux composition, density, particle size, and binder formulation (B3, B21, G1, H5, S2). The moisture in SMAW electrodes can be either chemically bound to the silicate binder or physically absorbed onto the surfaces of the flux particles or the binder. Thermogravimetric analyses show that the physically absorbed moisture can be removed at a lower temperature than the chemically absorbed moisture. Some have suggested that the physically absorbed moisture may not transfer to the weld pool due to resistive heating of the electrode during operation driving off this weakly bound water.

As can be seen in figure 1.4, not all of the available hydrogen is transferred to the weld. The potential hydrogen level can vary more than an order of magnitude with the same resulting weld hydrogen level when different welding processes are considered. Obviously, there must be other factors involved in the transfer of hydrogen than simply the potential hydrogen level.

Chemical thermodynamics can be applied to quantify these differences and gain some insight into the mechanisms of hydrogen absorption into the weld pool. Many people have assumed that the weld pool will become saturated with hydrogen at 1 atmosphere. However, as can be seen in figure 1.5, the equilibrium solubility of hydrogen in iron will vary with the amount of hydrogen partial pressure above the molten iron as well as with the temperature of the pool. Thus, in order to model the absorption phenomenon, one must know the temperature of the reaction as well as the amount of hydrogen in the gas phase.

The most fundamental relationship to describe the equilibrium absorption of hydrogen in molten iron is the well known Sievert relationship, which is derived from the reaction:



for which the equilibrium constant of:

$$K = a_H / (P_{H_2})^{1/2} \quad (1.3)$$

can be determined. If one assumes that the hydrogen concentration is within the Henrian activity region and an infinitely dilute standard state is used, the most popular form of Sievert's law is obtained:

$$C_H = K (P_{H_2})^{1/2} \quad (1.4)$$

where C_H is the amount of absorbed hydrogen, K is a constant which is often taken as the equilibrium constant or the solubility at 1 atmosphere, and P_{H_2} is the pressure of hydrogen gas above the surface. Although it can be argued that hydrogen in the arc atmosphere is monatomic and Sievert's law is applicable only for diatomic gases, many people have assumed that some form of this square root relationship holds true. An example is shown in figure 1.6 (C7). The methods used to gather this data will be discussed in detail in section 1.4.

From equation 1.4 and the basic thermodynamic law:

$$G = G^0 + RT \ln K \quad (1.5)$$

one can make estimates of the reaction temperature at which hydrogen absorption takes place for various systems. These estimates have been made for some welding operations which were not at equilibrium. However,

these "effective equilibrium reaction temperatures" can provide insight into the gas-metal reactions occurring and allow one to make predictions about other systems of interest. Reaction temperatures determined for welding systems represent the temperature at which the kinetic processes become too slow for equilibrium to be maintained.

For example, splat cooling is used in the study of slag-metal reactions to freeze equilibrium as close to the reaction temperature as possible. In welding, the cooling rate is not fast enough to freeze equilibrium, and one must wait until a low temperature is achieved before the kinetics are sluggish enough to stop transport of the hydrogen.

Chew and Willgoss studied hydrogen additions to GTAW at various currents and determined the equilibrium reaction temperature to be 1840 C at 100 amps and 1570 C at 200 amps (C7). These results appear to be counter intuitive, as one would tend to expect increased currents to increase pool temperature. Chew and Willgoss argue that higher heat inputs lead to slower cooling rates and slower cooling rates lead to lower effective reaction temperatures. They also explained their results by reasoning that the larger weld pool at higher currents enabled hydrogen to escape from the solidifying weld more rapidly (C7).

Determinations of "equilibrium hydrogen absorption temperatures" in SMAW have been as high as 2300 C (C6). White (W8), studying hydrogen additions to GMAW, found that the apparent weld pool temperature increased with increasing hydrogen contents. Savage, et al. (S6) found

an equilibrium temperature of 1870 C when comparing the amount of moisture versus the amount of hydrogen absorbed.

Christensen and Chipman (C10), studying SAW, found an effective reaction temperature of 2000 C for manganese distribution between metal and slag. This same reaction temperature was found by Belton, Moore, and Tankins while studying silicon/silica partitioning in SAW. Others have determined the temperatures to be from 1640 C to 1670 C for silicon deoxidation (C16). The higher reaction temperatures can be understood by realizing that the kinetics for silicon or manganese transport are far slower than for hydrogen. However, the cooling rates are far slower for SAW than GTAW due to the insulating slag layer and the generally larger heat inputs used for SAW.

The situation is actually more complicated than the above analysis can model, even in GTAW, perhaps the simplest welding system. Howden and Milner (H18) argued that the bulk of the absorption actually takes place in a hot spot directly beneath the arc in the center of the pool, and that the cooler regions of the arc give off hydrogen at a slower rate so that the gas content throughout the pool approximates that in the absorption zone. They found weld metal hydrogen contents which were 1.4 times greater than the melting point solubility and estimated the reaction temperature in the hot zone to be 2100 C. They also determined that hydrogen absorption in iron was lower than in other metals. For example, the solubility of hydrogen in aluminum welds is 70 times the melting point solubility.

Howder and Milner also found that vaporization of iron at higher temperatures would reduce the hydrogen partial pressure above the pool (H18). Thus, at the boiling point there would be no solubility of hydrogen in iron since the atmosphere above the weld pool would be entirely metal vapor. The resulting solubility curves, which include their metal vapor correction calculations, are reproduced in figure 1.7.

Block-Bolten and Eagar (B12, B13) have shown that the boiling temperature of iron can never even be reached since evaporative cooling will maintain a steel weld pool at a maximum temperature which they estimate at 2500 C.

In more complicated systems such as SMAW, Chew (C5) suggests that the reaction of interest actually occurs on the molten droplets which form on the electrode tip before they reach the weld pool. Grong and Christensen (G20), studying oxygen, carbon, silicon, and manganese levels in GMAW, have calculated reaction temperatures of: 1600 C at the electrode tip, 2400 C in the molten droplets, and 1800 to 2000 C in the hot region of the weld pool.

It is also possible that the oxidizing tendency of many shielding gases will help reduce the hydrogen absorption into the weld pool due to the reaction:



(1.6)

Christensen has postulated that as Q increases, H decreases according to this reaction (C9). This seems to be an interesting avenue of research since most GMAW is performed with 95% Ar / 5% O_2 , or 98% Ar / 2% O_2 . This could also be a mechanism of reducing the absorbed hydrogen when welding with CO_2 which would break down in the high temperature arc plasma into CO and O_2 .

Another consideration is that the free energy data used in the above studies is for hydrogen absorption in liquid iron, whereas all the experiments were performed on steel. The simultaneous effect of a number of alloying elements on the solubility can be calculated through use of a Taylor expansion method as shown by Wagner (W2). This method results in the use of free energy interaction coefficients to describe the effects of concentrations of dilute components on the activity coefficient of a selected dilute constituent. Elliot has shown the effect of alloying elements on the solubility of hydrogen, and has tabulated the first and second order interaction coefficients for most of the alloying elements used in steelmaking (E5). A first order approximation of the effect of the alloying elements typically found in a high strength steel (M10) on the solubility of hydrogen at the melting temperature can be calculated from:

$$\Delta G = 8720 - 11.02 T - RT \ln K$$

(1.7)

thus,

$$\log K = 1.36 - \log \underline{H} + \log f_H - 1/2 \log P_{H_2} \quad (1.8)$$

If one wishes the solubility at 1 atmosphere hydrogen, the fugacity can be determined from the interaction coefficients tabulated by Elliot:

$$\log f_H = e_H^C (\%C) + e_H^{Mn} (\%Mn) + \dots \quad (1.9)$$

Using this method, the solubility of hydrogen in the steel used in this study is found to be 21.9 ppm instead of 23 ppm in pure iron at the melting temperature. The solubility difference at .01 atmospheres amounts to less than 5%. This shows that using free energy data for hydrogen in pure iron is a useful approximation in the study of hydrogen in steel.

Once the maximum concentration of hydrogen has been reached in the molten weld pool, the weld will cool and a large portion of the hydrogen will diffuse into the surrounding base metal Heat Affected Zone (HAZ) or escape to the atmosphere. Karppi, et al. (K3) suggests that the cracking phenomenon can be more closely modeled by the amount of hydrogen remaining after the weld has cooled to 100 C. To understand this point one must understand the diffusion of hydrogen in the solid state.

1.4 DIFFUSION OF HYDROGEN

Hydrogen will diffuse away from regions of high chemical potential towards regions of low chemical potential until there is no further gradient in chemical potential. Hydrogen molecules are relatively large, so only the atomic form of hydrogen can effectively diffuse through a steel lattice. This diffusion can be mathematically determined through the use of Fick's Laws and kinetic theory (S1, S15, S18). When a concentration gradient exists in an unstressed body of uniform temperature, the steady state flux of atoms crossing a plane is given by Fick's first law:

$$J = -D \left(\frac{dC}{dx} \right)_t \quad (1.10)$$

where J is the flux of (hydrogen) atoms, D is the diffusion coefficient, and $\left(\frac{dC}{dx} \right)_t$ is the concentration gradient at a fixed time. If steady state does not exist, that is, if the concentration at some point is changing with time, a more convenient form is Fick's second law:

$$\frac{dC}{dt} = \frac{d}{dx} \left(D \frac{dC}{dx} \right) \quad (1.11)$$

The driving force for diffusion of hydrogen can be: 1) a gradient in the chemical potential which results from a gradient in the lattice

hydrogen concentration, 2) a gradient in the hydrostatic component of an elastic stress field, or 3) a gradient in an electric field (B8, M1). The driving force due to a concentration gradient may be opposed or augmented by a stress gradient, since it is the chemical potential which is the actual driving force.

Hydrogen will diffuse toward an elastic stress field that is tensile in character. This is because the energy of the interstitial hydrogen is lower in tensile stressed regions (the lattice opens up and has more room for the hydrogen atom). The localization of hydrogen at triaxially stressed regions, such as those caused by a notch or other sharp defect, is known to be a very important factor in the characteristic delayed fracture behavior of steels containing hydrogen (L8).

The rate of hydrogen diffusion is proportional to both the chemical potential gradient and the diffusion coefficient (D). In theory, the diffusion coefficient varies with temperature according to the Arrhenius equation:

$$D = D_0 \exp (-Q/RT) \quad (1.12)$$

where D_0 is a preexponential term, Q is an activation energy, R is the universal gas constant, and T is the absolute temperature. In actual practice, measurements of D tend to be somewhat scattered as is shown in the compilation in figure 1.8. The variations in D are due to differ-

ences in measuring techniques, amount of cold work of the material, and differences in steel composition.

The biggest influence on the diffusivity measurements of hydrogen in iron, especially below 250 C, is the presence of traps. The mobility and solubility of dissolved hydrogen can be heavily influenced by the presence of structural imperfections caused by factors such as cold working. The phenomenon of hydrogen trapping has been extensively researched to determine the density, depth, and interaction energies of the various trapping sites such as dislocations, solid-solid interfaces, voids, solute elements, and microcracks (B8, B9, H4, H10, H11, K6, K11, O5, P12, R3, T7, Z2). Unfortunately, the results of this research have rarely been applied to the field of welding.

During welding, the diffusing medium (i.e. steel) will not be at a uniform temperature or an unstressed state, and the diffusion coefficient (D) will undergo rapid changes. Coe and Chano have combined experimental results and diffusion theory to develop a number of hydrogen distribution plots for their weldments as a function of time (C13). Terasaki, et al. (T2, T5) have assumed a rectangular weld bead and applied finite element techniques using superposition of one-dimensional solutions to determine the optimum size of a diffusible hydrogen specimen, but did not actually calculate a hydrogen distribution plot.

Peng (P4), using the cooling curve for various welding conditions, estimated the diffusion effect at various points along the curve, and

added up the results to determine the residual amount of hydrogen remaining at the fusion line after the weld had cooled to 100 C. Since his specimens cracked along the fusion line, he calculated that hydrogen embrittlement occurred at .74 ml/100g (which is approximately .81 ppm) in HY-80 steel weldments, and at .5 ml/100g in X-80-W steel (which had a yield strength of 94 ksi).

Peng's calculated values for embrittlement are somewhat lower than the values found by other studies. For example, Graville (G15) found that a bulk value of 1 ppm caused embrittlement in his highly susceptible quenched steel. This discrepancy between Peng and Graville could be due to the welded microstructure being more susceptible, the fusion zone being an unmixed region, or exhibiting segregation, or perhaps a low temperature hydrogen transport phenomenon such as dislocation movement actually increased the amount of hydrogen at the fusion line during Peng's implant test time.

Even though calculations are available for the amount or distribution of hydrogen remaining directly after welding (C13), a number of authors have estimated that about half of the hydrogen determined from a standard diffusible hydrogen test (to be explained in the next section) remains after welding. Using this assumption, they have calculated the time needed to reduce the average hydrogen level at the center of a weldment to a fixed percentage of the initial hydrogen content using solutions previously derived by Russell (R6). An example of one of these curves used for a rough prediction of postheat temperature and time is

reproduced in figure 1.9.

1.5 METHODS OF MEASURING HYDROGEN CONTENT

Before discussing actual testing techniques, some background on the behavior of gaseous elements in metals is required. The fundamental physical and chemical principles involved in the determination of gases in metal must be understood to obtain reliable and useful analytical information.

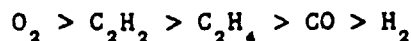
Gas-metal interactions are classified into four general categories: physical adsorption, chemical adsorption, solution formation, and bulk compound formation (H6). Adsorption reactions are confined to the surface, while in the last two types, the gas is absorbed into the metal. All four types are of concern because of their effect on the analytical results obtained in any test.

The first step in a gas-metal reaction involves the gas molecules striking a metal surface and being adsorbed by physical or chemical forces. In physical adsorption, van der Waals forces weakly hold the gas molecule in place. This process is reversible, and the gas can be removed by reducing the pressure since the exothermic heat of adsorption is usually less than 20,000 Joules/mole (5 kcal/mole).

In chemical adsorption, usually called chemisorption, a very stable

bond is formed between the gas and the metal. The bonds formed are almost as stable as those existing in stoichiometric compounds (M9). Vigorous treatments are often required to remove a chemisorbed layer from a metal surface, as their heats of adsorption are usually 80,000 to 400,000 Joules/mole (20-100 kcal/mole).

The adsorption of gases onto the clean surface of iron has been classified along with most other metals (H6), and Trapnell has established the general order of affinity (T9) as:



The adsorption of these gases on iron is a rapid and probably nonactivated process detectable at 300 K and 10^{-4} torr pressure (H6). When the surfaces of most metals are carefully prepared for analysis, the relative quantity of gas on the surface is usually insignificant compared to the bulk quantity. Problems can arise, however, if low bulk contents are being analyzed or if the specimen has a high surface to volume ratio.

Iron is classified as an "endothermic occluder". As such, it will only form a solid solution with hydrogen and will not form a bulk compound. Thus, the fourth category described above does not relate to iron, but may be important for describing the effect of hydrogen as it reacts with some of the precipitates. In pure iron, hydrogen will only

be present as an interstitial solid solution.

Although the effect of alloying elements on the solubility of hydrogen in a liquid melt was shown previously, there is little information on the effect of solubility in the solid. However, there have been some studies on the distribution of hydrogen among the phases that result from the addition of these elements.

Autoradiographic techniques using tritium have shown that hydrogen will segregate to MnS and Al_2O_3 (T13). Through use of a similar method, Caskey (C2) has demonstrated that this technique can be applied to welded materials and has shown that hydrogen segregates at dislocations, grain boundaries, and inclusion interfaces--particularly carbides.

Chemical methods for distinguishing between atomic, molecular, and oxidized hydrogen in steel have been used to show that water or hydroxyl groups were associated with inclusions (K8). Direct evidence for the presence of hydrogen as methane in microvoids in solid steel has also been obtained (P9). In fact, it has been found that only a small fraction of the hydrogen present in as-fabricated steel at temperatures less than 200 C is in the form of interstitial solid solution (H8).

Methods which can be used to determine the amount of hydrogen in metals have been extensively reviewed by Eborall (E3). The determination of hydrogen in steel has been covered by Acosta (A1), Wojcik (W9), and Martin, et al. (M2). Among the vast array of techniques used, some of

the more common are: vacuum fusion, vacuum extraction, inert-gas fusion, inert-gas extraction, equilibrium pressure, isotope dilution, and combustion (M9). A more recent method using a pyroelectric katharometer has promised ultra-high sensitivity (G21).

After years of evolution, the preferred method for determining hydrogen in steel appears to be extraction from a solid sample in vacuum or inert gas. Several commercially available analyzers have been developed which are based on this method of analysis, the most recent of which utilize a gas chromatograph to ensure that only the hydrogen gas is being measured.

The values which are measured by any method will depend on the technique, sample preparation (surface roughness and cleanliness), temperature (of extraction, not necessarily ambient), pressure (vacuum or inert-gas), and the materials used within the instrument as well as the type of crucible. All of these must be understood, as well as the fact that hydrogen may be in various traps or in the form of methane or water, in order to accurately use the values which are measured.

Several tests have been developed for the measurement of weld metal hydrogen content (G21, I8, I9, I10, J2, P10). The two most widely used methods for the measurement of this quantity are probably also the most inaccurate. They are very similiar in that they allow the welded specimen to degas in some form of eudiometer tube filled with a collecting fluid. The evolved gases are collected in the upper portion of the tube

over the fluid and the resulting volume is measured. Results are calculated as the volume of gas collected per unit mass of weld deposited.

A major problem with these techniques is that the results can vary significantly with fairly minor variations in the testing procedure (B17, B18, F1, O1, Q3). The two most widely used techniques involve the use of either glycerin or mercury. Results are difficult to compare between these two techniques, however, since the temperatures are typically different between these tests and the solubility of gases is different in the two types of fluids. In fact, one source (C15) states that most of the published results using these tests are worthless since the exact procedure is seldom recorded. Thus, the results are of little use because they cannot be reproduced. Numerous variations of this test have been put forth, including the use of different collecting fluids (F1, O1, S16).

An alternative method is to use gas chromatography, which is much more reproducible and reliable (I10, P10, Q4). Also, extraneous gases are not included in the resulting volume, since the thermal conductivity analyzer ensures that only hydrogen is being measured.

The moisture content in the electrode coatings can be determined by a number of techniques. A popular method consists of igniting the sample in a stream of pure dry oxygen (C15, L5, M13). The water expelled or formed by combustion in this operation is collected in a suitable absorbent and weighed. Another method is the use of a Karl Fischer titration

technique. This technique is apparently more precise and a recent article compares this method with some of the other popular methods (M12). Thermogravimetric analysis (TGA) is yet another method which may be used (G1, R4).

The recently introduced Leco HW-100 and HW-200 both measure diffusible hydrogen, but they make the determination at different temperatures (L3). The HW-200 performs its analysis at 400 C, whereas the HW-100 can operate from 25-200 C. As shown in the last section, this may result in different measurements due to trapping of the hydrogen at dislocations or inclusions.

Increased hydrogen values can be expected when the analyzing procedure uses a higher extraction temperature. This is because much of the hydrogen can be bound to traps which do not release the hydrogen until a certain threshold temperature.

1.6 MEASURED VALUES OF DIFFUSIBLE WELD HYDROGEN CONTENTS

Florian and Neumann (F5) have studied the effects of adding known amounts of hydrogen to the shielding gas of GTA welds. Their results show that weld parameters such as current and voltage change in the presence of hydrogen (shown in figure 1.10). They found that this variation adds to the scatter in experimental data, but has little effect on the overall weld hydrogen level (figure 1.11). Although they concentrated on

strain rate and acoustic emission data, they did determine the effect of percent hydrogen in the shielding gas on the resulting diffusible weld hydrogen as shown in figure 1.12.

Savage, et al. studied hydrogen and moisture additions to GMAW and found that pulsed current produced the most stable arc (S6). They also found that moisture additions resulted in more hydrogen being added to the weld than if hydrogen had been added directly (i.e. 1% H_2O resulted in more added hydrogen than 1% H_2). Unfortunately, they offered no explanation for either of these occurrences. White (W8) also studied hydrogen additions to GMAW and found that Sievert's Law could not be used directly to explain her results. Both groups of researchers found that high levels of hydrogen added to the shielding gas will create porosity in the weld which will decrease the amount of hydrogen measured in the diffusible hydrogen test.

Terasaki, et al. (T4) have also studied the effect of weld current and voltage on hydrogen absorption. They developed a method which allows one to calculate the initial hydrogen content absorbed into the molten weld based on the amount of hydrogen remaining in the diffusible hydrogen test. The method consists of measuring the cooling rate of the weld and converting the temperature versus time curve into a diffusion coefficient versus time curve. The area under this curve (which they term the "thermal factor") is then related to the amount of hydrogen which has left the specimen. Differences in heat input (by changing voltage and current), preheat, and time to quench the specimen are then related to the amount

of hydrogen remaining in the specimen. An example of their results is shown in figure 1.13. This is the only known work which attempts to calculate the actual amount of hydrogen initially absorbed by the molten weld pool.

Other researchers studying the amount of hydrogen remaining in a weld have had conflicting results as is evidenced by the differing effective equilibrium reaction temperatures quoted in section 1.3. The majority of this type of research has been performed for SMAW to find the amount of hydrogen absorbed as a function of moisture in the electrode coating. Unfortunately, ultra-low moisture levels are not currently possible in SMAW so the amount of diffusible hydrogen is quite large. The level of hydrogen in SMAW can easily promote cracking in the high strength steels being evaluated in this study.

1.7 EFFECT OF HARDNESS AND COMPOSITION ON CRACKING

Early work in the field of hydrogen embrittlement recognized the importance of hardness as a prerequisite for hydrogen cracking, especially in the Heat Affected Zone (HAZ). Knowledge of the hardness itself, however, is incomplete as a measure of hydrogen susceptibility, and erratic results soon showed that the type of microstructure was of even more importance (S17). Figure 1.14 shows that the HAZ hardness of a particular steel may be used as a means of detecting the degree of embrittlement, but that this relationship can vary substantially for dif-

ferent types of steel. The various microstructures found in ferritic steels can be qualitatively ranked in terms of increasing hydrogen crack susceptibility and generally follow the following trend (P11):

Quenched and tempered, or spheroidized steels have less susceptibility than normalized and tempered steels; followed by normalized steels; then by untempered bainite; and finally untempered martensite.

Chemical composition must also be considered since two steels may have identical microstructures but widely different cracking behavior due to different alloying additions. Heat treatment history is also of importance since fine and round carbide shapes are more resistant to embrittlement than coarse and angular ones (P11).

The microstructure produced in any steel is dependent upon the cooling rate through the transformation temperature of the steel and the composition and hardenability of the steel. The hardenability of a steel is difficult to quantify, and rankings such as the one given above are not always applicable. In an effort to find a useful way of describing hardenability, a Carbon Equivalent (CE) is often used which takes account of the important elements which are known to affect hardenability. An enormous number of carbon equivalent formulae have been postulated over the years. On a particular material or series of materials, these can be of benefit for making predictions concerning crack susceptibility. These predictions are usually based on empirical fits to data, and then either interpolated or extrapolated, which can lead to erroneous results.

Figure 1.15 shows that the carbon equivalent can be used to determine what hardness will be obtained for a given cooling rate (or vice versa). Although these types of graphs are useful for establishing welding procedures for previously characterized steels, they cannot always be fully relied upon. For example, two steels may have identical CE but one may crack whereas the other will not.

Other researchers have related hydrogen embrittlement to the percent martensite in the HAZ rather than the hardness (C8, P2). This method works quite well with the steels used in those investigations, but the applicability of this method for other steels remains in question (K5).

Through the judicious use of preheat, a cooling rate can be chosen which will produce the desired microstructure. Isothermal transformation curves (TTT diagrams) (A4) can be useful for predicting the desired cooling rate, and also for predicting what type of microstructure will be developed. Preheat provides the additional benefit of allowing more hydrogen to diffuse out of the weldment by reducing the cooling rate and keeping the weldment at an elevated temperature longer.

1.8 MECHANISMS OF HYDROGEN EMBRITTLEMENT

A number of mechanisms have been proposed to explain the phenomenon of hydrogen embrittlement. Since many of these mechanisms have been discussed in detail, only a brief list will be given here based on work by

Louthan and McNitt in 1976 (L7).

1) Precipitation of hydrogen as a gas at internal defects. The pressure developed by this precipitation is added to the applied stress and thus lowers the apparent fracture stress. This mechanism was initially proposed by Zapffe (Z2).

2) Interaction of dissolved hydrogen to reduce the cohesive strength of the lattice. This model was proposed by Troiano (T12) and modified by Oriani (O7).

3) Adsorption of hydrogen to reduce the surface energy required to form a crack and thus lower the fracture stress. This theory was first proposed by Petch (P5, P6).

4) Absorption of hydrogen to increase the ease of dislocation motion or generation, or both. This mechanism, proposed by Beachem (B7), differs in general from the previous models in that hydrogen is assumed to enhance local plasticity rather than truly embrittle the lattice.

5) Formation of a hydrogen-rich phase whose mechanical properties differ from those of the matrix. This model was generalized by Westlake (W6) and is most readily associated with hydride, methane, or steam embrittlement.

6) Association of hydrogen with dislocations either to restrict

dislocation mobility or to provide localized hydrogen accumulations and thereby embrittle the lattice. The dislocation-hydrogen association was proposed by Bastien and Azou (B5) and refined by Tien (T7).

It is generally acknowledged (e.g. I2, T6) that none of these proposed mechanisms are general enough to account for all observed cases of hydrogen embrittlement. Rather, it seems as though several of the proposed mechanisms may be active at the same time, depending on the particular experimental conditions. These mechanisms have rarely been applied to welding.

1.9 METHODS OF DETERMINING WELD HYDROGEN CRACK SUSCEPTIBILITY

Determination of the degree of hydrogen embrittlement of a particular steel can be a complicated task. The best method ultimately depends on the specific application intended for the weldment of interest. There are two classes of tests: direct and indirect. Direct tests are typically self-restrained joints that simulate production weld joints. Indirect tests subject hydrogen charged specimens to an external load or strain. Borland (B19) has reviewed many types of cracking tests and discussed their characteristics and limitations.

The Controlled Thermal Severity (CTS), Tekken, Cruciform, and Lehigh restraint tests are four of the most widely used direct tests for studying hydrogen cracking in weldments. A benefit of direct tests is that the full range of HAZ microstructures can be evaluated. They are useful for quick evaluations of weldability, but they require large amounts of material. The length of the test weld in a direct test should be at least 12 inches in order to develop maximum longitudinal residual stresses. Also, the restraint stresses are difficult to determine and can vary with changes in the welding procedure.

Indirect tests allow independent control over the hydrogen level, stress level, and microstructure. Two of these types of tests include the constant load rupture test and the notched tensile test. The constant load rupture test involves heating a notched tensile specimen in

hydrogen and quenching in a blast of argon. This treatment charges the sample with hydrogen, but only simulates a specific region of the HAZ. A series of these specimens is then loaded at various stresses to give a "static fatigue" curve such as is shown in figure 1.16. Bonisewski and Moreton have observed that hydrogen introduced by this means may not behave in the same way as does that introduced by an actual welding process (B16).

In response to the problems associated with the above types of tests, Granjon (G13) introduced the implant test. The implant test consists of the static loading of a notched cylindrical test piece which has been inserted (or implanted) through a hole in a base metal "specimen plate". A test weld is then deposited on the top surface of the specimen plate in order to (1) fuse it to the top end of the cylindrical test piece, (2) introduce a controlled amount of hydrogen, and (3) create a weld HAZ that now contains the notch. A diagram of this is presented in figure 1.17. The notch can be located in a specific area of interest in the HAZ, or a helical notch (similar to the threads of a screw) can be used so that the notch is always in an area of highest crack susceptibility. By varying the test conditions it is possible to determine the time and stress values needed for cracking or fracture.

The implant test has the following advantages over many of the other hydrogen cracking tests (S13):

1. The stress imposed is independent of the welding procedure or amount of restraint.
2. The effect of welding procedure on microstructure can be inves-

tigated independently.

3. The amount of hydrogen introduced can be controlled by adjusting the moisture content of the electrode or the hydrogen content of the shielding gas.

4. The test specimens are small, and since the size and notch dimensions are standardized, by using this test a vast data base of research performed by other investigators may be utilized.

5. The test weld and specimen plate can be of a composition different from that of the test specimen, since they do not actively participate in the test.

The cracking susceptibility is rated by varying the static load applied to the specimen and noting the time to fracture. A lower stress value will be reached where failure will not occur for an arbitrarily long time. This stress value is defined as the lower critical stress (LCS), and can be used as an indication of the ability of the material to resist hydrogen embrittlement. Another indication termed the "Embrittlement Index," I , can be calculated from the relationship:

$$I = (NTS - LCS) / NTS,$$

where NTS is the short-time notch tensile strength, and LCS is the lower critical stress defined above. As the susceptibility to cracking increases, the Embrittlement Index also increases.

The implant method has become one of the most widely used tests for studying the hydrogen cracking tendency of steels (G15). Although there is no standard method of performing implant testing, the IIW has proposed a good method (I7), and researchers have studied the effect of various test procedures on test results (B22).

1.10 METHODS OF PREDICTING AND PREVENTING HYDROGEN EMBRITTLEMENT

A number of researchers have proposed solutions or methods of preventing hydrogen embrittlement in weldments. These typically rely on empirical relationships which are then presented as a series of equations or nomographs such as in figure 1.18. This technique is usually quite adequate if the relationship being used was developed for that specific material (or series of materials). The fact that these relationships do not all agree with one another indicates that the use of them without extreme caution is ill advised.

Hydrogen embrittlement prevention relationships are usually based on determining the critical preheat temperature to prevent cracking as a function of the arc energy (or heat input), thickness of the materials to be welded (or combined thickness), and some form of carbon equivalent.

There have been a number of variations of these relationships. Pavaskar and Kirkaldy (P2) based their critical preheat temperature on the HAZ hardness, percent martensite, and the hydrogen content as determined by the IIW diffusible hydrogen test. Christensen and Simonsen (C8)

Other researchers in Scandinavia (K5) have taken into account the stress field pattern around the specimen notch or an actual weld joint geometry. Thus they have made it possible to relate test results to fabrication procedures.

Karppi, et al. (K5) have used a more rational hydrogen value for their relationships than the result obtained in a diffusible hydrogen test. They use the amount of hydrogen remaining in the weld after it has cooled to 100 C, which is when cracking actually begins to occur. This procedure allows them to take into account the fact that much of the hydrogen will diffuse away from the weld region and take no part in the cracking phenomenon. Their relationships use the HAZ hardness rather than the percent martensite. Furthermore, they use a stress field parameter to account for stresses rather than the thickness of the material.

Okuda, et al. (O4) developed a single equation for the preheat temperature which they claim is valid for submerged arc welds made on steels with a strength of between 100 and 140 ksi. This temperature is based solely on the strength of the steel and the hydrogen content as found in the diffusible hydrogen test. Ueda and Kim (U1) determined that each of their steels required a different equation for the preheat temperature. This temperature is based on the composition (a carbon equivalent-like formula), the thickness, the hydrogen content (as determined by the diffusible hydrogen test), and an efficiency of hydrogen transfer rating for the type of electrode used.

Satoh, et al. (S5) developed a graph to predict the required preheat for the first four passes of a multi-pass weld. This temperature is based on the composition (using a carbon equivalent formula), the diffusible hydrogen content, and the intensity of restraint. Alcantara and Rogerson (A2) developed a nomograph to determine the amount of cracking

(termed the average cracking coefficient) only in the weld. This relationship is based only on the arc energy and the diffusible hydrogen content. Ito, et al. (I11) developed a series of graphs to predict the implant rupture strength based on the diffusible hydrogen content, preheat temperature, plate thickness, and composition.

Suzuki, et al. (S25 through S33) have developed a series of relationships which perhaps takes into account the largest number of factors. These relationships are delineated in a number of papers regarding aspects of what is alternately called the "hydrogen accumulation cracking parameter" and the "cold cracking parameter". The most recent revision (S.33) predicts the critical preheat temperature to prevent cracking based on nine different factors. These factors include the time to cool to 100 C (which in turn is dependent on the preheat temperature), the composition, the hydrogen content (again, dependent on the preheat temperature), the heat input or arc energy, the joint geometry, the intensity of restraint, and the efficiency of hydrogen transfer (which varies with the electrode type).

The choice of a relationship to determine which preheat temperature to use will ultimately depend on the application and the material. Obviously, if others have studied the same steel as one's application, then their relationship will probably be the most accurate. It seems as though no single relationship can account for all the factors involved in hydrogen embrittlement for all materials. Even if such a relationship could be found, it would probably be too cumbersome to use.

1.11 CONCLUSIONS

Based on a thorough literature review and conversations with many of the experts in the field of hydrogen embrittlement, the following areas of research were found to be of particular interest in Gas Metal Arc Welding of high strength steels:

1) Examine hydrogen measurement methods for accurately measuring the relevant hydrogen content of welds.

2) Determine the effect of oxygen and carbon dioxide content in the shielding gas on the amount of hydrogen absorbed by the weld pool.

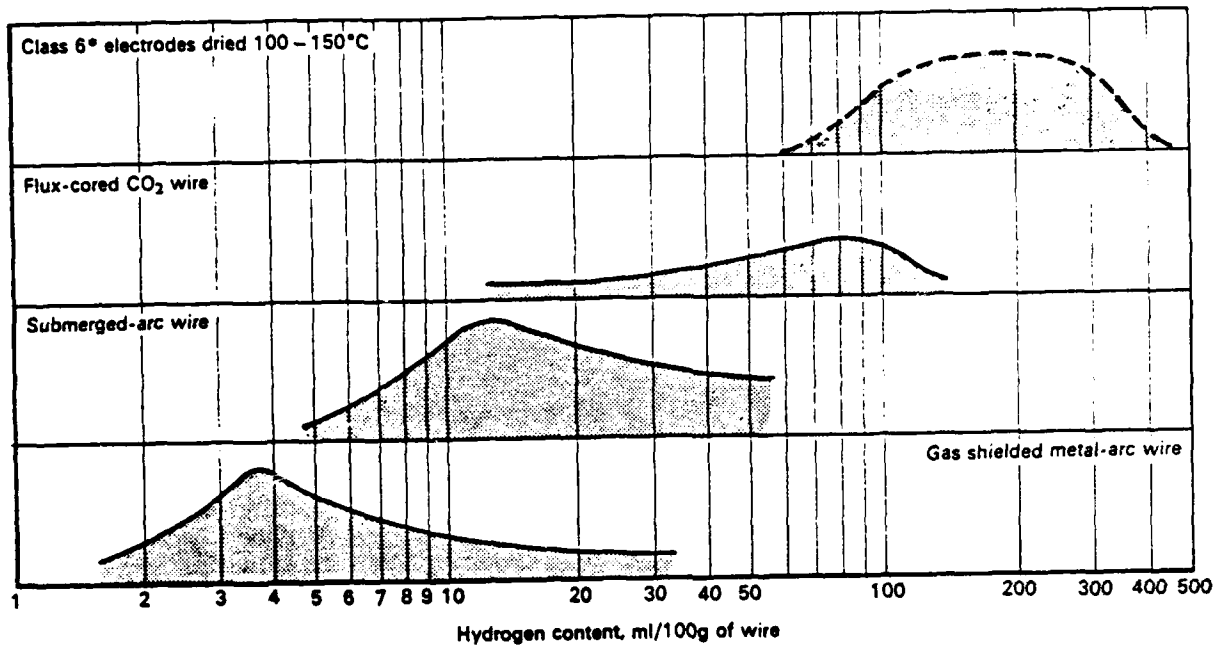
3) Model the mechanism of hydrogen absorption into the molten weld pool for low values of hydrogen in the arc atmosphere.

4) Quantify the sources of hydrogen in welding and predict the effect of each source on the resulting level of hydrogen in the weld pool and in the weld.

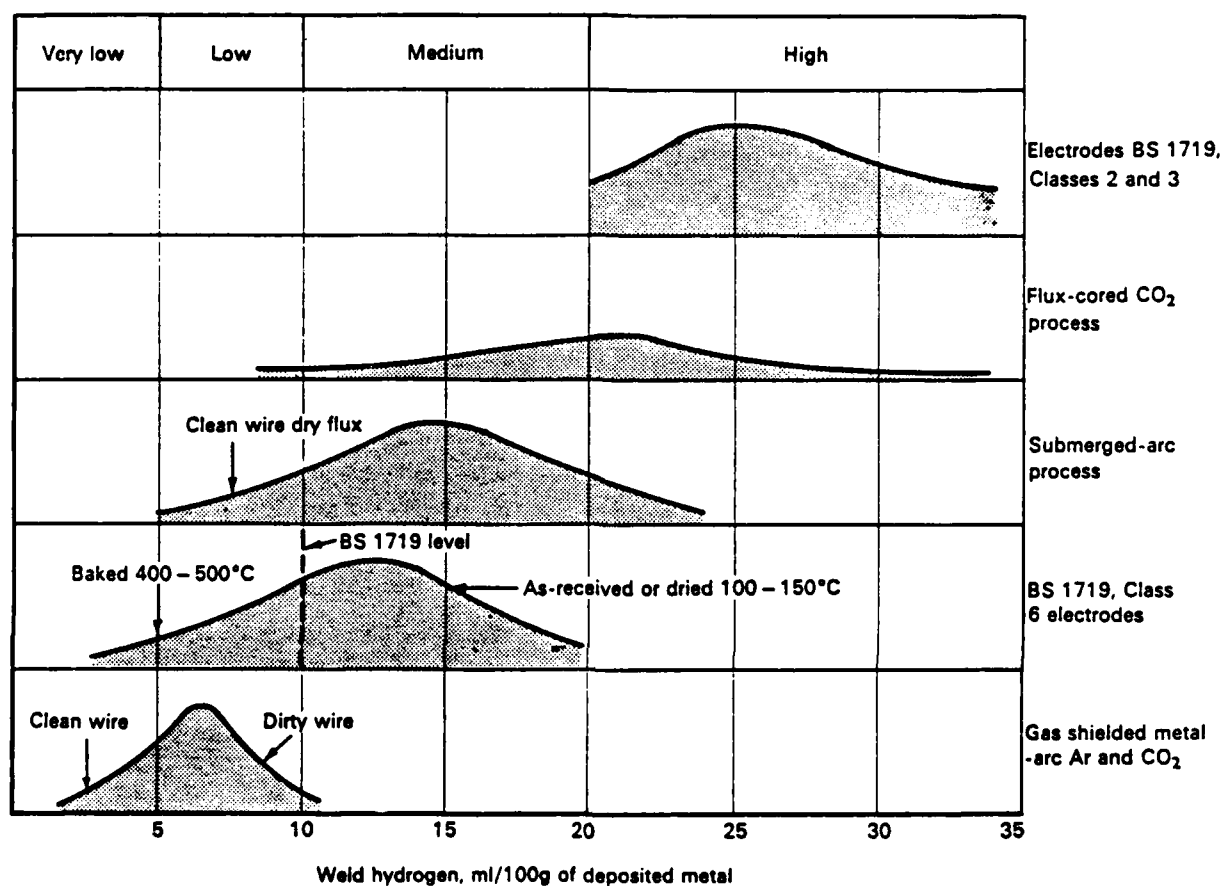
5) Examine the effect of these hydrogen sources on the actual cracking of high strength steel welds.

6) Utilize previous research available on hydrogen trapping, hydrogen embrittlement mechanisms, thermodynamics, and analytical chemis-

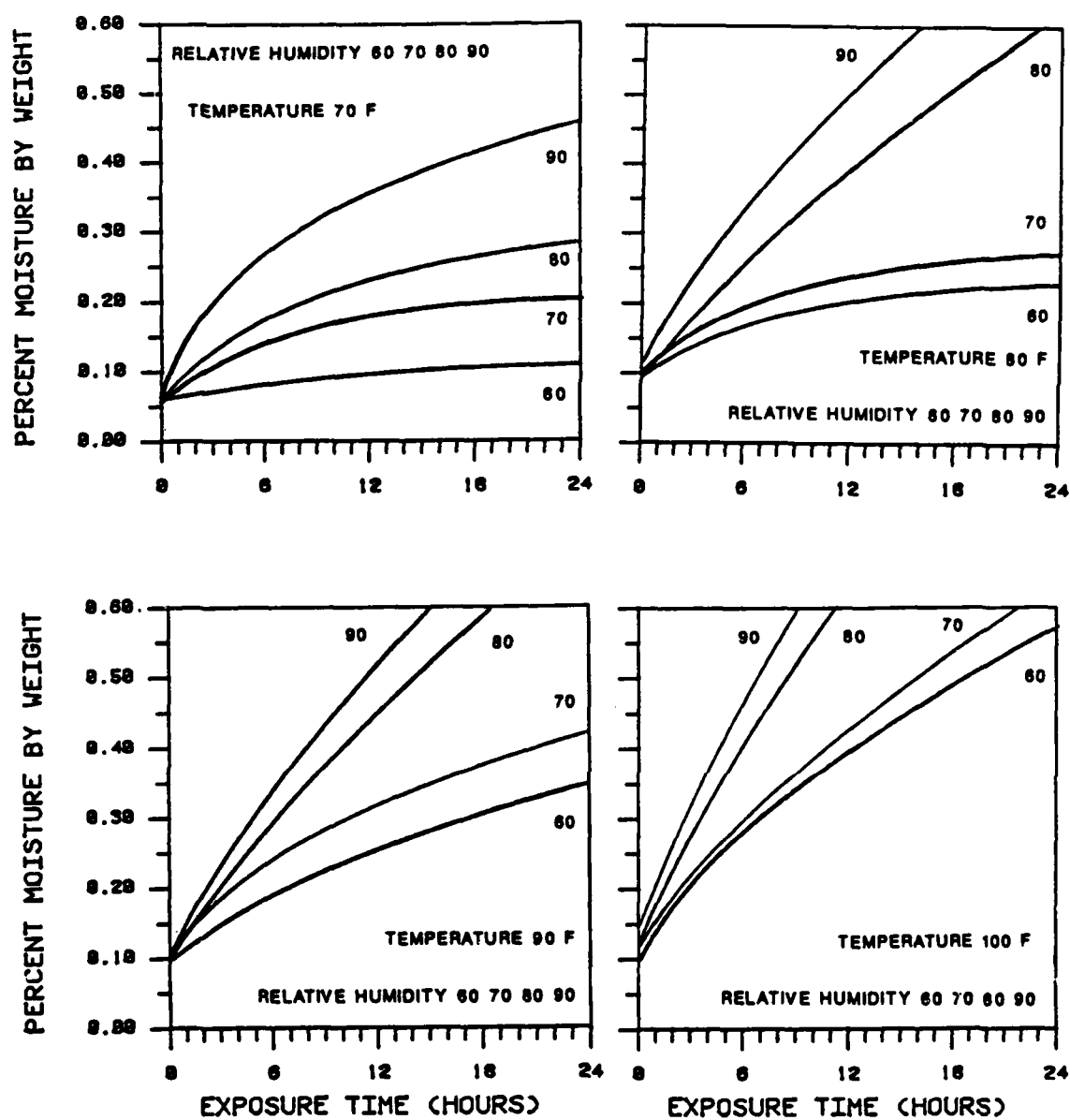
try as they relate to the field of welding.



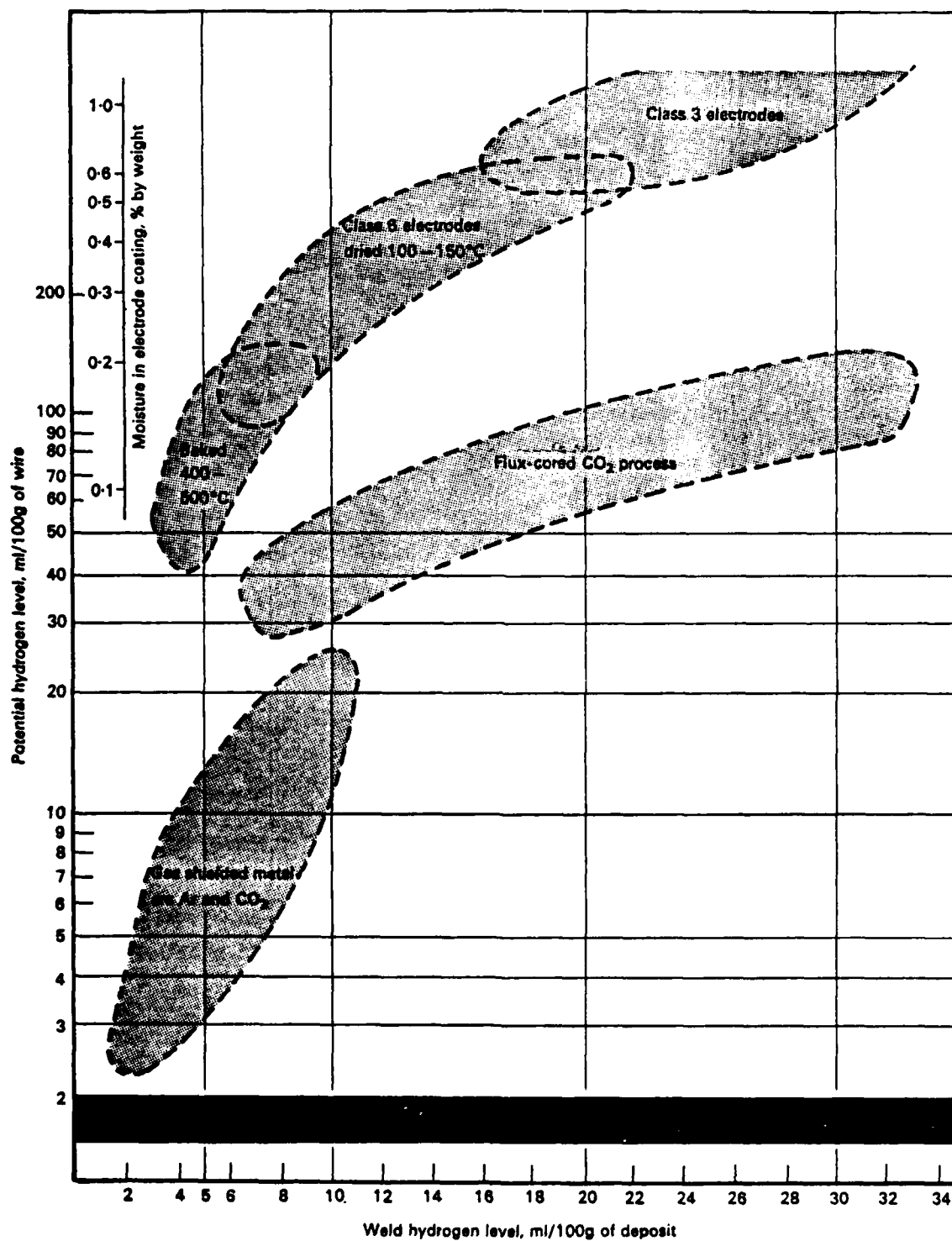
- 1.1 Typical hydrogen content of various electrode wires. The curve height indicates the relative frequency of test results for each type of consumable. (Ref C.15)



- 1.2 Typical moisture content of various fluxes and coatings. The curve height indicates the relative frequency of test results for each type of consumable. (Ref C.15)

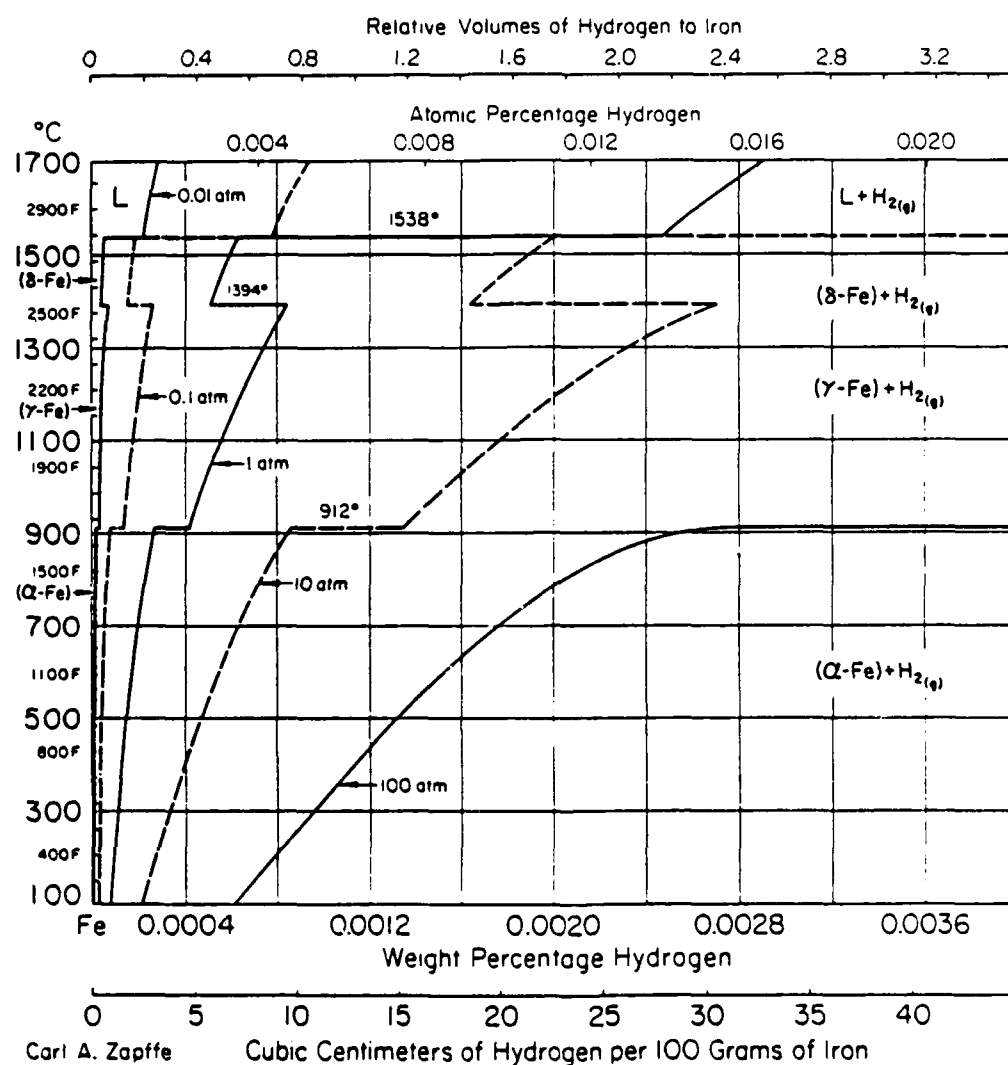


1.3 Effect of temperature and humidity on moisture levels of a low moisture E7018 electrode. (Redrawn from Ref N.1)

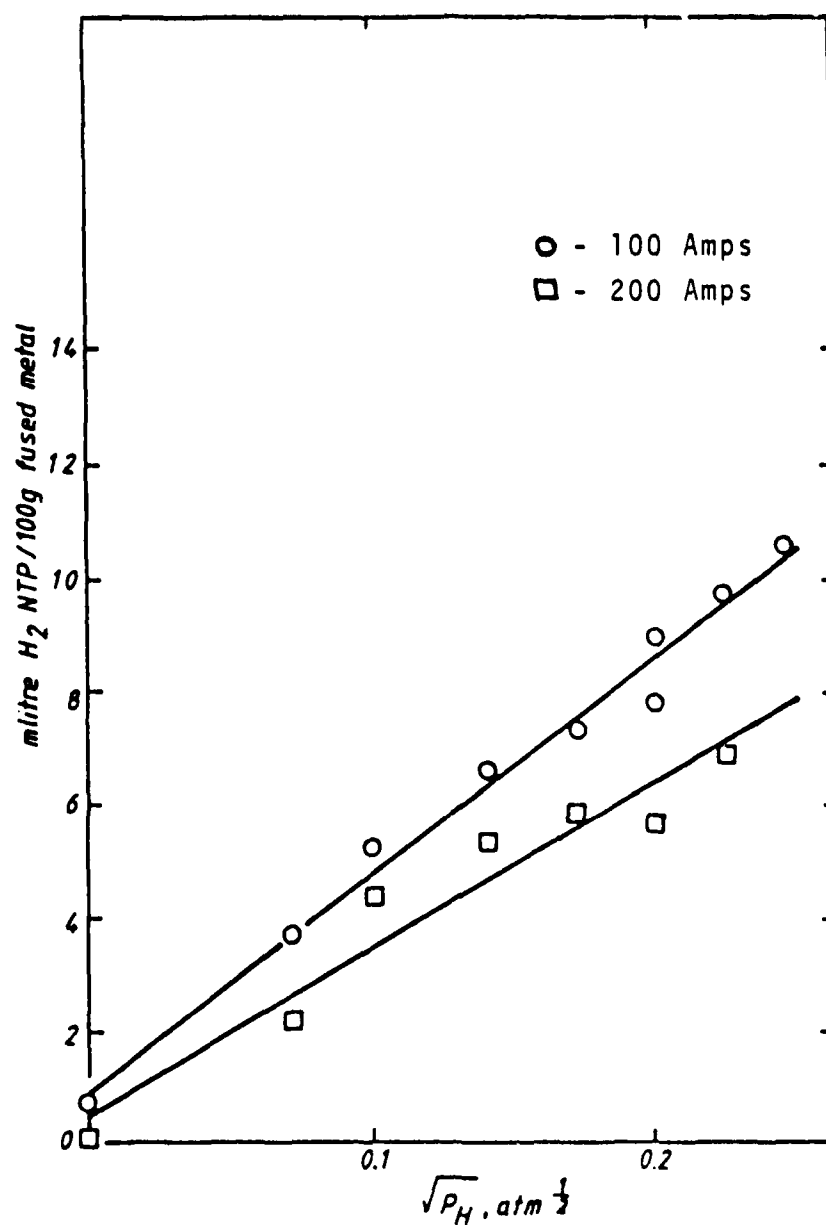


1.4 Relationship between potential hydrogen and weld hydrogen
(Ref C.15)

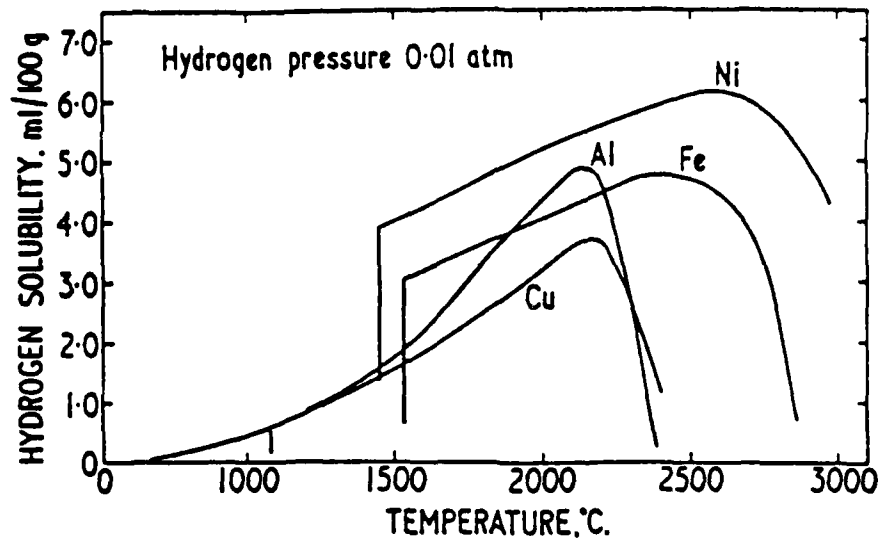
Fe-H Iron-Hydrogen



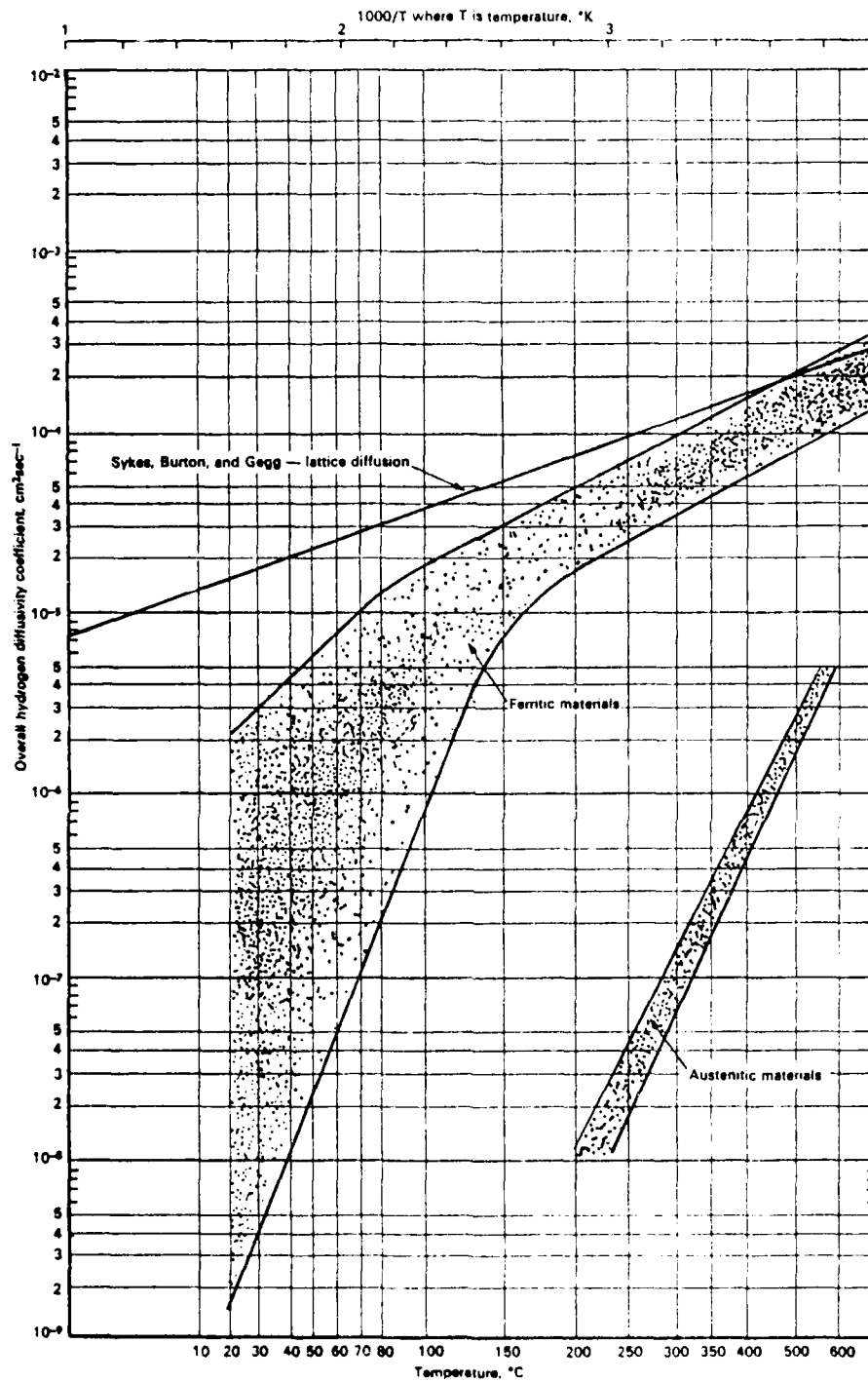
1.5 Iron-Hydrogen phase diagram. (Ref H.1)



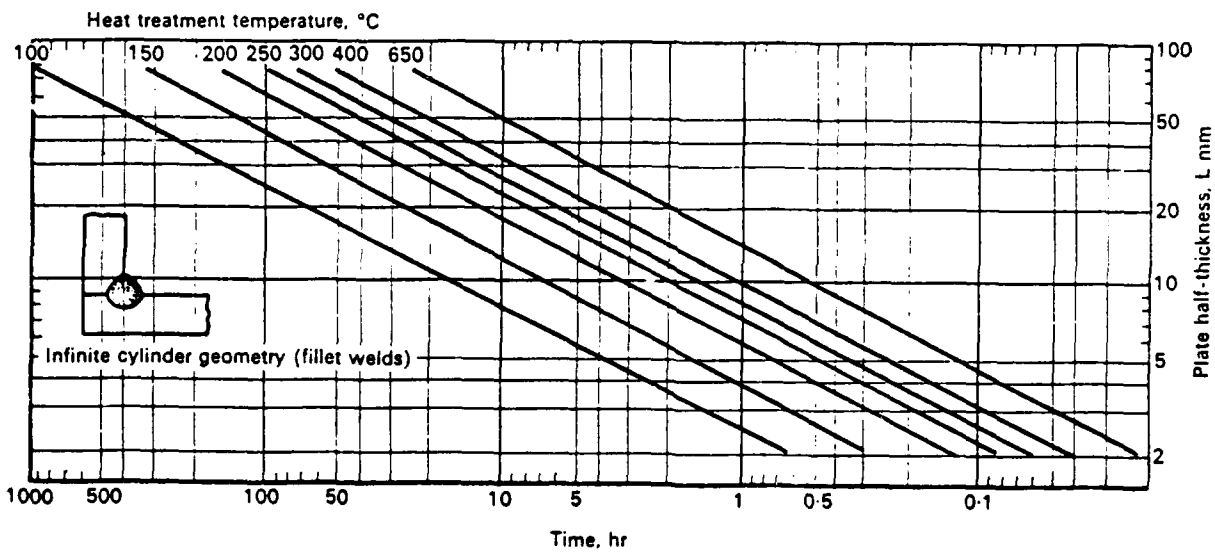
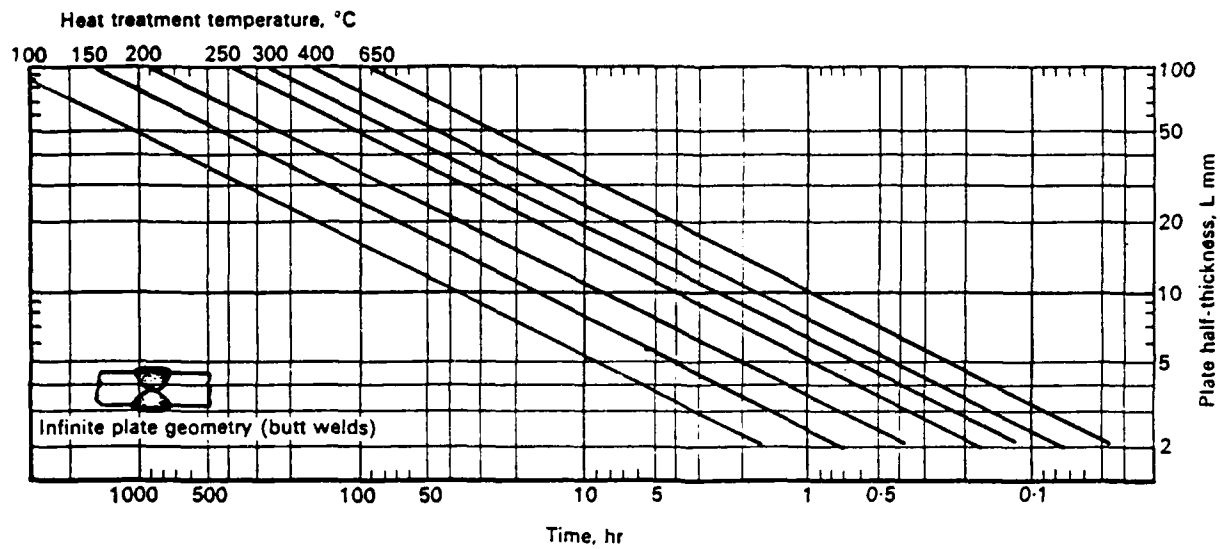
1.6 Measured hydrogen content of weld metal as a function of the square root of hydrogen partial pressure. (C.7)



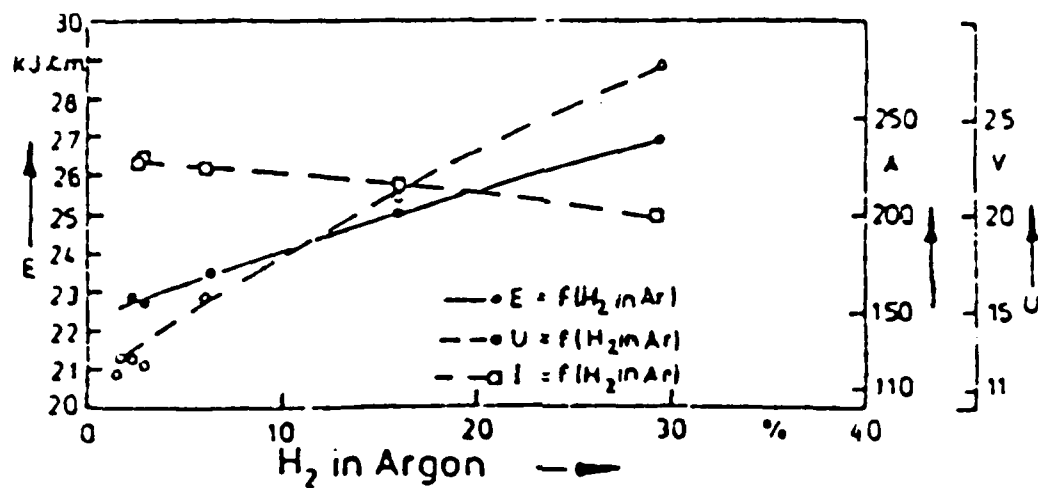
- 1.7 Hydrogen solubility versus temperature curves. The low-temperature part of the curves is derived from known experimental data, the high-temperature portion is obtained by extrapolating these data and then applying a correction for metal vapor. (Ref H.18)



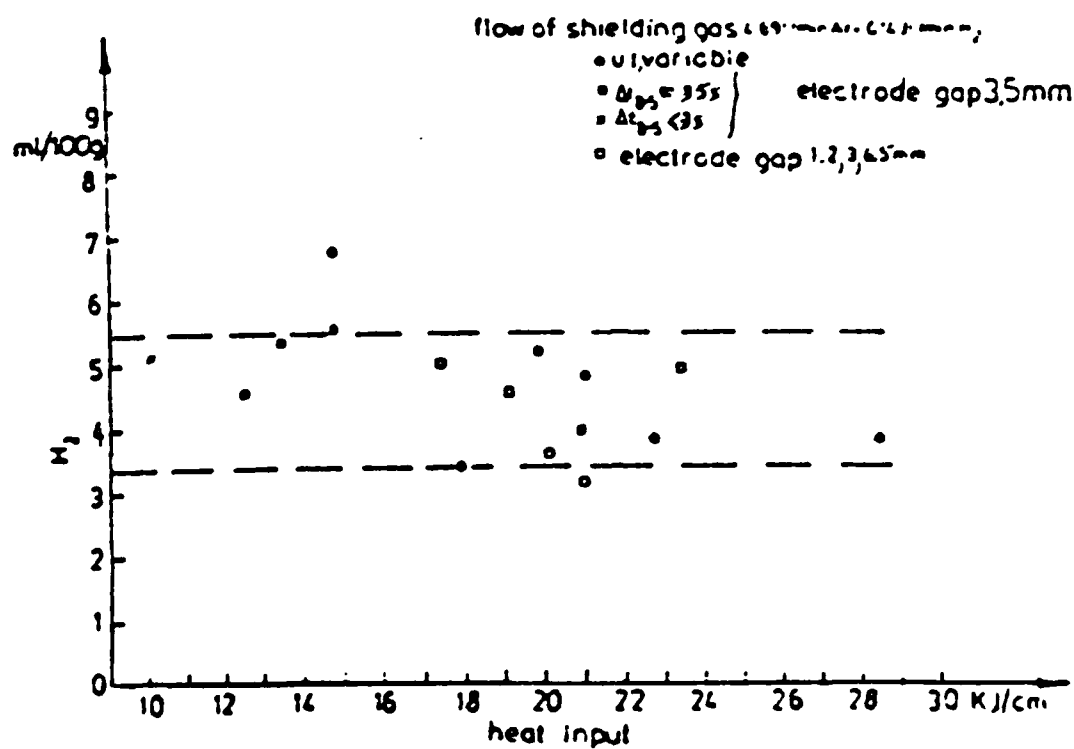
1.8 Variation in overall diffusivity coefficient, D , as a function of temperature. (Ref C.15)



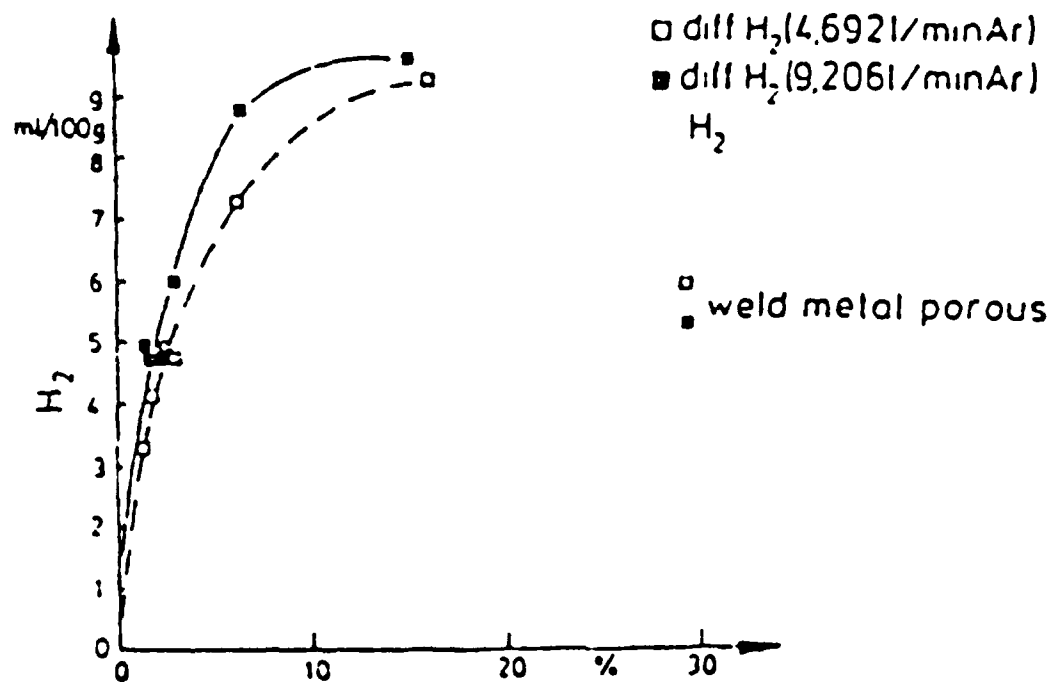
1.9 Approximate times for removing 75% of the original hydrogen:
 (a) butt welds, (b) fillet welds. (Ref C.15)



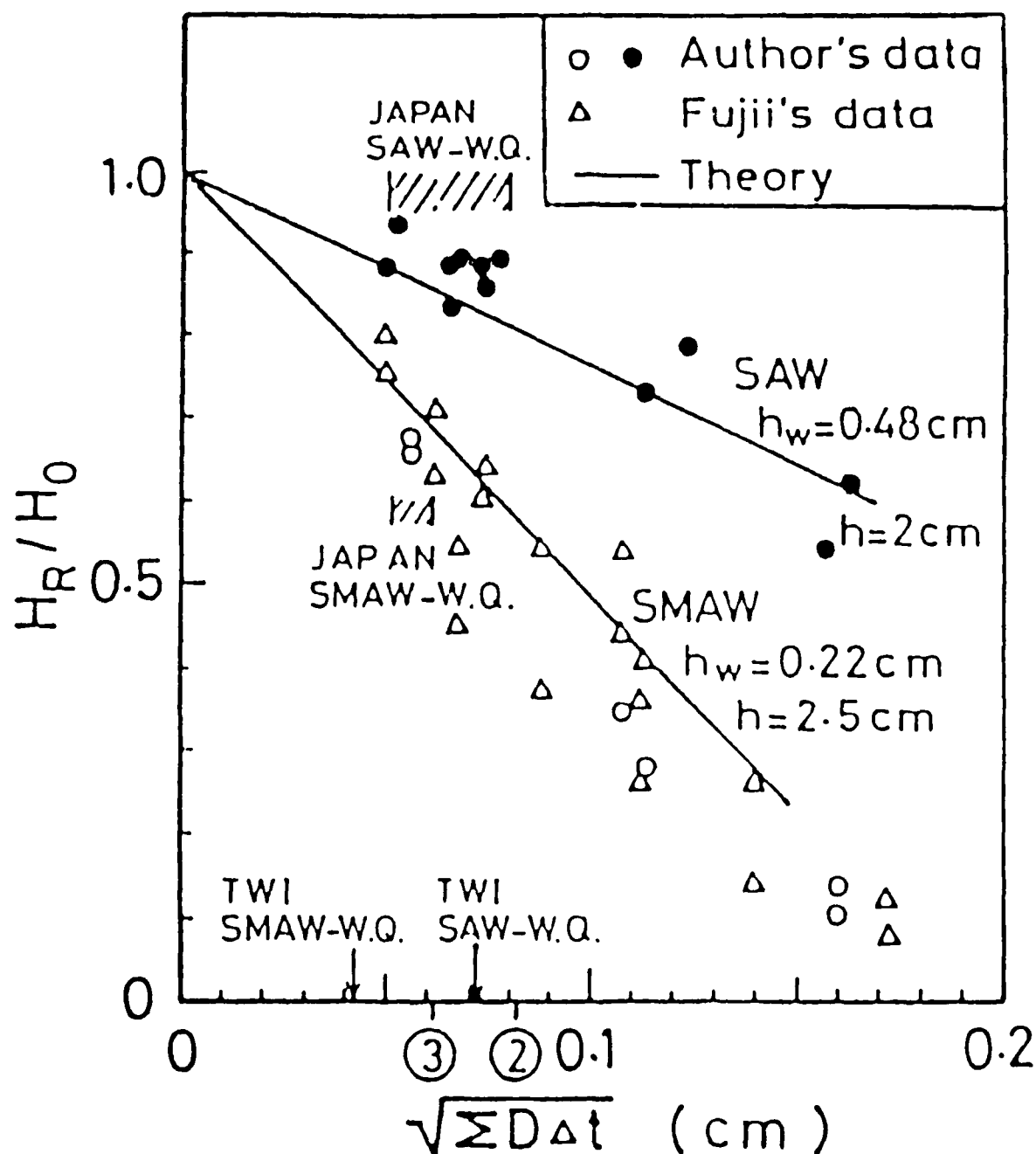
1.10 Variation in weld current and voltage as a function of hydrogen in the shielding gas. (Ref F.5)



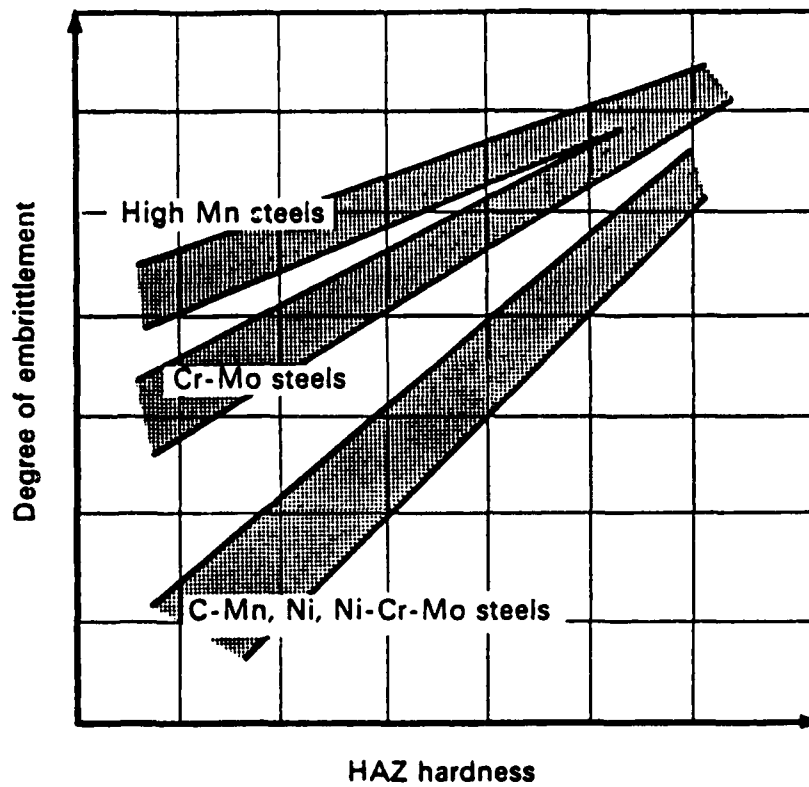
1.11 Variation in the diffusible hydrogen content as a function of heat input. (Ref F.5)



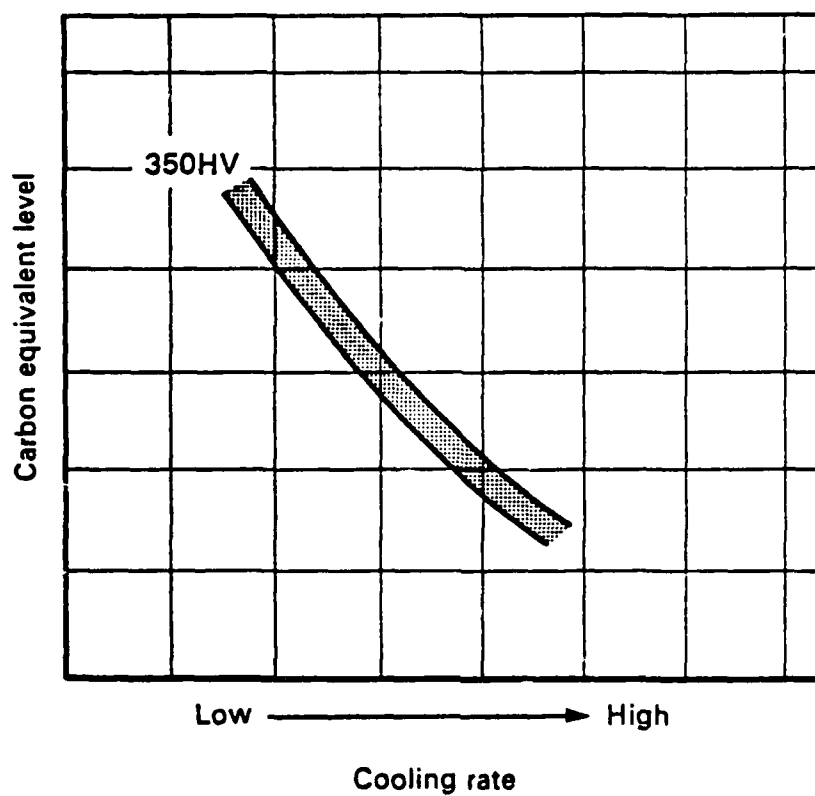
1.12 Diffusible hydrogen content of GTA welds as a function of hydrogen in the shielding gas. (Ref F.5)



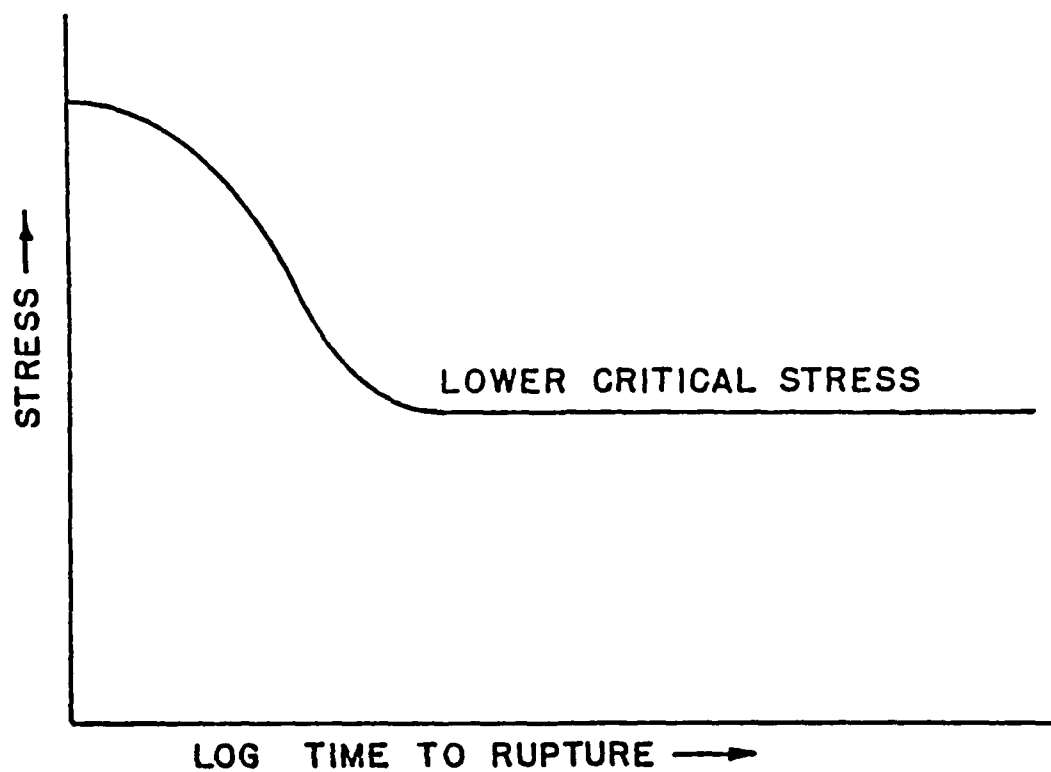
1.13 Comparison between experimental and theoretical results of retained diffusible hydrogen content. H_R/H_0 is the ratio of retained hydrogen to originally absorbed hydrogen. h_w is the bead width, and h is the specimen thickness. (Ref T.4)



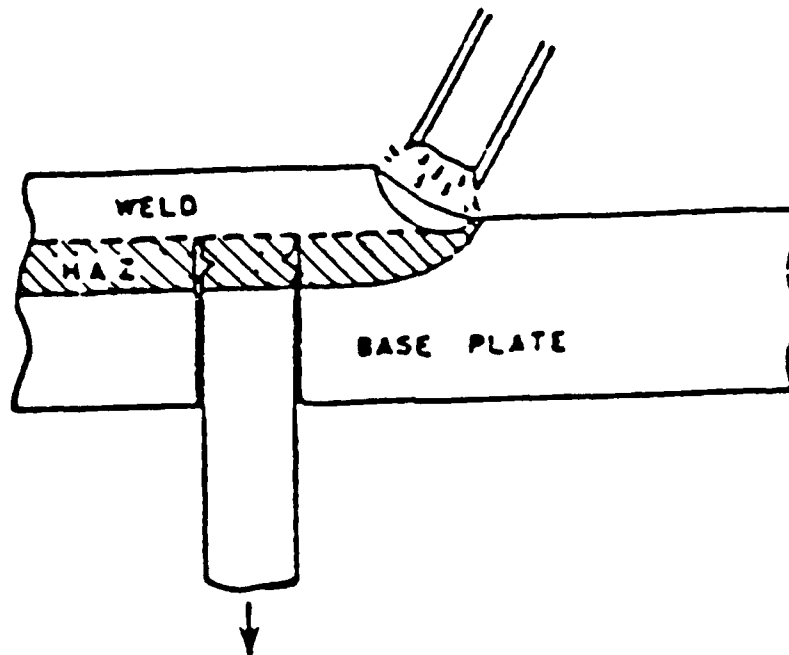
- 1.14 Hydrogen embrittlement as a function of HAZ hardness for three different steels. (Ref C.15)



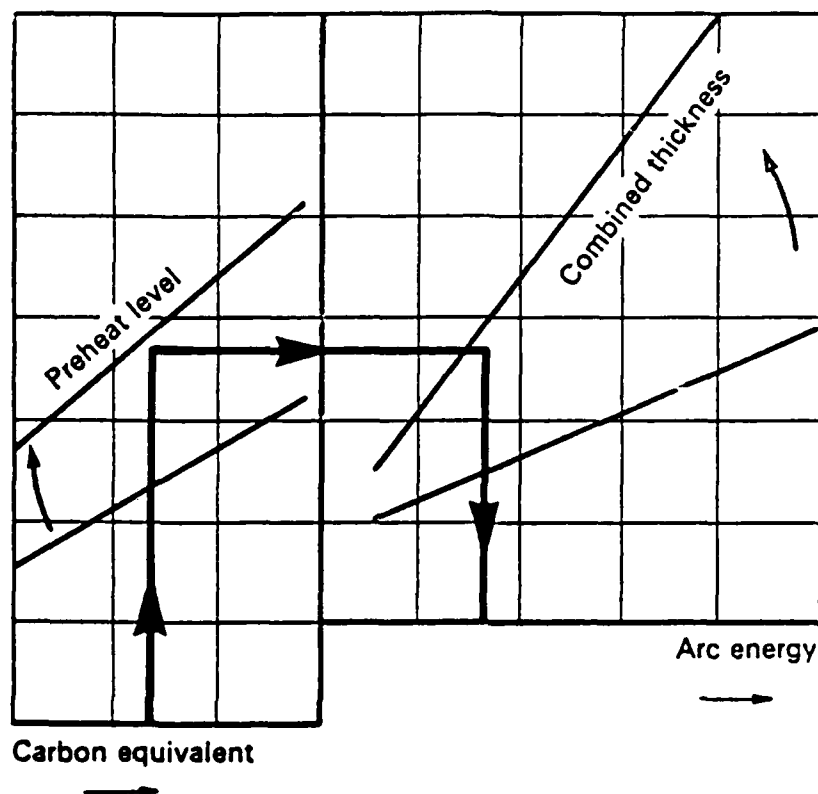
1.15 Demonstration of the effect of carbon equivalent and cooling rate on hardness. (Ref C.15)



- 1.16 Schematic plot of a "static fatigue" curve from constant load rupture tests.



1.17 General diagram of the implant test. (Ref S.13)



- 1.18 Prediction nomograph using material composition (carbon equivalent), and plate thickness to select preheat and arc energy to avoid cracking. (Ref C.15)

MEASUREMENT OF HYDROGEN IN WELDS

2.0 ABSTRACT

The primary objective of this experimental portion of the research program is to determine the amount of hydrogen initially absorbed into the molten weld pool, and to determine the amount of hydrogen responsible for causing hydrogen assisted cracking in weldments. These desired hydrogen values will be used in the theoretical discussions in chapters 3-5.

In order to accomplish this, the diffusible hydrogen test is studied to understand how the hydrogen values measured in this test can be used to determine the hydrogen values desired.

The method of measuring weld hydrogen content is investigated to determine how technique variations affect the accuracy and reproducibility of the final numerical results. Technique variations studied include: specimen size, outgassing temperature, calibration procedure of the gas chromatograph, and time delay between weld completion and quench.

The effect of welding process variations on hydrogen content are then investigated. Welding variations studied include: shielding gas composition, droplet transfer mode, preheat, and steel composition.

A method of determining the amount of hydrogen initially absorbed into the molten weld pool is developed based on a method originally developed by Terasaki. A method of determining the amount of hydrogen at the cracking zone is developed based on a hydrogen distribution model initially developed by Coe.

2.1 INTRODUCTION

At the outset of this research effort, the most widely recognized standard in the world for measuring weld hydrogen content was the International Institute of Welding (IIW) document IIS/IIW-805-85 (I9). This is commonly referred to as the "mercury method" which determines the diffusible hydrogen content. In this test, a weld is made on a specimen which is then quenched to lock in the hydrogen. The temperature of the specimen is later raised, and the volume of outgassed hydrogen measured. The salient characteristics of the IIW test include:

- A 10mm X 15mm X 30mm specimen machined from mild steel with a surface ground finish and degassed at 650 C for 1 hour prior to welding;
- Quenching the specimen as soon as possible after weld completion (no specified time requirement);
- Outgassing under a mercury collecting fluid (no specified temperature or time requirement);
- Measuring the volume of gas evolved with a eudiometer tube.

A number of specifications and standards have been based on this method of measurement or one of many modifications (E10, F1, G21, I8, I10, J2, K3, O1, P10, Q4, S16, S19, T5, W4). Modifications include using glycerin, water, or oil as the collecting medium. All of these tests have been criticized (B17, B18, C14, C15, O2, Q3) for variations in the measured values from lab to lab as well as for validity of the results.

The initial need for the IIW test was to differentiate between the quality and moisture content of welding consumables. It was known that

certain compounds added to an electrode could reduce the amount of as-deposited hydrogen even though the moisture may have remained constant. This test was used rather than measuring the moisture content since the effectiveness of a manufacturer's electrode formulation could be tested.

Since this test was already in existence, a large number of researchers have used this technique for an entirely different purpose: to predict hydrogen cracking of weldments, or hydrogen absorption reaction temperatures. However, much of the initial hydrogen diffuses away and plays no part in the embrittling phenomenon, and the diffusible hydrogen test does not directly measure the amount of hydrogen absorbed; it measures the amount retained a few seconds after solidification.

From a practical point of view, there is nothing wrong in principle with determining the critical IIW diffusible hydrogen value required to eliminate cracking in a specified application with a specified material, preheat, postheat, heat input, and applied stress. The only problem is to ensure reproducible measurements to control quality of the final product.

From a scientific point of view, the precise amount of hydrogen absorbed by the weld and the amount of hydrogen which actually causes cracking are the important values. These values could be used to develop a rational model for the absorption of hydrogen into the weld pool during welding. Also, these values can be used to more fully understand the

hydrogen cracking mechanisms of steel weldments.

This study has 3 objectives:

- 1) to understand the influence of testing technique variations and weld process variations on the resulting value of weld hydrogen content;
- 2) to understand how much hydrogen is initially absorbed by the weld, and how much remains at the time of cracking; and
- 3) to determine an accurate and reproducible technique for measuring the hydrogen content of a weld. This is especially needed for low hydrogen contents, since at low hydrogen levels the experimental scatter can be as high as the value of hydrogen being measured.

2.2 FUNDAMENTALS OF ANALYTICAL CHEMISTRY

The field of analytical chemistry deals with methods for the identification of one or more of the components in a sample of matter, and the determination of the relative amounts of each. Much can be learned from this advanced field to understand how to measure the amount of hydrogen in steel weldments and to understand what the results mean.

The choice of analytical method is based on such considerations as speed of analysis, accuracy, reproducibility, concentration range of the

analyte, and availability of equipment. Success or failure of an analysis is often critically dependant on the proper selection of the method as well as the technique.

The simplest, and for centuries the most accurate, method of chemical analysis was gravimetric analysis. The sensitivity is often in the range of one or two parts in 1000. Today, this method of analysis is generally used in precipitation or volitization methods. For simple systems, containing more than 1% of the analyte, this method is seldom surpassed by other methods (S22). Unfortunately, in the measurement of hydrogen contents, the amount of hydrogen is so small, and the weight of hydrogen so minute, that this method is not feasible for steel weldment samples.

With the introduction of carefully calibrated glassware, the volumetric method of measurement became possible. This method is often as accurate as the gravimetric method when used with the titration process. In the field of welding, the titration process (with Karl-Fischer reagent) is often used to very accurately measure the amount of moisture in a sample of flux.

The commonly used "mercury method" or "glycerin method" of measuring the amount of hydrogen in welds does not have nearly the accuracy of other volumetric methods of analysis. There are a number of sources of error in these methods currently being used by the welding field. Unfortunately, many of these sources of error are not systematic, but are

variable, thereby making corrections for them difficult.

The first error is due to the fact that a number of gases can outgas from the weld sample, all of which are collected in the calibrated eudiometer tube. The resulting measured volume of gas is not necessarily the amount of hydrogen. Another error is the solubility of hydrogen in the collecting fluid. This solubility problem is slight in the case of mercury, but mercury is an unattractive medium due to its toxicity and dangerous embrittlement potential.

Glycerin has been used extensively in the United States as a collecting medium. Glycerin is safe to use, but hydrogen is very soluble in it. Some have attempted to solve this limitation by bubbling hydrogen through the liquid to saturate it. However, this will introduce a large concentration gradient across the glycerin container, and hydrogen will diffuse down this gradient and increase the volume measured in the eudiometer tube. Hydrogen solubility in water and oil also render these media unacceptable.

The accuracy and reproducibility of the mercury or glycerin method are difficult to estimate, but they have been criticized for lack of both. A conservative estimate of the accuracy of the mercury method would be about one part in ten. The accuracy of the glycerin method is much worse.

The introduction of the gas chromatograph (GC) has significantly

improved the ability to measure the amount of gaseous elements in a metal. Chromatography refers to processes that are based on differences in rates at which individual components in a mixture migrate through a stationary medium under the influence of a moving phase. This technique is beyond doubt the most extensively employed instrumental analytical separation method (Ell). Although a GC can be used for a huge number of applications, this discussion will be centered around a system for measuring hydrogen in steel welds.

The essential parts of a GC are shown in figure 2.1. The moving phase in this system will be the argon gas, the sample will be hydrogen gas, and the stationary medium in the column is chosen so that the components (e.g. argon, nitrogen, and hydrogen) will migrate through it at different rates. The hydrogen can be extracted from the steel weldment by heating it in an enclosed container for some period of time. The time and temperature chosen will affect the amount which outgases from the weld sample. Since hydrogen is naturally gaseous at room temperature, a GC for this analysis need not be enclosed in an oven as is shown in figure 2.1.

The differential detector most often used for measuring hydrogen is a thermal conductivity (TC) detector. This form of detector consists of temperature sensitive resistors used in two arms of a Wheatstone bridge. The electrical circuit of a TC detector is shown in figure 2.2. An increase in current causes a rise in temperature of both R_1 and R_2 and hence a change in their resistance, upward for a metallic wire and down-

ward for a thermistor. The change is equal for both arms, and the bridge remains balanced. If, however, the gas surrounding one of the resistors is different, the heat developed in the two arms will be conducted away through the gases at different rates. The two arms will then be at different temperatures, and the bridge will no longer be balanced.

The TC detector signal will be balanced (or zeroed) with pure argon being passed over both sides of the Wheatstone bridge. When the sample gas is introduced into the gas stream at the sample injection port, the difference in thermal conductivities of the gases will cause the detector to signal peaks such as are shown in figure 2.3. If more than one gas is in the sample (i.e. hydrogen and nitrogen) they will move through the packed column at different rates, and two peaks will be detected. Due to the fact that the entire sample component is consumed, the integrated area under the signal-time curve must equal the mass of substance detected. The height of the curve at any point is proportional to the mass flow rate of the sample $v_s = dm/dt$; hence the area beneath the recorded curve equals:

$$A = \int v_s dt = \int (dm/dt) dt = m \quad (2.1)$$

If the area can be properly integrated, this measurement of the amount of hydrogen can be quite accurate. The area can be integrated by an approximation method, by manually measuring the area off a strip chart recorder, by using a planimeter, or by using an integration unit built

into the electronics of the GC unit.

Since hydrogen will travel through the column at a different rate than any other gases evolved from a steel weld specimen, this method will eliminate the error of counting numerous gases in the measured hydrogen content.

If a GC is properly used, the major consideration remaining for the measurement of hydrogen in a steel weld is the choice of how to remove the hydrogen from the sample. This will inevitably depend on what the final values will be used for. The factors affecting these values will be studied in the following sections.

2.3 EXPERIMENTAL OUTLINE

Based on the literature survey, it was determined that the optimum measuring technique would utilize a Gas Chromatography method to increase the sensitivity and eliminate the possibility of measuring gases other than hydrogen. From an economic standpoint, it was decided to perform the bulk of the testing on a Yanaco hydrogen analyzer model G-1006 (sold in the U.S. by Oerlikon). This unit uses a thermistor type thermal conductivity detector, argon carrier gas, and molecular sieve 5A in the column. The advertised measurement error is 0.01ml per 2ml. The Yanaco unit also measures the amount of nitrogen in the gas being analyzed. This is useful for detecting leaks in the outgasing chamber.

The IIW technique was used with a number of variations which were systematically evaluated. These included:

- 1) calibration procedure for the Yanaco unit,
- 2) specimen size,
- 3) specimen surface finish,
- 4) outgassing temperature,
- 5) outgassing time, and
- 6) time delay between weld completion and quench.

During the course of this experimental program, the American Welding Society (AWS) initiated commission A4.3-86 to develop a new standard for diffusible hydrogen measurement of steel weldments. The results of this commission were also studied in the present investigation wherever time permitted.

After a standard method of diffusible hydrogen measurement was determined with the above experiments, the effect of welding variations was studied. The variations studied included:

- 1) the amount of hydrogen in the weld shielding gas,

- 2) the composition of the weld shielding gas,
- 3) droplet transfer mode,
- 4) base metal composition, and
- 5) preheat.

2.4 RESULT OF HYDROGEN MEASUREMENT TECHNIQUE VARIATIONS

2.4.1 CALIBRATION PROCEDURE OF THE GAS CHROMATOGRAPH

The calibration procedure supplied with the Yanaco unit (W3) was examined to determine if differences in the procedure would cause a difference in the measured hydrogen value.

The Yanaco unit has an internal calibrated tube which holds a known amount of hydrogen. This tube is filled with hydrogen, and then the amount is measured by the Gas Chromatograph (GC) portion on the Yanaco unit. The resulting output of the unit is then adjusted to Standard Temperature and Pressure (STP) and should agree with the value supplied by the manufacturer. If the output is different than the value supplied by the manufacturer, the sensitivity is adjusted so that the numbers agree. The procedure is repeated until the output reading remains steady, at which point the measurement of the hydrogen in the specimens is performed (one reading for each specimen).

This calibration procedure was examined for its accuracy and reproducibility under different conditions with the following experiment. The specimen holding chamber (shown in figure 2.4) has a valve on the top which will let gas flow through any of the four chambers or bypass all four. Chamber one was left empty, and a blank (hydrogen free) specimen was placed in chamber two. The calibration procedure was then performed

with the valve in the bypass, chamber one, and chamber two positions. The sensitivity dial was not adjusted between measurements. The resulting measurements are tabulated in table 2.1 for a 12 X 25 X 80 mm specimen size.

When this procedure is followed with the sample holder in the bypass position, a different number is found than when the procedure is followed using a specimen chamber with a specimen in it. This average difference of about .05 ml will cause a consistent discrepancy between the measured value and the actual value of the diffusible weld hydrogen content.

Also demonstrated in table 2.1 is the reproducibility of the calibration procedure. The standard deviation among the readings is about .02 ml. Also noted during this portion of the experiment was that the Yanaco unit required a warm up time of about 15-20 minutes before it stabilized. Any readings attempted before that time resulted in extremely erratic fluctuations.

2.4.2 SPECIMEN SIZE

The initial diffusible hydrogen determinations were performed using the IIW specimen size. These results as a function of varying hydrogen content in the GMAW shielding gas are shown in figure 2.5. As can be seen, there is a large amount of experimental scatter in the data. In many cases the scatter is almost as large as the data itself (i.e. $.07 \pm$

.05 ml H_2). This large amount of experimental scatter made reasonable scientific correlations difficult.

By increasing the specimen size, the amount of hydrogen available for measurement was also increased substantially. The increased size was chosen as the maximum width and depth that could fit into the Yanaco chamber without dramatic alterations to the specimen holder. This was also the cross-section size chosen by AWS standard A4.3-86. Therefore a size of 25 X 12 X 80 mm (1 X 1/2 X 3 1/4 in.) was used in the present study so that all of the dimensions, including the length, agreed with the AWS standard.

Figure 2.6 shows the diffusible hydrogen content found in the larger specimens, hereafter referred to as the AWS specimen size, as a function of hydrogen content in the weld shielding gas. As can be seen, the amount of experimental scatter is less for the AWS size than for the IIW size. During all portions of these and ensuing tests, certified mixtures of shielding gas were used to ensure that the percent hydrogen and oxygen were consistent. This helped reduce the scatter due to variations in the mixture caused by the rotometer usually used.

2.4.3 SURFACE CONDITION

The effect of specimen surface condition was briefly examined. Specimens were welded in the as-rolled condition (hot-rolled A36) as well

as after careful machining. The amount of hydrogen measured in the as-rolled specimens was 20% lower than in the machined specimens. These results, tabulated in table 2.2, show that the surface condition can alter the amount of hydrogen which escapes from the specimen. A number of specimens were also bead blasted after quenching but before outgassing. This increased the amount of hydrogen outgassed by about 8 - 10%. The remaining specimens were not bead blasted.

2.4.4 OUTGASSING TEMPERATURE AND TIME

Outgassing temperature was examined to quantify the effect on the resulting diffusible hydrogen value. This can be especially important since many investigators have used different outgassing temperatures. The Leco HW-100 analyzes 12 specimens each hour after outgassing at 25 to 200 C. The Leco HW-200 analyzes 1 specimen at 400 C for one hour and then heats the sample to 650 C to analyze what Leco terms the residual hydrogen. White (W8) performed her outgassing at 200 C. The IIW allows both 25 C and 45 C. The new AWS standard specifies either 45 C or 150 C.

The Yanaco specimen holders used in the present study had viton 'O' rings which failed at temperatures above 100 C. These were replaced with teflon 'O' rings for the higher temperature extractions. It was found that higher extraction temperatures resulted in more hydrogen diffusing out of the specimen, but that substantial leaking also occurred. Since these tests were inconclusive, this portion of the research program was

discontinued.

Outgassing time was varied to find the minimum time at which most of the hydrogen left the specimen. The resulting data for outgasing performed at 45 C is shown in figure 2.7.

2.4.5 TIME DELAY BETWEEN WELD COMPLETION AND QUENCH

The time delay between weld completion and quenching was varied to quantify the effect on the remaining weld hydrogen. The results for a GMAW shielding gas composition of 2% H_2 / 1% O_2 / Ar are shown in figure 2.8. As can be seen, the resulting diffusible hydrogen level decreases with time. Also, the scatter in the data decreases with time.

The remaining hydrogen content decreases approximately linearly with the log of time and eventually remains constant. The amount of hydrogen remaining in the specimen after 24 hours has been tabulated in table 2.3 for a variety of shielding gas compositions.

2.5 DISCUSSION OF HYDROGEN MEASUREMENT TECHNIQUE VARIATIONS

2.5.1 CALIBRATION PROCEDURE

The experiments performed on the calibration procedure of the Yanaco unit show that great care must be taken in order to obtain accurate and reproducible results. The zero level of the unit tends to float during the course of an analysis, and the unit must be rezeroed often. If the unit is not sufficiently stabilized by being left on for at least 15 minutes prior to analysis, the results are extremely scattered. The internal tube should also be filled in a consistent manner (i.e. filled

for 5 seconds, followed by a 5 second delay) otherwise the calibration procedure will produce variations in the output.

Also, if the argon carrier gas cylinder pressure falls below 350 psig, the unit cannot be zeroed due to erratic fluctuations in the readout. Discussions with a gas cylinder manufacturer (K7) disclosed the fact that almost empty cylinders may have large amounts of residual impurities and should never be completely emptied. The author has been unable to find any references to this phenomenon in the literature. This could be an important point since these impurities could lead to welding defects. If the erratic fluctuations in the GC readout due to these impurities are at all realistic, then hydrogen contents of over 100 ppm are left in an almost empty cylinder (new cylinders are typically certified at about 10 ppm moisture).

The results in table 2.1 show that the calibration procedure will produce a different result depending on the position of the specimen chamber valve. This is probably due to the machine's being peak sensitive. It should be recalled from section 2.2 that the integration of the area under the hydrogen peak can alter the resulting measurement of the total amount of hydrogen. A peak width and height variation will produce variations in the integrated number determined by the GC. When a larger specimen and chamber are used, the hydrogen peak will be more spread out and the integration portion of the Yanaco unit will calculate a smaller value for the hydrogen content. In the bypass position, the peak will be taller and narrower. Even though the same amount of hydrogen is being

analyzed in both cases, the taller peak will be seen by the integrator as having a higher hydrogen content.

In order to obtain accurate results, this variation in the hydrogen peak height between different sizes of specimen chambers must be accounted for. If this calibration factor is not included, the resulting measured values of hydrogen content will be lower than the true value.

Before analyzing the hydrogen content of a specimen, the unit must be calibrated with the specimen chamber valve in the bypass position. The value desired on the digital readout is .045 ml greater than that which the standard calibration procedure would normally indicate. If this adjustment is not made, all of the readings will be about .45 ml/100g too low (.045 times 100 divided by the deposited weld metal weight of about 10 grams). This necessary correction in the calibration procedure was first postulated by Kotecki (K10).

2.5.2 SPECIMEN SIZE

As the results in figure 2.5 demonstrate, the IIW specimen size is too small for accurate measurement of low diffusible hydrogen concentrations. The first reason for this is that the amount of hydrogen which can be collected in such a small specimen is on the same order of magnitude as the experimental uncertainty. Thus, any statistical confidence limits on the data are quite small. The second reason is that a signifi-

cant amount of hydrogen can diffuse out of the specimen before it can be quenched after weld completion.

A small specimen size is desired to reduce the amount of time needed for total evolution of hydrogen from the specimen, thus reducing the time needed to perform a measurement. A small size is also desired to fit into an isolation chamber in which to outgas. However, a large specimen size is required to retain all of the hydrogen absorbed by the weld pool during welding.

Terasaki, et al. used a numerical analytical model of superpositioned one dimensional analyses to theoretically determine the optimum specimen size to meet all of these conditions. Their theoretical results showed that a specimen size of 10 X 20 X 40 mm was sufficiently large to collect most of the hydrogen produced by a 4 mm diameter SMAW electrode with an arc energy of less than 17 kJ/cm (T2). Later, using experimental data, they determined that a specimen size of 12 X 40 X 40 mm was more appropriate for a wide range of welding processes and arc energies (T3).

Terasaki, et al. developed a theoretical equation for the minimum specimen width as a function of the bead width and thermal factor (T2). Substituting the maximum GMAW bead width and thermal factor used in the present study, the required specimen width was determined to be 21 mm. Using a similar set of equations for the minimum specimen thickness, a 12 mm thickness was found to be more than adequate. Terasaki, et al. also found that the diffusible hydrogen content determined with 40 mm and 80

mm specimen lengths were virtually equivalent (although the scatter was slightly smaller for the longer length). Thus, they chose the smaller length as being adequate. The present study was performed using the 80 mm length so that a larger amount of hydrogen could be collected. This is especially needed since very small amounts of hydrogen were being measured. Thus the 12 X 25 X 80 mm specimen size was chosen as the optimum size for the present study. This size also conforms with AWS standard A4.3-86.

Of course some of the hydrogen absorbed by the molten weld pool will escape through the surface rather than through the bulk of the specimen. Thus, no matter how large the specimen is, some hydrogen will escape before the specimen can be quenched to freeze in the remaining hydrogen. The amount of hydrogen absorbed directly by the molten weld pool must be somewhat higher than the diffusible hydrogen test can directly measure.

2.5.3 SURFACE CONDITION

The fact that specimen surface finish can affect the final value of diffusible hydrogen is not surprising. The oxide coating on a hot-rolled specimen will prevent diffusion of hydrogen across the surface. A similar observation has also been found by researchers studying SMAW. Boniszewski and Morris (B18) found that shot blasting the specimen after welding allowed approximately 10% more hydrogen to diffuse across the surface than wire brushed samples (figure 2.9). However, they also found

that shot blasting resulted in more experimental scatter (probably due to residual compressive stresses caused by the shot blasting). The need to shot blast or wire brush the specimen is greater for SMAW which has a thick slag coating over the weld, than for GMAW. Whichever technique is used, it should be explicitly stated by any researchers presenting their results. In the present study the GMAW specimens were carefully machined prior to welding, and not bead blasted or wire brushed after welding, since the effect was found to be slight.

If the expensive machining step could be eliminated, the cost of preparing specimens would be significantly reduced. However, mill scale effects the amount of hydrogen which can diffuse out of the specimen. Since the amount of mill scale will be different from one set of specimens to another, this will result in an increase in experimental error. Thus, it is advisable to carefully machine the specimen surfaces to obtain reproducible results. The IIW and AWS standards do not specify a single method of surface preparation, but rather suggest a variety of methods.

2.5.4 OUTGASSING TEMPERATURE AND TIME

Due to the limitation of the experimental apparatus, the diffusible hydrogen as a function of outgassing temperature could not be quantified. This is unfortunate since this may be a significant effect which is often overlooked. It is known that hydrogen becomes bound to various types of

imperfections in the steel specimen at different trapping sites. This area of research has been extensively studied by physical metallurgists for some time, and the specific types of trapping sites have been a topic of much debate. The basic idea is that each trapping site will have a different binding energy associated with it. Hydrogen will remain trapped at that site until a critical temperature is reached, at which point the trap will release its hydrogen.

In actual binding energy experiments, the hydrogen will not all be released at a specific temperature; rather, the rate of hydrogen evolution will exhibit a maximum at a certain temperature. An example of a thermal analysis for the determination of trapping sites in three types of steel is shown in figure 2.10 (14). A careful analysis of this figure shows that a number of fairly distinct peaks can be discerned for each type of steel. Lee, et al. have classified these peaks and identified the type of trapping site associated with each. Their resulting tabulation is reproduced in table 2.4. The height and location of these peaks (and hence the binding energies) also vary with the amount of cold work and amount of ferrite-carbide interfaces as is shown in figures 2.11 and 2.12.

As a result of differences in binding energy from trapping site to trapping site in different steels, diffusible hydrogen experiments performed by a method which uses a higher outgassing temperature may result in a higher value than that found using a lower temperature. The increased solubility of hydrogen at the higher temperature is an insigni-

ficant fraction of the amount which will outgas. This is an area of research which should be carefully evaluated in order to determine if the various diffusible hydrogen testing temperatures need to be standardized. The effect will also probably vary from one steel to another.

The results in figure 2.7 show that the IIW and AWS outgassing recommendation of 72 hours at 45 C should indeed result in the vast majority of the hydrogen being allowed to outgas. This result has also been theoretically confirmed by Terasaki (T2) as is shown in figure 2.13. Obviously, any change in outgassing temperature will require a different outgassing time. The higher the outgassing temperature the less time required.

2.5.5 TIME DELAY BETWEEN WELD COMPLETION AND QUENCH
(METHODS FOR DETERMINING INITIALLY ABSORBED HYDROGEN CONTENT AND
HYDROGEN REMAINING IN THE CRACKING ZONE)

As was shown in figure 2.8, if the weld is allowed to cool on its own for some time before quenching, hydrogen will diffuse out of the specimen. Researchers have found that hydrogen cracking will only occur once the weld has cooled to about 100 C (K5), and that the amount of hydrogen which diffuses out before that temperature will play no role in the cracking phenomenon.

Terasaki has theoretically modeled the amount of hydrogen which remains in the specimen as a function of the summation of diffusion-time increments (which he terms the "thermal factor"). If the cooling curve of temperature versus time is known, along with the diffusivity versus temperature, a theoretical curve of hydrogen remaining versus time after welding can be calculated. This theoretical curve is shown in figure 2.14, which shows experimental data as well as the theory.

Terasaki's theoretical line correlates well with his plotted experimental data. However, it is not clear how he found experimental data for H_0/H_R since it is impossible to experimentally determine H_0 directly. Unfortunately, no mention is made of how the data was obtained or modified for his graph. This question does not necessarily detract from the validity of Terasaki's theory, which was primarily aimed at finding an

optimum specimen size. It makes sense that the amount of hydrogen will be related to Terasaki's "thermal factor" since the solution of Fick's laws will result in a $(Dt)^{1/2}$ term.

It is the author's opinion, however, that the Terasaki model is fairly conservative since he does not consider the amount of hydrogen which will escape from the weld through the weld surface. Rather, he only calculates the amount which will diffuse out of the specimens' sides and bottom. Coe and Chano (C13) have shown that hydrogen will rapidly diffuse out of the top surface of the weld. The fact that some hydrogen will diffuse out the top will shift Terasaki's theoretical curves downward (i.e. the H_R value will be lower than his calculation shows). Also, hydrogen will be able to escape from the beginning of the weld during the time it takes to complete the weld (i.e. hydrogen will escape from the first 10mm of the weld while the last 10 mm is being welded). Calculating the exact extent of this difference would be extremely difficult and is beyond the scope of this investigation. However, Terasaki's results graphically show that the amount of hydrogen measured by the diffusible hydrogen test is different from the amount initially absorbed by the weld pool. Thus the use of diffusible hydrogen values in calculating an equilibrium reaction temperature will result in a substantial error.

By knowing the diffusible hydrogen content and the cooling curve of the specimen, Terasaki's method will yield an approximation of the original hydrogen content of that weld. These values of the original hydrogen content can then be used to model the mechanism of hydrogen absorption

from the arc atmosphere into the molten weld pool. The experimental diffusible hydrogen values determined in this study will be converted to initially absorbed hydrogen for the theoretical analysis to be performed in chapter 3.

By extending the Terasaki analysis to much longer times (24 hours rather than 3 seconds), one can obtain information about the amount of hydrogen remaining in a specimen to cause cracking in an implant or other cracking test. However, due to the errors inherent in the diffusivity data below 250 C, the Terasaki analysis will also have an inherent error if extended to very long times. Another important error will arise due to the fact that the solubility and diffusivity of hydrogen will vary under an applied stress. Therefore, the weld residual stresses, or the applied stress in an implant test, will invalidate the long time Terasaki values.

Numerous researchers have proposed mechanisms of hydrogen embrittlement which postulate that hydrogen will continually be supplied to the advancing crack tip (e.g. as a Cottrell atmosphere). The numerical value of this additional hydrogen will not be addressed in the present discussion.

This discussion is concerned with the bulk hydrogen at the weld fusion line which is where the implant fractures occur in the high strength steels used in this study. The hydrogen distribution in a weld has been modeled by Coe and Chano (C13). A sample of their distribution

plots is shown in figure 2.15. The effect of time on the hydrogen distribution is determined by the non-dimensional value r . This value is defined as:

$$r = D t / l_0^2 \quad (2.2)$$

where D is the diffusivity, t is time, and l_0 is the bead depth.

As can be seen, hydrogen will become more evenly distributed throughout the weld and HAZ as time progresses. For the welding conditions in the present study, r is about .5 one hour after welding, and about 1.0 twenty-four hours after welding. These values are higher if preheat is used. Figure 2.16 shows the hydrogen concentration at various locations near the weld as a function of r (the fusion line is at $l_0 = .3$).

Therefore, if the implant test specimen is loaded 24 hours after welding, the hydrogen will be uniformly distributed in the weld and HAZ with a concentration of 10 - 20% of the original content in the weld bead. In order to account for errors in the diffusivity data, the ratio of Q/Q_0 can be experimentally determined at various welding conditions (and time after welding) to find the hydrogen concentration at the fusion line for that value of r . In other words, Q/Q_0 can be used to more accurately find the hydrogen concentration than r . If the implant test specimen is loaded shortly after welding, the hydrogen concentration at

the fusion line will vary as the test progresses.

The stress associated with fracture for both of these loading times will be presented in chapter 5. The hydrogen concentration at the fracture zone will be chosen with the aid of the model developed by Coe and Chano.

2.6 RESULT OF WELD PROCESS VARIATIONS ON HYDROGEN CONTENT

Following the conclusion and analysis of the above results, the effect of weld process variations on hydrogen content was studied. It was decided to standardize on the AWS method of diffusible hydrogen analysis, using the Yanaco gas chromatography unit. All of the following data was collected using the 12 X 25 X 80 mm specimen size machined from A36 hot rolled bar stock. The specimens were outgased at 45 C for 72 hours. Most of the specimens were quenched within 3 seconds after weld completion, but some were quenched after 24 hours when the effect of preheat was studied. The Yanaco unit was adjusted so that the correct calibration was obtained with the AWS sized specimen chamber.

2.6.1 EFFECT OF SHIELDING GAS COMPOSITION

Welding parameters were initially chosen to produce a sound weld when welding with a 98% Ar / 2% O₂ shielding gas. The addition of hydro-

gen to the Ar/2%O₂ shielding gas caused arc instability and a slight decrease in arc length. The droplet transfer mode also changed from stable spray to globular (or in some cases to a combination of spray and short circuiting transfer). For a given current and contact tube to work distance, it was found that an increase in voltage would restore the transfer mode to stable spray. This "transition voltage" was different for each gas mixture. The transition voltage also varied with the base material and electrode composition. The weld current could also be varied to restore stable spray transfer, but the weld voltage had a stronger effect on the transfer mode when switching between gases.

In order to eliminate the effect of changing transfer modes from one gas mixture to another, the majority of diffusible hydrogen tests were performed using weld parameters which produced a sound weld with globular transfer. Table 2.5 shows the welding parameters used for all tests unless otherwise noted. The effect of increasing the weld voltage into the spray transfer region will be separately examined in section 2.6.2.

Many of the experiments on the effect of weld shielding gas composition were performed at the U.S. Army Construction Engineering Research Laboratory (CERL). CERL used linear mass flowmeters and "zero standard gases" in order to study a wide variety of gas compositions. These facilities were not available at MTL where all the other welding was performed.

In order to ensure that the CERL results were consistent with the

MTL results, MTL reproduced a number of the critical welds by purchasing premixed certified gas cylinders. Other means of ensuring consistency included shipping material from the same heats of steel (both A36 and 46100) to CERL, and monitoring the welding parameters directly rather than using the readouts on the front of the welding power supplies. The specific procedures and gas compositions studied at CERL are described in detail in appendix 2A. The results are discussed in the main body of this chapter.

The effect of varying the shielding gas hydrogen and oxygen concentration on the diffusible weld hydrogen content is shown in figure 2.17. This figure depicts the amount of weld hydrogen in ml / 100g of deposited metal on the ordinate versus the amount of hydrogen in the shielding gas on the abscissa. Each curve on this figure shows a different amount of oxygen in the three gas mixture. As can be seen, increasing the oxygen content also increases the amount of hydrogen absorbed by the weld (for a given percent hydrogen in the shielding gas and identical welding parameters).

It must be noted, however, that welds made without oxygen had a poor bead appearance. Oxygen is needed to increase arc stability, decrease spatter, promote wetting, and help prevent undercut. Carbon dioxide serves a similar function when added to argon.

The effect of varying the shielding gas hydrogen and carbon dioxide concentration on the diffusible weld hydrogen content is shown in figure

2.18. The results indicate that differences in carbon dioxide content from 2-10% seem to have little effect on the amount of hydrogen absorbed by the weld. The three curves showing carbon dioxide content in figure 2.18 basically overlap once experimental uncertainty is considered.

If no carbon dioxide is added, the amount of hydrogen absorbed is reduced. Once again, however, some amount of carbon dioxide is needed for good arc stability and bead shape.

Figure 2.19 compares the amount of hydrogen absorbed for 2% CO_2 versus 2% O_2 . When no hydrogen is added to the shielding gas, the amount of hydrogen absorbed is about equivalent (or slightly lower for the oxygen). The carbon dioxide is more effective at preventing added amounts of hydrogen from absorbing into the weld pool.

2.6.2 EFFECT OF DROPLET TRANSFER MODE

Regions of droplet transfer mode are mapped on a voltage versus current graph for different electrode extensions in figure 2.20. The regions are also mapped for different gas compositions in figure 2.21.

At low hydrogen concentrations in the shielding gas, increasing the voltage to go from globular to spray transfer has little to no effect on the diffusible hydrogen content. At higher hydrogen concentrations, however, the transfer mode has a pronounced effect. Figure 2.22 shows

the effect of voltage on hydrogen content for welds made with .5% H_2 in the shielding gas. The voltage has little effect on the amount of weld hydrogen until the transition to spray transfer is reached. At this point the amount of hydrogen absorbed increases over 3ppm.

2.6.3 EFFECT OF BASE METAL COMPOSITION

The use of different steel for the diffusible hydrogen specimen, rather than the standard mild carbon (A36) steel, was examined. Four steels were evaluated: a high strength armor steel conforming to MIL-A-46100, a 1018 cold-rolled mild carbon steel, a 1044 hot-rolled carbon steel, and the standard A36 hot-rolled mild carbon steel. The compositions of these steels are tabulated in table 2.6. An analysis of the carbon contents of these steels revealed that the A36 had .16% carbon. The other steels had the same carbon content as is listed in the table. The GMAW electrode composition used is shown in table 2.7.

A wide range of base metal compositions can thus be compared, as well as the difference between hot and cold rolling. The results of diffusible hydrogen content versus percent hydrogen added to the GMAW shielding gas for each material are tabulated in table 2.8.

Figure 2.23 shows how the base metal affects the amount of diffusible hydrogen as a function of hydrogen in argon. The diffusible hydrogen content of high strength steel is consistently 2 to 3 ppm more than the

A36 mild steel. This trend is repeated with 2% oxygen in the shielding gas as is shown in figure 2.24. The fact that welds made with 2% CO_2 absorb less hydrogen than those made with 2% O_2 is also repeated for the high strength steel as is shown in figure 2.25.

2.6.4 EFFECT OF PREHEAT

Preheat is often used to lower the rate of cooling. This increased time at temperature effectively increases the amount of hydrogen which diffuses out of the weld. In the diffusible hydrogen results shown in table 2.9, the specimen was allowed to cool in air for 24 hours rather than quenching immediately after welding. As can be seen, preheat lowers the amount of hydrogen remaining in the weld. The numerical results of this set of experiments are later used in studying the effect of preheat on hydrogen cracking during an implant test.

2.7 DISCUSSION OF THE EFFECT OF WELD PROCESS VARIATIONS ON THE DIFFUSIBLE HYDROGEN CONTENT

2.7.1 EFFECT OF SHIELDING GAS COMPOSITION

All of the results in figures 2.17 through 2.19 are presented in terms of hydrogen absorbed (in ml H_2 /100g deposited) as a function of percent hydrogen added to the shielding gas. In this way the "effective-

ness" of preventing hydrogen absorption for each gas mixture can be assessed. This effectiveness does not necessarily imply that one gas mixture is better than another. Other important considerations such as amount of spatter, arc stability, oxidizing tendency, penetration, and fluidity and shape of the weld bead also need to be assessed to determine which gas composition is the "best".

The composition of the welding electrode and base metal also strongly influences which gas composition would be the best for a particular application. An example of this interdependence is that when welding with a very oxidizing gas to obtain short circuiting transfer for out-of-position welding, the electrode must have extra silicon or other deoxidizers in order to prevent degradation of the mechanical strength of the weld.

A thorough review of the interdependence of the gas, electrode, and base plate composition is beyond the scope of this research effort. However, one must be aware of the limitations of the ensuing discussion when attempting to adapt the present results for a different set of electrode/base metal. The following discussion will be primarily concerned with the use of a Linde 95X .045" GMAW electrode to weld MIL-A-46100 high strength steel. These compositions were listed in tables 2.6 and 2.7.

Increasing the oxygen content of the shielding gas increases the amount of hydrogen absorbed into the weld pool. This trend applies when welding either A36 or 46100. The trends for the hydrogen content of the

weld as a function of shielding gas hydrogen are all repeated if the diffusible hydrogen results are replotted in terms of ml/100g fused instead of deposited metal. For consistency and brevity, all the discussions in this chapter will be in terms of deposited metal.

From figure 2.19, Ar/2% CO₂ will result in less hydrogen absorption than Ar/2% O₂. This becomes an important consideration if high amounts of hydrogen are anticipated. In a fabrication environment, spools of electrode wire are often left for long times to pick up moisture, rust, dirt, and oil. This hydrogen contamination will be less dangerous if a shielding gas containing 2-10% CO₂ is used. Bead appearance and spatter are about the same whether oxygen or carbon dioxide is added to the argon shielding gas.

Before one could make a final choice between the two gas compositions, however, the mechanical properties associated with each may need to be determined. The effect of increasing the carbon content of the weld deposit when using Ar/2-10% CO₂ may alter the choice of electrode to one containing less carbon. Thus, even though this research has shown the promise of using Ar/2-10% CO₂ over Ar/2% O₂, the ultimate choice of which gas to use may be influenced by other factors as well.

Welding with pure argon will result in little absorbed hydrogen, but as was mentioned, poor bead appearance, low puddle fluidity, and undercutting, make this an unattractive choice of shielding gas for most steel welding applications.

The effect of oxygen and carbon dioxide on the absorbed hydrogen content will be theoretically studied with the aid of newly developed Fe-H-O and Fe-C-H-O phase diagrams in chapter 4.

2.7.2 EFFECT OF DROPLET TRANSFER MODE

Figure 2.22 shows that the voltage will primarily affect the weld hydrogen concentration by altering the droplet transfer mode. Spray transfer is often desired in welding applications because of superior bead shape, smooth operation, and decreased spatter. If hydrogen cracking is a potential problem, however, this research shows that globular transfer may be desired instead of spray. At low hydrogen concentrations, the transfer mode has little effect on weld hydrogen.

The primary reason for studying this phenomenon in the present research was for the purpose of choosing a set of welding parameters which could be used to study the effect of shielding gas composition on the amount of absorbed hydrogen. It has been shown that the effect of metal transfer will vary with the amount of hydrogen. It has also been shown that the amount of hydrogen will alter the transition voltage and current. In order to eliminate these effects, a set of welding parameters was chosen so that the mode of metal transfer was consistently globular. The lower voltages in globular transfer may also decrease the effect of humidity on the resulting diffusible hydrogen content as was shown by Quintana (Q4).

The specific reason for increased hydrogen absorption when welding with spray transfer is unknown at the present time. It may be that the increased ratio of surface area to volume in spray transfer allows more hydrogen to be absorbed onto the droplet surface during its traverse across the arc. This should be an interesting area for future research.

2.7.3 EFFECT OF BASE METAL COMPOSITION

The experimental findings in table 2.8 show that the use of a different material than the standard mild carbon steel test specimen results in a different value of diffusible hydrogen.

The high strength steel diffusible hydrogen content was about 2-4 ppm higher than the mild steel hydrogen content. By examining the effect of alloying elements on the solubility of hydrogen in steel (as was performed in the first chapter), one can determine that the extra alloying elements in this steel result in a .7ppm reduction in the solubility compared to mild steel. This will not cause a 2 ppm increase.

Figure 2.26 plots the diffusible hydrogen content versus the (analyzed) carbon content in the steels for various levels of percent hydrogen added to the shielding gas. As can be seen, increasing the carbon content increases the amount of diffusible hydrogen. This experimental result is contrary to the fact that carbon reduces the solubility of hydrogen. This may be because increasing carbon content will

decrease the oxygen partial pressure which has been shown to decrease the amount of absorbed hydrogen.

The effect of carbon content on hydrogen absorption will be further examined in the analysis presented in chapter 4, where Fe-C-H-O phase equilibria will be studied.

2.7.4 EFFECT OF PREHEAT

This experimental section is primarily performed in order to provide data required for the hydrogen assisted cracking discussion in chapter 5. In chapter 5 the implant fracture strength and fracture mechanics will be used to assess the various proposed mechanisms of hydrogen cracking.

The hydrogen distribution model developed by Coe and Chano (C13) can be used to determine the amount of hydrogen present in the fracture zone. The preheat data in table 2.9 can be used to determine Q/Q_0 . This value will then be used to find the r associated with that preheat from figure 2.16. The hydrogen concentration in the fusion zone at that r can then also be determined from figure 2.16.

2.8 CONCLUSIONS

1) Variations in the IIW diffusible hydrogen method were studied to determine the accuracy and reproducibility of this test. Results show that:

a) The specimen size should be increased to 15mm X 30mm X 80mm. This is in conformance with the results found by Terasaki and AWS A4.3-86.

b) While the gas chromatography method can be more accurate and reproducible than other methods of measurement, it must be properly calibrated and operated or the results will be erroneous.

c) Variations in the carbon content of the specimen will result in different diffusible hydrogen contents.

d) Variations in the time to quench after welding will affect the reproducibility of the diffusible hydrogen results.

e) Standardizing on one specified outgassing temperature should be considered.

2) Gas Metal Arc Welding process variations were studied to determine the effect on the diffusible hydrogen content. Results show that:

a) Welds made with argon / 2 - 10% CO₂ shielding gas will absorb less hydrogen than welds made with argon / 2% O₂.

b) Increasing the oxygen content of the weld shielding gas will result in increased amounts of hydrogen absorbed by the weld.

c) Welds made with spray transfer absorb more hydrogen than welds made with globular transfer. This effect is not as strong at very low hydrogen levels.

3) The amount of hydrogen initially absorbed into the molten weld pool can be found by determining the amount of diffusible hydrogen per 100 grams of fused weld metal, and then converting this value into origi-

nally absorbed hydrogen by using a relationship derived by Terasaki. For this study, the amount of hydrogen remaining in the diffusible hydrogen specimen was found to be about 70% of the amount originally absorbed.

4) The hydrogen concentration in the cracking zone can be approximated by using the hydrogen distribution model developed by Coe and Chano. These values will be more uniform if the implant specimen is not loaded until 24 hours after welding.

TABLE 2.1

	BYPASS	CHAMBER #1 (empty)	CHAMBER #2 (w/specimen)
VALUES	1.96	1.87	1.93
	1.96	1.85	1.94
	1.96	1.83	1.91
	1.95	1.83	1.90
	1.95	1.86	1.90
	1.94	1.84	1.88
	1.97	1.85	1.90
	1.91	1.83	1.88
	1.95	1.83	1.90
MEAN	1.950	1.843	1.904
STANDARD DEVIATION	.017	.015	.020

TABLE 2.2

Effect of Surface Condition of Measured Diffusible Hydrogen

(Results shown are for Ar/.1% H₂/2% O₂ on A36, AWS Specimen)

	As - Received (ml H ₂ /100g Deposited)	Machined (ml H ₂ /100g Deposited)
	3.56	4.41
	2.71	4.04
	3.11	3.78
	3.39	4.28
	3.72	4.78
	4.62	4.44
	3.16	5.08
	3.29	3.85
MEAN	3.45	4.33
STANDARD DEVIATION	.56	.45

TABLE 2.3
Tabulated Values of Diffusible Hydrogen
Remaining in AWS Specimen After 24 Hours

<u>% H₂</u>	<u>% O₂</u>	<u>ml H₂/100g Deposited Metal</u>
0	2	.74
.01	2	1.09
.1	2	1.23
.5	2	1.96
.5	1	1.80
2	1	2.19

TABLE 2.4

Temperature where maximum hydrogen release occurs
for various trapping sites (Ref. L.4)

classification of trapping site		heating rate (°C/min)	peak temp. (°C)
grainboundary (pure iron)		3.88	118
F-C interface (0.49% C steel)		2.6	129
F-C interface (AISI 4340 steel)		3.4	115
dislocation (pure iron)		3.88	253
dislocation (0.49% C steel)		2.6	205
dislocation (AISI 4340 steel)		3.4	272
microvoid (pure iron)		3.88	311
microvoid (0.49% C steel)		2.6	-
microvoid (AISI 4340 steel)		3.4	338
405 °C peak (pure iron)		3.88	-
405 °C peak (0.49% C steel)		2.6	387
405 °C peak (AISI 4340 steel)		3.4	405
MnS interface (pure iron)		3.88	-
MnS interface (0.49% C steel)		2.6	-
MnS interface (AISI 4340 steel)		3.4	495

TABLE 2.5

Welding Parameters Used Throughout
This Study Unless Otherwise Stated

<u>Process</u>	<u>GMAW</u>
Voltage	25 Volts
Current	220 Amps
Travel Speed	20 in/min.
Wire Feed Rate	295 in/min.
Contact Tip-to-Work	3/4"
Preheat	75°F
Electrode Diameter	.045"
Polarity	DCRP
Gas Flow Rate	60 c f h

TABLE 2.6

Composition of the Steels Used in This Study

	C	Si	Mn	Cu	P	Ni	S	Al	Cr	Mo
A36	.29 MAX	---	.60-.90	---	.04 MAX	---	.05 MAX	---	---	---
1018	.15-.20	---	.60-.90	---	---	---	---	---	---	---
1044	.43-.50	---	.30-.60	---	---	---	---	---	---	---
MIL-A-46100	.31	.41	.97	.38	.011	1.21	.008	.044	.51	.50

TABLE 2.7

GMAW Electrode Composition

Type	C	Mn	Si	S	P	Mo	Ni	Cr
Linde 82 (ER-70S-3)	.10	1.05	.60	.020	.012	---	---	---
LINDE 95 (ER-100S-1)	.06	1.65	.35	.020	.007	.35	1.75	.10

TABLE 2.8

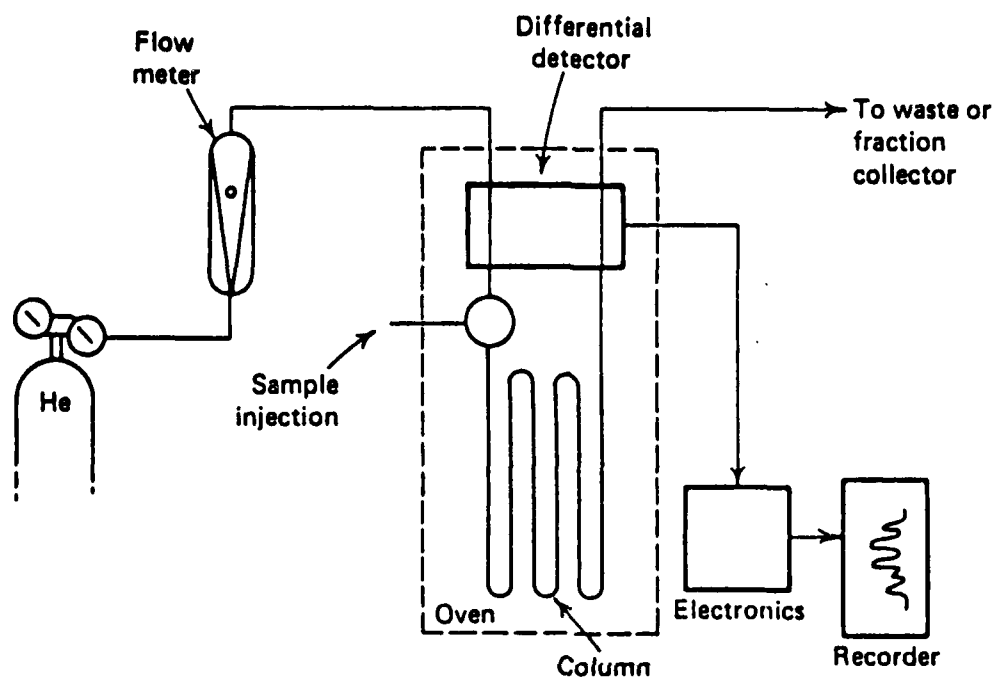
Diffusible Hydrogen Content
Determined on Different Steels

Material	%H ₂	%O ₂	Diffusible Hydrogen (ml H ₂ /100g Deposited)
1018	0	2	3.38
A36	0	2	2.14
1044	0	2	2.76
46100	0	2	2.93
1018	.1	2	4.65
A36	.1	2	4.52
1044	.1	2	5.73
46100	.1	2	5.19
1018	.5	2	8.98
A36	.5	2	8.28
1044	.5	2	--
46100	.5	2	12.0
1018	2	2	--
A36	2	2	14.2
1044	2	2	9.58
46100	2	2	18.0

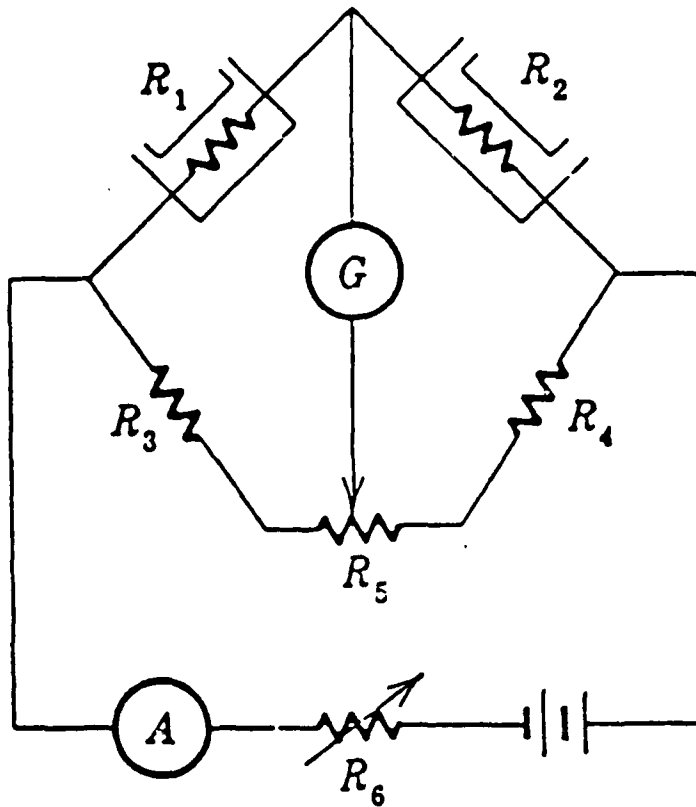
TABLE 2.9

Tabulated Values of Diffusible Hydrogen
Remaining in AWS Specimen After 24 Hours
as a Function of Preheat

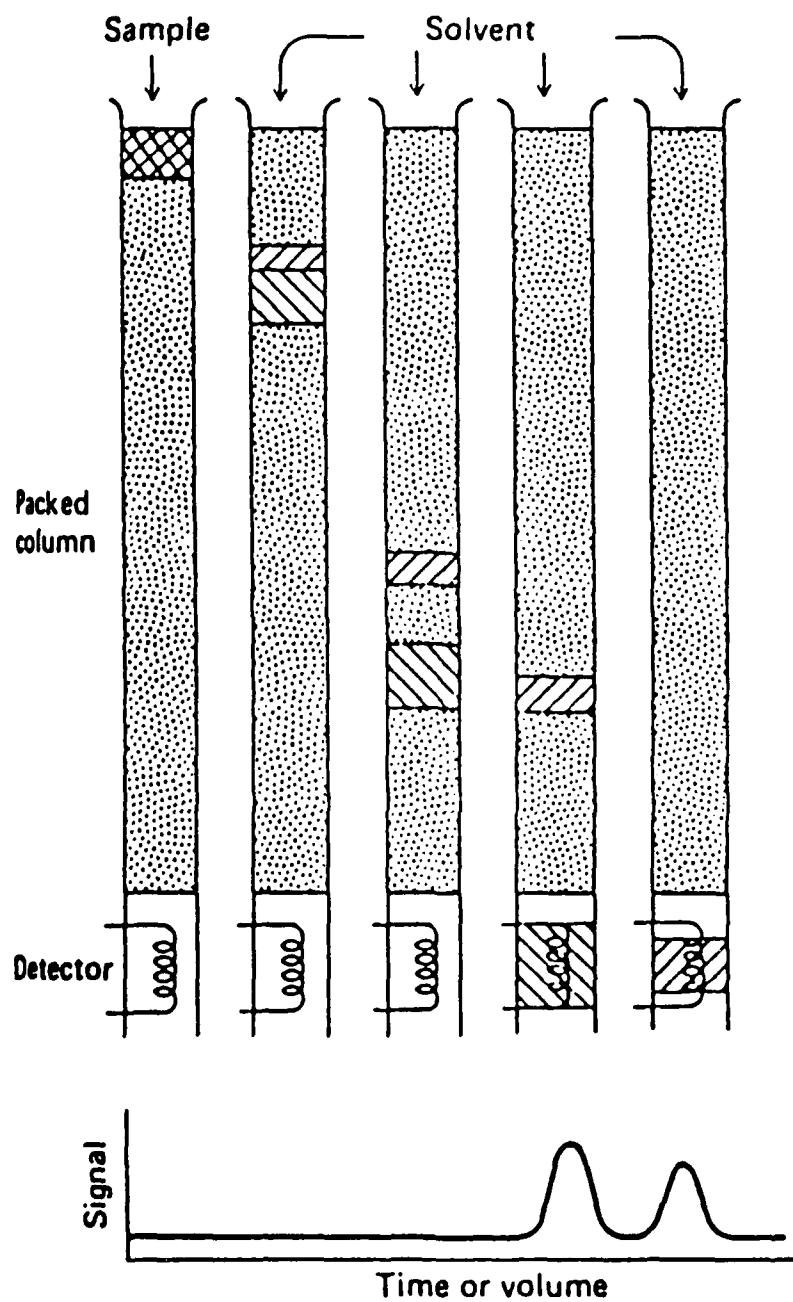
$\% \text{H}_2$	$\% \text{O}_2$	No Preheat	250°F Preheat
0	2	.74	.22
.01	2	1.09	---
.1	2	1.23	.42
.5	2	1.96	---
.5	1	1.80	1.58
2	1	2.19	1.31



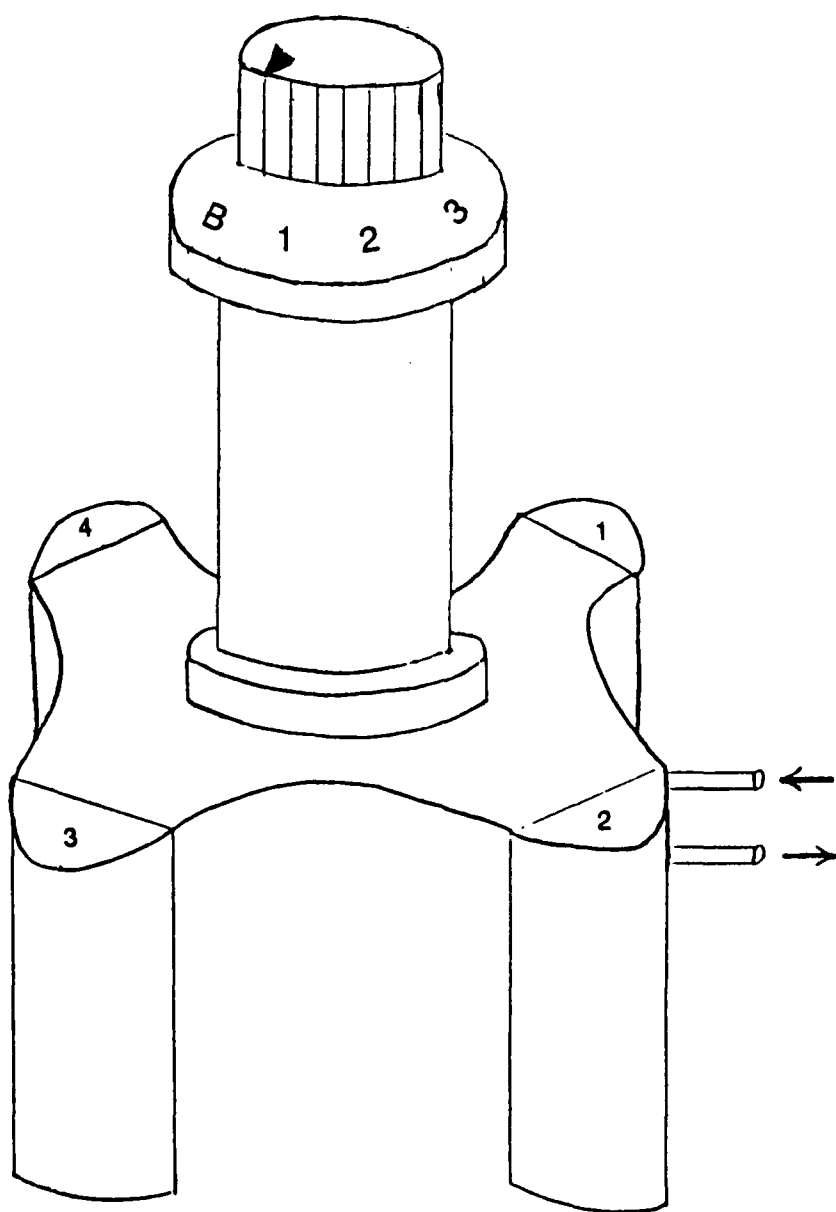
2.1 Schematic of a typical Gas Chromatograph (Ref E.11)



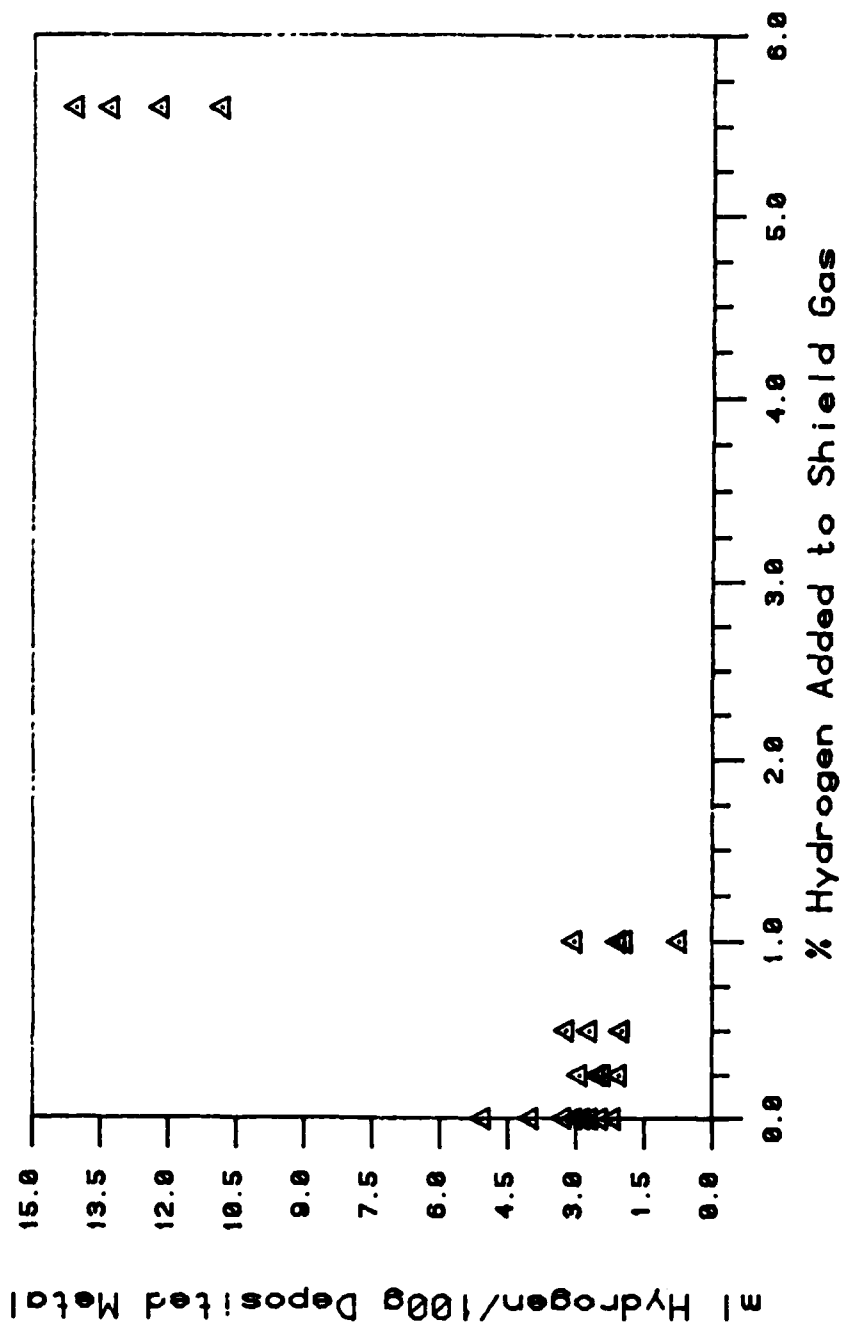
2.2 Electrical circuit of a thermal conductivity detector. R_1 and R_2 are temperature sensitive elements, R_3 and R_4 are ratio arms, R_5 is a zero adjustment, and R_6 is a current limiter. In practise the galvanometer G is replaced by a voltmeter. (Ref E.11)



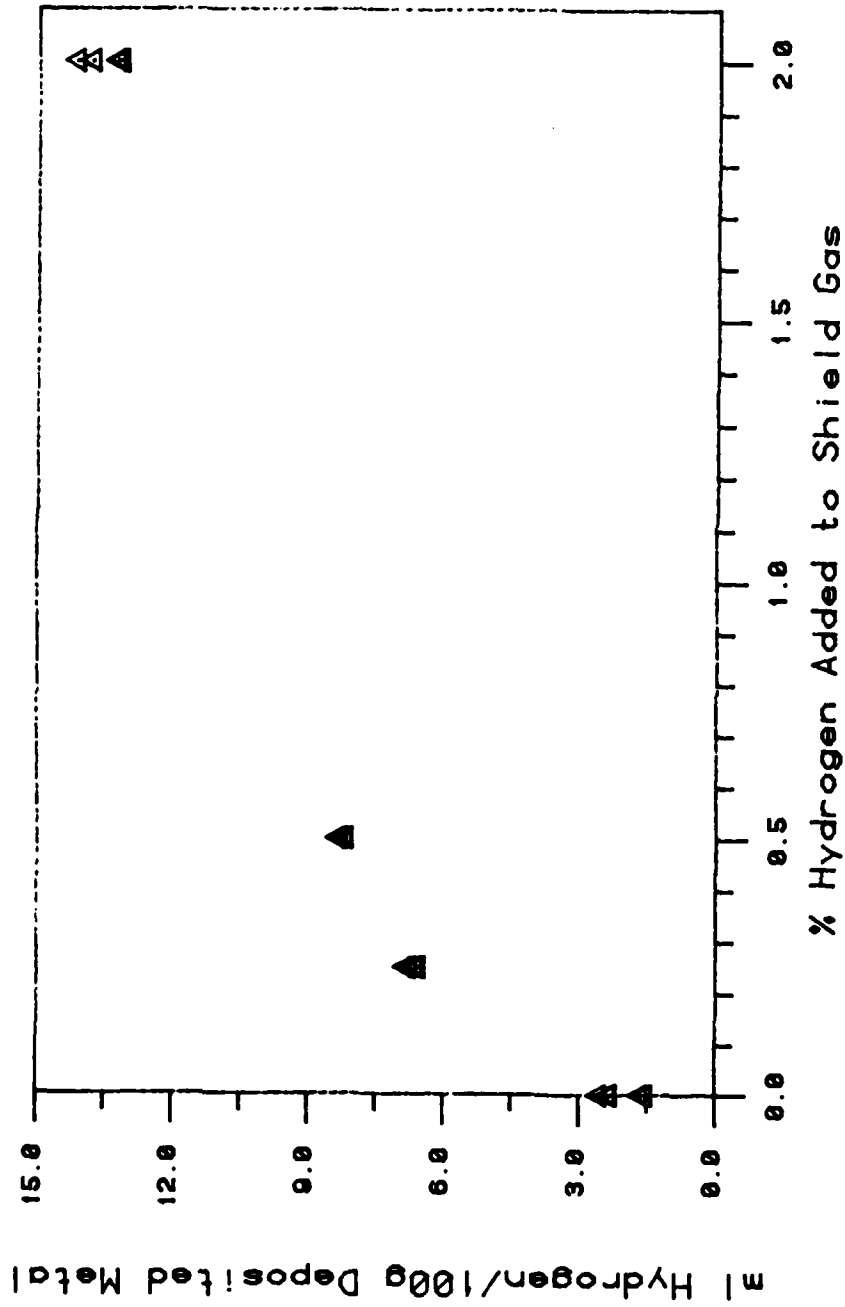
2.3 Schematic of an elution chromatographic separation of a two-component mixture. (Ref S.22)



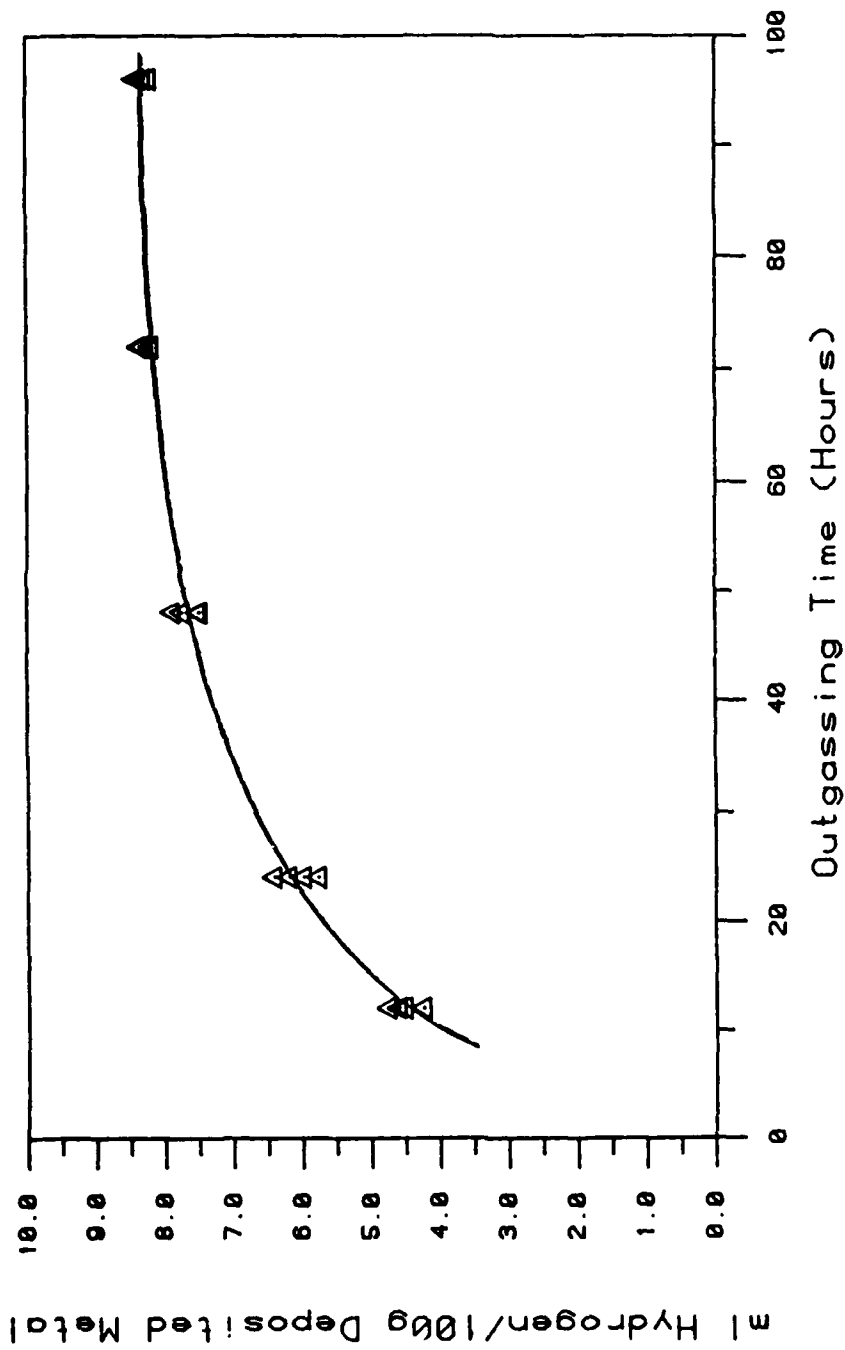
2.4 Diagram of the specimen holding chamber for the Yanaco gas chromatography unit.



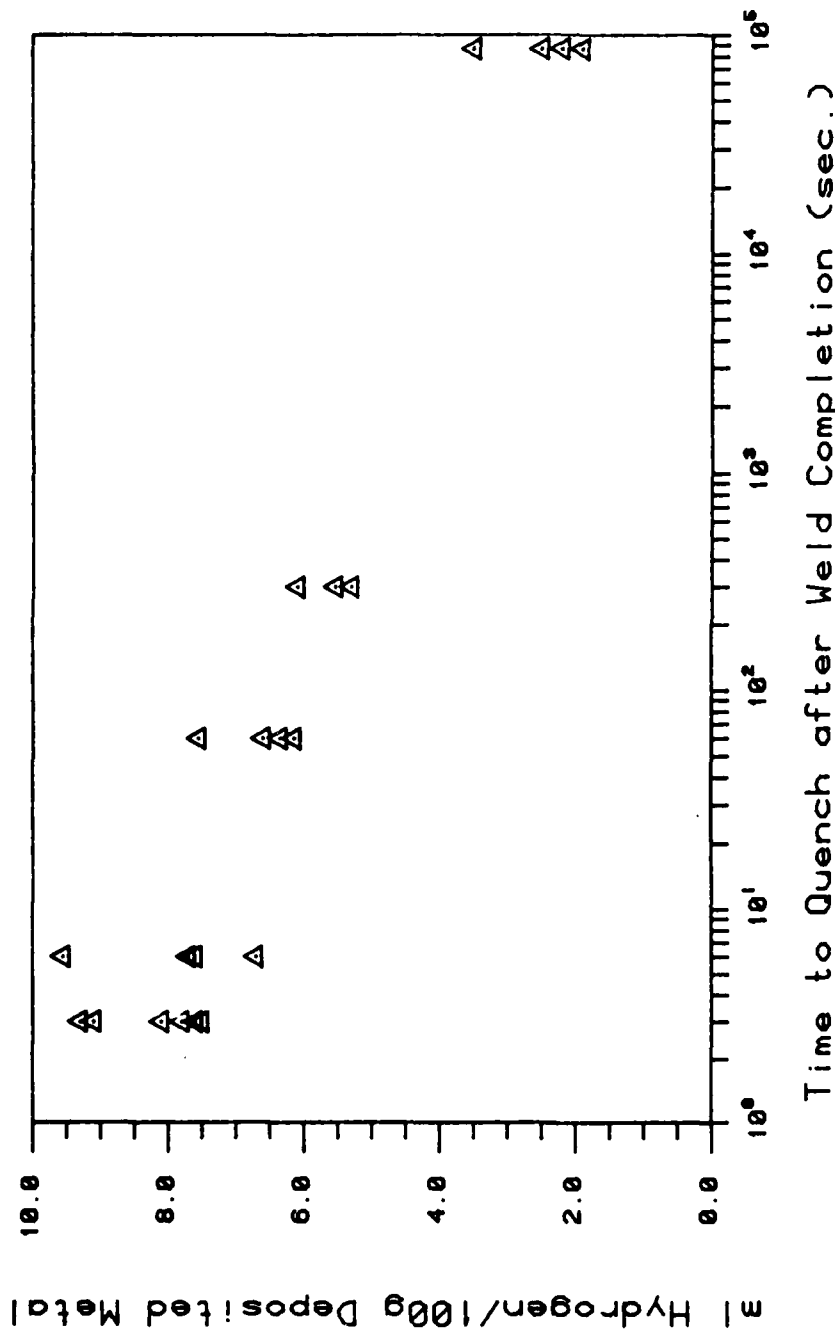
2.5 Diffusible hydrogen in an IW size specimen as a function of percent hydrogen added to Ar/2%₂ shielding gas.



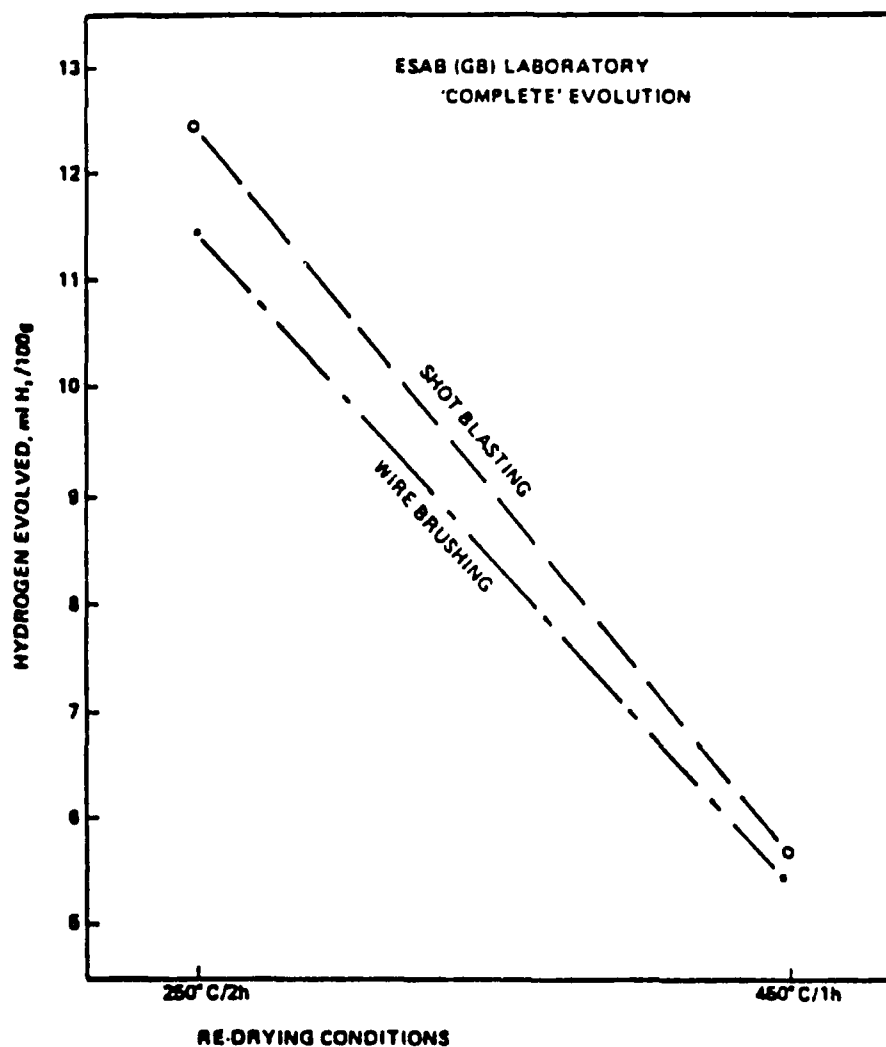
2.6 Diffusible hydrogen in an AWS size specimen as a function of percent hydrogen added to Ar/25O₂ shielding gas.



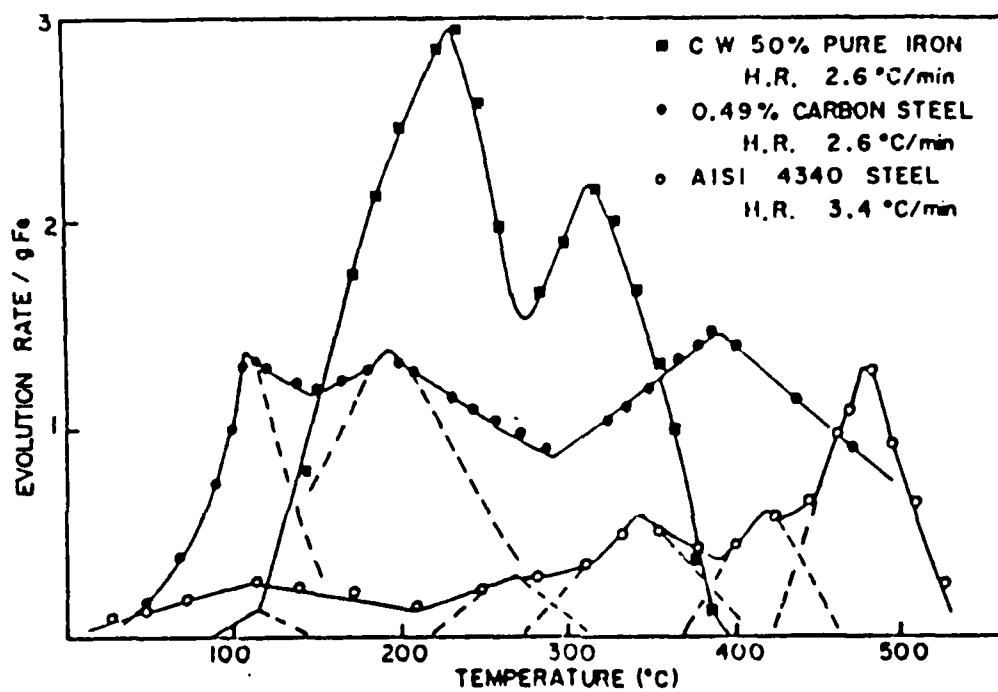
2.7 Diffusible hydrogen measurement versus time for an outgassing temperature of 45 C. (A36, AWS, Ar/.5%H₂/2%O₂)



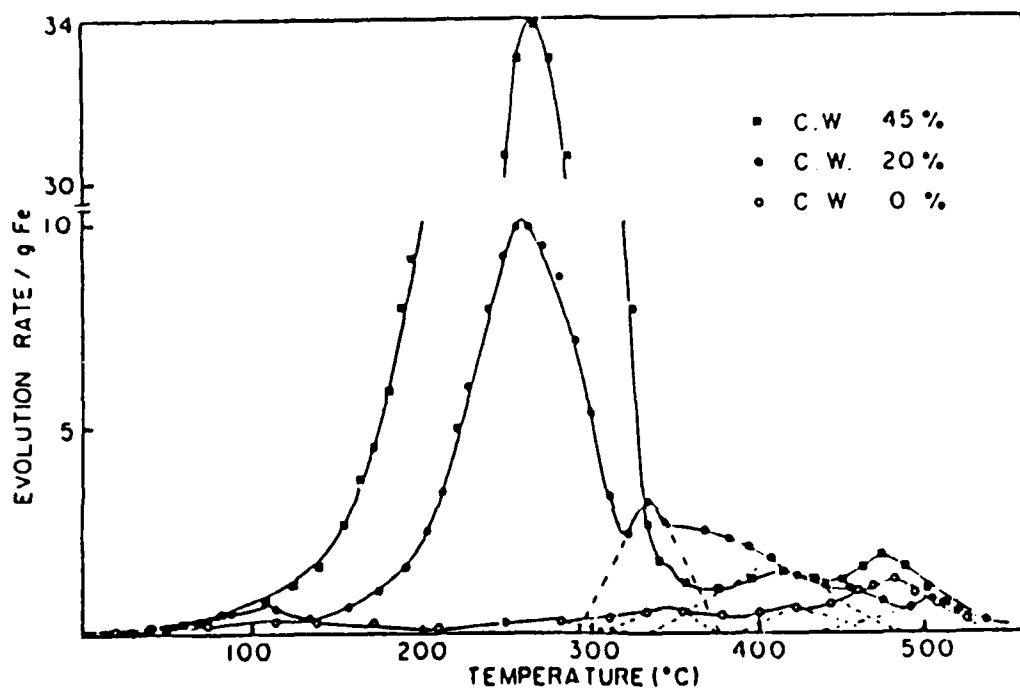
2.8 Effect of the delay between weld completion and quench on the measured hydrogen content. (A36, AWS, Ar/1%O₂/2%H₂)



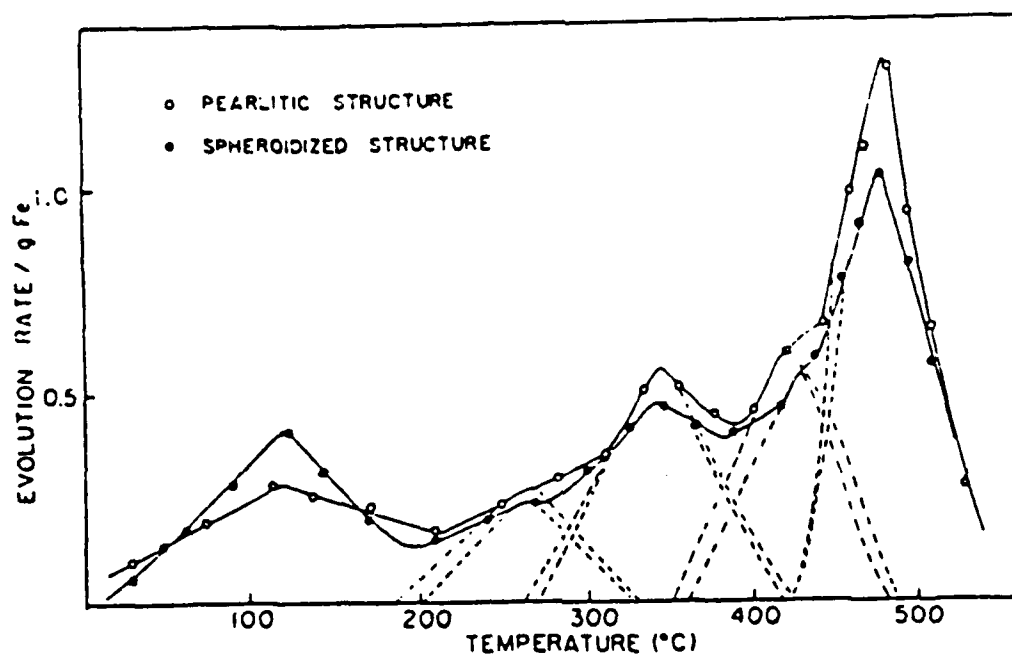
2.9 Average diffusible hydrogen content after "complete" evolution as a function of sample cleaning method and electrode re-drying conditions. (Ref. B.18)



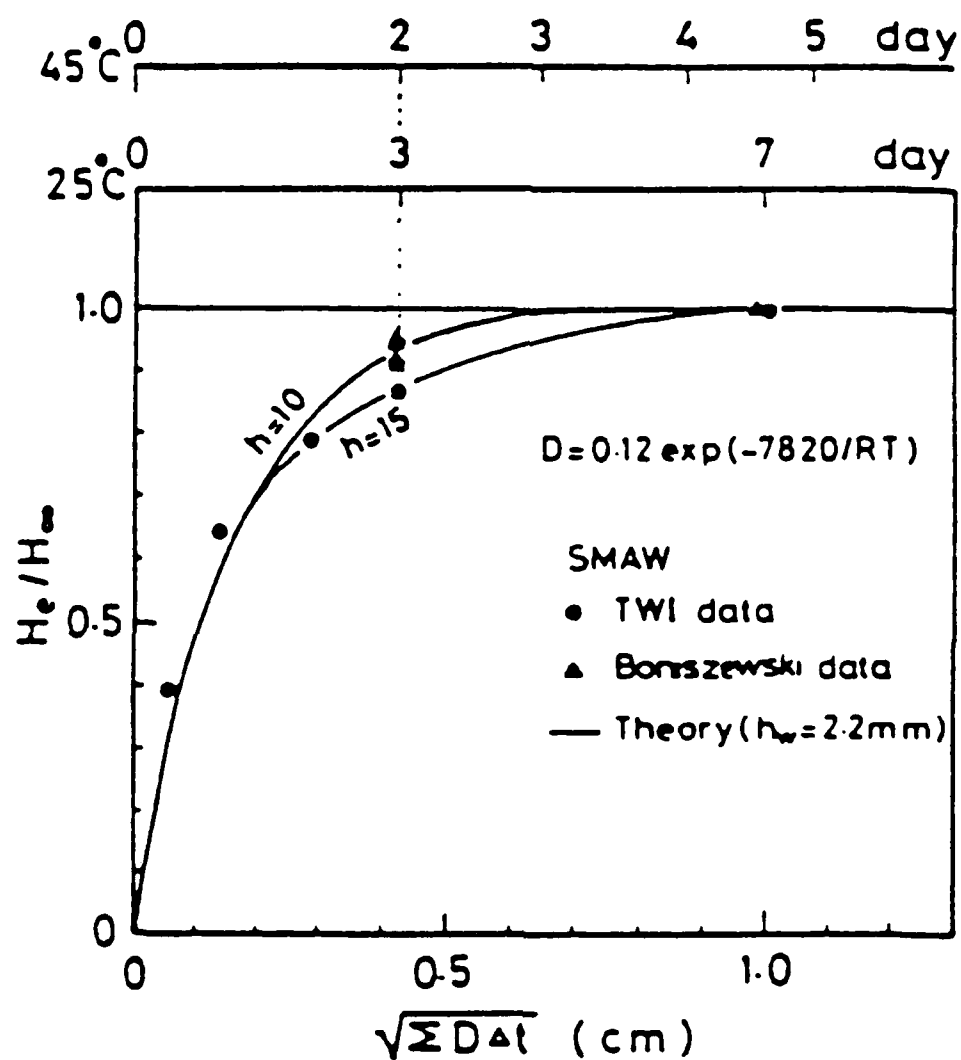
2.10 Thermal analysis peaks of hydrogen in pure iron, 0.49% carbon steel, and AISI 4340 steel furnace cooled at 850 C. (Ref. L.4)



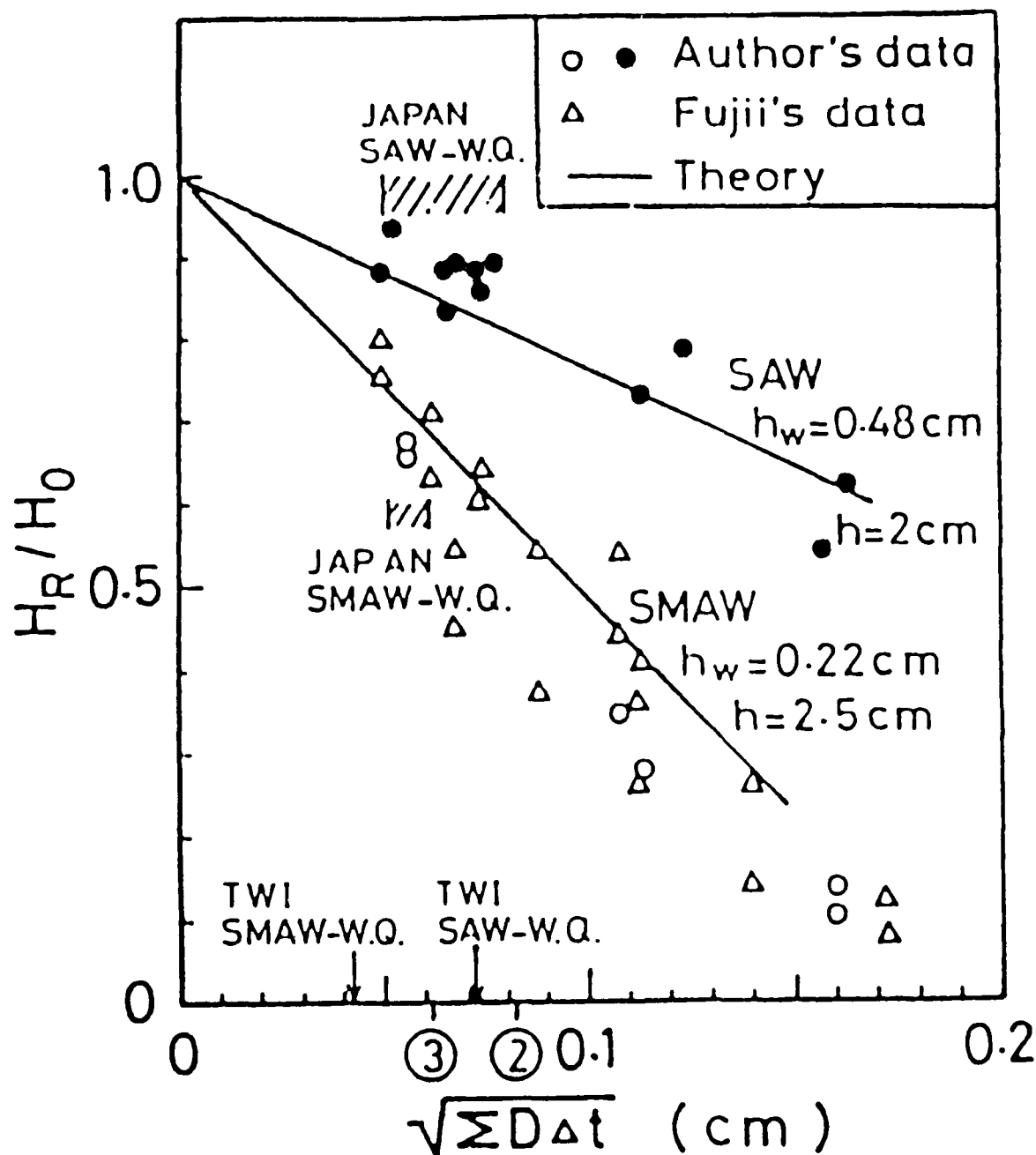
2.11 Dependence of the hydrogen peak height as a function of the amount of cold work. (Ref. L.4)



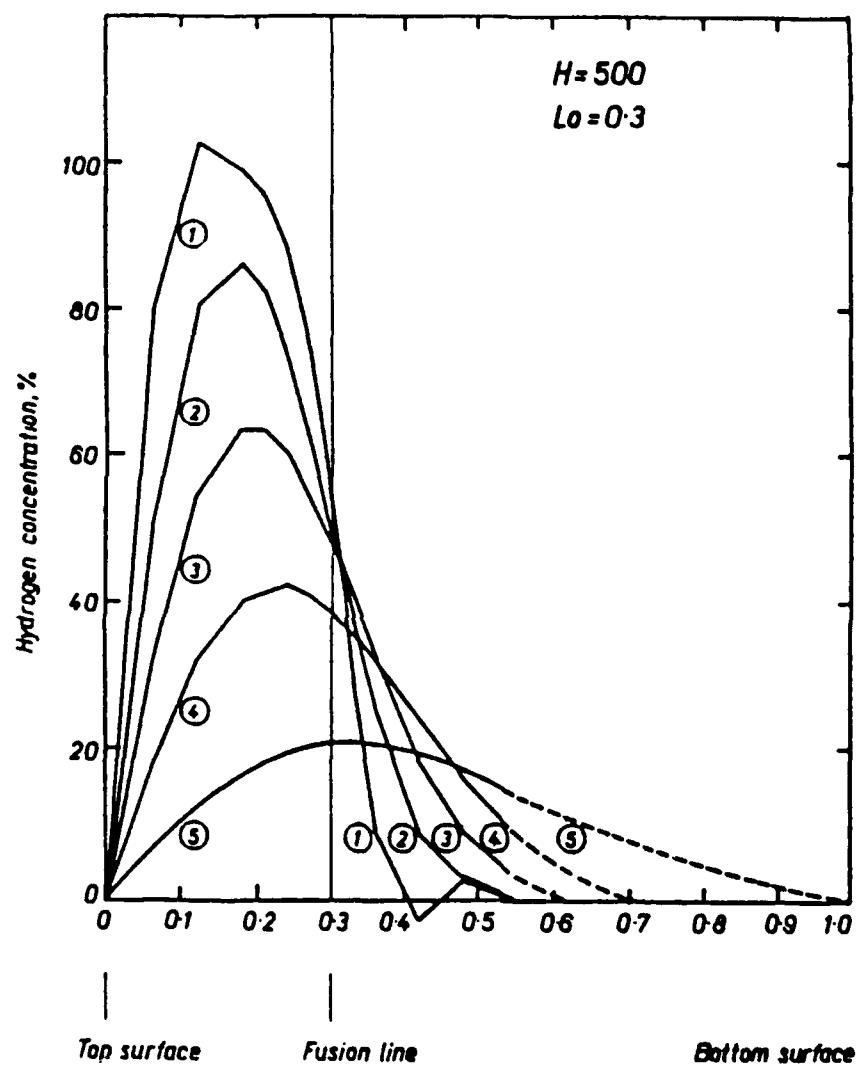
2.12 Dependence of the hydrogen peak height as a function of the amount of ferrite-carbide interface. (Ref. L.4)



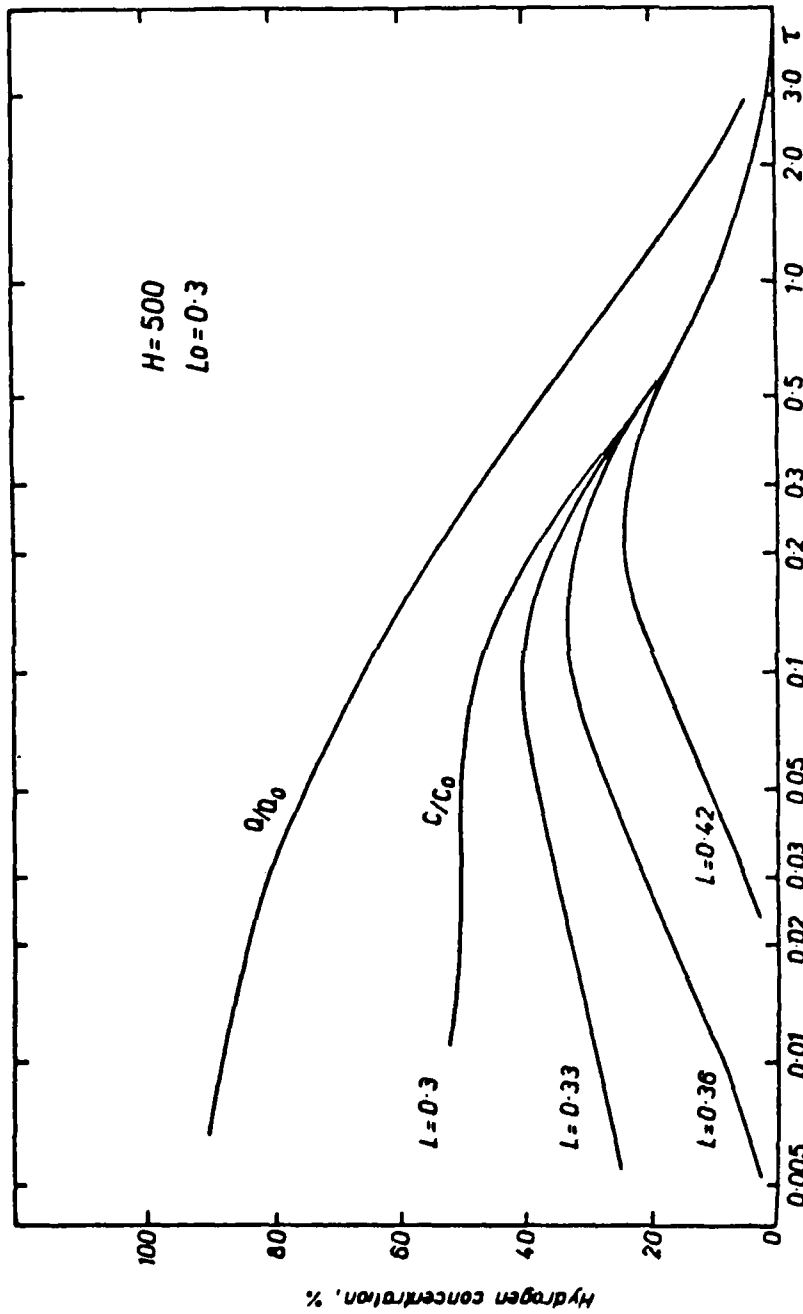
2.13 Comparison between experimental and theoretical hydrogen evolution curve. (Ref T.2)



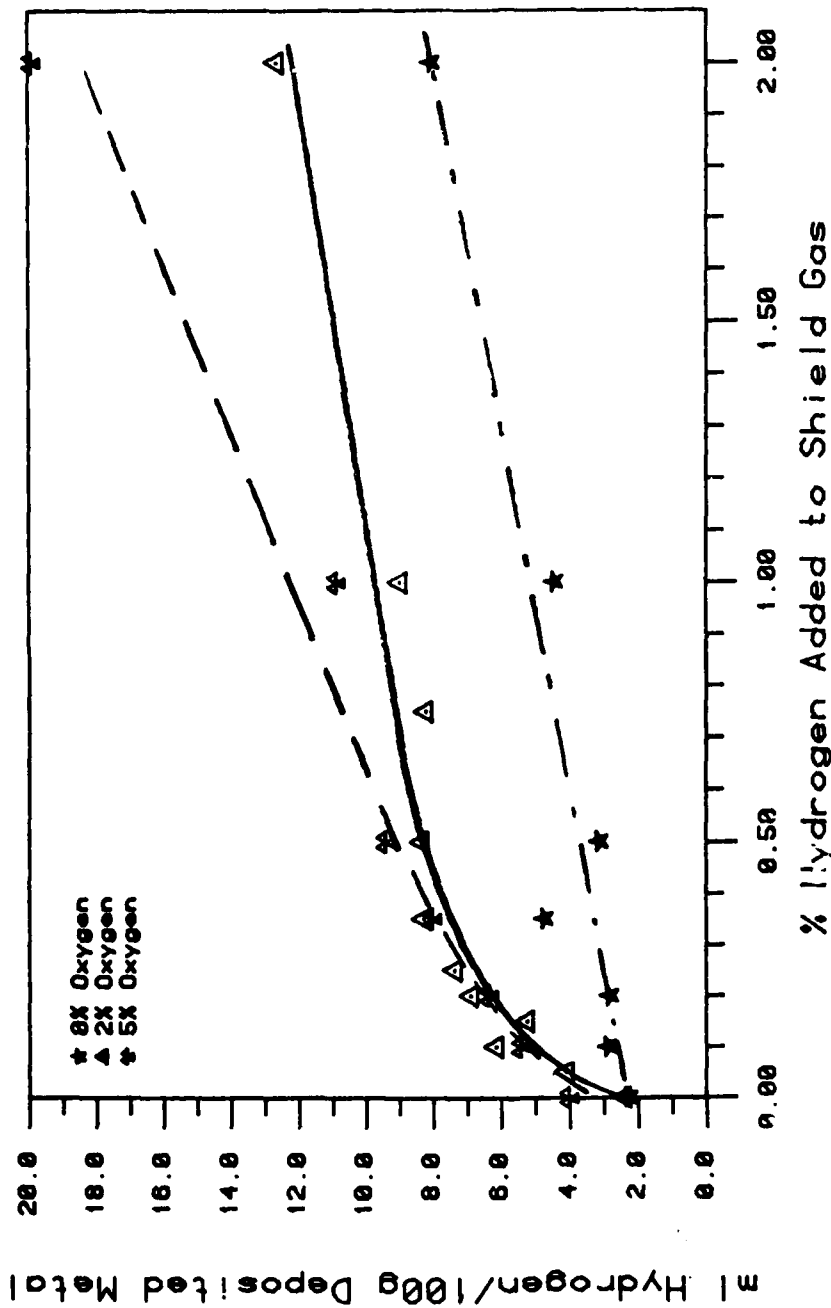
2.14 Comparison between experimental and theoretical results of retained diffusible hydrogen content. H_R/H_0 is the ratio of retained hydrogen to originally absorbed hydrogen. h_w is the bead width, and h is the specimen thickness used in the theoretical calculation. (Ref T.4)



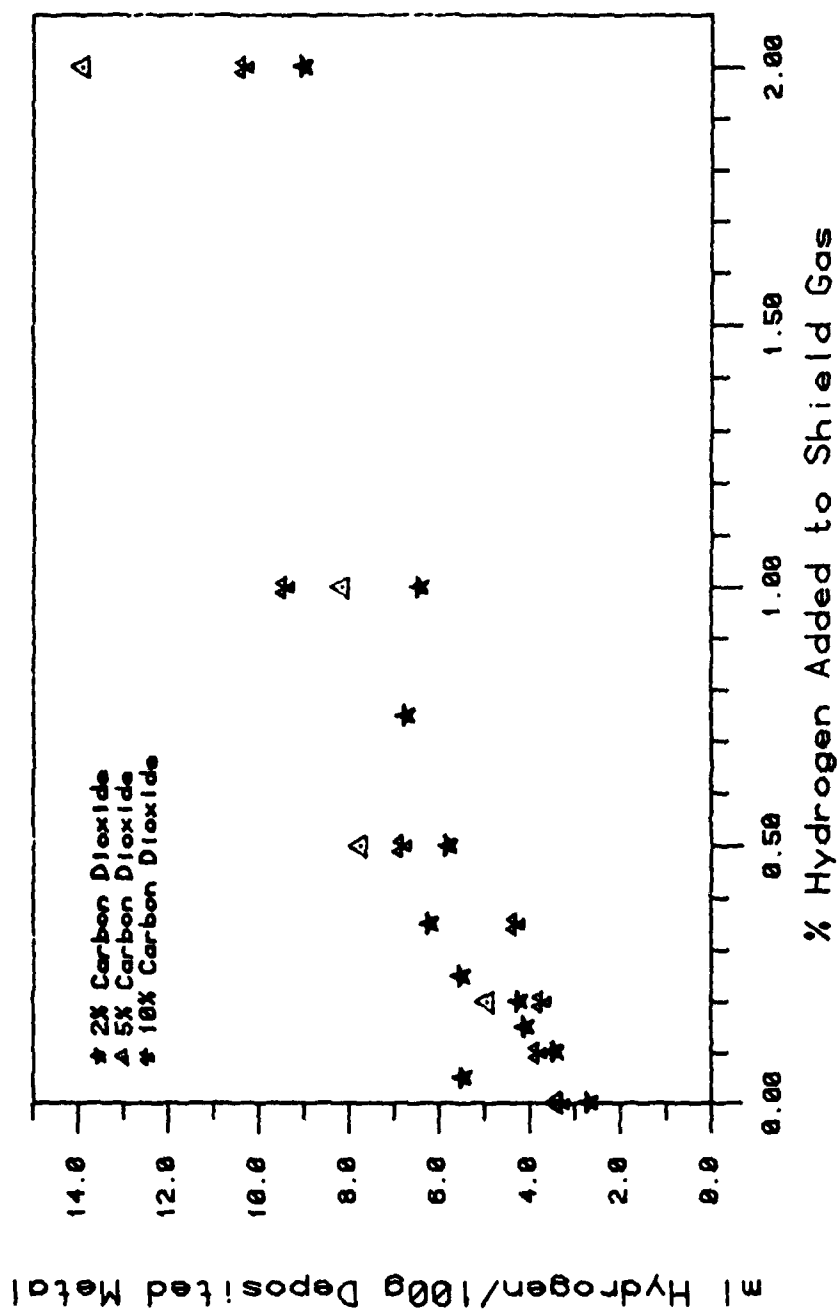
2.15 Hydrogen distribution as a function of distance in the weld for $\tau = 0.011, 0.044, 0.10, 0.20$, and 0.50 . (Ref. C.13)



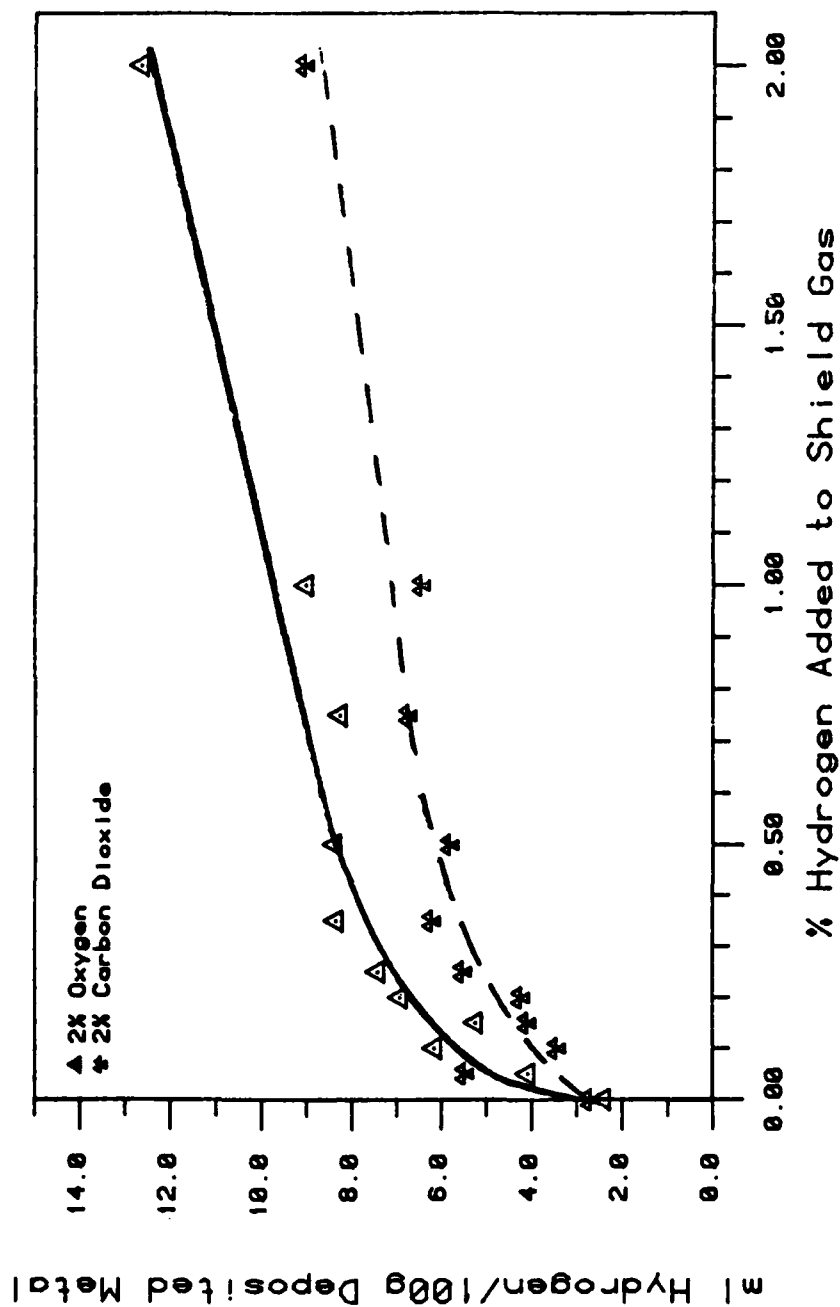
2.16 Hydrogen concentration as a function of τ for different locations in the weld. C_0 is the amount of hydrogen initially in the weld, and Q is the total amount in the weld region.



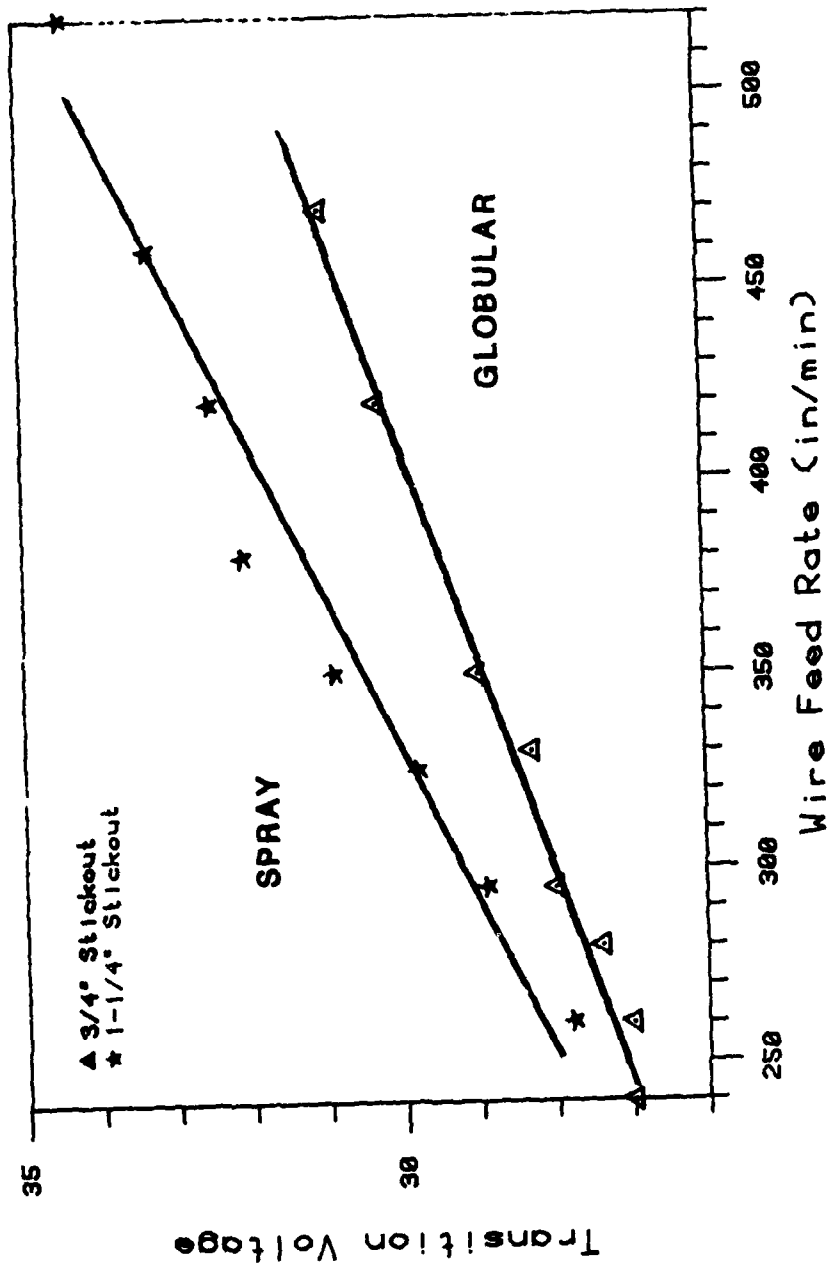
2.17 Diffusible hydrogen as a function of hydrogen in the GMAW shielding gas. Curves depict Ar with 0%, 2%, and 5% Oxygen. (A35, AWS)



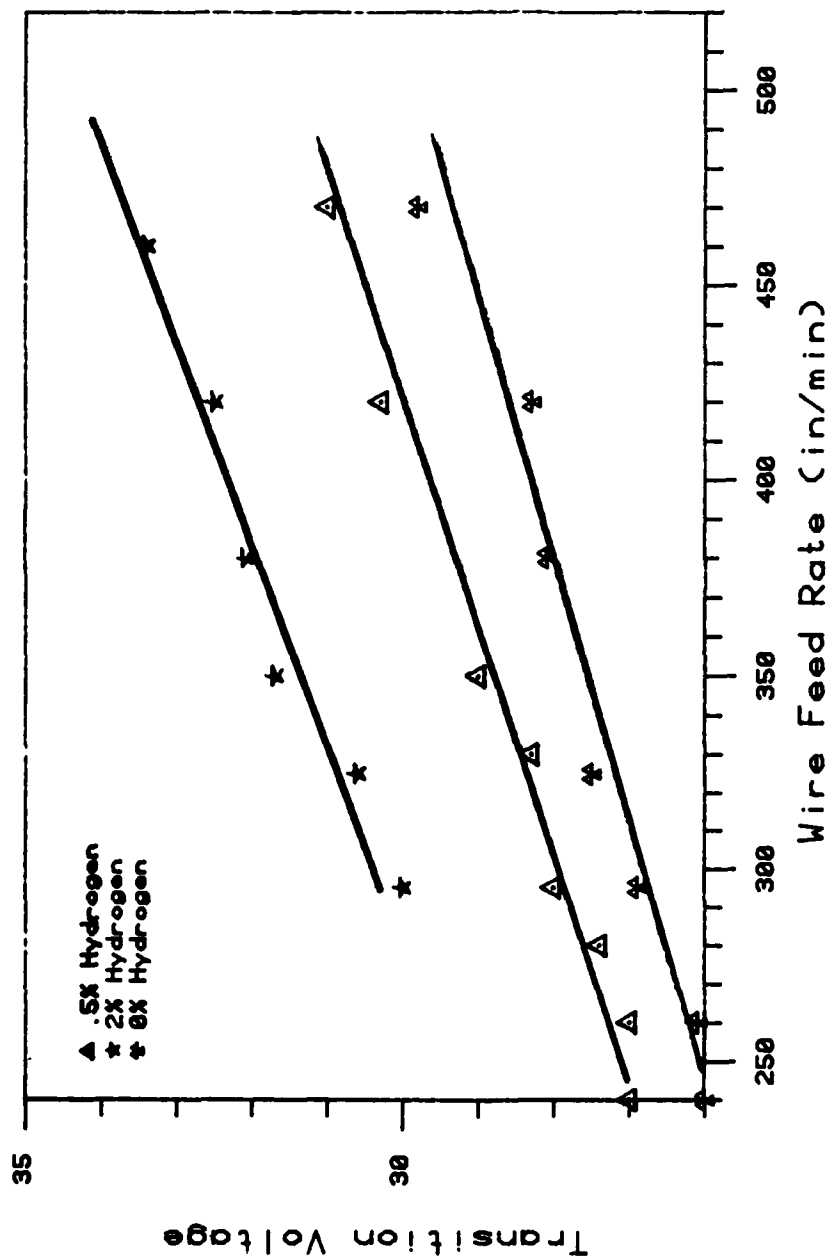
2.18 Diffusible hydrogen as a function of percent hydrogen in a shielding gas with different amounts of carbon dioxide in argon. (A36, AWS)



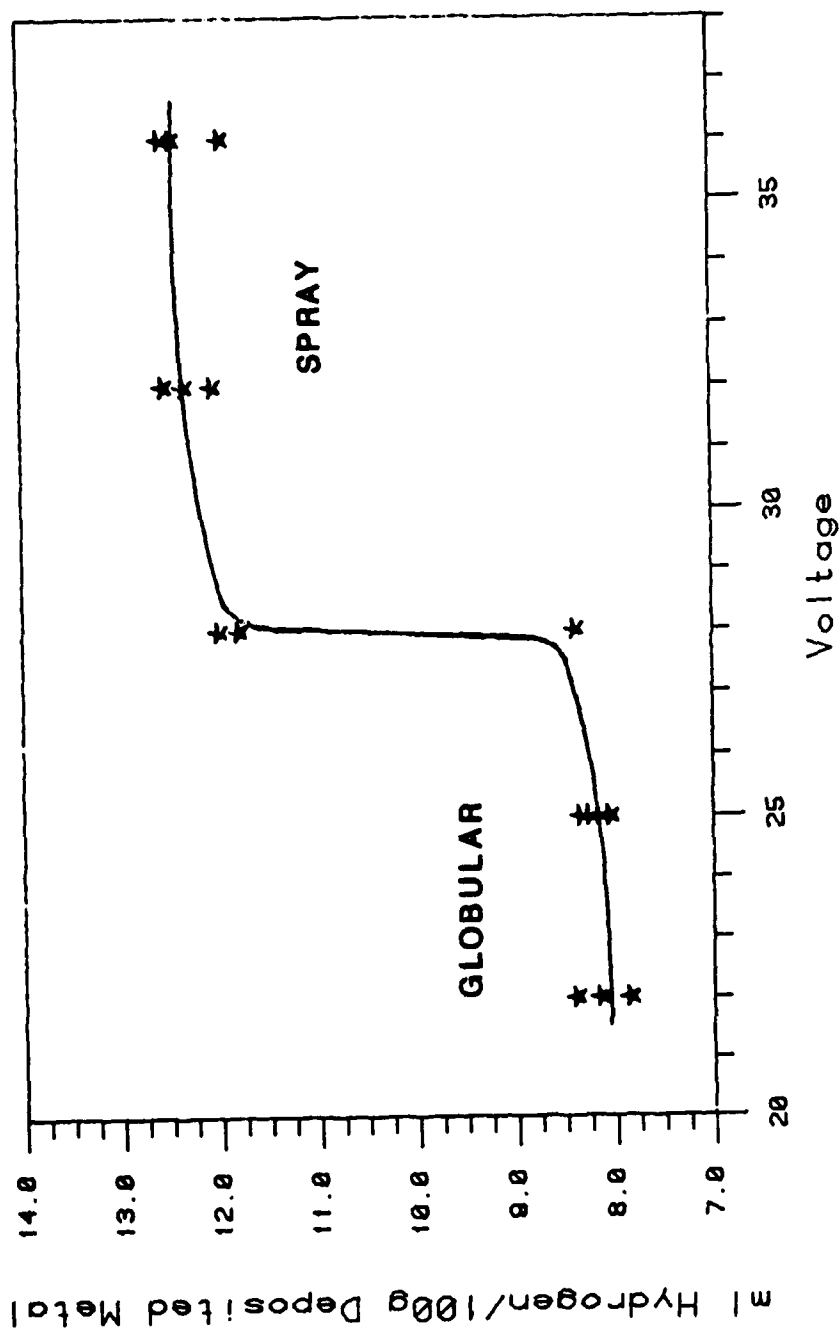
2.19 Comparison of the effect of 2% oxygen and 2% carbon dioxide in the shielding gas. (A36, AWS)



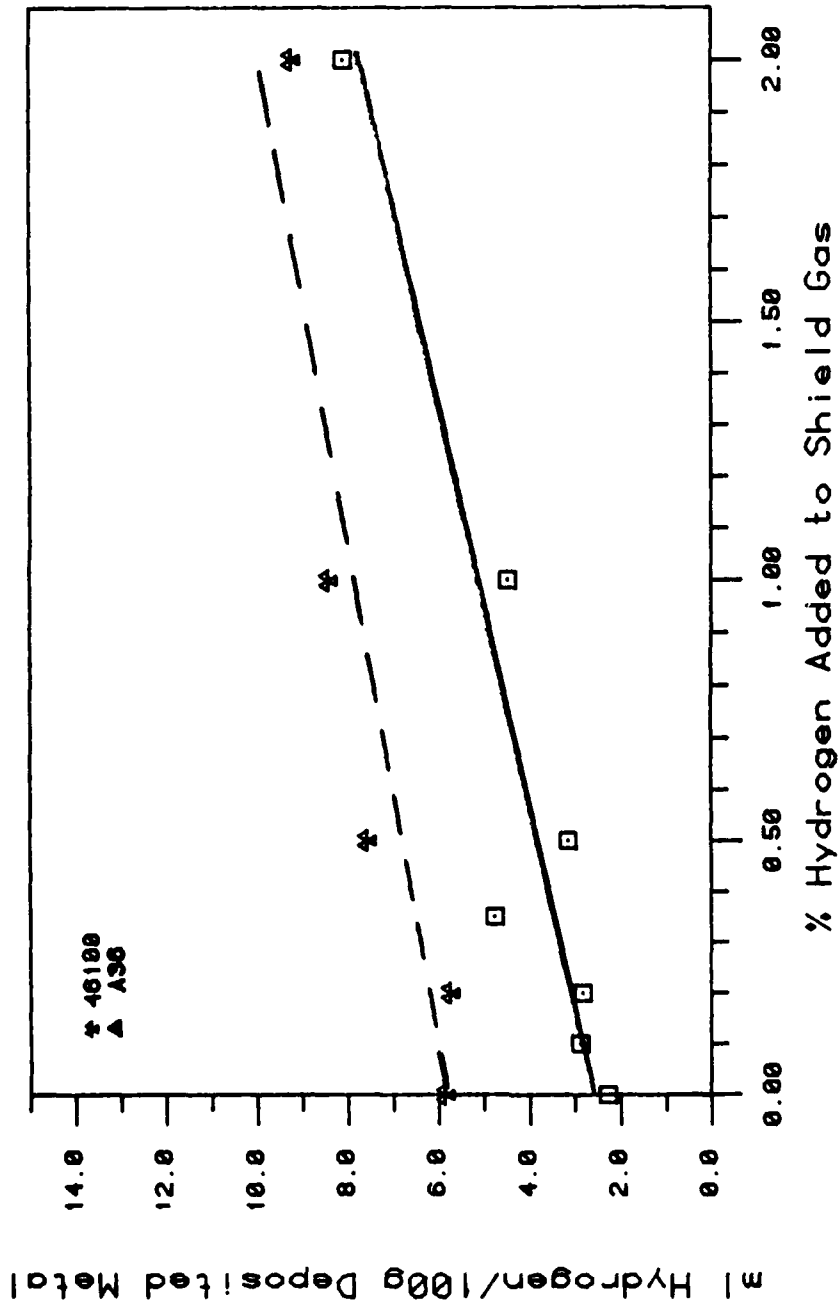
2.20 Metal transfer mode regions as a function of voltage and wire feed rate (wire feed determines the current) for 3/4" and 1-1/4" tip-to-work distances. (A36)



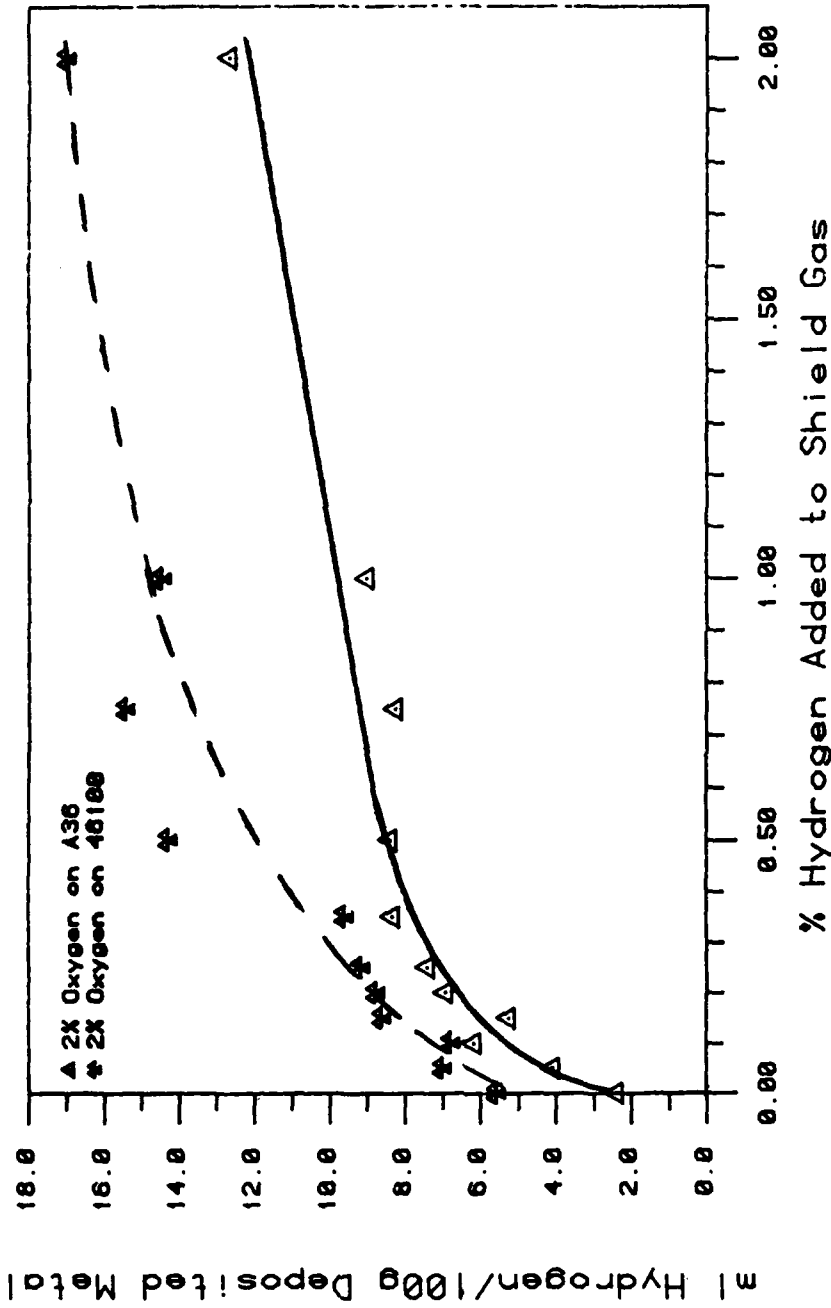
2.21 Metal transfer mode regions as a function of voltage and wire feed rate for various shielding gases.



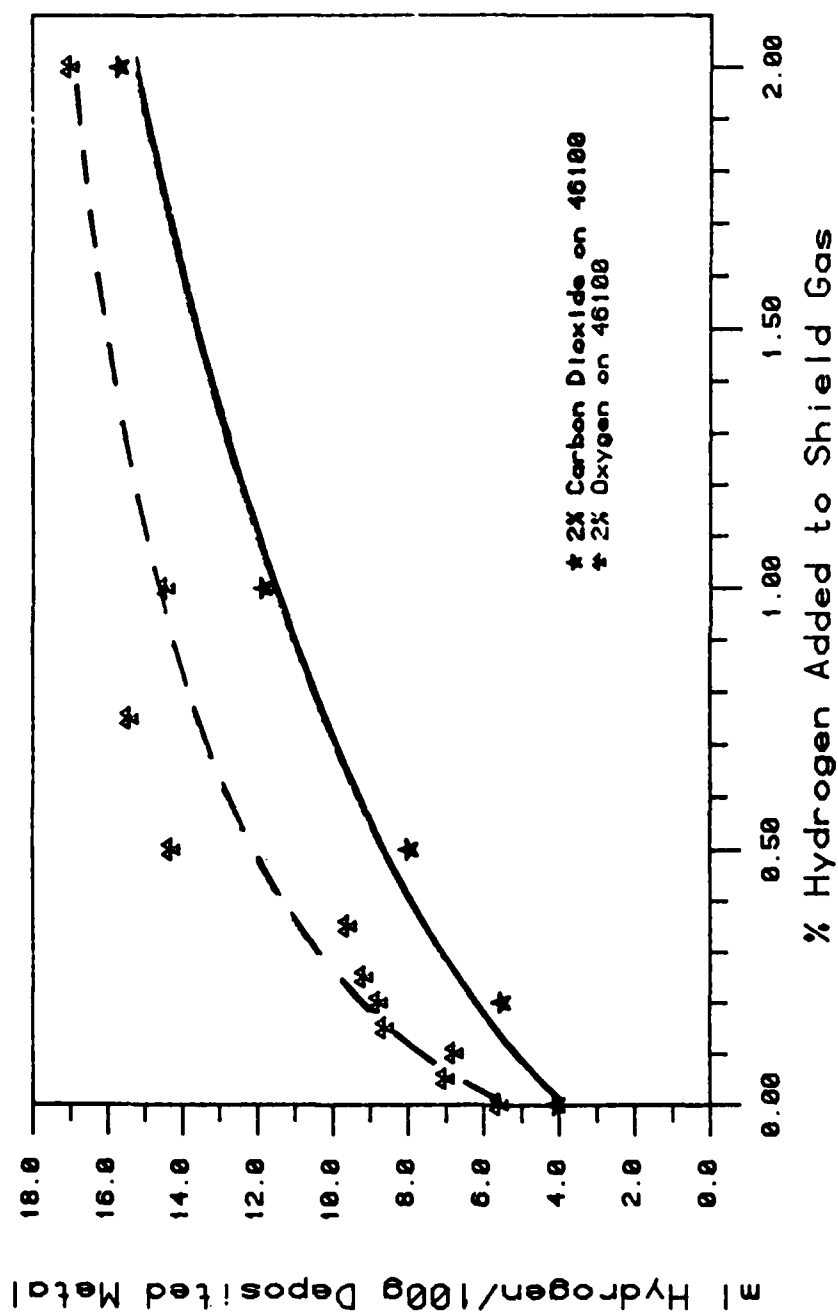
2.22 Effect of voltage on diffusible hydrogen content. The transition voltage from globular to spray is 28 Volts.



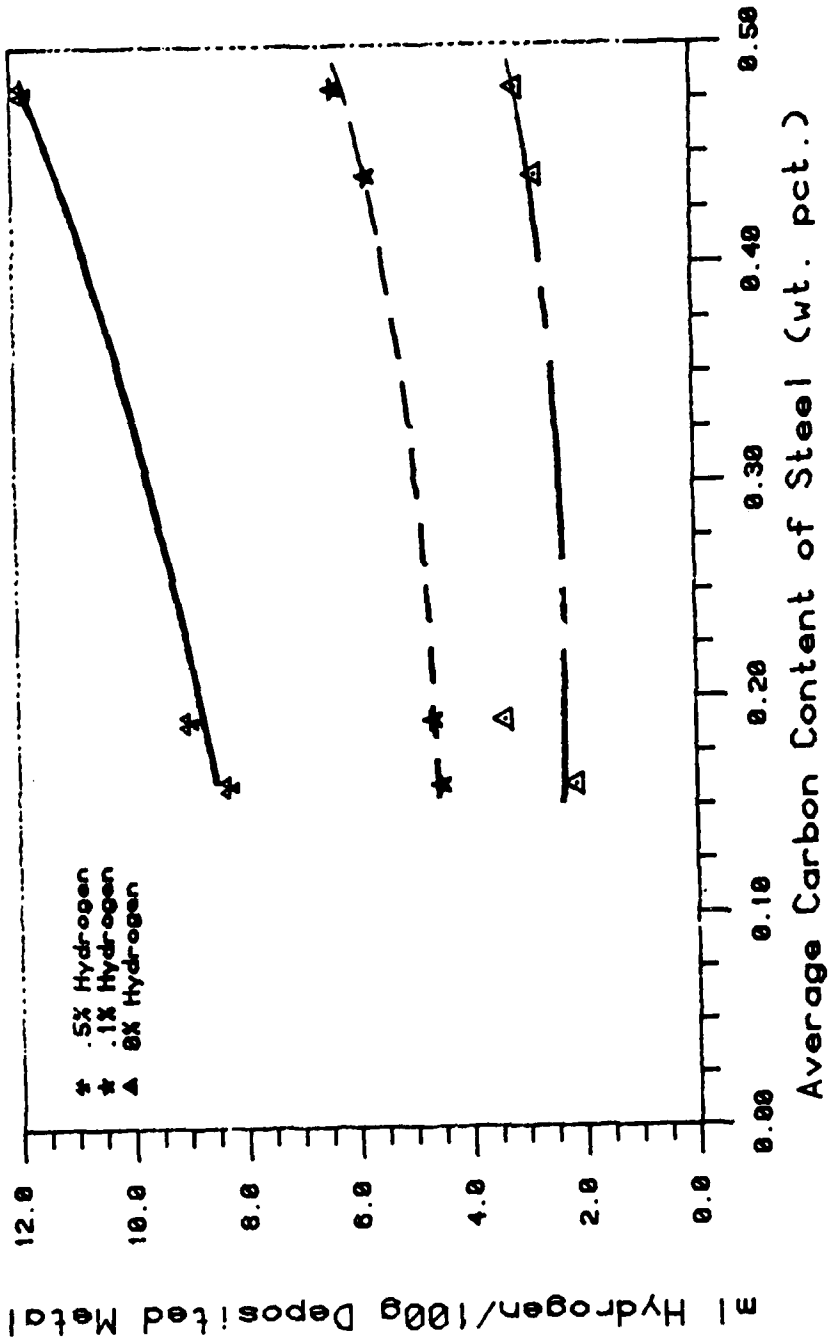
2.23 Diffusible hydrogen versus hydrogen in pure argon shielding gas for A36 and 46100 steel.



2.24 Diffusible hydrogen versus hydrogen in Ar/2% O₂ shielding gas for A36 and 46100 steel.



2.25 Diffusible hydrogen content of 46100 versus hydrogen in the shielding gas for Ar/2% O₂ and Ar/2% CO₂.



2.26 Diffusible hydrogen content as a function of the carbon content of the steels tested. Each curve represents a different amount of hydrogen in the Ar/2% O₂ shielding gas.

APPENDIX 2A

A portion of the diffusible hydrogen measurements presented in this document was performed at the U.S. Army Construction Engineering Research Laboratory (CERL). These results were monitored by Steven Gedeon of the U.S. Army Materials Technology Laboratory under MTL contract AW-6-MD0045.

This research used linear mass flowmeters to study the effect of shielding gas variations on the diffusible hydrogen content of Gas Metal Arc Welds (GMAW). Zero gas standards were used for the input gases for all tests. The steel used was MIL-A-46100 and A36 shipped from MTL specifically for use in this study. The AWS A4.3-86 method of specimen preparation was used. The welding parameters were designated by MTL and conform to those listed in table 2.4. The shielding gas compositions to be studied were also designated by MTL.

The method of diffusible hydrogen measurement is based on the method originally developed by Maria Quitana of the General Dynamics Electric Boat Division, and used by Dawn White at CERL for her Ph.D. thesis at the University of Illinois at Champaign. All of the experimental apparatus was already available at the start of this research effort. The method used essentially consists of injecting a known amount of helium into the outgassing chamber and then ratioing the hydrogen peak against the helium peak and multiplying by the known amount of helium

injected. This value is then adjusted to standard temperature and pressure.

The resulting diffusible hydrogen values measured in this study, along with the calculated mean and standard deviation, are presented in the following pages. The experimental scatter is larger than that experienced at either MTL or Electric Boat. After discussions with Marie Quintana and Dawn White, it is felt that this is due primarily to variations in humidity from one test to another. Another possible source of error is that the amount of helium injected into the outgassing chambers varied somewhat. Also, the weld was not always placed in the center of the diffusible hydrogen specimen.

The values found in this portion of the study were independently verified at MTL by using certified gas mixtures. Due to the cost of these specially mixed cylinders, only a limited number of verifications could be made. However, the MTL results coincide very closely with the average of those found at CERL.

2% O₂ On A36 (#1-53)

<u>% H₂</u>	<u>mlH₂/100g Deposited</u>	<u>Mean</u>	<u>Standard Deviation</u>
0	2.8920 <u>1.9117</u>	2.40	.69
0.05	3.0914 3.8804 5.2660 <u>4.1071</u>	4.09	.90
0.1	6.8156 <u>5.4947</u>	6.16	.93
0.15	5.1709 <u>5.3130</u>	5.24	.10
0.20	7.7435 6.7542 6.5651 <u>6.6219</u>	6.92	.55
0.25	<u>7.4118</u>	7.41	x
0.35	8.4533 7.7522 <u>8.7894</u>	8.33	.53
0.5	8.3373 <u>8.4036</u>	8.37	.05
0.75	7.7285 10.3458 <u>6.6355</u>	8.24	1.91
1.0	9.1322 <u>8.8735</u>	9.00	.18
2.0	12.1744 13.0247 12.7477	12.65	.43

5% O₂ on A36 (#210-219; 231-248)

<u>% H₂</u>	<u>mlH₂/100g Deposited</u>	<u>Mean</u>	<u>Standard Deviation</u>
0	3.7402 4.3032 <u>4.0642</u>	4.03	.28
0.1	4.7354 6.0129 <u>5.6162</u>	5.45	.65
0.2	6.1698 6.3547 6.0359 <u>7.0757</u>	6.41	.46
0.35	7.4026 7.7290 <u>9.1036</u>	8.08	.90
0.5	8.2388 11.2143 <u>8.9081</u>	9.45	1.56
1.0	13.4148 9.5208 <u>9.7435</u>	10.89	2.19
2.0	19.5907 16.1694 24.2070 25.3774	21.34	4.25

2% CO₂ on A36 (#108-147)

<u>% H₂</u>	<u>mlH₂/100g Deposited</u>	<u>Mean</u>	<u>Standard Deviation</u>
0	4.9568 3.2279 1.7327 <u>0.9473</u>	2.71	1.77
0.05	5.7895 7.7716 7.4193 <u>1.0269</u>	5.50	3.10
0.1	5.1194 3.0217 3.0197 <u>2.6645</u>	3.46	1.12
0.15	9.3697 2.2751 2.2850 <u>2.5038</u>	4.11	3.51
0.2	7.6431 3.0007 2.7604 <u>3.5796</u>	4.25	2.29
0.25	6.0513 3.2141 4.4754 <u>8.4190</u>	5.54	2.24
0.35	9.1749 3.1533 <u>6.3529</u>	6.23	3.01
0.5	8.5233 3.8666 6.3397 <u>4.6035</u>	5.83	2.07
0.75	8.7295 8.6188 5.2026 <u>4.5091</u>	6.76	2.22
1.0	10.7216 4.3199 <u>4.3026</u>	6.45	3.70
2.0	9.2524 8.6284 9.2558	9.05	.36

5% CO₂ on A36 (#307-322 & 339-342)

<u>% H₂</u>	<u>mlH₂/100g Deposited</u>	<u>Mean</u>	<u>Standard Deviation</u>
0	3.9520 1.9460 4.2395 <u>3.6095</u>	3.44	1.03
0.2	2.7730 5.5496 6.0402 <u>5.4342</u>	4.95	1.47
0.5	3.1301 10.8136 6.9023 <u>10.2457</u>	7.77	3.54
1.0	6.6946 9.4806 <u>8.4021</u>	8.19	1.40
2.0	14.5822 10.6615 15.3135 15.1244	13.92	2.19

10% Co₂ on A36 (#251-278)

<u>% H₂</u>	<u>mlH₂/100g Deposited</u>	<u>Mean</u>	<u>Standard Deviation</u>
0	2.0994 3.7001 3.9393 <u>3.5823</u>	3.33	.83
0.1	2.6388 3.3637 3.5319 <u>5.7963</u>	3.83	1.37
0.2	2.3227 3.7770 3.8246 <u>5.0181</u>	3.74	1.10
0.35	3.3655 <u>5.2934</u>	4.33	1.36
0.5	5.0688 <u>8.6417</u>	6.85	2.52
1.0	11.5887 4.9544 11.5857 <u>9.6325</u>	9.44	3.13
2.0	8.3934 7.6844 16.5026 8.8071	10.35	4.13

Ar & H₂ on A36 (#148-209)

<u>% H₂</u>	<u>mlH₂/100g Deposited</u>	<u>Mean</u>	<u>Standard Deviation</u>
0	1.9248 1.6789 <u>3.2790</u>	2.29	.86
0.1	2.7365 <u>3.0513</u>	2.89	.22
0.2	2.2136 3.0066 2.9747 <u>3.1156</u>	2.83	.42
0.35	2.4331 9.3354 <u>2.5238</u>	4.76	3.96
0.5	2.2678 2.8766 4.1922 <u>3.2063</u>	3.14	.60
1.0	3.3505 4.1516 5.0351 <u>5.3307</u>	4.47	.90
2.0	7.2573 8.2558 9.2971	8.1	.98

2% O₂ on 46100 (#338-507)

<u>% H₂</u>	<u>mlH₂/100g Deposited</u>	<u>Mean</u>	<u>Standard Deviation</u>
0	6.4317 <u>4.7721</u>	5.60	1.17
0.05	9.0601 7.0239 <u>4.9704</u>	7.02	2.04
0.1	4.8294 <u>8.7713</u>	6.80	2.79
0.15	10.2599 6.4932 <u>9.1355</u>	8.63	1.94
0.20	<u>8.8049</u>	8.80	X
0.25	12.9049 7.7106 <u>6.9542</u>	9.19	3.24
0.35	11.2936 8.5345 <u>9.0641</u>	9.63	1.46
0.5	6.3706 <u>22.2348</u>	14.30	11.20
0.75	12.1575 18.7786 <u>15.3624</u>	15.43	3.31
1.0	17.3131 11.2589 <u>14.8204</u>	14.46	3.04
2.0	17.6170 17.7107 17.5036 <u>15.2101</u>	17.01	1.20

2% CO₂ on 46100 (#25-44)

<u>% H₂</u>	<u>mlH₂/100g Deposited</u>	<u>Mean</u>	<u>Standard Deviation</u>
0	2.6490 3.5821 4.3232 <u>5.8740</u>	4.10	1.67
0.2	3.5261 <u>7.5014</u>	5.51	2.81
0.5	12.6684 5.2132 <u>6.0286</u>	7.97	4.09
1.0	8.5532 17.3838 7.0843 <u>14.4568</u>	11.87	4.86
2.0	13.9732 17.3901	15.68	2.42

10% CO₂ on 46100 (#45-64)

<u>% H₂</u>	<u>mlH₂/100g Deposited</u>	<u>Mean</u>	<u>Standard Deviation</u>
0	5.1011 3.3617 <u>8.6672</u>	5.71	2.70
0.2	7.8993 5.5505 4.7507 <u>6.4205</u>	6.15	1.35
0.5	15.3540 14.2542 9.5945 <u>6.1836</u>	11.34	4.25
1.0	10.7631 <u>18.8795</u>	14.81	5.74
2.0	10.7631 22.0751 13.5683 21.9977	17.10	5.81

H_2 & Ar on 46100 (#65-84)

<u>% H_2</u>	<u>ml H_2/100g Deposited</u>	<u>Mean</u>	<u>Standard Deviation</u>
0	7.1329 5.7466 <u>4.7137</u>	5.86	1.22
0.2	9.4826 3.8709 <u>3.8897</u>	5.75	3.23
0.5	9.4128 4.1828 <u>9.1127</u>	7.57	2.94
1.0	7.2129 4.2305 <u>13.8652</u>	8.44	4.93
2.0	10.2575 7.0758 8.4323 11.1698	9.23	1.83

T.I.M.F. on A3C (#54-97)

<u>% H₂</u>	<u>mlH₂/100g Deposited</u>	<u>Mean</u>	<u>Standard Deviation</u>
0	3.0338 5.6354 5.9676 <u>1.9111</u>	4.14	1.98
0.05	4.1184 6.9220 5.1174 <u>6.8615</u>	5.75	1.37
0.1	3.6126 7.8183 6.9525 <u>4.2928</u>	5.67	2.03
0.15	10.3039 9.0542 9.0437 <u>6.1229</u>	8.63	1.77
0.2	4.9479 10.6787 7.3529 <u>6.9680</u>	7.49	2.37
0.25	6.8425 10.9941 9.9801 <u>8.1316</u>	8.99	1.86
0.35	11.8535 9.4178 <u>9.5759</u>	10.28	1.36
0.5	9.4284 7.7086 12.1923 <u>8.6724</u>	9.50	1.93
0.75	13.6326 12.1768 <u>10.6553</u>	12.15	1.49
1.0	14.5302 16.8255 9.3040 <u>10.5915</u>	12.81	3.48
2.0	14.5786 13.5561 <u>13.7440</u>	13.96	.54

Simulate T.I.M.E. w/o O_2 on A36 (#279-306)

<u>% H_2</u>	<u>ml H_2/100g Deposited</u>	<u>Mean</u>	<u>Standard Deviation</u>
0	2.4373 2.2960 5.9925 <u>3.1336</u>	3.46	1.72
0.1	7.6293 5.6572 5.5997 <u>5.7361</u>	6.16	.98
0.2	12.8156 4.8952 <u>10.0022</u>	9.24	4.02
0.35	14.3084 12.5478 <u>7.6149</u>	11.49	3.47
0.5	18.2111 18.0093 6.6839 <u>6.7611</u>	12.42	6.58
1.0	15.5454 5.9214 12.2972 <u>7.2128</u>	10.24	4.48
2.0	14.3301 16.5347 18.8947	16.59	2.28

THERMOCHEMICAL ANALYSIS OF HYDROGEN ABSORPTION IN WELDING

3.0 ABSTRACT

Many researchers have used Sievert's law to describe hydrogen absorption in weld pools. Sievert's law is based on the equilibrium absorption of diatomic gases and neglects the effect of dissociation which can occur in the high temperature region of the welding arc plasma. A thermodynamic analysis is applied in order to quantify the effect of dissociation on the theoretical hydrogen absorption levels, and the ensuing effect on the reaction temperature obtained.

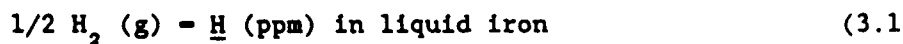
Previous researchers have used diffusible hydrogen measurements to determine an "effective" equilibrium reaction temperature. It is shown that if the actual amount of hydrogen initially absorbed into the molten weld pool is used, then Sievert's law predicts impossibly high absorption temperatures. Sievert's law is shown to be invalid for modeling hydrogen absorption in weld pools.

Experimental results on hydrogen absorption in Gas Metal Arc Welds are used to develop a new hydrogen absorption model including the effect of dissociation in the high temperature region of the arc. The effect of temperature distribution in the weld pool is also considered and results indicate that the majority of hydrogen absorption actually occurs due to monatomic hydrogen absorption into the outer region of the weld pool.

3.1 CALCULATION OF HYDROGEN ABSORPTION REACTION TEMPERATURE

USING SIEVERT'S LAW NEGLECTING DISSOCIATION

The most often used equation to describe the absorption of hydrogen in steel is the well known Sievert relationship. Sievert's law is based on the equilibrium reaction:



The free energy of this reaction has been found to be:

$$G = 8720 - 11.02 T - - RT \ln K \text{ (Kcal/mole)} \quad (3.2)$$

where:

$$K = \underline{H} / (P_{H_2})^{1/2} \quad (3.3)$$

These equations can be used to plot the absorbed hydrogen as a function of the diatomic hydrogen partial pressure for various assumed equilibrium reaction temperatures as is shown in figure 3.1. This data has been replotted in figure 3.2 as the amount of absorbed hydrogen as a

function of the assumed reaction temperature for various hydrogen partial pressures. As can be seen, the amount of absorbed hydrogen increases with both temperature and hydrogen partial pressure.

The simultaneous effect of a number of alloying elements on the solubility of hydrogen in steel has been calculated in section 1.3. The results show that the free energy of hydrogen absorption in steel is within 5% of the free energy of hydrogen absorption in pure iron. Thus, the data in table 3.1 is appropriate for steel welding research.

Many previous investigators have used the results of diffusible hydrogen measurements in their hydrogen absorption reaction temperature calculations. This is a gross error since the value of hydrogen measured in this test does not equal the amount of hydrogen initially absorbed by the weld pool. Some have even used results in terms of ml/100g deposited rather than fused metal. Diffusible hydrogen measurements can be converted to initially absorbed hydrogen values by using Terasaki's theoretical analysis shown in figure 3.3. This conversion was described in detail in section 2.5.5. The thermal factor associated with an AWS sized specimen quenched 3 seconds after weld completion is indicated in the figure. Thus, dividing the diffusible hydrogen content (calculated in ml H_2 /100g FUSED metal) by .7 will provide a reasonable estimate of the amount of hydrogen initially absorbed by the weld pool.

Using the diffusible hydrogen results obtained in the previous chapter, converting from ml/100 g deposited to ml/100 g fused metal using

the results shown in figure 3.4, and applying the conversion factor from figure 3.3, the hydrogen initially absorbed as a function of hydrogen in the weld shielding gas can be found for various gas mixtures. For convenience, the data will also be converted to parts per million using the conversion:

$$1 \text{ ml H}_2/100 \text{ g steel} = 1.1 \text{ ppm} \quad (3.4)$$

The resulting data for hydrogen initially absorbed by the weld pool as a function of diatomic hydrogen added to the GMAW shielding gas are shown in figures 3.5 through 3.7.

Comparing this data with figure 3.1 (using Sievert's law in equations 3.2 and 3.3), the reaction temperature found for the absorption of hydrogen in GMA welds is in excess of 3000 C.

This value is unreasonably high. Block-Bolten and Eagar (B12) have shown that evaporative cooling of iron vapors will limit the maximum temperature of a weld made on steel to 2500 C. Howden and Milner (H18) have shown that iron vaporization will also limit the amount of hydrogen which can come into contact with the weld pool at high temperatures. Spectroscopic research by Quigley, et al. (Q1) has shown that vaporization will significantly reduce the arc power transferred to the workpiece, and they showed the weld pool to be between 2400 and 2750 K (i.e a maxi-

mum of under 2500 C). Other research by Quigley, et al. (Q2) found that evaporation is the dominant mechanism for energy loss from the weld pool, and estimate the center pool temperature to be 2500 K, but no more than 2750 K.

Chew and Willgoss (C7), studying GTAW, realized that they were not analyzing the initially absorbed hydrogen and instead measured what they termed an "effective reaction temperature". Thus, their results were strongly dependent on the heat input (and thus the cooling rate) as is shown in figure 3.8. If their diffusible hydrogen results are converted to initially absorbed hydrogen (since they followed the IIW procedure, a time to quench of 5 seconds is assumed in this conversion) their hydrogen absorption reaction temperature would have been in excess of 2500 C.

Another important point is evidenced in figure 3.8: an increase in current decreases the amount of hydrogen and decreases the effective reaction temperature. Thus, Chew and Willgoss' effective reaction temperature does not at all reflect the absorption temperature, but rather reflects a decrease in the cooling rate, which allows more hydrogen to escape. Numerous reseachers have mistakenly reported their effective reaction temperatures as absorption reaction temperatures.

Investigators working with GTAW, SMAW, and SAW have published effective reaction temperatures of between 1600 C and 2300 C using Sievert's law (references in chapter 1). These temperatures are meaningless, however, since Sievert's law applies only to equilibrium absorption of

diatomic gases. The data of the above researchers includes the additional effects of solidification and diffusion of hydrogen away from the weld pool. If the results of these investigations are reinterpreted to account for the loss of hydrogen through diffusion before the specimen is quenched, then the absorption temperatures calculated using Sievert's law are in excess of 2500 C.

Salter, collecting data by arc melting metal on a water-cooled copper hearth, found that the arc significantly aided hydrogen transfer to the pool. His data indicated that hydrogen was absorbed into the "hot spot" of the pool at a temperature well in excess of 2500 C; a temperature now known to be impossible to reach. He also found that increasing the hydrogen content of the gas increased the temperature of the weld pool.

White (W8), studying hydrogen in GMAW, did not establish an equilibrium reaction temperature, but rather concluded that increasing hydrogen contents increased the temperature of the weld pool. Her reasoning was that hydrogen made the arc unstable, and that an increase in current aided in stabilization, thus increasing the temperature. Research by Florian and Neumann (F5) on GTAW, reproduced in figure 3.9, shows that the presence of large amounts of hydrogen increases heat input, but by increasing the voltage rather than the current. White's diffusible hydrogen data is reproduced in figure 3.10. The fact that she did not report her values in terms of ml/100 g fused metal makes it difficult to

use her values to examine hydrogen absorption. However, if the results from the present study for the ratio of fused metal to deposited metal as a function of hydrogen and oxygen content in the shielding gas are used (figure 3.4) along with the conversion to initially absorbed hydrogen (figure 3.3), then the reaction temperatures associated with her data are in excess of 2500 C; an impossibility.

Savage, et al. (S6) studied the effect of adding hydrogen gas or water vapor to the shielding gas of GMAW. They found that water vapor added more hydrogen to the weld than did an equal amount of hydrogen gas. They also found that a pulsed arc was more stable in the presence of hydrogen than welding with direct current reverse polarity (DCRP). They did not attempt to explain either of these occurrences, but a reproduction of their data, plotted as ppm hydrogen in the fused weld metal, is shown in figure 3.11.

Savage, et al. reported a reaction temperature of 1870 C by seemingly arbitrarily choosing the solubility of hydrogen as 43 ppm at one atmosphere. If the correct solubility of hydrogen is used (about 23 ppm), the equilibrium reaction temperature which best fits their results is about 2225 C. Unfortunately, their results cannot be used directly to accurately examine the amount of hydrogen initially absorbed by the molten weld pool since they waited approximately 10 seconds after welding before quenching the specimen. Also, their use of silicon oil for a collecting fluid adds doubt to the validity of their diffusible hydrogen measurements. The fact that much hydrogen will be lost during their 10

second delay, and that hydrogen is soluble in silicon oil, will mean that their reaction temperatures are actually in excess of 2500 C.

Howden and Milner (H18) used a stationary arc in an enclosed chamber to study both the hydrogen absorbed in the molten pool and the hydrogen retained in the solidified metal. They found that thoroughly deoxidized iron will absorb much less hydrogen than iron which contains a normal amount of oxygen. Figure 3.12 shows their results for hydrogen solubility in pure deoxidized iron (as well as nickel, copper, and aluminum). Figure 3.13 shows that dramatically more hydrogen will be absorbed into iron containing oxygen. Using Sievert's law, the reaction temperature associated with the hydrogen absorption in normal iron (containing oxygen) is well in excess of 2500 C.

Research performed on the solubility of nitrogen in arc melted iron examined the possibility that the nitrogen became dissociated before absorption (I6). That research concluded that nitrogen absorption obeyed Sievert's law, but that the arc resulted in a substantial increase in solubility. They attributed this to "energy acquired by nitrogen molecules in the anode boundary zone through interaction between electrons and neutral particles". However, this does not rule out the possibility that hydrogen will not dissociate because the dissociation energy for hydrogen is far less than for nitrogen as is shown in figure 3.14.

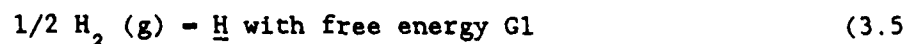
One final consideration is that residual hydrogen is not measured in a diffusible hydrogen test. If the residual hydrogen is added to the

diffusible hydrogen test values of all the previous researchers, the calculated absorption temperatures would be even higher.

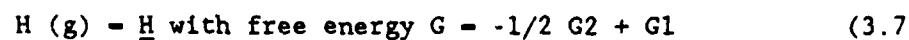
Thus, by systematically analyzing previous research on hydrogen absorption, it has been shown that Sievert's law cannot be directly used to assess the hydrogen absorption reaction temperature. Previous research using Sievert's law has been shown to not accurately reflect a true hydrogen absorption temperature, but rather reflect an "effective" temperature at which the kinetics are sluggish enough to slow down hydrogen diffusion away from the weld region. The major assumption in the Sievert relationship, that diatomic gas alone is being absorbed by the weld pool, must be reconsidered. In order to understand this, the dissociation of hydrogen in the high temperature arc plasma must be examined.

3.2 ABSORPTION OF MONATOMIC HYDROGEN INTO THE WELD POOL

Basic thermodynamics can be used to combine thermodynamic data to calculate the free energy of a reaction of interest:



can be combined into the reaction:



Using the thermodynamic data in table 3.1, the free energy associated with equation 3.7 is equal to:

$$\Delta G = -44,780 + 3.38 T \text{ (kcal/mole)} \quad (3.8)$$

Thus, one can plot the amount of absorbed hydrogen as a function of

the partial pressure of monatomic hydrogen for various assumed reaction temperatures as is shown in figure 3.15. This is replotted as absorbed hydrogen as a function of assumed reaction temperature for various partial pressures of monatomic hydrogen in figure 3.16. These graphs show quite a different relation than for the non-dissociated hydrogen in figure 3.1 and 3.2, namely, that the amount of absorbed hydrogen decreases with temperature rather than increases. It can also be seen that at the reaction temperatures quoted in the literature (which vary from 1600 C to 2300 C), the amount of absorbed hydrogen (assuming that all of the hydrogen in the arc is fully dissociated) is unreasonably large.

The fact that the solubility of "active" gases increases with decreasing temperature is a well known phenomenon in high temperature systems (F4). Gaseous solubility in aqueous solutions can be described as "physical" or "chemical". In some systems both types may be present.

Physical solubility has been theoretically modeled by calculating the work associated with creating a cavity or so-called "hole" in the fluid, and then fitting a gaseous molecule into the cavity with an additional energy term representing the interaction of the gas with the surrounding solvent molecules. Since the number of holes increases with temperature, the solubility of physically absorbed molecules increases as well. Physical solubilities are usually low in magnitude and are accompanied by endothermic partial molar heats of mixing. However, the overall heat effect for dissolution could still be exothermic because of the predominance of the heat contribution due to condensation (F4).

The solubility of diatomic hydrogen in liquid iron may be described as "physical".

The solubility of monatomic hydrogen in liquid iron may be described as "chemical". The partial molar heat effects for chemical solubility are usually exothermic and the excess entropies of mixing are expected to be negative.

Since the amount of hydrogen absorbed from even a minute amount of dissociated hydrogen gas is quite large at low temperatures, the degree of dissociation must be further investigated.

3.3 HYDROGEN DISSOCIATION IN THE WELDING ARC

The degree of hydrogen dissociation as a function of temperature has been previously calculated by Christensen (C9), and is reproduced in figure 3.17. At first glance, it seems as though the degree of dissociation at the reaction temperatures quoted in the literature are negligibly small and so can be ignored. However, it must be noted that the dissociation curve in figure 3.17 is for a pressure of 1 atmosphere hydrogen. During a welding operation the partial pressures of hydrogen can be as low as .0001 atmospheres (.01% H_2 in the shielding gas). Thus the percent dissociation needs to be calculated for lower partial pressures of total hydrogen (diatomic plus monatomic).

A sample calculation for the percent dissociation resulting from 5% diatomic hydrogen gas in an inert argon shielding gas will now be performed at a specified temperature. This method can then be repeated for varying hydrogen partial pressures and temperatures to recalculate the percent dissociation as a function of both temperature and pressure. This particular calculation and ensuing graph have never before been published in the open literature.

Table 3.2 lists the known and unknown quantities used in the following series of calculations. The initial partial pressures being introduced to the high temperature region of the arc are designated with a prime. The initial molar fraction of each component is designated with

a primed letter n and the resultant molar fraction after exposure to the high temperature is unprimed. Since argon is inert, its final number of moles must be equal to its initial number of moles. The final molar fractions of diatomic and monatomic hydrogen yet need to be determined. Since this is an "open system", the total pressure must remain at 1 atmosphere by definition.

A number of relationships exist between the molar fractions and the partial pressures. For example:

$$P_t - 1 = P_{Ar} + P_{H_2} + P_H \quad (3.9)$$

$$P_{Ar}' = (n_{Ar}'/n_t') P_t = n_{Ar}'/n_t' = .95 \quad (3.10)$$

$$P_{Ar} = (n_{Ar}/n_t) P_t = n_{Ar}/n_t = n_{Ar}' / (n_{Ar}' + n_{H_2}' + n_H') \quad (3.11)$$

Since one molar fraction of diatomic hydrogen will dissociate into two molar fractions of monatomic hydrogen, the following is also known:

$$n_{H_2}' = n_{H_2} + 1/2 n_H \quad (3.12)$$

Thus, the final total molar fraction will be somewhat more than one and the final partial pressure of argon in equation 3.11 will be less than .95 atmospheres. A set of equations similar to 3.10 and 3.11 can be written for the molar fractions of diatomic and monatomic hydrogen.

From the free energy of dissociation in equation 3.6, the relationship between the partial pressures of diatomic and monatomic hydrogen as a function of temperature is known. Namely:

$$-53,844.6 / T + 14.49 = \ln (P_H)^2 / P_{H_2} \quad (3.13)$$

at a specified temperature -- let's say 3000 K -- equation 3.13 can be rewritten:

$$P_H^2 = .0314 P_{H_2} \quad (3.14)$$

which in terms of molar fractions is:

$$(n_H/n_t)^2 = .0314 (n_{H_2}/n_t) \quad (3.15)$$

or,

$$(n_H)^2 = .0314 n_{H_2} n_t = .0314 n_{H_2} (.95 + n_H + n_{H_2}) \quad (3.16)$$

Now, using the known value for n_{H_2} of .05 in equation 3.12:

$$.05 = n_{H_2} + 1/2 n_H \quad (3.17)$$

Thus, two equations (3.16 and 3.17) and two unknowns (n_{H_2} and n_H) are obtained. This set of equations can be solved to determine the final molar fractions of diatomic and monatomic hydrogen, which are:

$$n_H = .03274 \quad \text{and} \quad n_{H_2} = .03363$$

this results in a percent dissociation of:

$$((.03274 / 2) / .05) 100 = 32\% \quad (3.18)$$

This methodology can be followed for varying initial hydrogen concentrations and temperatures to calculate figures 3.18 and 3.19. This computation was performed on an IBM PC.

As can be seen in figure 3.18, neglecting to consider the reduced pressure can result in a large variation in the percent dissociation anticipated. Thus, at a temperature of 3000 K, the percent dissociation

risks from 8% to 32% by reducing the pressure of hydrogen from 1 atmosphere to .05 atmospheres. It rises to virtually 100% at .0001 atmospheres.

This large amount of hitherto unanticipated dissociation will now be shown to have a large effect on the amount of hydrogen absorbed by the weld pool.

3.4 THE EFFECT OF DISSOCIATION ON THE AMOUNT OF HYDROGEN ABSORBED INTO THE WELD POOL

It was shown in section 3.1 that the use of Sievert's law results in impossibly high predicted hydrogen absorption reaction temperatures. One possible explanation for this is that Sievert's law neglects the effect of dissociation.

Table 3.3 shows the resulting hydrogen absorption if diatomic hydrogen first dissociates into the proper amounts of monatomic and diatomic hydrogen (according to figure 3.18) and then the monatomic hydrogen and diatomic hydrogen separately absorb into the weld pool (according to equations 3.8 and 3.2 or figures 3.15 and 3.1, respectively).

Figure 3.20 graphically shows the total absorbed hydrogen as a function of the reaction temperature assumed in table 3.3 for three amounts of diatomic hydrogen added to the shielding gas. As can be seen, the

curves for each percentage original hydrogen exhibit a maximum. The temperature at which this maximum occurs reduces with a reduction in original hydrogen content.

Comparing these theoretical absorbed hydrogen values with the experimental results in figures 3.5 through 3.7, it can be seen that the predicted values (for reasonable temperatures) are almost high enough to be in agreement with the experimental results.

This analysis can be further refined to take into account the fact that the dissociation reaction may take place at a higher temperature than the absorption reaction.

3.5 THE EFFECT OF NON-EQUILIBRIUM DISSOCIATION IN THE WELDING ARC ON THE AMOUNT OF HYDROGEN ABSORBED INTO THE WELD POOL

The previous section implicitly assumed local thermodynamic equilibrium (LTE). However, due to the extremely large temperature gradient from the weld pool surface to the arc plasma, reactions occurring in or near the cathode boundary layer will probably not be at LTE. In GMAW (normally performed with reverse polarity), the weld pool will be the cathode. In GTAW (normally straight polarity), the weld pool will be the anode.

The vast majority of arc plasma physics research has been performed

on the anode boundary layer rather than the cathode due to the added complexity of the cathode region. Quigley (Q2), however, has estimated the cathode boundary layer to be about 10^{-6} m thick. The temperature immediately above this layer must be greater than 8000 K in order to ionize the argon so that current can flow across the arc. Current flow across the cathode boundary layer is due to thermionic emission, positive ion bombardment, and field emission.

Dinulescu and Pfender (D4), studying anode boundary layers, found that substantial deviations from LTE occurred. A detailed numerical calculation using plasma physics showed that a number of different boundary layers are involved. The thermal boundary layer is approximated by the energy exchange free path, λ_E , which can be interpreted as the distance traveled by an electron in the direction of the electric field over which it loses its excess energy by collisions with the heavy particles. The diffusion boundary layer is approximated by the recombination free path, λ_r , which can be interpreted as the distance traveled by an electron in the direction of the electric field between two successive ionization-recombination collisions.

The electrons contained in a layer adjacent to the anode of thickness λ_E will arrive at the anode without suffering any further energy losses by collisions with heavy particles (D4). By analogy, a proton (or ionized monatomic hydrogen) contained in a layer adjacent to the cathode of thickness λ_E will arrive at the cathode at a substantially higher temperature than the heavy species (i.e. argon). Thus, the temperature of

monatomic hydrogen will probably be higher than the temperature of either the weld pool surface or the argon in the cathode region. Dinulescu and Pfender (D4) estimate λ_E to be about .2mm and λ_r to be about .3 to .6mm. Quigley, et al. (Q1) also found that there would be virtually no electron collisions across the anode boundary layer (which is about 6 to 10 times thicker than the cathode boundary layer).

Based on these values, a positive hydrogen ion in the high temperature arc could travel through the cathode boundary layer and strike the weld pool without losing its thermal or kinetic energy through collision. The fact that the cathode requires positive ion bombardment in order to allow current flow further supports this hypothesis. Thus, it is quite reasonable to assume that the hydrogen dissociation which occurs in the high temperature region of the arc may not completely recombine before it strikes the weld pool. This deviation from LTE can be approximately modeled by assuming two different equilibrium reaction temperatures.

Table 3.4 demonstrates the resulting hydrogen absorption if the dissociation reaction and absorption reaction occur at different temperatures. As can be seen, high enough hydrogen absorption values can readily be calculated if the dissociation temperature is about 10% to 20% higher than the absorption temperature. By using this model, a reasonable weld pool temperature can be used for absorption, and then a dissociation temperature can be determined so that the amount of hydrogen absorbed will equal experimental observations.

Using an estimated weld pool temperature for hydrogen absorption of 2300 C, a dissociation reaction temperature of 2500 will result in hydrogen absorption values which are in close agreement with experimental observations. If a 2000 C weld pool temperature is assumed, then a dissociation temperature of about 2100 C will result in experimentally determined hydrogen contents.

The agreement between experimental and theoretical results now rests on the choice of weld pool temperature. The choice of weld pool temperature will dictate the resulting calculated dissociation temperature. This is important since hydrogen absorption must take place at the same temperature as the weld pool surface. However, since the weld pool temperature is far from homogeneous, the effect of temperature distribution must now be considered.

3.6 THE EFFECT OF RADIAL TEMPERATURE DISTRIBUTION AND A MOVING WELD POOL

In the previous discussion, a homogeneous weld temperature and dissociation (or boundary layer) temperature have been implicitly assumed. The effect of radial temperature distribution will now be considered.

A reasonable estimate of temperature as it varies across the weld pool surface is shown in figure 3.21. Only recently, the first actual measurements of the weld pool surface temperature have been accomplished. These unpublished results (performed in 1987 at INEL by H. Krause on

GTAW) were unavailable at the time of this writing. What is known is that the maximum temperature near the center cannot be greater than 2500 C, and that dT/dx at the edge of the weld pool must be greater than zero in order for thermal conduction to be operative. Vigorous convection will make the boundary layer thickness near the edge of the weld quite narrow, so that the temperature will remain fairly constant throughout the rest of the pool.

Based on the research of Dinulescu and Pfender (D4), a homogeneous cathode boundary layer thickness (and temperature) will be assumed. It is quite possible that the boundary will be thicker near the outer radius of the weld pool, and thus cooler. However, this consideration is well beyond the scope of the present research.

If a dissociation temperature of 2500 K is assumed, figure 3.22 shows the resulting amounts of hydrogen absorbed at various locations in the weld pool. An immediate observation is that the majority of the hydrogen absorption will take place around the outer edge of the weld pool. This is a direct contradiction to the postulates of others who have looked at Sievert's law and deduced that the maximum absorption occurred at the high temperature central region.

Most of the hydrogen absorbed into the outer region of the weld pool will become evenly distributed throughout the pool through convection. However, near the trailing edge of the pool, solidification may overtake the diffusion of hydrogen out from this stagnant region. Chew and

Willgoss (C7) found that hydrogen will accumulate in the weld pool near the trailing edge even though they postulated that hydrogen was absorbed into the center of the weld pool.

Hydrogen will diffuse through this stagnant region according to Fick's laws. During a specified period of time, hydrogen will diffuse a distance of approximately:

$$x = 2 (Dt)^{1/2} \quad (3.19)$$

Taking the diffusion coefficient of hydrogen in liquid steel at its melting point to be $10^{-7} \text{ m}^2 \text{ sec}^{-1}$ (H12), hydrogen will diffuse about $2.0 \times 10^{-4} \text{ m}$ in .1 second. Using the travel speed from the welds made in the present investigation of 20 in/min, the weld pool will advance a distance of $8.5 \times 10^{-4} \text{ m}$ in that same time. Thus, much of the hydrogen absorbed into the trailing edge of the weld pool will become trapped in the solidifying weld metal. The previous quick calculation is based on the assumption that the stagnant boundary layer (defined as the region over which hydrogen movement is diffusion controlled rather than convection controlled) is at least $2.0 \times 10^{-4} \text{ m}$ thick. A precise analysis of this boundary layer would entail a detailed numerical calculation which is beyond the scope of the present effort. In any case, it is apparent that some hydrogen is likely to become trapped by the advancing solidification front.

Another rationale for the hypothesis that hydrogen is trapped rather than rejected by the advancing solidification front, is the fact that little porosity is found in steel welds. If substantial amounts of hydrogen were being rejected, significant levels of porosity would be evidenced as well (such as is found in aluminum welds).

Howden (H15) also postulated that hydrogen would be "pumped" into the solidifying weld metal rather than the hydrogen being rejected by the solidification front, as had been thought by some up until that time. His research results agree with the present trapping hypothesis even though he assumed that the majority of the hydrogen was initially absorbed into the center of the weld pool.

If one assumes that the hydrogen content of the molten weld pool is approximated by the amount initially absorbed into the trailing edge of the weld, the absorption reaction temperature of interest will be approximately 1540 C. Using this absorption temperature, the calculated dissociation temperature (at the outer edge of the cathode boundary layer) which results in the experimentally determined hydrogen content, will be about 1900 - 2000 K (about 10% greater than the absorption temperature). In actuality, the hydrogen will probably only absorb onto the top surface of the weld stagnant layer. In this case, the dissociation temperature will be substantially higher.

Due to the complexity of the proposed mechanism and the many assumptions and estimates involved, an exact calculation for the temperature of

dissociation is not appropriate. From all of the above considerations, however, it is apparent that the temperature of dissociation is about 10% to 30% higher than the weld pool temperature at the point of absorption. The logical conclusion of this hypothesis is quite important: hydrogen will absorb into the outer region of the weld rather than into the hot central portion. This revolutionary new theory needs to be substantially quantified before any realistic numbers can be assigned to the dissociation reaction temperature. One fact is clear, however: The simple model of hydrogen absorption using Sievert's law usually used by most researchers is not valid, and arc phenomena in the anode and cathode boundary regions must be carefully considered before any realistic chemical reaction mechanisms can be proposed.

3.7 FUNDAMENTALS OF THE SIEVERT RELATIONSHIP

In the chemical reaction:



the two end conditions (hydrogen gas and hydrogen in solution) are thermodynamic state functions. State functions are conditions which can be completely specified by their extensive parameters (mole fraction, volume, and internal energy) and a combination of intensive parameters (i.e. temperature and pressure). In Sievert's law, a theoretical analysis is developed which relates the difference between the two state

functions. This relationship is valid under equilibrium conditions (i.e. isothermal, closed system).

However, in welding, this simple, equilibrium, closed system model is not valid. Work, heat, and matter all cross the boundary in this open system. While the end conditions remain fixed (the experimental data for hydrogen solubility versus hydrogen partial pressure), there will be an infinite number of paths between these two states of hydrogen.

The hypothesis proposed in this thesis is that the energetically favored path consists of hydrogen dissociation followed by monatomic hydrogen absorption. Using this path, the calculated temperatures of the weld pool are meaningful and realistic. When the Sievert law path of direct diatomic hydrogen absorption is assumed, the calculated temperatures are unrealistically high.

Some previous researchers have applied the Sievert law relationship to their data which resulted in somewhat reasonable temperatures (the temperatures were within the realm of the possible). However, these values are not meaningful as they do not accurately reflect the true temperature of absorption. Many researchers have concluded that an increase in current will decrease the equilibrium temperature; but this has no basis in fact. Increasing the current will allow more hydrogen to escape from the already solidified weld metal by slowing the cooling rate.

The final value of hydrogen content will be governed by three dis-

tinctly different phenomena: hydrogen absorption into the molten pool, hydrogen trapping or rejection from the solidification front, and hydrogen diffusion away from the solidified weld. These are separate occurrences which can be separately modeled (by absorption theory, solidification theory, and diffusion theory). Any attempt to explain these separate occurrences with a single value is scientifically meaningless.

The fact that hydrogen solubility versus diatomic hydrogen pressure in the welding arc can be approximated by a parabolic function is a spurious relationship which has, unfortunately, led many researchers to assume that Sievert's law was responsible for the shape of the curve. The functional relationship resulting from the present hypothesis between the absorbed hydrogen and hydrogen partial pressure is a very complex function. This function may resemble a square root function, but this does not mean that, in fact, it is a result of Sievert's law.

Hopefully, a more fundamental approach to the chemical reactions occurring within the weld pool (which also consider the cathode or anode boundary regions) such as taken in this work will also be useful for other gas-metal reactions occurring during welding.

3.8 SUMMARY

The use of Sievert's law to calculate the hydrogen absorption reaction temperature has been shown to be invalid by a systematic review of previous research. In order to account for this, a new model of hydrogen absorption is proposed.

This model uses a novel calculation of the hydrogen dissociation as a function of both pressure and temperature, and proposes that the hydrogen dissociation reaction is governed by the higher temperature of the cathode boundary layer, and that the hydrogen absorption reaction is governed by the surface temperature of the weld pool. Following this hypothesis further, the majority of the hydrogen will actually absorb into the outer portion of the weld pool rather than the central region as has been proposed by others. The hydrogen initially absorbed into the trailing edge of the weld pool will become trapped in the solidifying weld metal.

The dissociation reaction temperature has been estimated to be about 10% to 30% higher than the absorption reaction temperature.

Table 3.1 Thermodynamic Data used in this study (Ref E.6)

<u>Reaction</u>	<u>Free Energy</u>	
	M (pure)	= M (i.d. wt. %, liq) cal/g atom
$1/2 \text{ H}_2(\text{g}) = \underline{\text{H}}$ (ppm) in liq Fe	$G^0 = 8,720 - 11.02 \text{ T}$	
$1/2 \text{ O}_2(\text{g}) = \underline{\text{O}}$ (%) in liq Fe	$G^0 = -28,000 - .69 \text{ T}$	
$\text{H}_2(\text{g}) = 2\text{H}(\text{g})$	$G^0 = 107,000 - 28.8 \text{ T}$	
$\text{C (graphite)} = \underline{\text{C}}$ (%)	$G^0 = 5,400 - 10.1 \text{ T}$	
$\text{H}_2(\text{g}) + 1/2 \text{ O}_2(\text{g}) = \text{H}_2\text{O}(\text{g})$	$G^0 = -60,000 + 13.94 \text{ T}$	
$\text{C (graphite)} + 1/2 \text{ O}_2(\text{g}) = \text{CO}(\text{g})$	$G^0 = -28,200 - 20.16 \text{ T}$	
$\text{C (graphite)} + \text{O}_2(\text{g}) = \text{CO}_2(\text{g})$	$G^0 = -94,755 + .02 \text{ T}$	
$\text{H}_2(\text{g}) + 2 \text{ C (graphite)} = \text{C}_2\text{H}_2(\text{g})$	$G^0 = 52,000 - 11.80 \text{ T}$	
$2 \text{ H}_2(\text{g}) + \text{C (graphite)} = \text{CH}_4(\text{g})$	$G^0 = -22,100 + 26.45 \text{ T}$	

TABLE 3.2

Table of values for hydrogen dissociation calculation

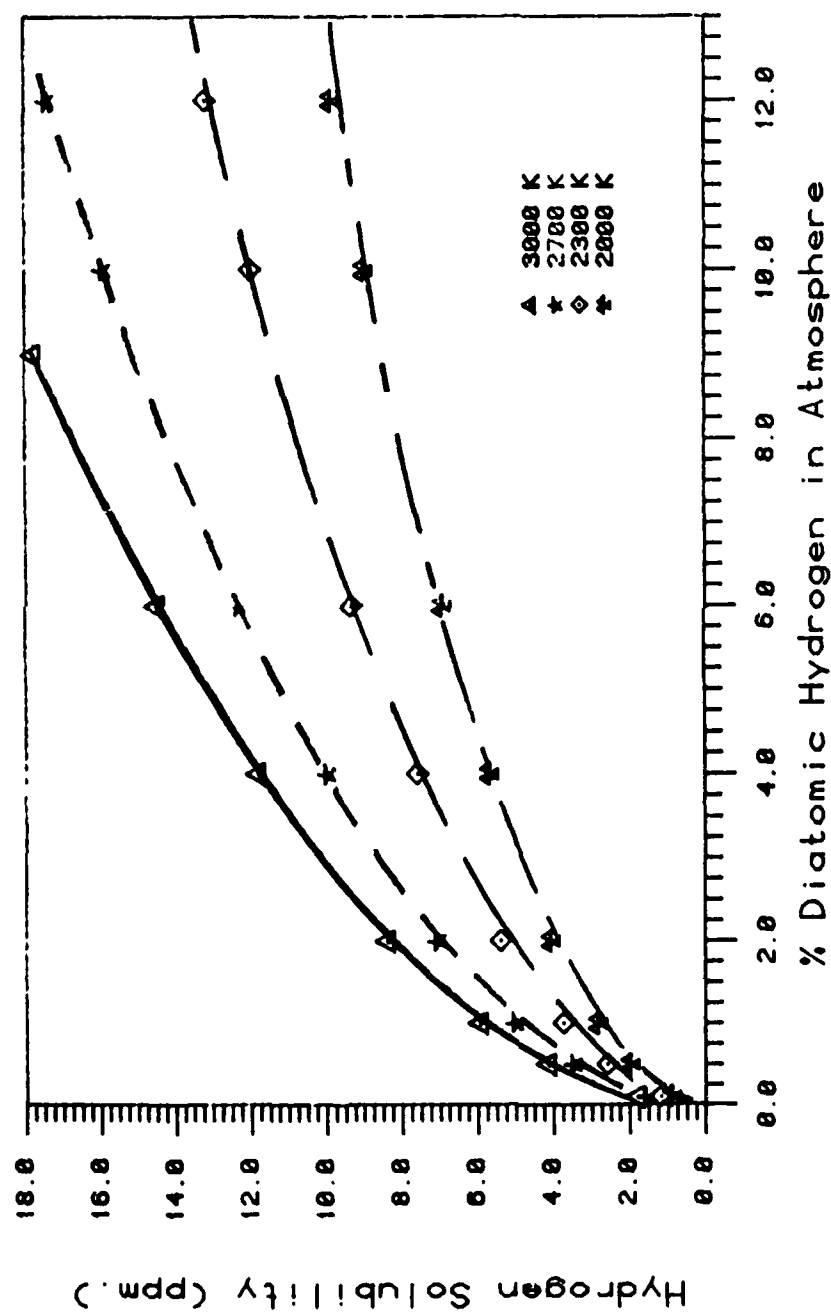
initial argon	$P_{Ar}' = .95$	$n_{Ar}' = .95$
initial diatomic hydrogen	$P_{H_2}' = .05$	$n_{H_2}' = .05$
initial monatomic hydrogen	$P_H' = 0$	$n_H' = 0$
initial total	$P_t' = 1$	$n_t' = 1$
final argon	$P_{Ar} = ?$	$n_{Ar} = .95$
final diatomic hydrogen	$P_{H_2} = ?$	$n_{H_2} = ?$
final monatomic hydrogen	$P_H = ?$	$n_H = ?$
final total	$P_t = 1$	$n_t = ?$

Table 3.3 Hydrogen adsorption as a function of assumed reaction temperature and percent hydrogen

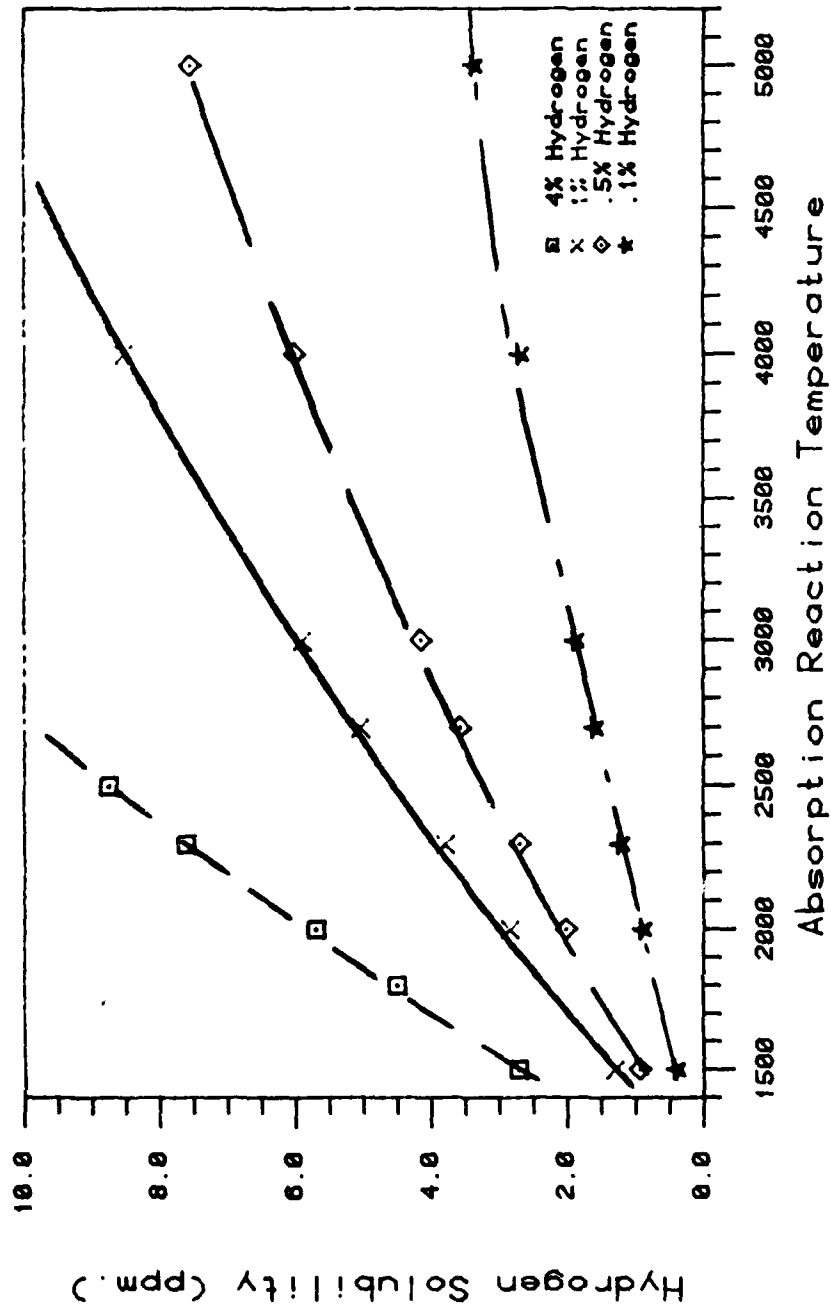
% Hydrogen	Temperature (degrees K)	% Dissoc	Pressure Diatomic (atm)	Pressure Monatomic (atm)	Hydrogen due to Diatomic (ppm)	Hydrogen due to Monatomic (ppm)	Hydrogen Total (ppm)
1%	2000 K	1.0 %	.0099	.0002	2.84	2.85	5.70
1%	2100 K	1.9 %	.00981	.00038	3.15	3.16	6.31
1%	2200 K	3.3 %	.00967	.00067	3.42	3.42	6.84
1%	2300 K	5.5 %	.00945	.0011	3.69	3.69	7.38
1%	2400 K	9.0 %	.0091	.0018	3.93	3.93	7.86
1%	2500 K	13.5 %	.00865	.0027	4.12	4.12	8.24
1%	2600 K	20.0 %	.0080	.0040	4.23	4.23	8.46
1%	2700 K	25.3 %	.00747	.0056	4.33	4.33	8.66
1%	2800 K	37.6 %	.00624	.00752	4.27	4.27	8.54
1%	3000 K	58.0 %	.0042	.0116	3.85	3.85	7.70
.5%	2100 K	2.3 %	.00487	.00026	2.21	2.21	4.42
.5%	2300 K	7.8 %	.00461	.00078	2.57	2.57	5.12
.5%	2400 K	12.5 %	.004375	.00125	2.73	2.73	5.46
.5%	2500 K	18.8 %	.00406	.00188	2.84	2.84	5.63
.5%	2600 K	27.0 %	.00365	.0027	2.86	2.86	5.72
.5%	2700 K	37.0 %	.00315	.0037	2.84	2.84	5.68
.1%	2000 K	3.1 %	.000969	.000062	.89	.89	1.78
.1%	2200 K	10.2 %	.000898	.000204	1.045	1.045	2.09
.1%	2400 K	25.5 %	.000745	.00051	1.15	1.13	2.26
.1%	2500 K	37.0 %	.00063	.00074	1.11	1.11	2.22
.1%	2600 K	49.0 %	.00051	.00102	1.07	1.07	2.14
.1%	2800 K	74.0 %	.00026	.00148	.85	.85	1.70

Table 3.4 Hydrogen adsorption as a function of assumed dissociation and adsorption reaction temperatures

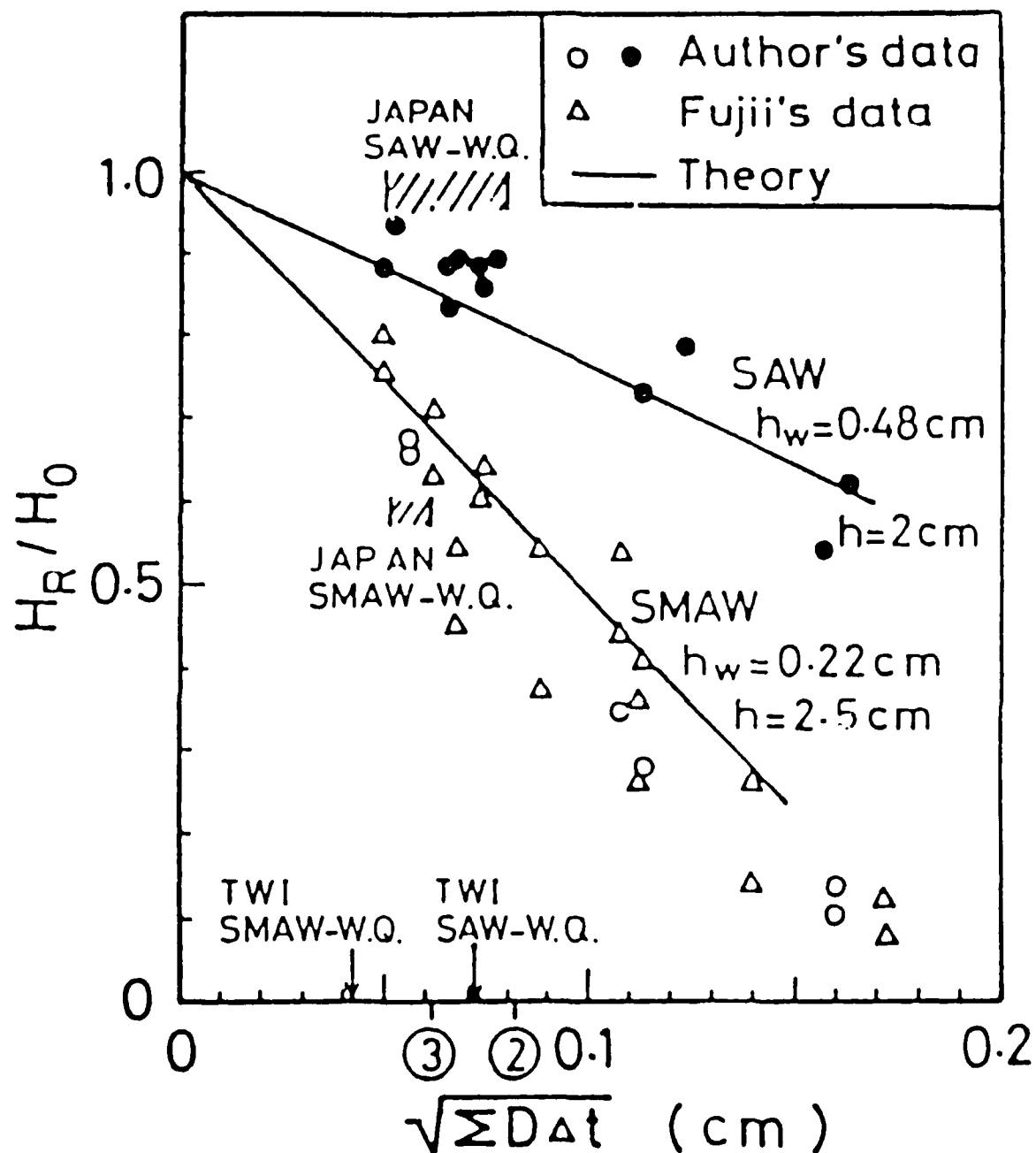
% Hydrogen	Dissociate Temperature (degrees K)	% Dissoc	Pressure		Adsorb Temp.	Hydrogen due to		Total Hydrogen (ppm)
			Diatomic (atm)	Monatomic (atm)		Diatomic (ppm)	Monatomic (ppm)	
1 %	3000 K	58.0 %	.0042	.0116	2100 K	2.05	96.9	98.95
1 %	3000 K	58.0 %	.0042	.0116	2300 K	2.46	38.1	40.56
1 %	3000 K	58.0 %	.0042	.0116	2500 K	2.87	17.4	20.27
1 %	3000 K	58.0 %	.0042	.0116	2700 K	3.27	8.9	12.17
1 %	2700 K	25.3 %	.00747	.0056	2100 K	2.74	46.8	49.54
1 %	2700 K	25.3 %	.00747	.0056	2300 K	3.28	18.4	21.68
1 %	2700 K	25.3 %	.00747	.0056	2500 K	3.83	8.4	12.23
1 %	2700 K	25.3 %	.00747	.0056	2700 K	4.33	4.33	8.66
1 %	2500 K	13.5 %	.00865	.00275	2100 K	2.95	22.9	25.85
1 %	2500 K	13.5 %	.00865	.00275	2300 K	3.53	9.0	12.53
1 %	2300 K	5.5 %	.00945	.0011	1900 K	2.47	28.4	30.87
1 %	2300 K	5.5 %	.00945	.0011	2100 K	3.08	9.2	12.28
1 %	2500 K	13.5 %	.00865	.0056	2250 K	3.39	11.2	14.59
1 %	2100 K	1.9 %	.00981	.00038	1900 K	2.52	9.82	12.34



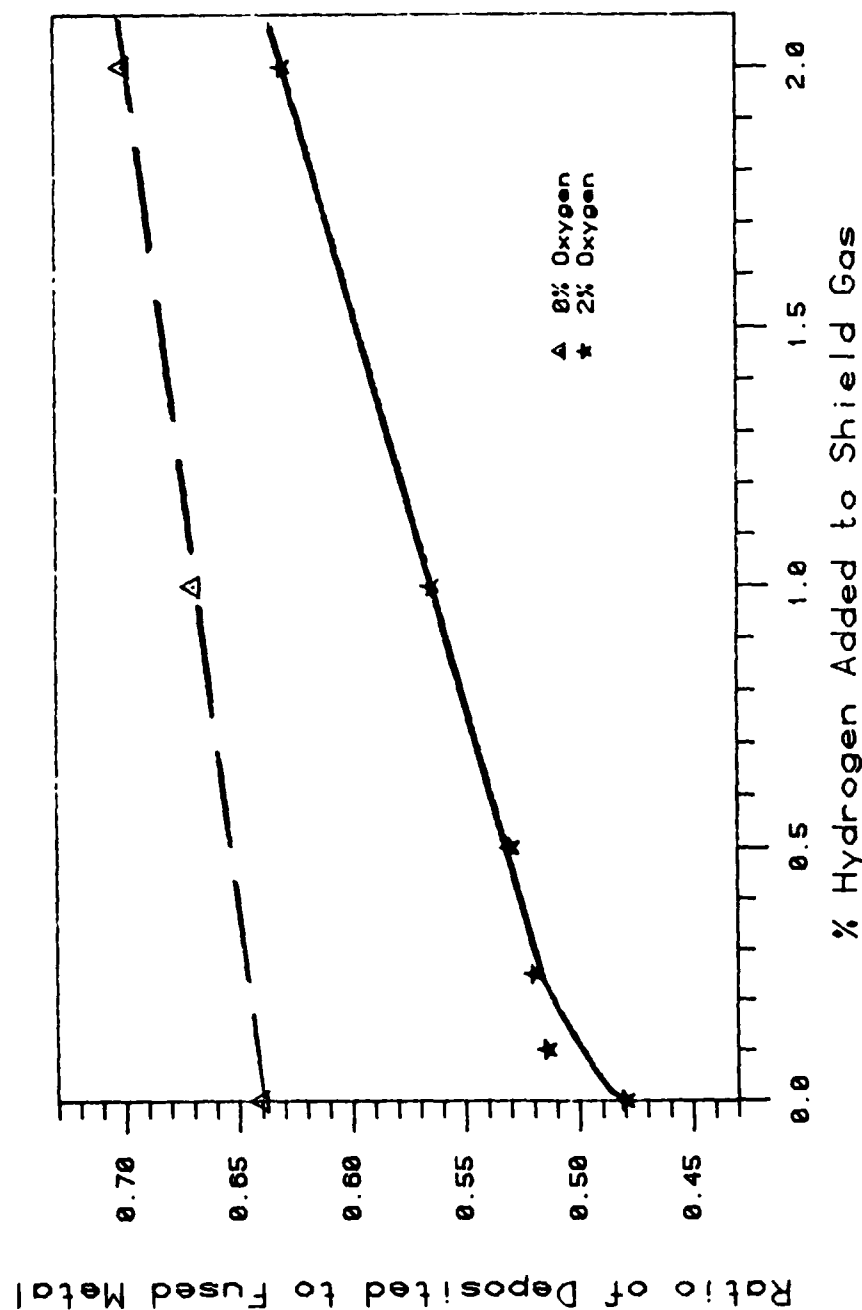
3.1 Equilibrium hydrogen solubility as a function of diatomic hydrogen partial pressure for various assumed absorption temperatures.



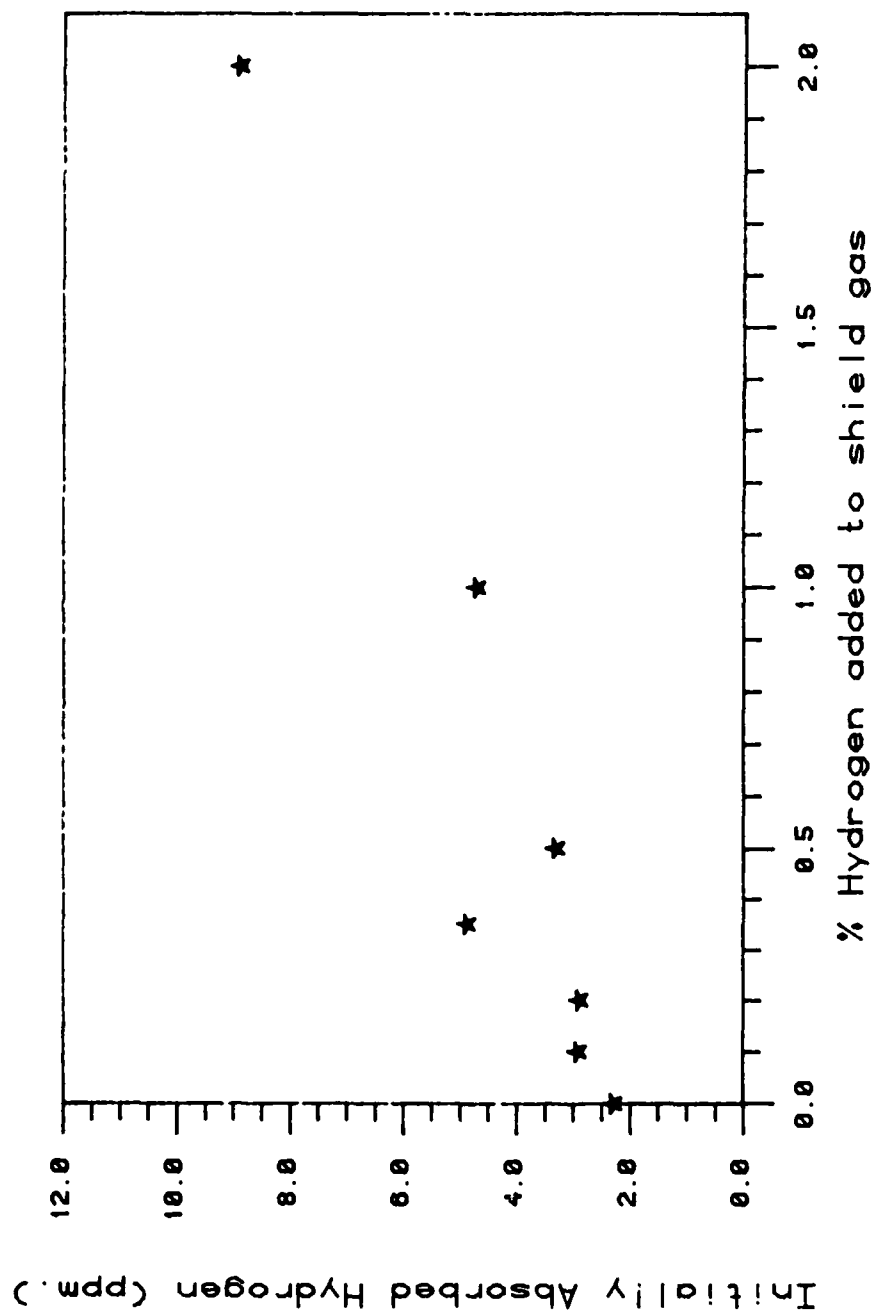
3.2 Equilibrium hydrogen solubility as a function of the absorption temperature for various diatomic hydrogen partial pressures.



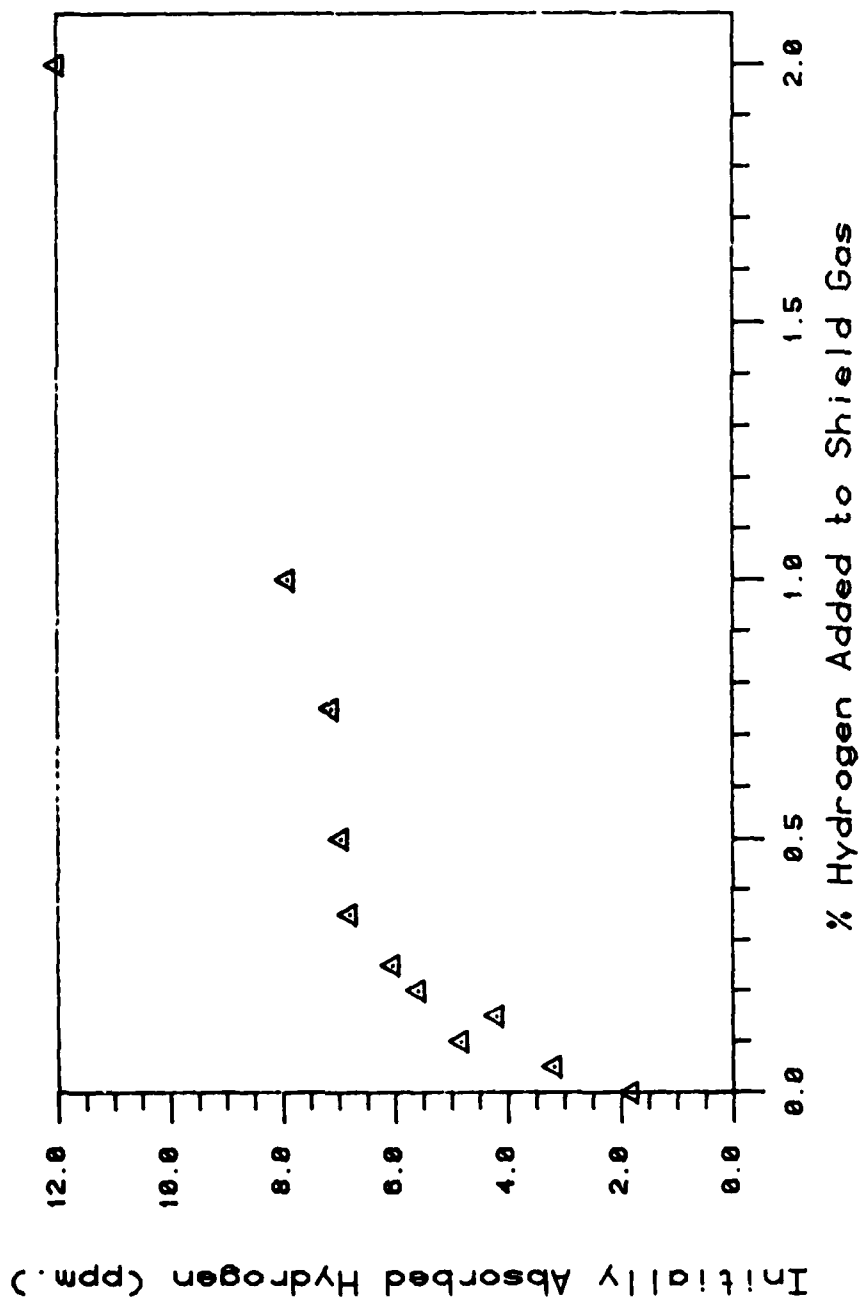
3.3 Ratio of retained hydrogen to initially absorbed hydrogen as a function of the "thermal factor". (Ref T.4)



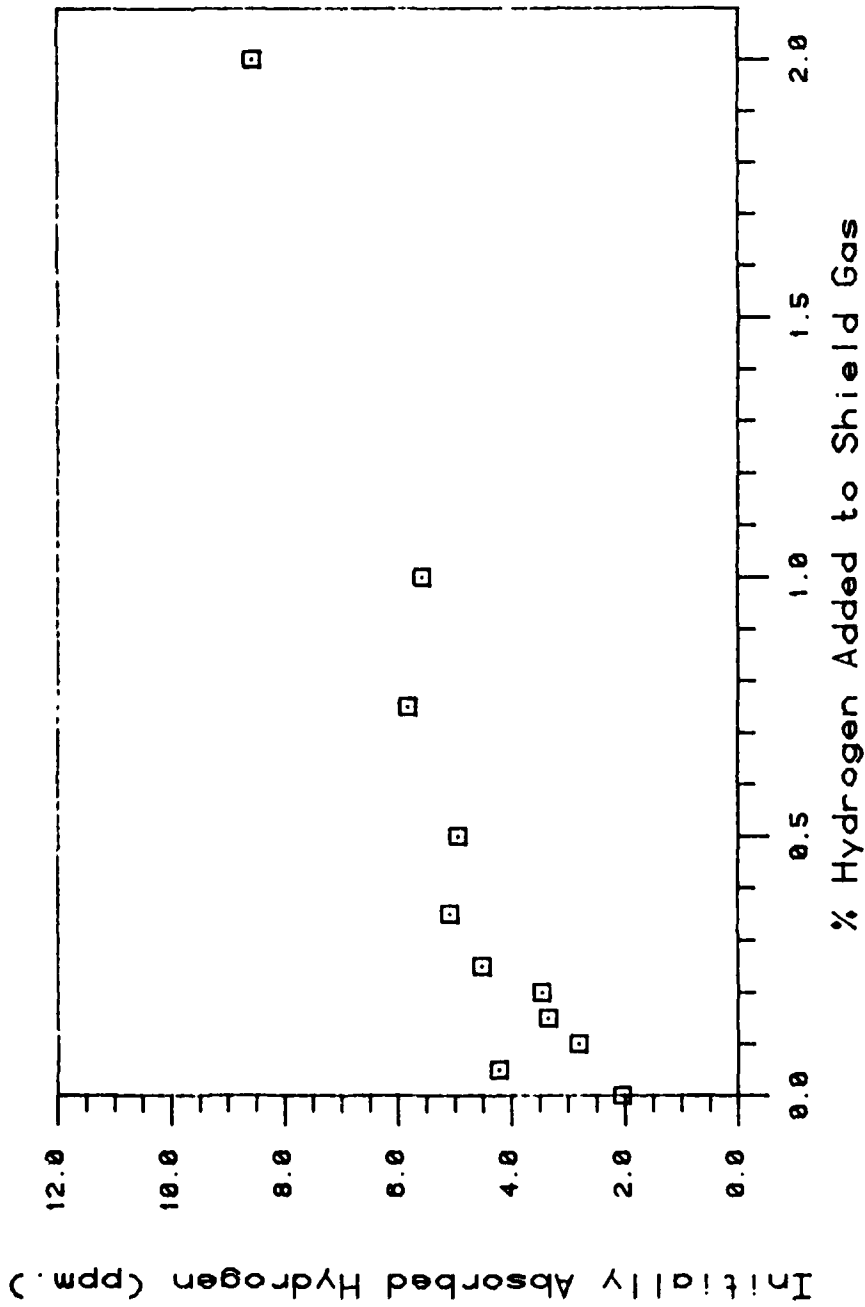
3.4 Ratio of deposited metal to fused metal as a function of hydrogen in the shielding gas for pure argon and Ar/2% O₂.



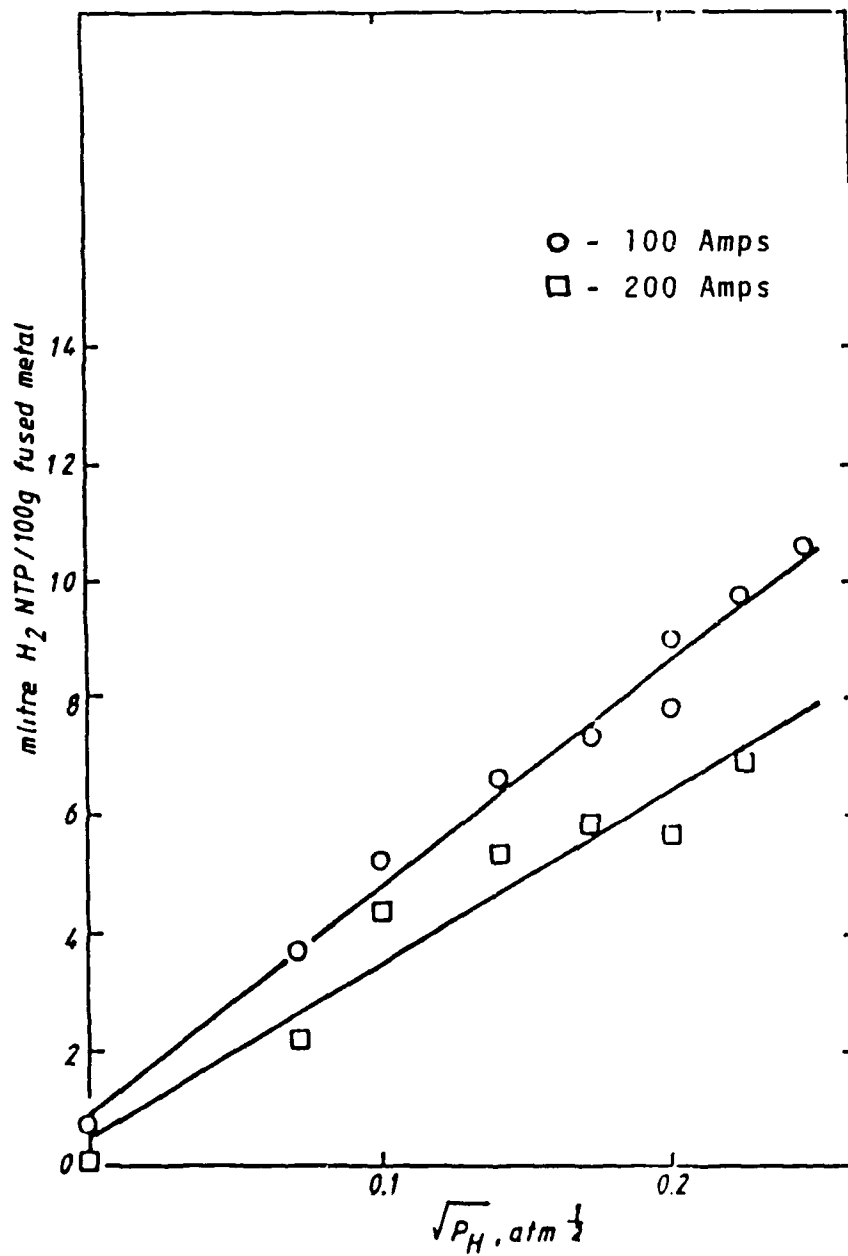
3.5 Initially absorbed hydrogen as a function of hydrogen in pure argon shielding gas. (A36)



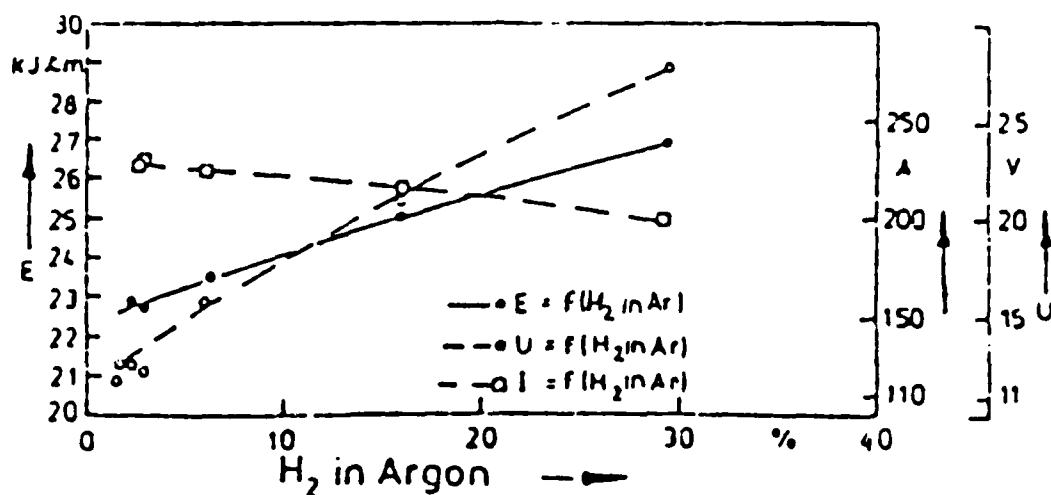
3.6 Initially absorbed hydrogen as a function of hydrogen in Ar/2% O₂ shielding gas. (A36)



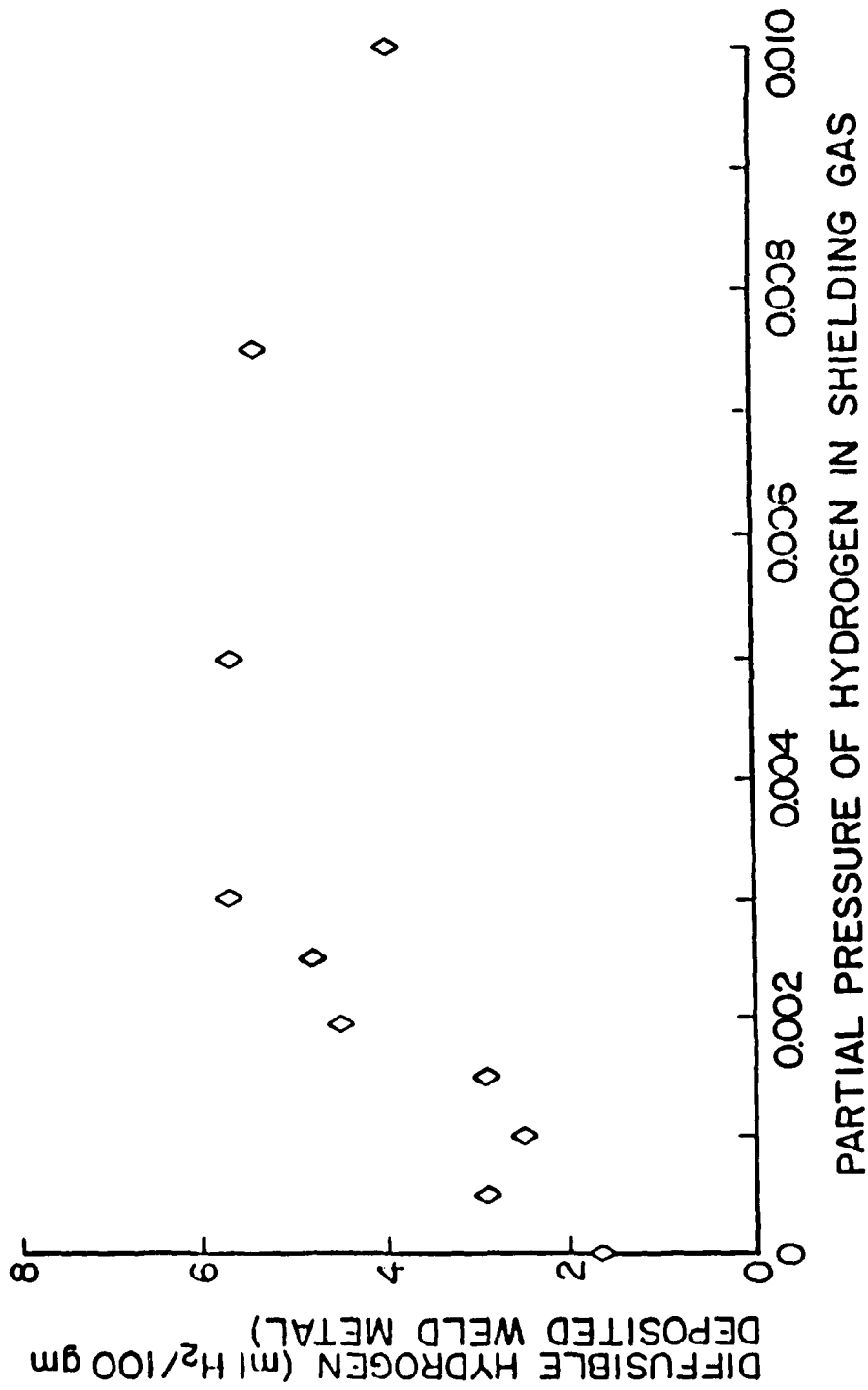
3.7 Initially absorbed hydrogen as a function of hydrogen in Ar/2% CO₂ shielding gas. (A36)



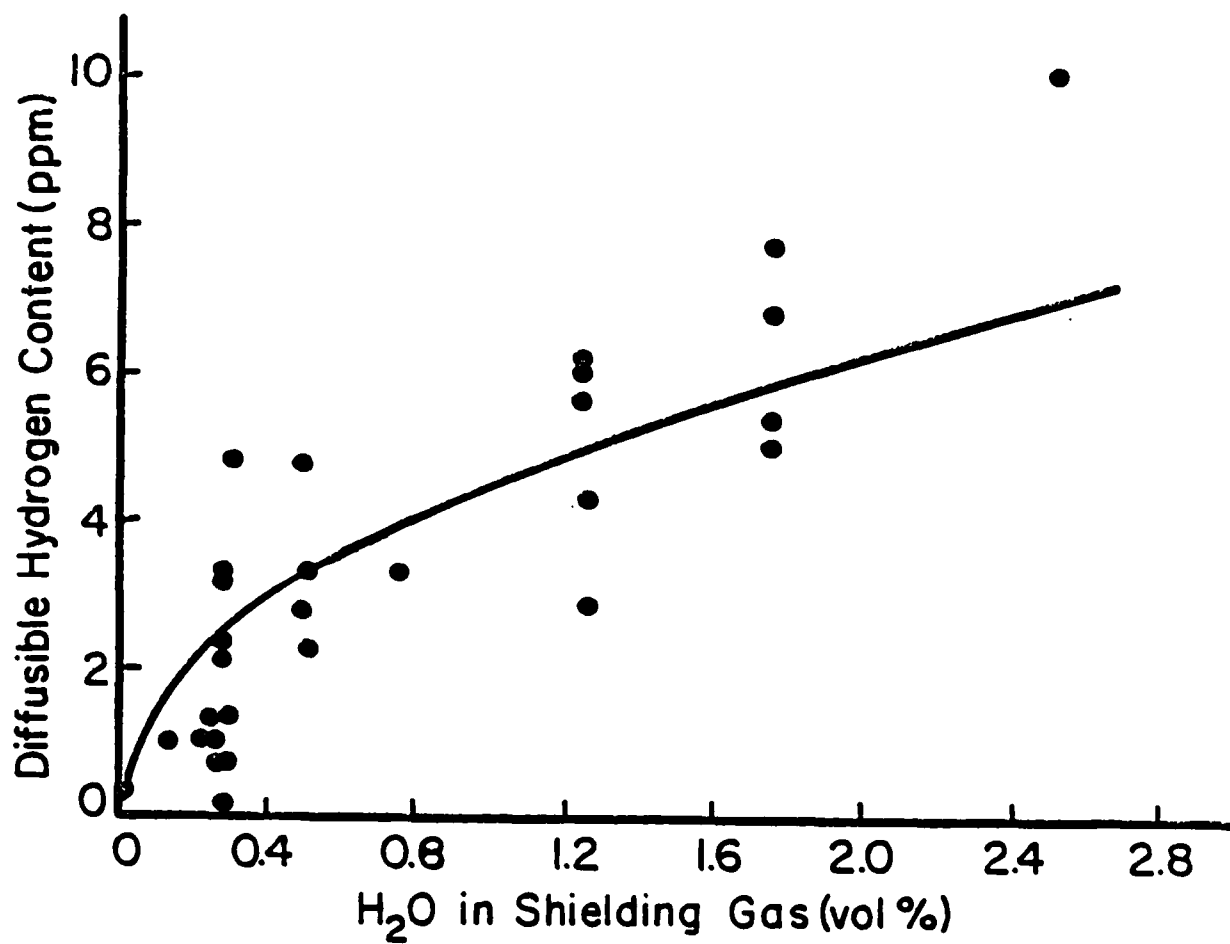
3.8 Measured hydrogen content of GTA weld metal as a function of the square root of hydrogen partial pressure. (Ref. C.7)



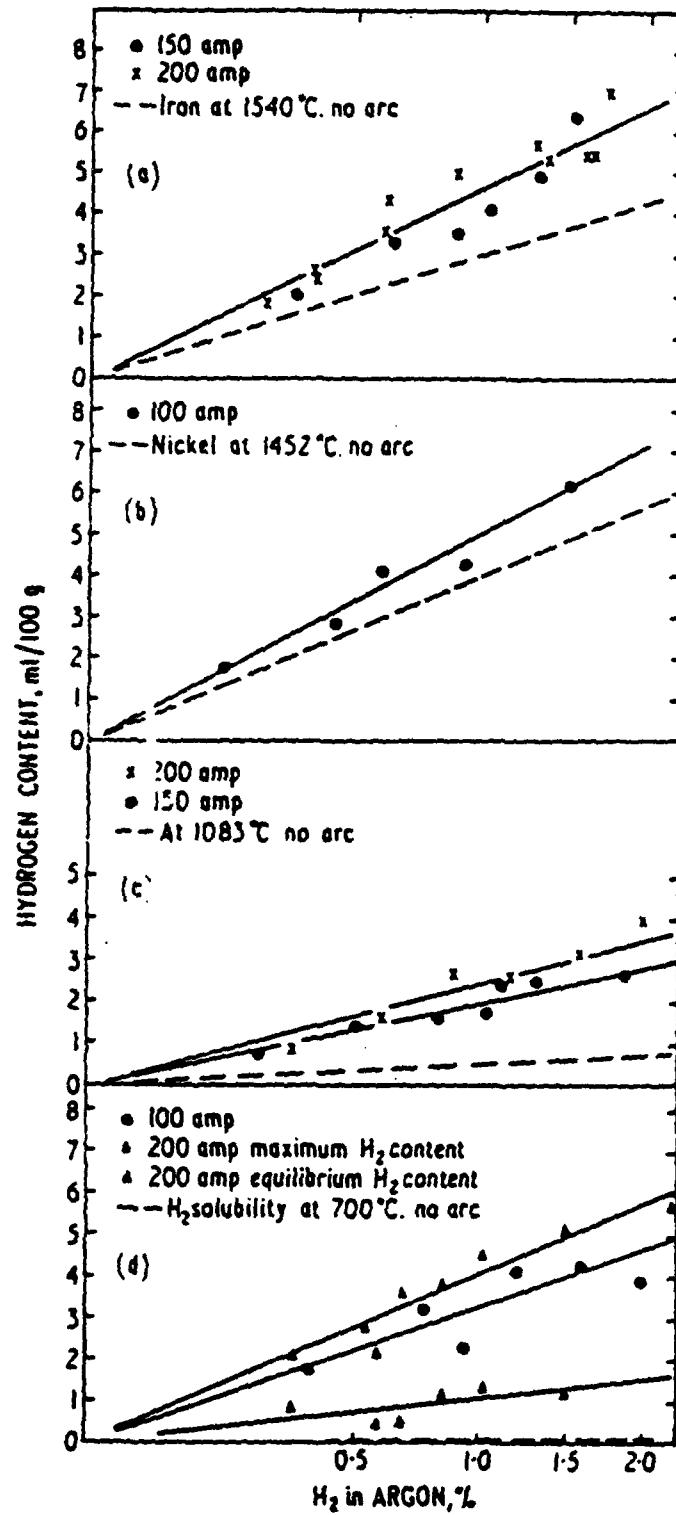
3.9 Variation in weld current, voltage, and heat input as a function of hydrogen in the shield gas. (Ref F.4)



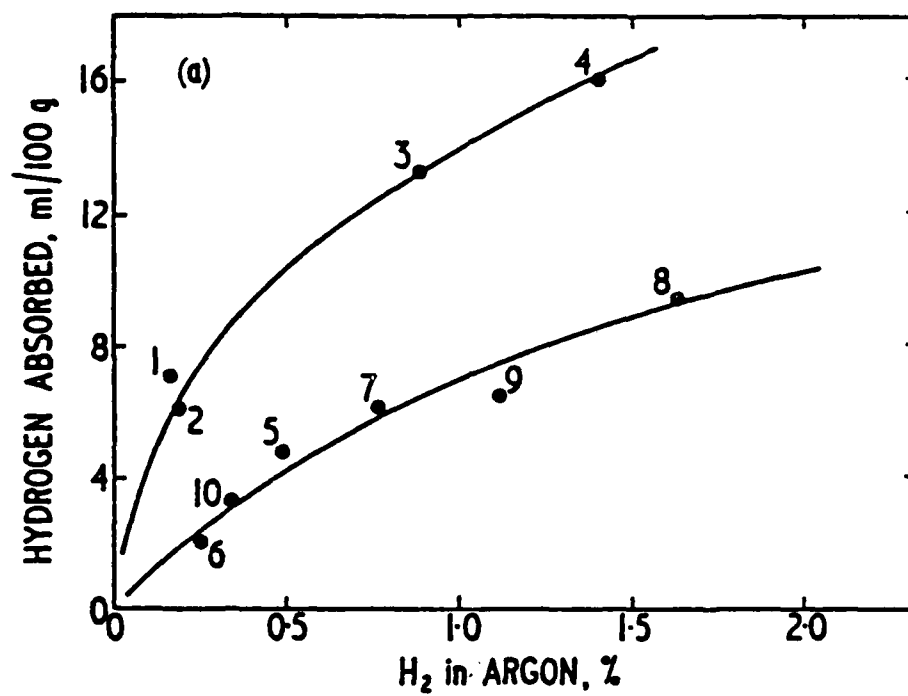
3.10 Diffusible weld hydrogen content as a function of GMAW shield gas hydrogen content. (Ref W.8)



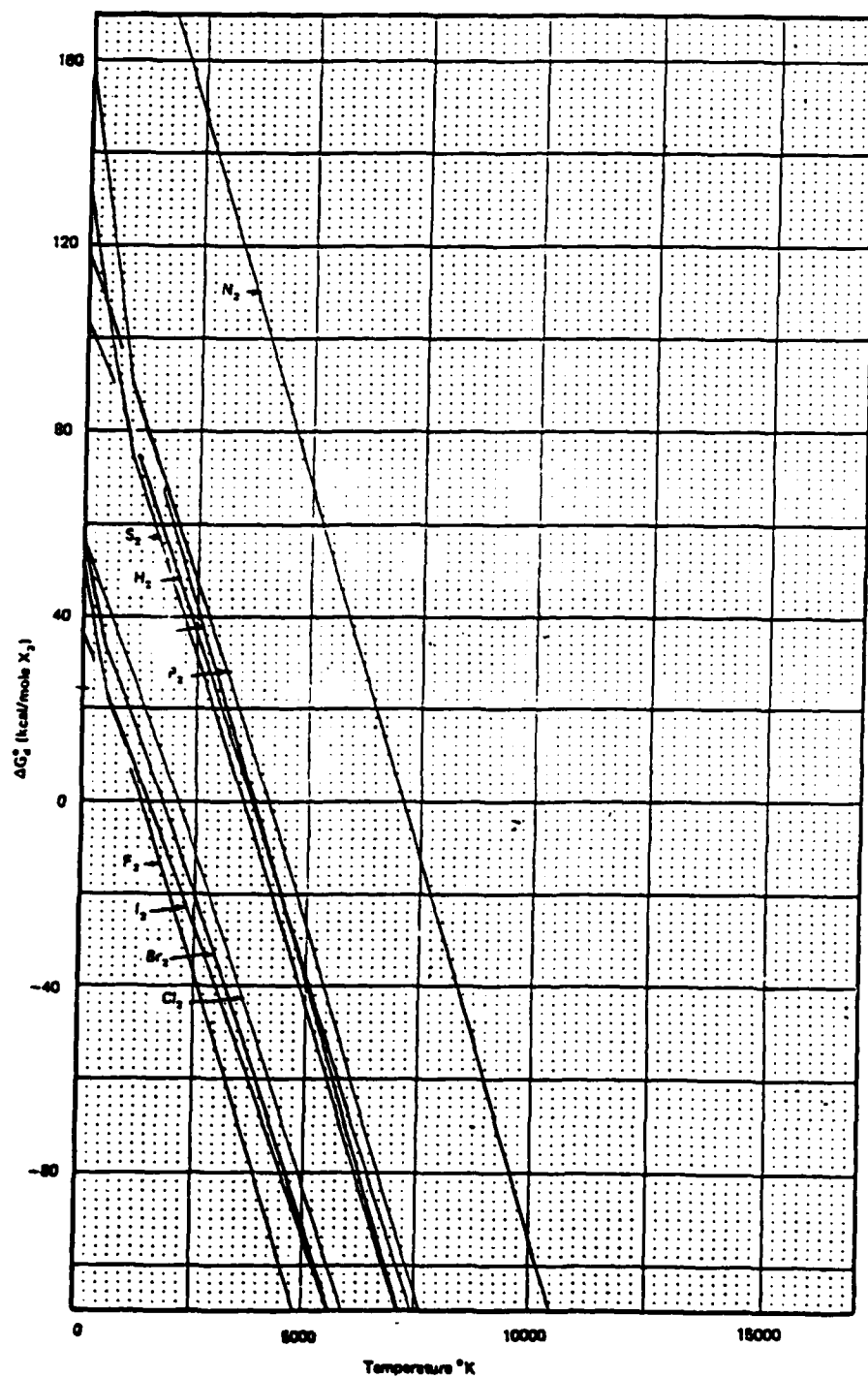
3.11 Diffusible hydrogen content of pulsed GMAW welds on a fusion zone basis with moisture additions to the shield gas. (Ref S.6)



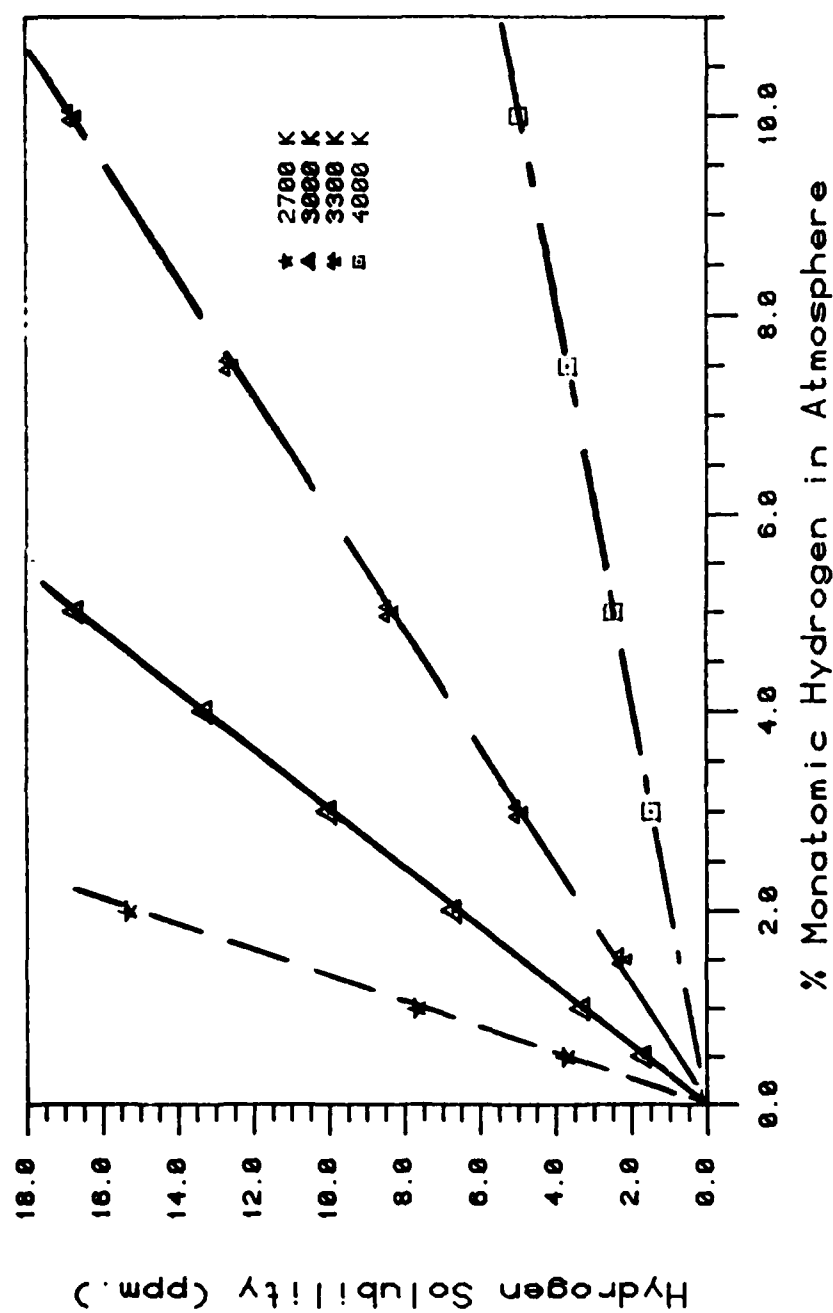
3.12 Variation of hydrogen content with hydrogen partial pressure at different currents for: (a) Armeo iron; (b) nickel; (c) copper; (d) aluminium. (Ref. R.17)



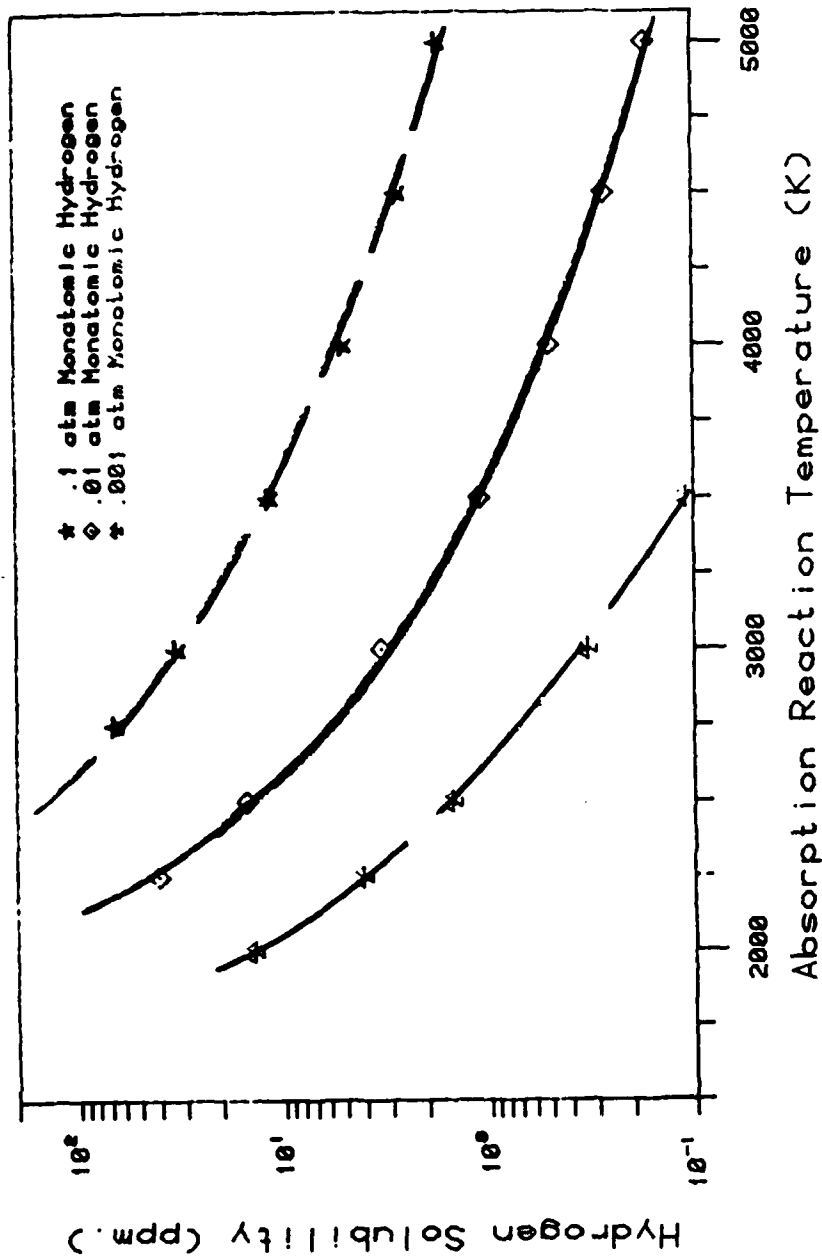
3.13 Results of a series of determinations of hydrogen absorption by iron containing oxide (numbers give the order of testing). (Ref H.18)



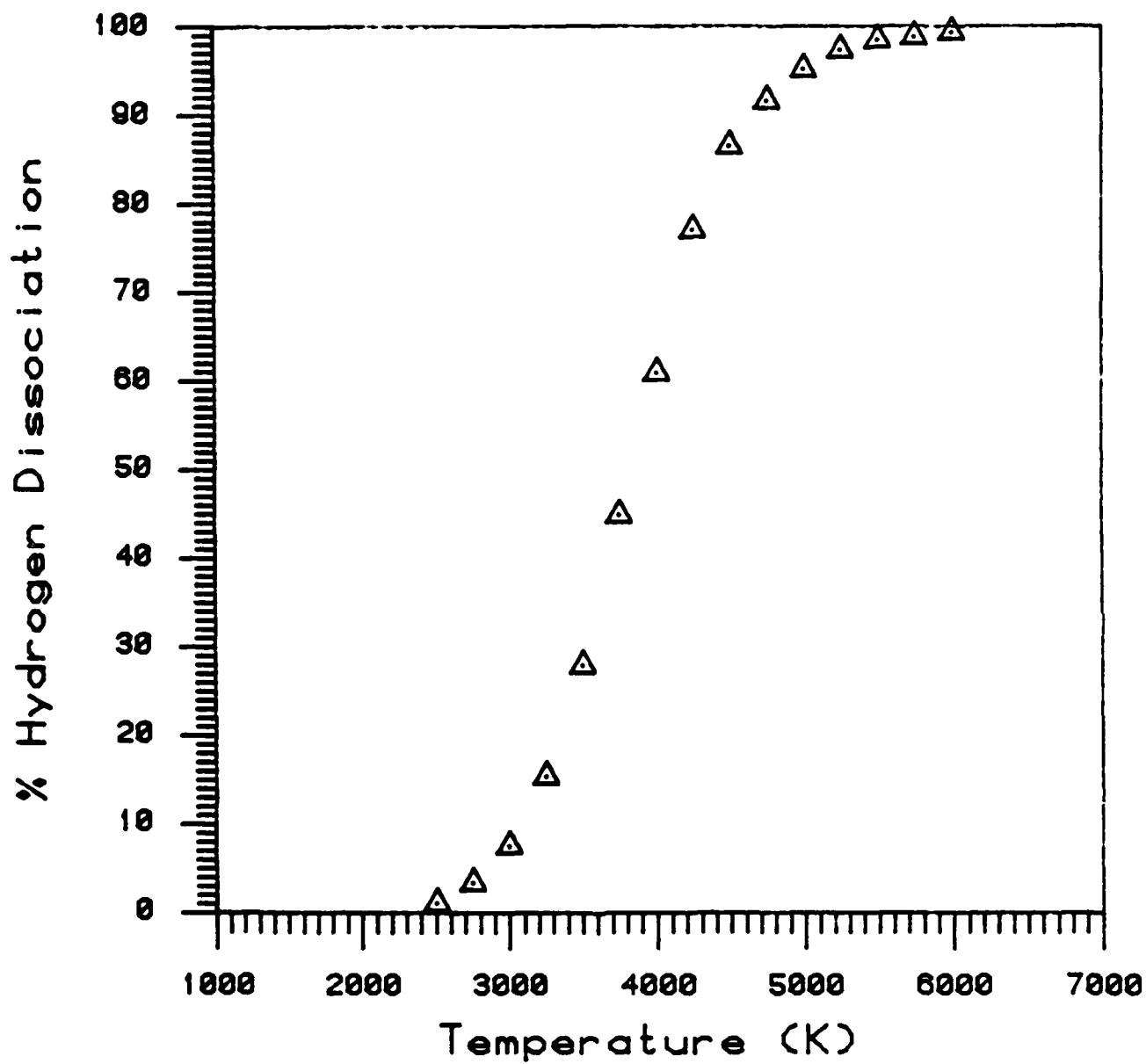
3.14 Free energy of dissociation of diatomic gases.



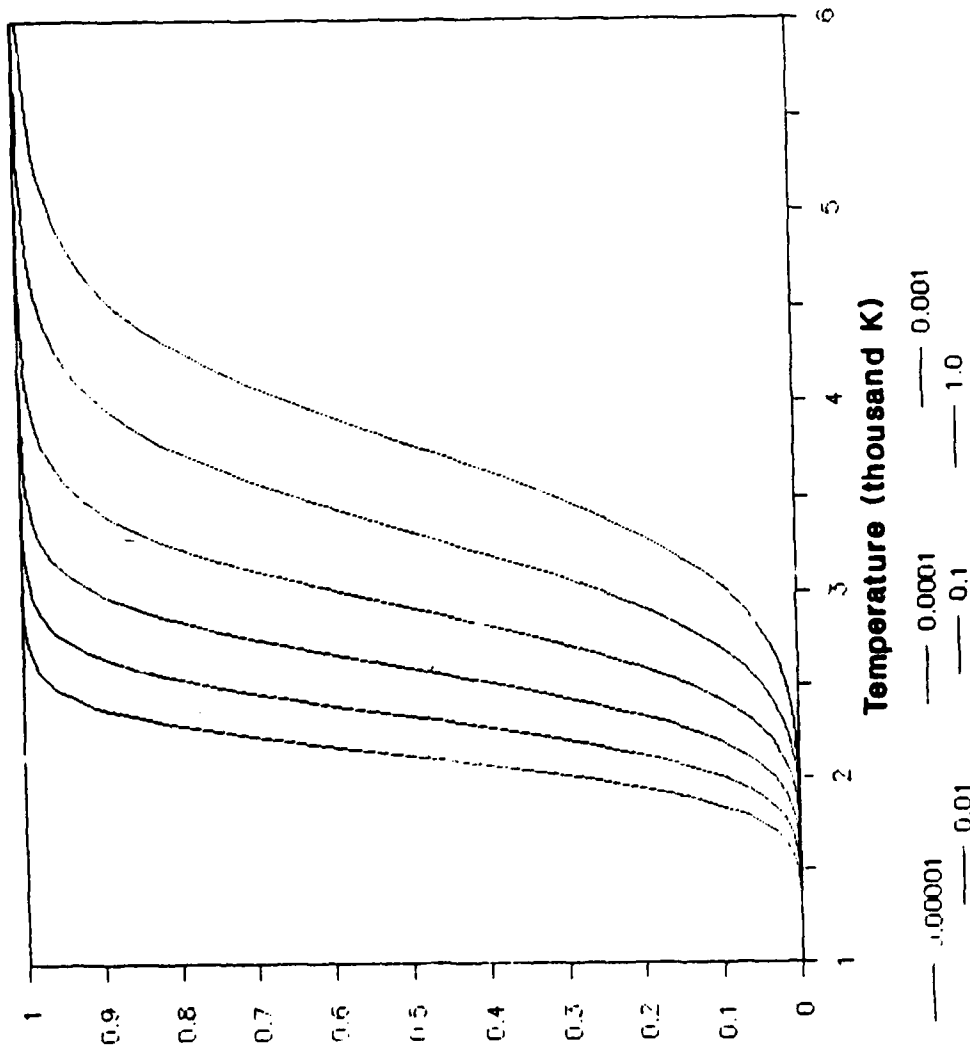
3.15 Equilibrium hydrogen solubility as a function of the partial pressure of monatomic hydrogen gas for various assumed absorption temperatures.



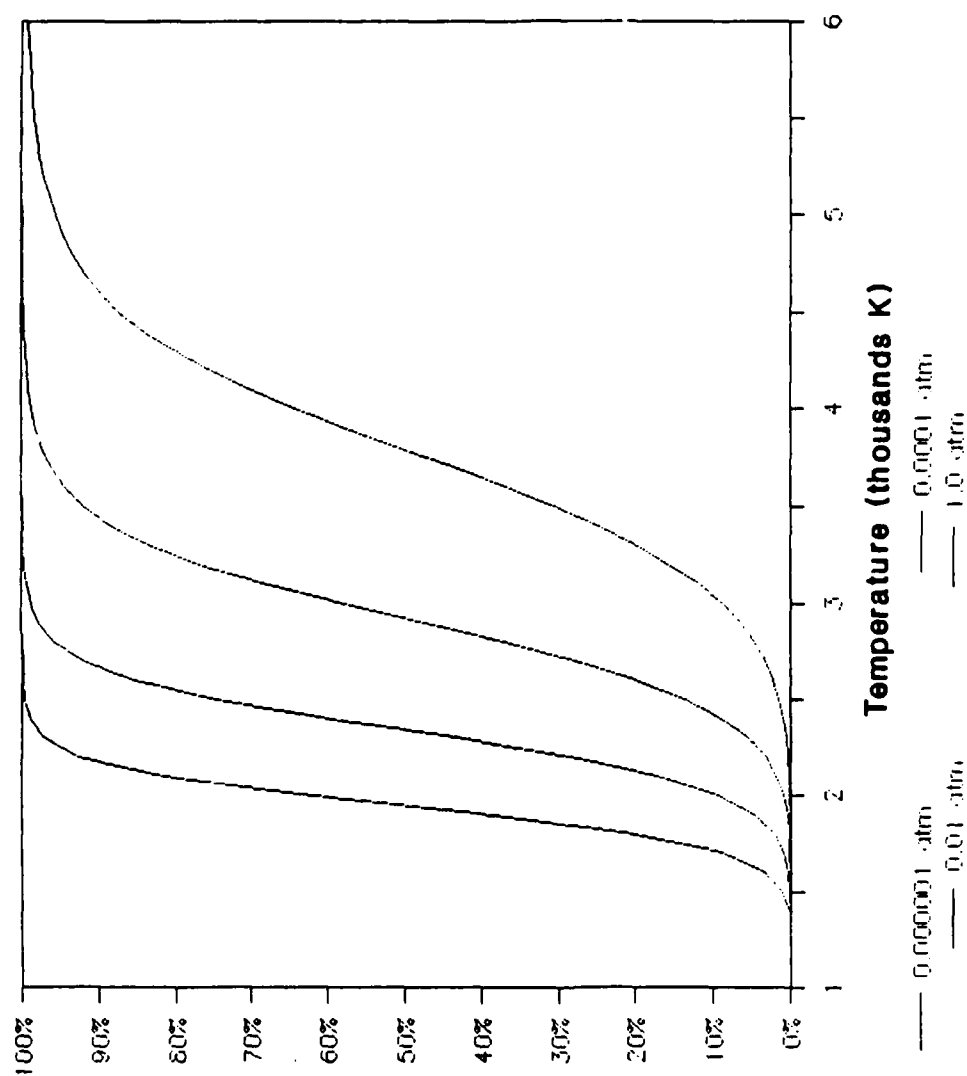
3.16 Equilibrium hydrogen solubility as a function of the absorption temperature for various partial pressures of monatomic hydrogen.



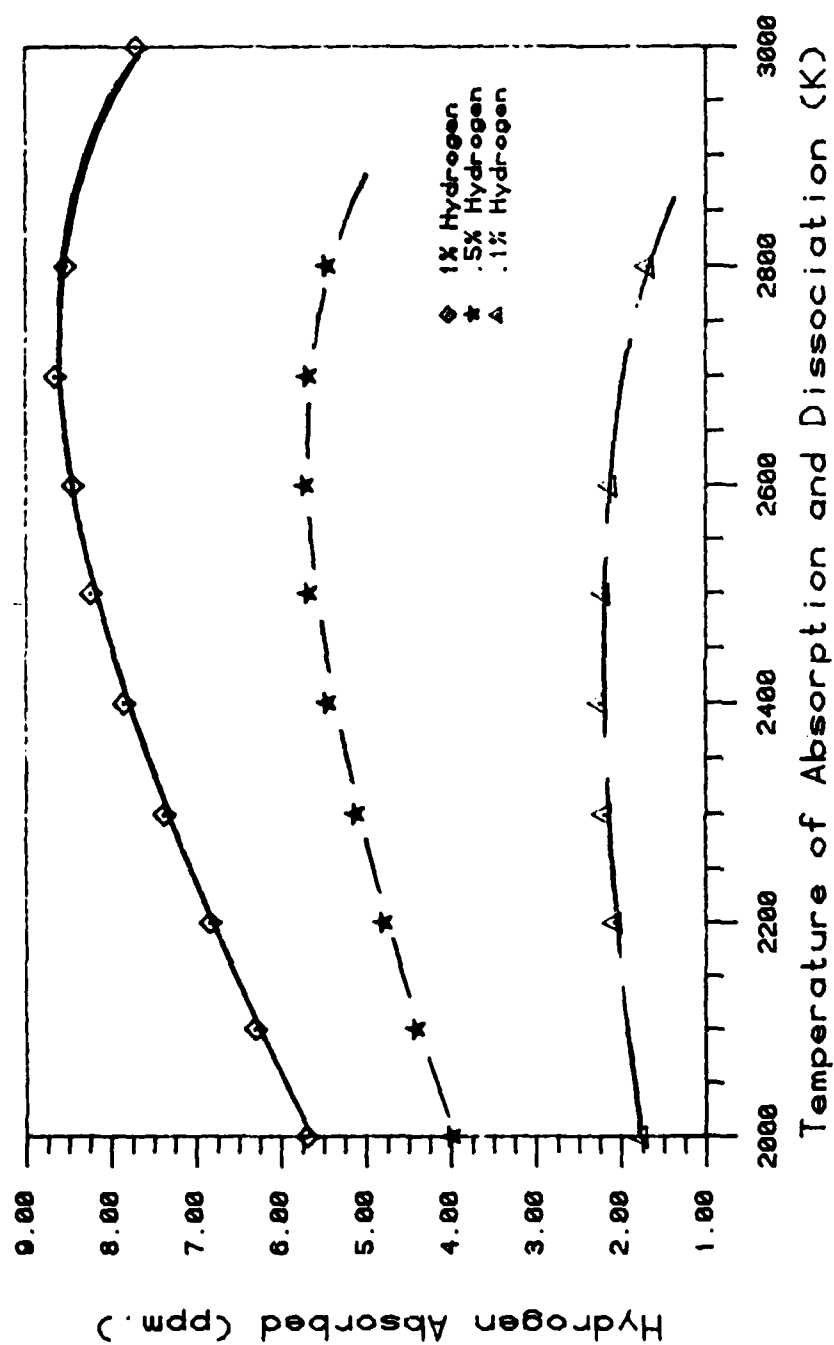
3.17 Percent hydrogen dissociation as a function of temperature, 1 atm pressure. (Ref. C.9)



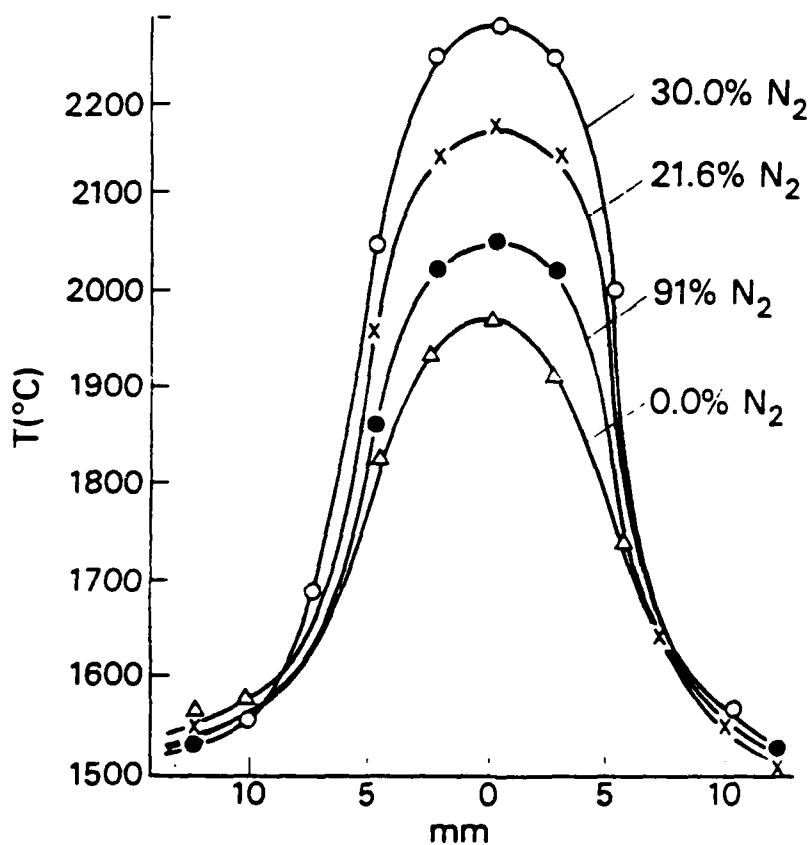
3.18 Percent hydrogen dissociation as a function of both pressure and temperature. Curves are from right: 1 atm, .1 atm, .01 atm, .001 atm, .0001 atm, and .00001 atm hydrogen partial pressure.



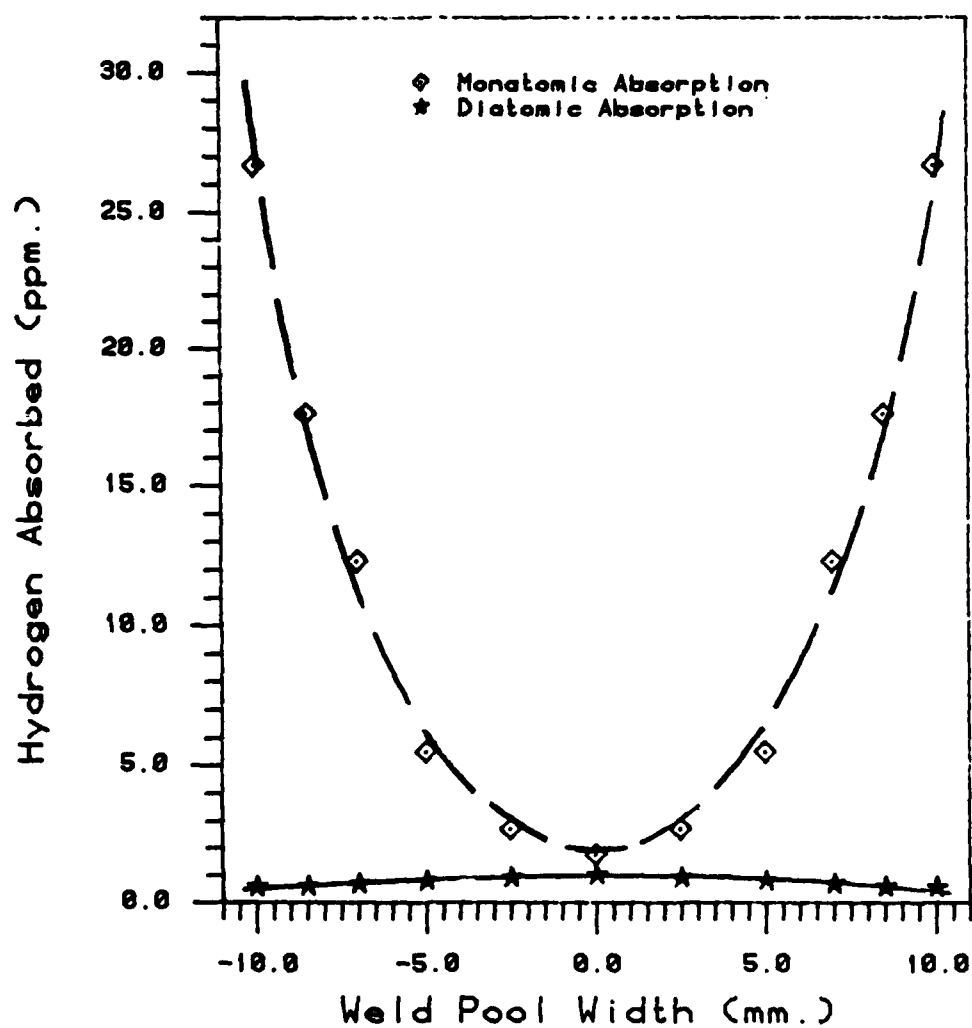
3.19 Percent hydrogen dissociation as a function of both pressure and temperature. Curves are from right: 10^0 atm, 10^{-2} atm, 10^{-4} atm, and 10^{-6} atm hydrogen partial pressure.



3.20 Theoretical hydrogen solubility as a function of assumed hydrogen dissociation and absorption temperature.



3.21 Temperature distribution on the surface of arc-melted iron. Shielding gas argon and various additions of nitrogen; current 80A. (Erokin 1978)



3.22 Theoretical hydrogen absorption due to monatomic and diatomic hydrogen as a function of weld pool location. Calculation assumes a dissociation temperature of 2500 C, an absorption temperature as given above, and .01 atm hydrogen.

THE EFFECT OF Fe-C-H-O PHASE RELATIONSHIPS ON
HYDROGEN ABSORPTION IN WELD POOLS

4.0 ABSTRACT

Available thermodynamic data has been used to construct Fe-H-O and Fe-C-H ternary phase diagrams which were never published previously. These ternary systems and the previously published system Fe-C-O are combined to develop slices through the quaternary Fe-C-H-O system. These systems are then used to explain the effect of weld shielding gas composition on the absorption of hydrogen in weld pools.

When welding with O_2 in the shielding gas, all available H_2 will be in the form of the more thermodynamically stable H_2O . Thus, hydrogen absorption will be governed by the Fe-H-O phase diagram.

When welding with CO_2 in the shielding gas, there will be finite amounts of both H_2 and H_2O . The ensuing hydrogen levels will be intermediate between welds made with O_2 (hydrogen absorption governed by the Fe-H-O phase diagram), and those made with pure argon (hydrogen absorption governed by the Fe-H phase diagram).

4.1 GENERAL PHASE EQUILIBRIA

Several good texts explaining the necessary conditions for phase equilibria and the rules for constructing multicomponent phase diagrams exist. Gaskell (G2) is an excellent introductory text and explains the basics of thermodynamic equilibrium in single and binary systems, as well as reactions involving gases and condensed phases. Rhines (R2) offers an explanation of the various types of binary and ternary systems. Masing (M3) provides a good introduction to applications of the phase rule in multicomponent systems. Other more complex and comprehensive treatments of multicomponent systems include Prince (P13), and Palatnik and Landau (P1).

Another excellent document which gives a short, concise explanation of some of the concepts involved in gas-metal reactions occurring in molten steel was written by Elliot (E5, E6). These concepts are needed to adequately construct new ternary and quaternary phase diagrams.

4.2 THERMODYNAMIC DATA

The problem of determining new phase diagrams can be approached with the aid of available thermodynamic data and the generalized rules governing phase diagrams treated in the above references. Data from the binary phase systems which bound the ternary are needed. For our systems of

interest we need Fe-H, Fe-C, Fe-O, H-O, C-O, and C-H.

Binary phase diagrams are shown in figures 4.1 - 4.4 for the Fe systems. Thermodynamic data, freezing point depression data, and segregation coefficients which can be found in the literature and are needed for this work, are shown in tables 4.1 - 4.3. Since the freezing point depression data for hydrogen in iron has never been determined experimentally, it must be calculated from basic principles (E7). The relationship between the segregation coefficient (k) and the effect of an alloying element on the melting point of iron can be derived with the use of the Gibbs-Helmholtz equation as was shown by Elliot (E5). If it is assumed that iron in the liquid and solid phases follows Raoultian behavior, the following equation can be written:

$$\ln \left[X_{Fe} (l) / X_{Fe} (s) \right] = \Delta H_m / R \left[1/T_m - 1/T \right] \quad (4.1)$$

where $X_{Fe} (l)$ and $X_{Fe} (s)$ are the mole fractions of iron in the equilibrium liquid and solid, respectively. ΔH_m is the enthalpy of fusion, T_m is the melting temperature, and R is the universal gas constant. Thus the freezing point coefficient for hydrogen in iron can be calculated to be 1500 degrees C per weight percent hydrogen (or .198 C/ppm). This value has been listed in table 4.2.

4.3 EQUILIBRIUM PHASE RELATIONSHIPS DURING SOLIDIFICATION

4.3.1 THE Fe-H-O TERNARY SYSTEM

For the purpose of illustrating the phase relationships of interest, a series of polythermal projections onto the basal Fe-H-O plane will be presented. These projections will then be used to understand the effect of oxygen on the absorption of hydrogen into the molten weld pool.

The equilibrium solubility of hydrogen and oxygen in liquid iron at 1538 C (the melting temperature of iron) can be calculated by combining the free energy data in table 4.1 into the following equation:

$$\text{H}_2\text{O (g)} = 2\text{H (ppm)} + \text{O (\%)} \quad (4.2)$$

for which the free energy is:

$$G^0 = 49440 - 36.67 T \text{ (cal/g atom)} \quad (4.3)$$

thus:

$$24879/T - 18.45 = \ln \frac{\text{H}^2 \text{ O}}{P_{\text{H}_2\text{O}}} \quad (4.4)$$

Figure 4.5 is a polythermal projection of this relationship. The lines represent surfaces of saturation of the liquid (or solid) with respect to another phase. The coordinates are solubility of hydrogen in parts per million vertically, and solubility of oxygen in weight percent horizontally. The figure shows that variations in the partial pressure of H_2O have a significant effect of the solubility of oxygen and hydrogen in liquid iron.

For consistency of presentation, the following series of polythermal projections at lower temperatures have been developed for .01 atmospheres water vapor except where noted otherwise. This system is relevant for welding applications using an argon-oxygen gas mixture contaminated with small amounts of hydrogen.

As the temperature is lowered, delta iron will precipitate out of the liquid phase. The resulting lines of two-fold saturation can be calculated from the freezing point depression data in table 4.2. The equilibrium freezing temperature of the liquidus is:

$$T_m - T = 69 (\% O) + .198 (\text{ppm } H) \quad (4.5)$$

The equilibrium freezing temperature of the solidus can be calculated by combining equation 4.4 with the distribution coefficients in table 4.3.

$$T_m - T = 69/.059 (\% \underline{O}) + .198/.27 (\text{ppm } \underline{H}) \quad (4.6)$$

The resulting polythermal projection at 1537 °C is shown in figure 4.6.

As the temperature is lowered to 1533 °C, the Fe-H phase diagram shows that delta iron will be in equilibrium with hydrogen gas according to the following reaction:



Also, the lines of two-fold saturation of the 2 phase field ($\delta + \text{liq}$) and the single phase field (liq) will touch. The ensuing projection is shown in figure 4.7. The 3-phase field ($\delta + \text{liq} + \text{gas}$) must touch at a point on the H-O binary edge of the phase diagram. This point can be calculated using the free energy data for:



which at 1806 °K is:

$$K = 16683 = P_{H_2O} / P_{H_2} P_{O_2}^{1/2} \quad (4.9)$$

The partial pressure of oxygen can be calculated from the reaction:

$$1/2 O_2 (g) = \underline{O} \quad (4.10)$$

for which:

$$K = \underline{O} / P_{O_2}^{1/2} \quad (4.11)$$

Knowing the solubility of oxygen at the point of 3-fold saturation in the polythermal projection in figure 4.7 to be .062%, the partial pressure of oxygen can be calculated from equation 4.11 and substituted into equation 4.9 to yield the ratio:

$$P_{H_2O} / P_{H_2} = .299 \quad (4.12)$$

Since the total gas pressure ($P_{H_2O} + P_{H_2} + P_{O_2}$) is .01 atm, the 3-phase field will touch the H-O binary at 92% hydrogen.

As the temperature is further reduced to 1538 C, the lines of 2-fold saturation shift to the positions shown in figure 4.8.

Upon further reduction in temperature, a monotectic reaction occurs in the Fe-O binary system. This results in the previous liquid phase being replaced with an oxygen rich liquid slag. In order to calculate the point where the 3-phase field intersects the H-O binary once the oxygen rich liquid enters the diagram, one must turn to the Fe-O binary system for information about the partial pressure of oxygen. Muan and Osborn have described this information on the phase diagram shown in figure 4.4, which indicates the partial pressure of oxygen above the liquid at various temperatures. At 1520 C, this value is about 10^{-9} atmospheres. Using this value, the resulting polythermal projection is shown in figure 4.9.

The ratio of water vapor to hydrogen will not change significantly even with the temperature decreasing to 1400 C. Below this temperature the oxygen rich liquid will solidify and no further hydrogen absorption is possible.

In order to examine the effect of varying the amount of oxygen and hydrogen in the weld shielding gas, a series of polythermal projections is shown for .001% and .05% water vapor in figures 4.10 - 4.12. Once below 1520 C, the oxygen rich liquid phase will control the partial pressure of oxygen, and all of the polythermal projections will be the same, even with variations in the water vapor percentage.

4.3.2 THE Fe-C-H TERNARY SYSTEM

Before the effect of CO_2 on hydrogen absorption in weld pools can be understood, the Fe-C-H ternary system must be established in order to construct the Fe-C-H-O quaternary. The Fe-C-H system will be developed by presenting a series of polythermal projections onto the basal plane in the iron rich corner of the ternary.

The equilibrium solubility of hydrogen and carbon in liquid iron at the melting temperature of iron (1538 C) can be determined with the free energy data in table 4.1 to yield:

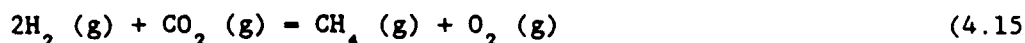
$$\text{CH}_4 \text{ (g)} = 4\text{H (ppm)} + \text{C (wt. pct.)} \quad (4.13)$$

for which the free energy is:

$$G^0 = 62,380 - 80.63 T \text{ (cal / g atom)} \quad (4.14)$$

Figure 4.13 shows the resulting solubility at various partial pressures of methane gas. The methane partial pressure of interest in this study was chosen by a brief analysis of how much would be present in a combination of CO_2 and H_2 gases at the melting temperature of iron. The

following reaction was chosen:



which has a free energy of:

$$G^\circ = 72,655 + 26.43 T \text{ (cal / g atom)} \quad (4.16)$$

therefore, at the melting temperature of iron:

$$2.86 \times 10^{-15} = (P_{\text{CH}_4}) (P_{\text{O}_2}) / (P_{\text{H}_2})^2 (P_{\text{CO}_2}) \quad (4.17)$$

If about .1% oxygen and 10ppm hydrogen are expected in the molten iron, the relationships $1/2 \text{ O}_2 (\text{g}) = \underline{\text{O}}$ and $1/2 \text{ H}_2 (\text{g}) = \underline{\text{H}}$ can be used to determine the partial pressures of oxygen and hydrogen. Substituting these values into equation 4.17 and knowing the total pressure to be 1 atmosphere, the partial pressure of methane will equal about 10^{-7} atmospheres.

The following series of polythermal projections onto the iron rich corner of the Fe-C-H basal plane will be presented for a methane partial pressure of 10^{-7} atmospheres.

As the temperature is lowered to 1533 C, the equilibrium freezing temperature of the liquidus and solidus will be governed by relations similar to equations 4.5 and 4.6 using the data in tables 4.2 and 4.3. At this temperature, the 2 phase δ + liquid field will touch the single phase liquid field creating the 3 phase δ + liquid + gas field. This 3 phase field can be determined to touch the C-H binary very close to 100% hydrogen. The ensuing lines of two-fold and three-fold saturation are shown in figure 4.14.

Once the temperature falls below 1495 C, the austenite peritectic reaction will occur. The ensuing projection at 1490 C is shown in figure 4.16. Note that liquid will still be present at this temperature. For the high strength steel used in the present study, there will still be liquid present until about 1460 C. Non-equilibrium solidification conditions will lower this temperature still further.

4.3.3 THE Fe-C-O TERNARY SYSTEM

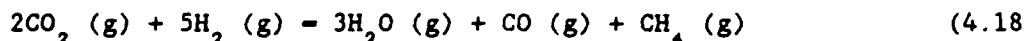
This ternary system has been developed in the doctoral thesis of Wright (W10). The polythermal projections developed by Wright at 1528, 1520, and 1490 C are reproduced in figures 4.17 through 4.19.

All of these ternaries were developed for a total pressure of one atmosphere carbon monoxide. A reduction in this pressure will not substantially alter the projections shown. The only difference will be that

carbon and oxygen will be slightly less soluble in the liquid phase.

4.3.4 THE Fe-C-H-O QUATERNARY SYSTEM

In order to develop the complete Fe-C-H-O quaternary phase diagram, the partial pressures associated with each of the three ternaries bordering the iron corner must be determined. The following equation must be solved:



for which the free energy is:

$$\Delta G = -40,790 + 48.07 T \text{ (Kcal/mole)} \quad (4.19)$$

Unfortunately, the complex and unknown relationship between the partial pressures during welding will preclude a detailed knowledge of the partial pressures in all three ternaries.

A more realistic task is to assume that the carbon content of the weld remains fairly constant and to develop slices through the quaternary at constant carbon content near the iron rich corner.

Figure 4.20 shows a slice through the Fe-C-H-O quaternary at 1528 C and .4% carbon. The intersection on the lines of two and three fold saturation with the Fe-O and Fe-H edges of this figure are found from the Fe-C-O and Fe-C-H ternaries at .4% carbon. All of the lines bordering the three phase regions will touch at the C-H-O side of the quaternary. The specific point where these lines meet will depend on the partial pressures above the molten iron.

Figure 4.21 is a slice at 1490 C and .4% carbon showing the resulting lines once equilibrium with γ and the FeO slag phases is established. Figure 4.22 shows a slice at a much lower carbon content (.1% carbon) at 1528 C.

4.4 THE EFFECT OF OXYGEN AND CARBON DIOXIDE IN GMAW SHIELDING GASES ON HYDROGEN ABSORPTION IN WELD POOLS

This theoretical discussion is aimed at using the previously developed phase diagrams to explain the experimental results presented in chapter 2. The principal experimental result is that welds made with oxygen in the shielding gas absorb more hydrogen than those made with carbon dioxide, which absorb more than those made in pure argon.

At molten weld pool temperatures, H_2O is more thermodynamically stable than either H_2 or O_2 (determined from equation 4.9). In fact, the

free energy of H_2O formation will remain negative until over 4000 K, which is well in excess of the relevant cathode boundary layer temperature calculated in chapter 3. Thus, as long as there is sufficient oxygen present in the weld shield gas, hydrogen absorption will be governed by the Fe-H-O phase diagram rather than the Fe-H phase diagram.

Consider a weld made with 1% H_2 and no oxygen. According to the equilibrium Fe-H phase diagram in figure 4.2, the resulting solubility in liquid iron at the melting temperature (1537 C) will be about 2 ppm. Non-equilibrium conditions result in the experimentally determined value of 5 ppm. Once at least .5% O_2 is added to the shielding gas, the solubility will be determined by the Fe-H-O phase diagram. According to the equilibrium Fe-H-O phase diagram in figure 4.6, the resulting solubility at 1537 C will vary from about 3 to 12 ppm. (depending on the amount of oxygen in solution). Non-equilibrium conditions result in the experimentally determined value of 10 ppm.

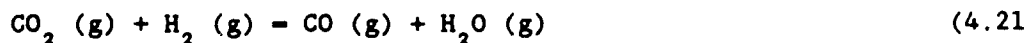
Thus, it can be understood that H_2O results in more hydrogen absorption than H_2 . This theoretical explanation also accounts for the experimental results found by Savage, et al. (S6). They found that moisture was absorbed more readily than hydrogen by GMA weld pools but did not attempt to explain this phenomenon. A sample of their results comparing the diffusible hydrogen contents in welds made with H_2O and H_2 is shown in figures 4.23 and 4.24. The experimental results of Howden and Milner (H18), shown in figure 3.13, are also explained by the increased solubility of hydrogen in melts containing oxygen.

The previous discussion adequately explains how the presence of oxygen increases hydrogen absorption in weld pools. The results can also be explained by the fact that molten iron has a high affinity for oxygen; If hydrogen happens to be bound to the oxygen being absorbed, then the hydrogen is readily absorbed as well.

In the case of welding with carbon dioxide in the shielding gas, the partial pressures governing the solubility of hydrogen are not as easy to determine. The reaction of interest shown in equation 4.18 cannot be solved directly. However, a simpler reaction can be written if the effect of methane is overlooked:



the free energy of which remains positive until slightly over 3000 K. This means that the CO_2 will break down in the arc atmosphere, and not completely recombine in the cathode boundary layer. This finite amount of oxygen will combine with the available hydrogen in the reaction:



for which the free energy equals:

$$\Delta G = 6,555 - 6.24 T \text{ (Kcal/mole)}$$

(4.22)

At the melting temperature K will equal 3.7. This means that there will be a finite amount of both H_2 and H_2O , as well as CO_2 and CO .

Thus, in welds made with carbon dioxide, the hydrogen absorption will be governed by both H_2O and H_2 . This explains the experimental result that welds made with carbon dioxide had more hydrogen than those made in pure argon (absorption governed by H_2) but less than those made with oxygen (absorption governed by H_2O).

The above discussions have explained the effect of carbon dioxide and oxygen additions to argon shielding gas on hydrogen absorption in GMA welds. The only experimental result still to be understood is the effect of carbon content as was shown in figure 2.26. One possible explanation is that the carbon will lower the melting temperature. As was previously shown, monatomic hydrogen absorption into the cooler outer edge of the weld pool will significantly increase the overall amount of absorbed hydrogen. Thus, a lowering of the temperature will increase hydrogen absorption. A second explanation is that increased carbon levels may decrease the partial pressure of oxygen in the arc atmosphere. Reducing the oxygen pressure has been shown to reduce the amount of hydrogen absorbed.

The influence of carbon content on hydrogen absorption is incompletely understood at the present time, and the possible explanations

presented are only tentative. However, it is hoped that the phase diagrams and discussions presented in this dissertation will make it easier for future researchers to analyze this topic.

Table 4.1 Thermodynamic Data used in this study (Ref E.6)

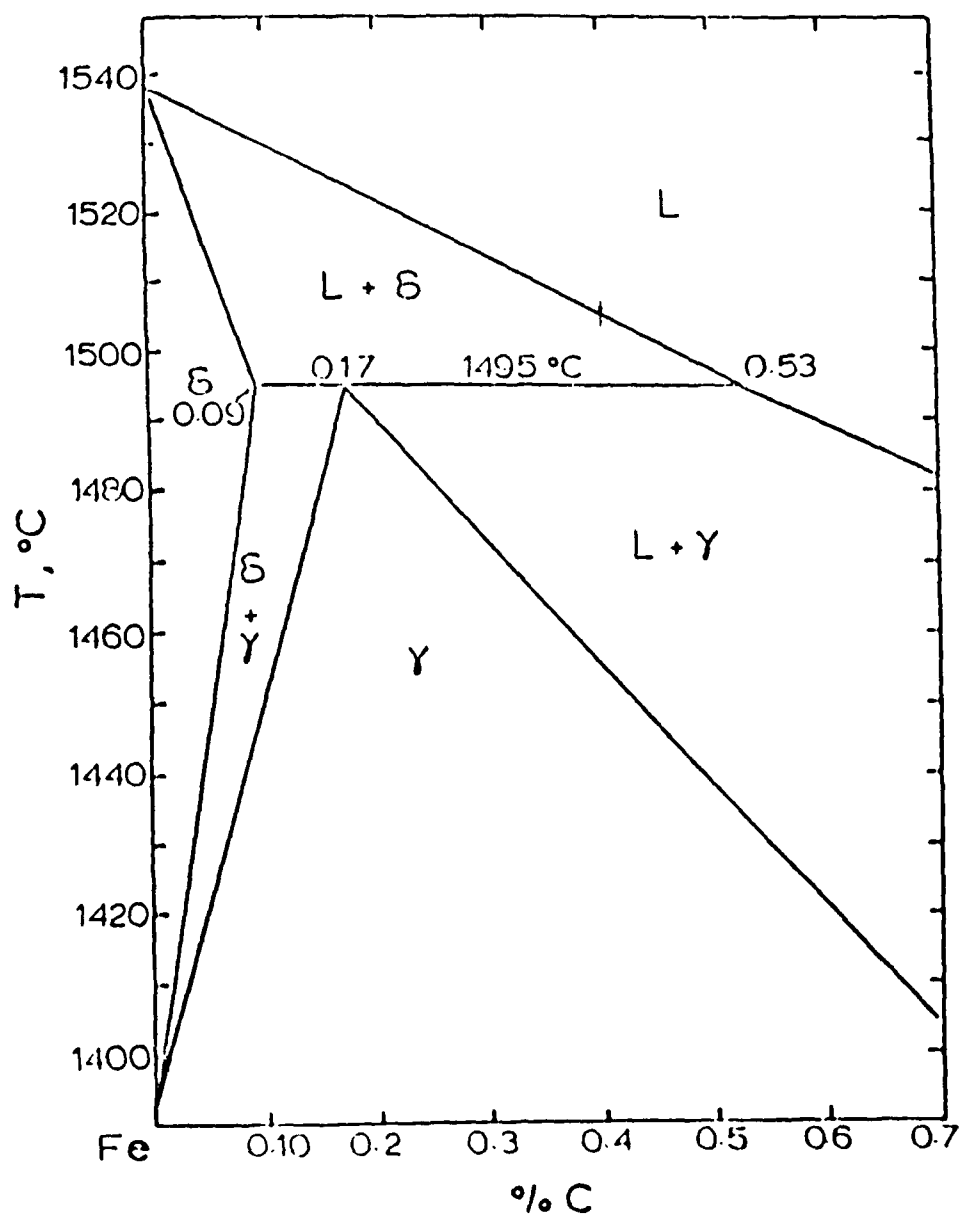
<u>Reaction</u>	<u>Free Energy</u>	
	M (pure)	= M (i.d. wt. %, liq) cal/g atom
$1/2 \text{ H}_2(\text{g}) = \underline{\text{H}}$ (ppm) in liq Fe	$G^0 = 8,720 - 11.02 \text{ T}$	
$1/2 \text{ O}_2(\text{g}) = \underline{\text{O}}$ (%) in liq Fe	$G^0 = -28,000 - .69 \text{ T}$	
$\text{H}_2(\text{g}) = 2\underline{\text{H}}$ (g)	$G^0 = 107,000 - 28.8 \text{ T}$	
C (graphite) = $\underline{\text{C}}$ (%)	$G^0 = 5,400 - 10.1 \text{ T}$	
$\text{H}_2(\text{g}) + 1/2 \text{ O}_2(\text{g}) = \text{H}_2\text{O}(\text{g})$	$G^0 = -60,000 + 13.94 \text{ T}$	
C (graphite) + $1/2 \text{ O}_2(\text{g}) = \text{CO}(\text{g})$	$G^0 = -28,200 - 20.16 \text{ T}$	
C (graphite) + $\text{O}_2(\text{g}) = \text{CO}_2(\text{g})$	$G^0 = -94,755 + .02 \text{ T}$	
$\text{H}_2(\text{g}) + 2 \text{ C}$ (graphite) = $\text{C}_2\text{H}_2(\text{g})$	$G^0 = 52,000 - 11.80 \text{ T}$	
$2 \text{ H}_2(\text{g}) + \text{C}$ (graphite) = $\text{CH}_4(\text{g})$	$G^0 = -22,100 + 26.45 \text{ T}$	

Table 4.3
Distribution Coefficient, k_i , -iron and liquid

Element, i	k_i	Reference
C	.20	E.6
O	.059	E.6
H	.27	

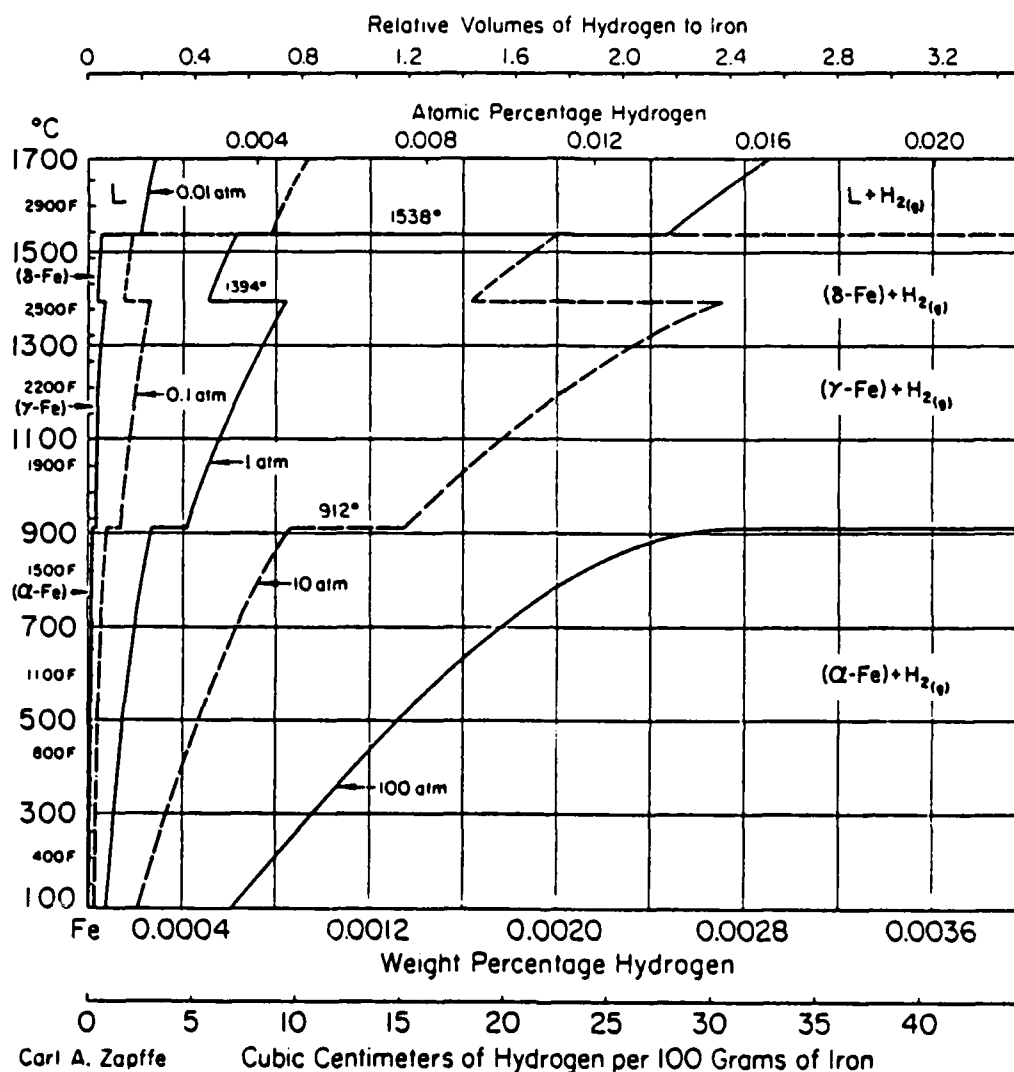
Table 4.2
Freezing Point Depression

Element, i	Constant, A_i ($^{\circ}\text{C}/\%$)	Reference
C	80	E.8
O	69	E.8

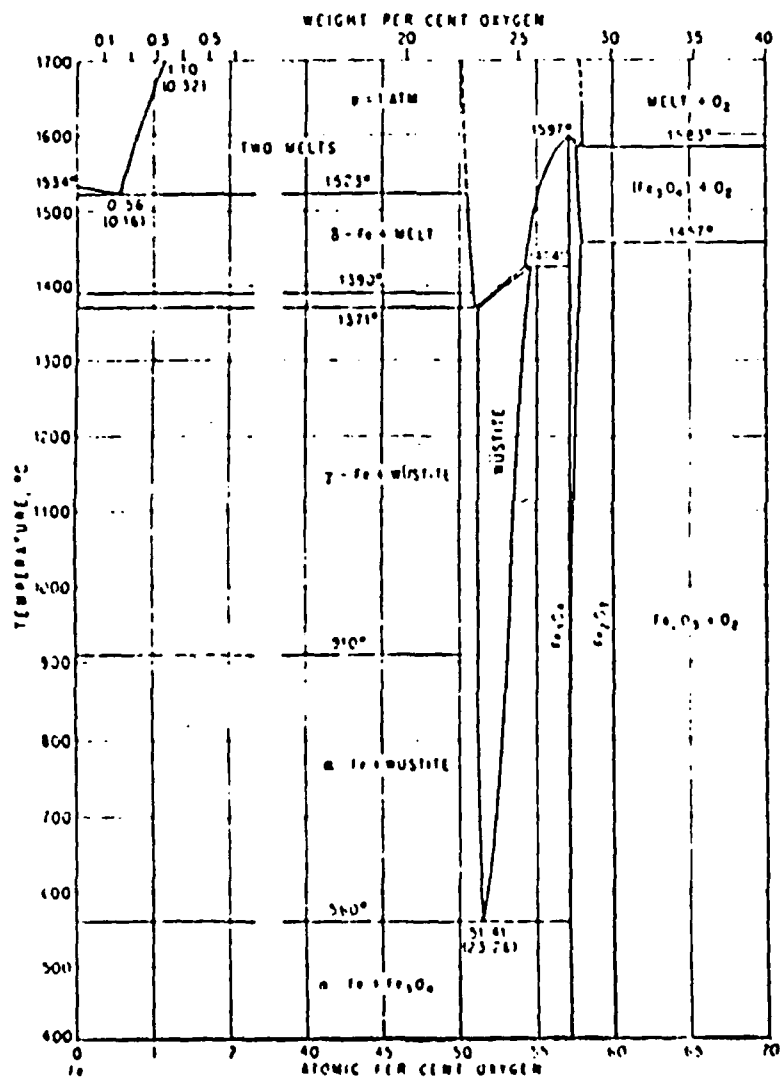


4.1 Iron - Carbon phase diagram. (ref H.1)

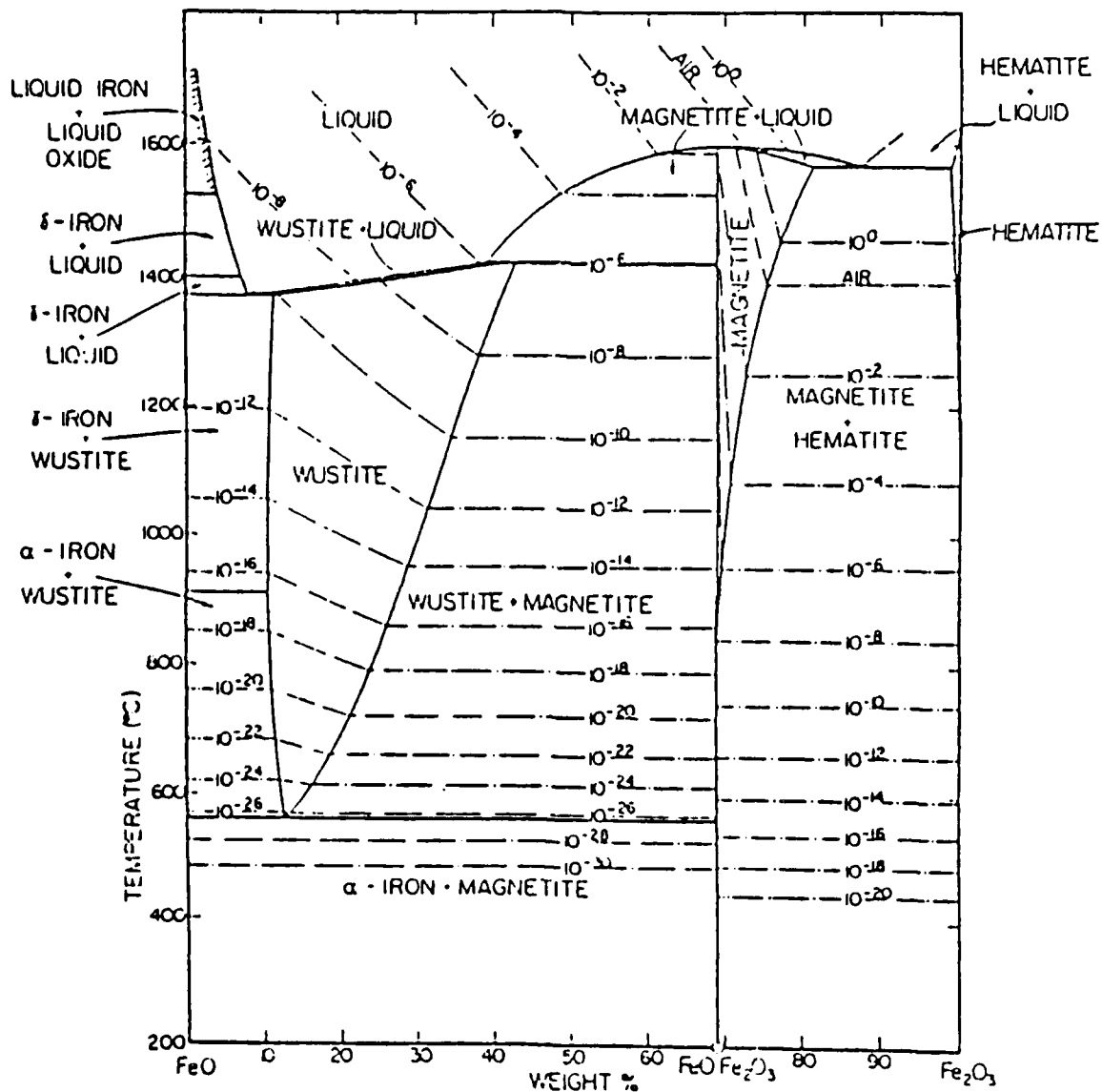
Fe-H Iron-Hydrogen



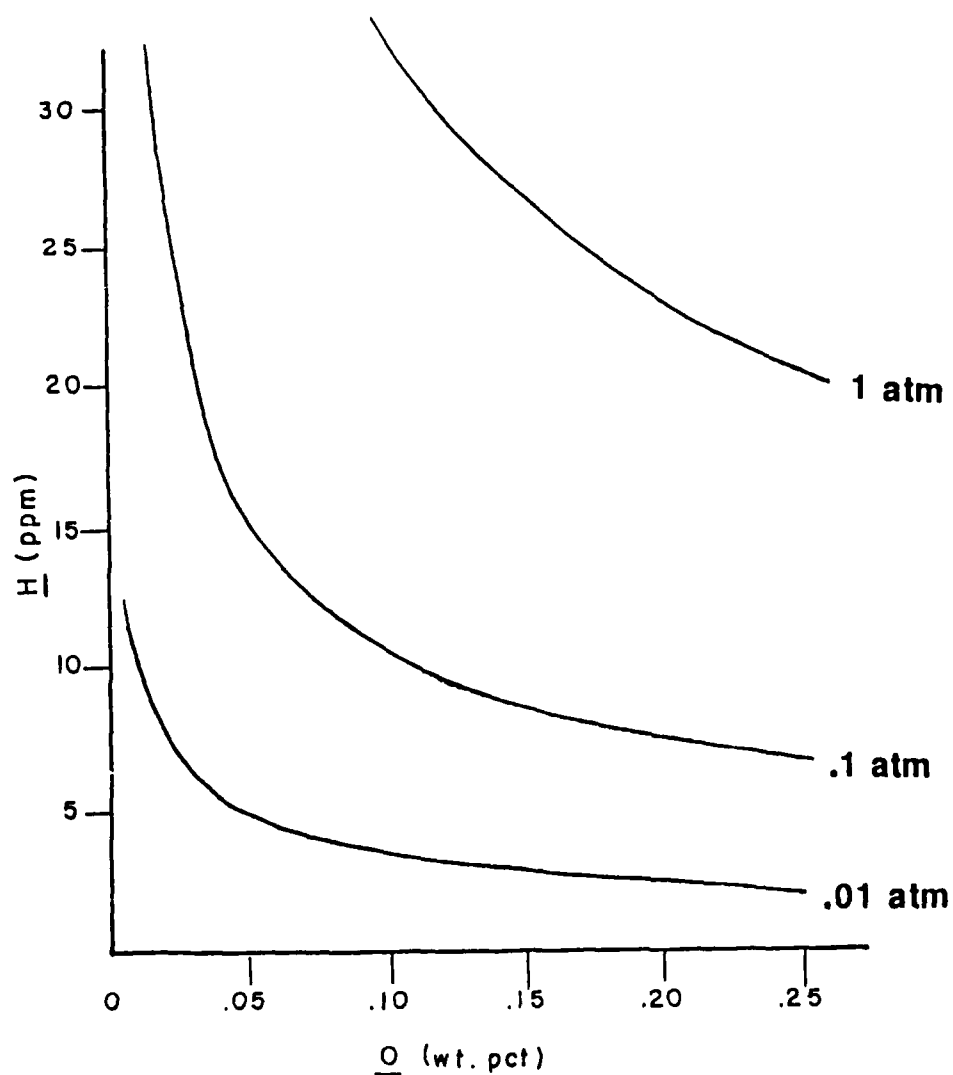
4.2 Iron - Hydrogen phase diagram. (ref H.1)



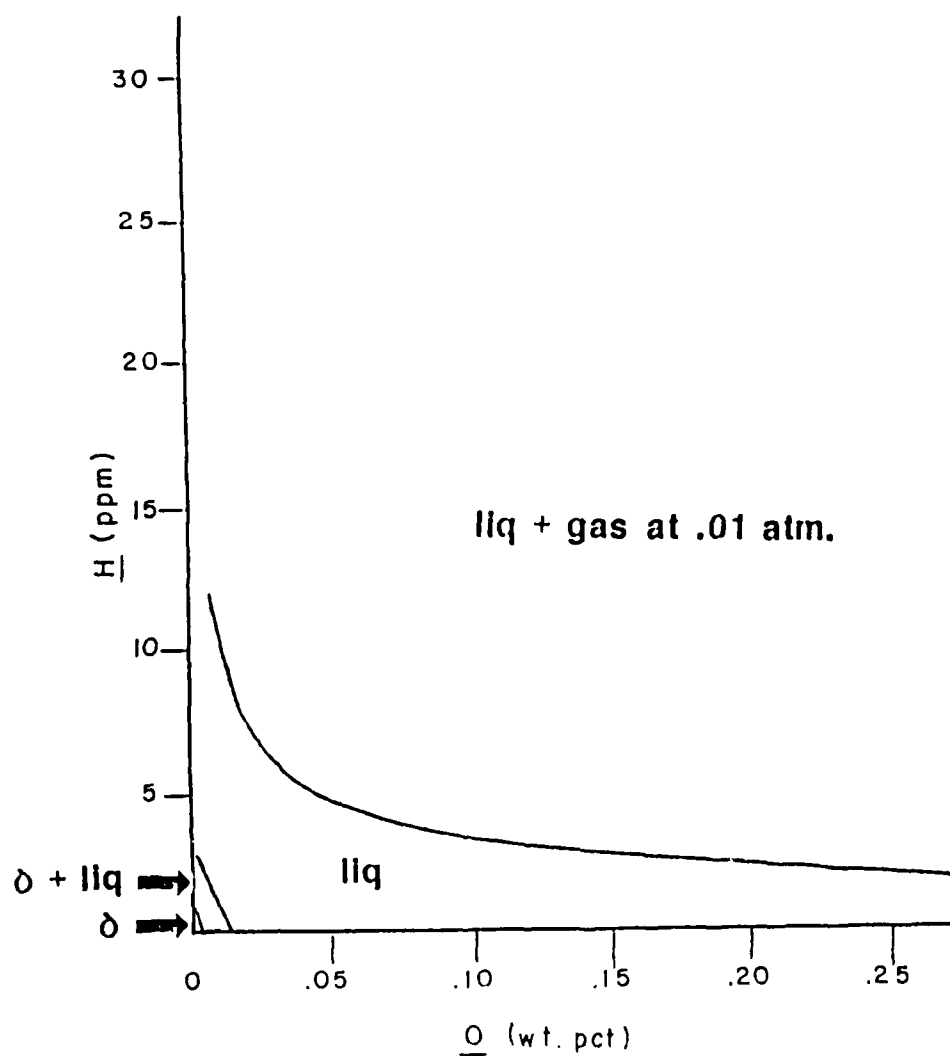
4.3 Iron - Oxygen phase diagram. (ref H.1)



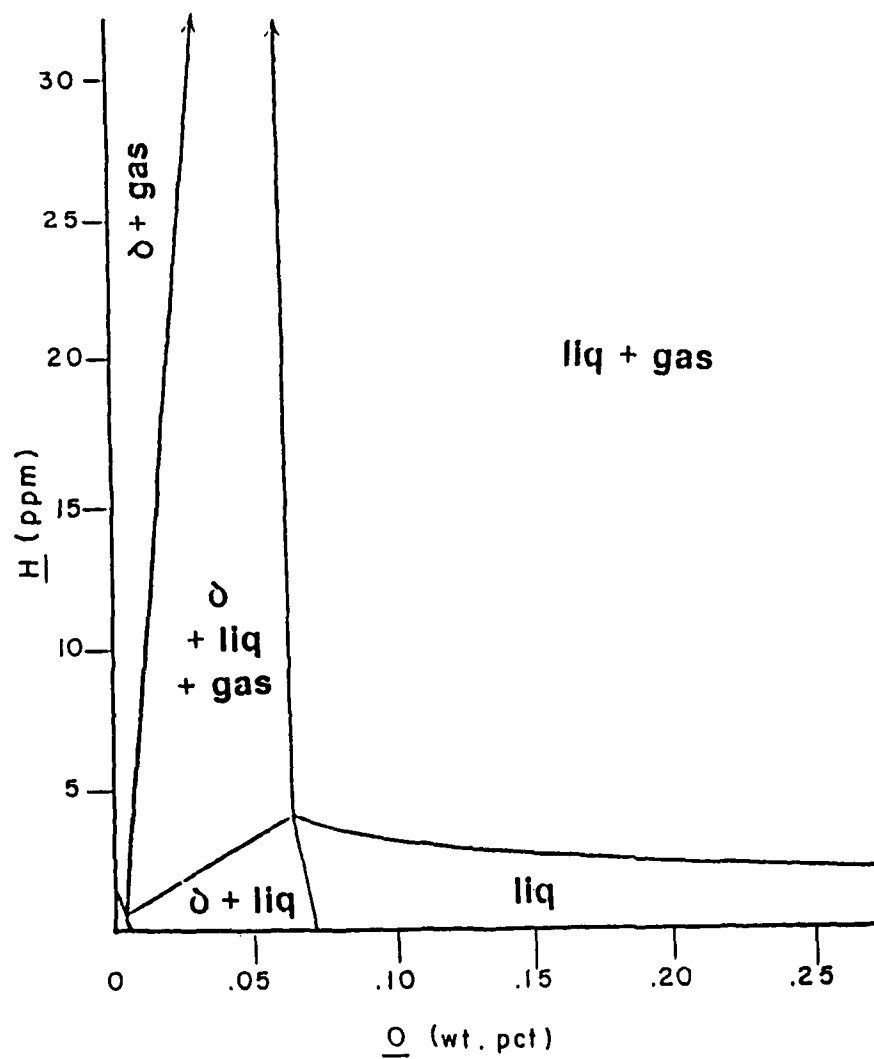
4.4 Iron - Oxygen phase diagram showing the partial pressure of oxygen gas. (Muan and Osborn)



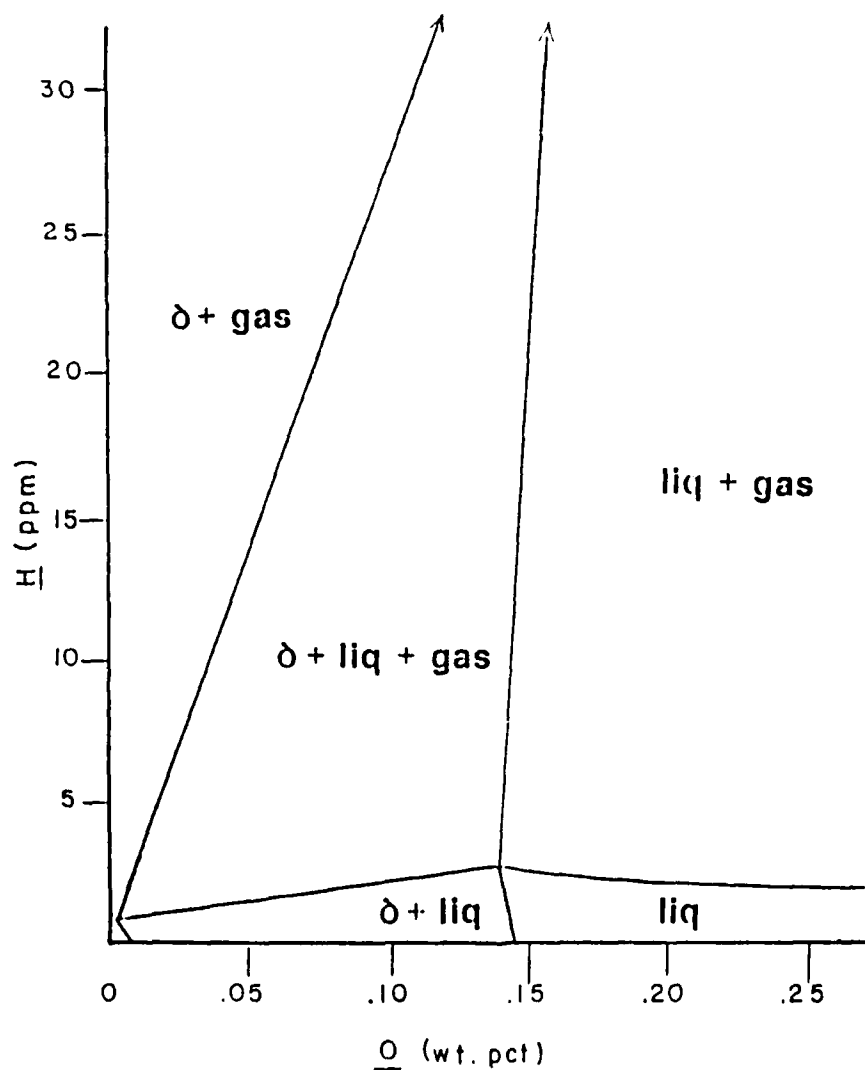
4.5 Isotherm of Fe-H-O at 1538 C. Each line shows the solubility of hydrogen and oxygen in the liquid iron at a specified pressure.



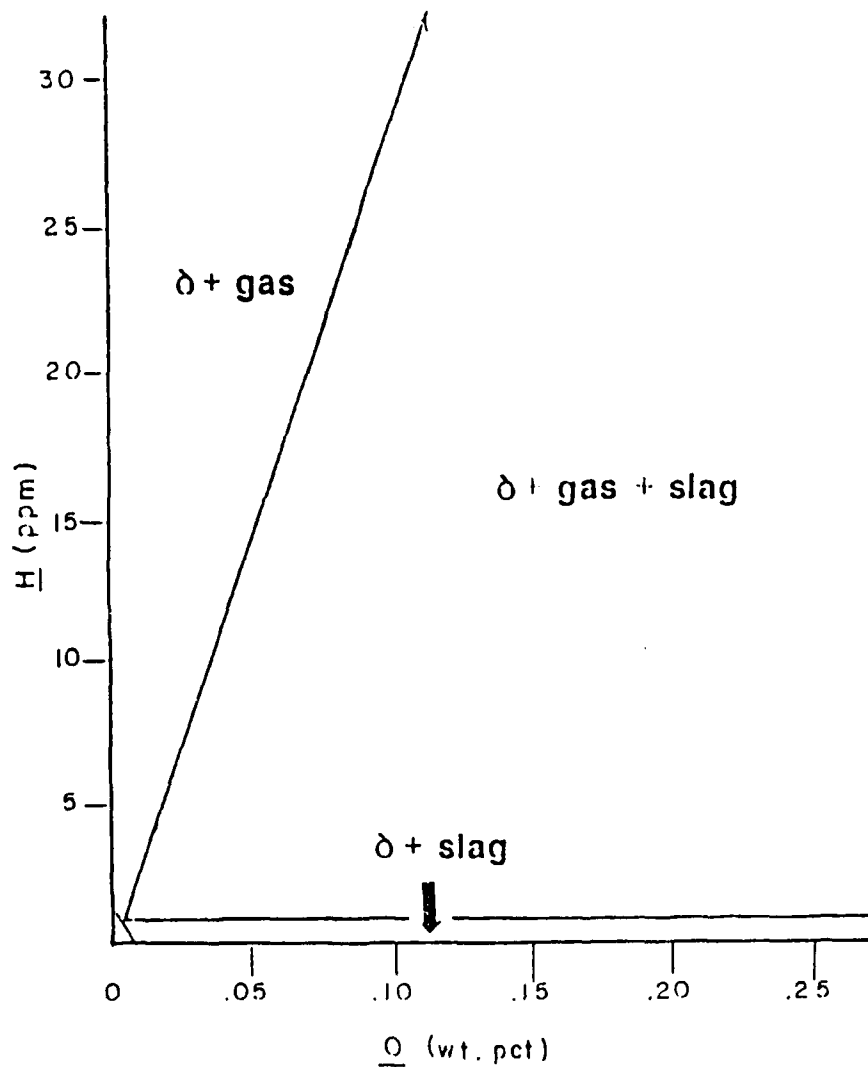
4.6 Isotherm of Fe-H-O at 1537 C and a moisture pressure of .01 atmospheres.



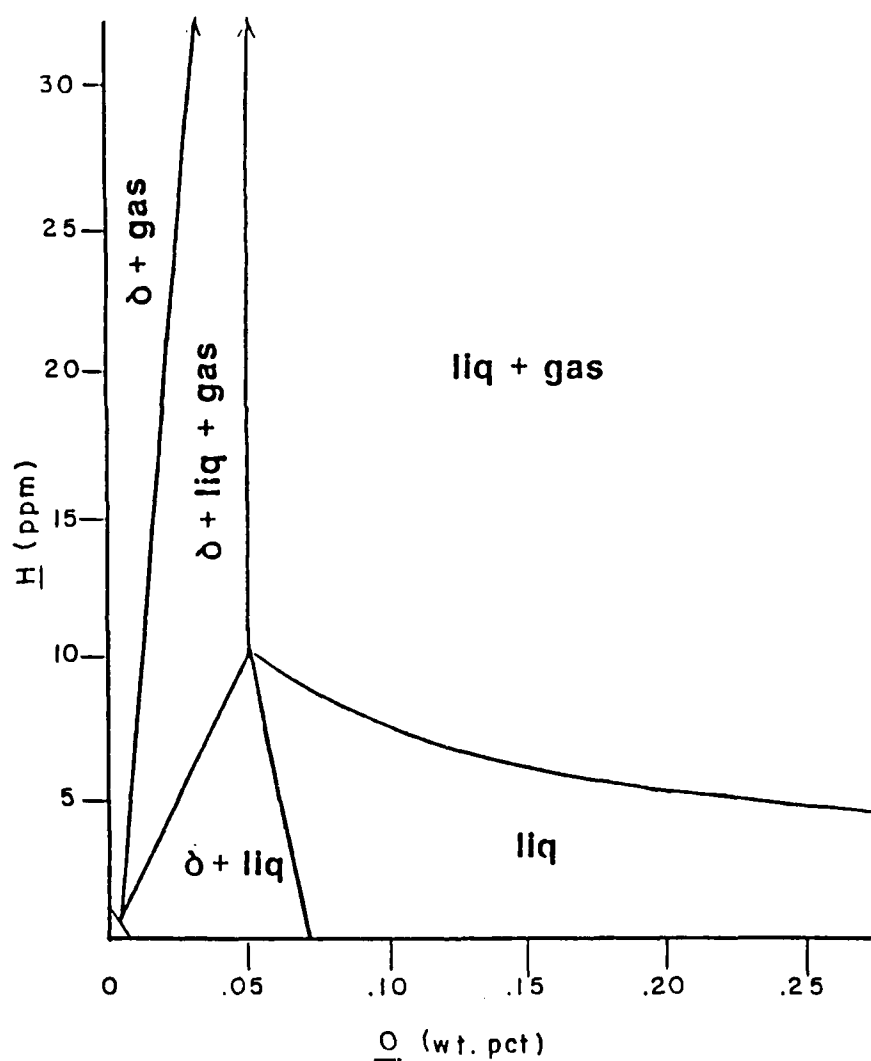
4.7 Isotherm of Fe-H-O at 1533 C and .01 atm moisture. The three phase region touches the H-O binary at a ratio of $P_{H_2O} / P_{H_2} = .299$



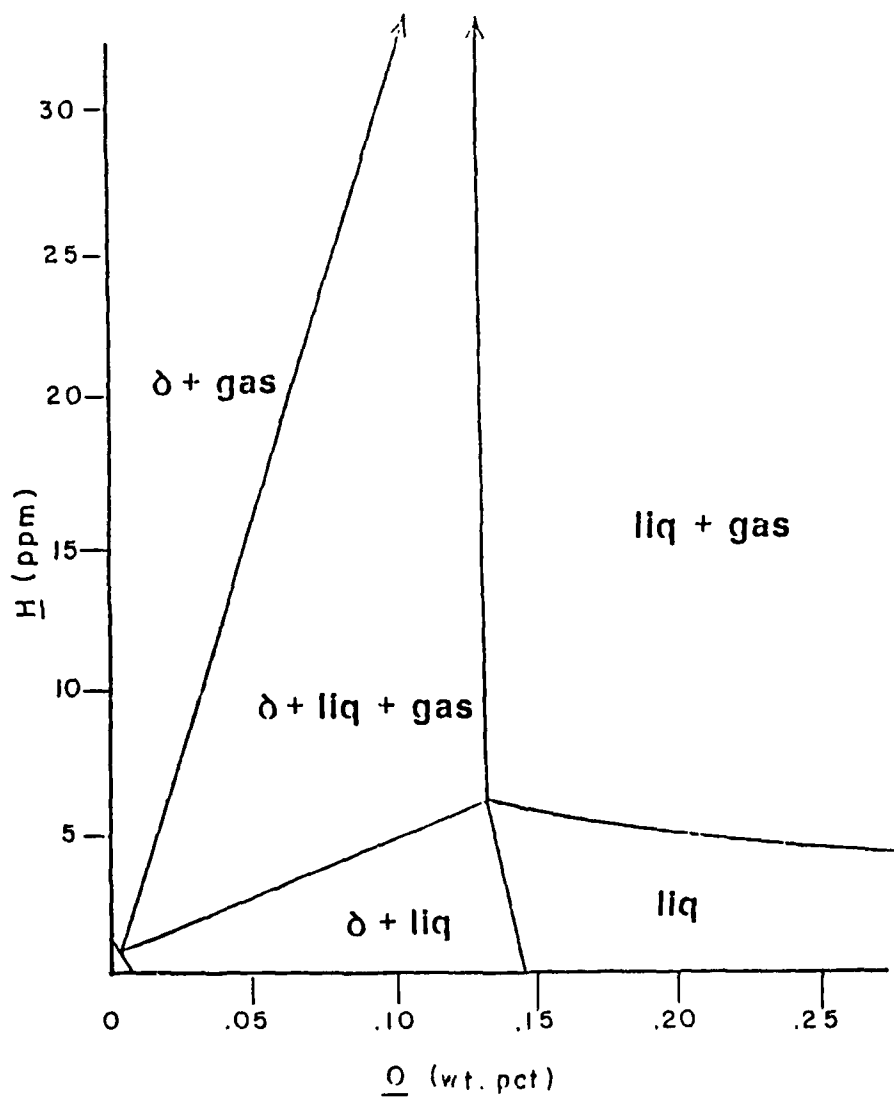
4.8 Isotherm of Fe-H-O at 1528 C and .01 atm moisture. The three phase region touches the H-O binary at a ratio of $P_{H_2O} / P_{H_2} = .692$



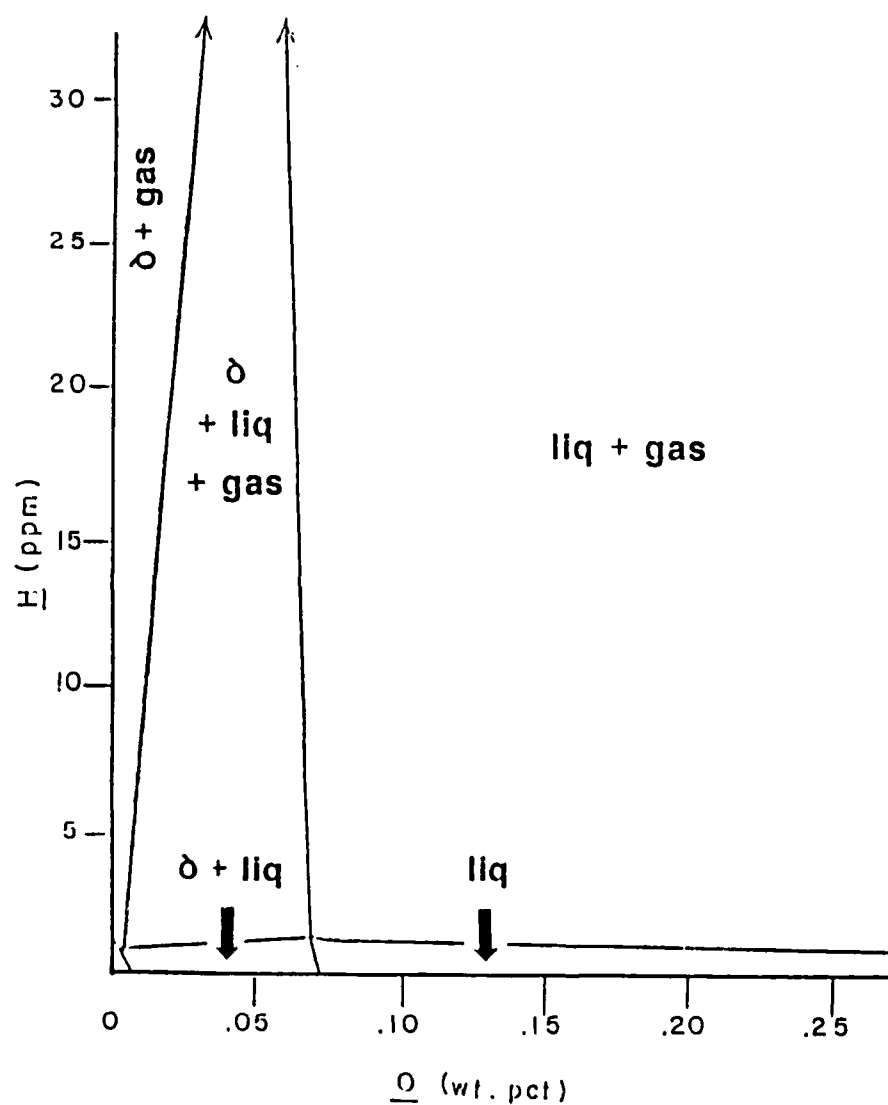
- 4.9 Isotherm of Fe-H-O at 1520 C and .01 atm moisture. The liquid phase is replaced with an FeO slag. The three phase region touches the H-O binary at a ratio of $P_{H_2O} / P_{H_2} = .60$



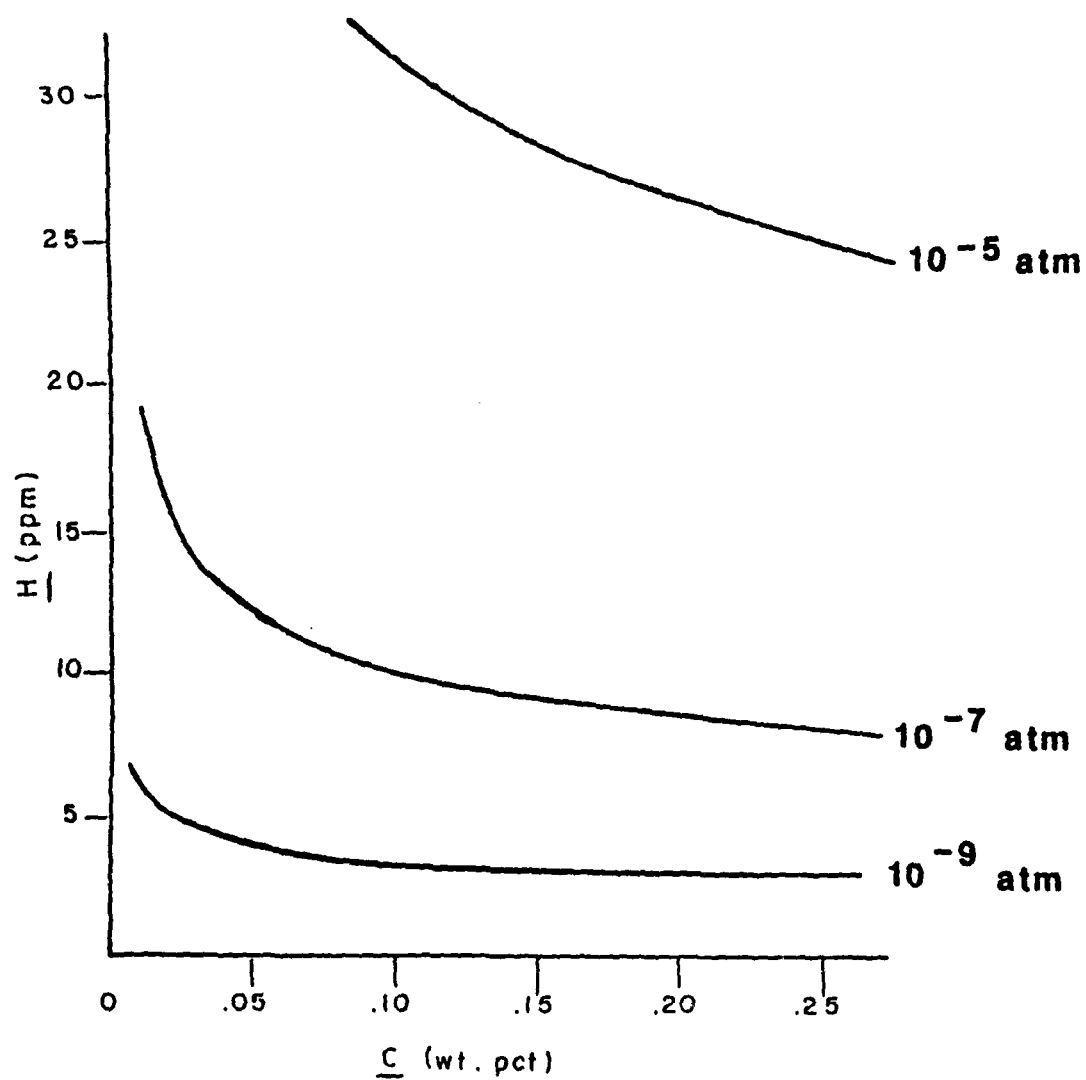
4.10 Isotherm of Fe-H-O at 1533 C and .05 atm moisture. The three phase region touches the H-O binary at a ratio of $P_{\text{H}_2\text{O}} / P_{\text{H}_2} = .237$



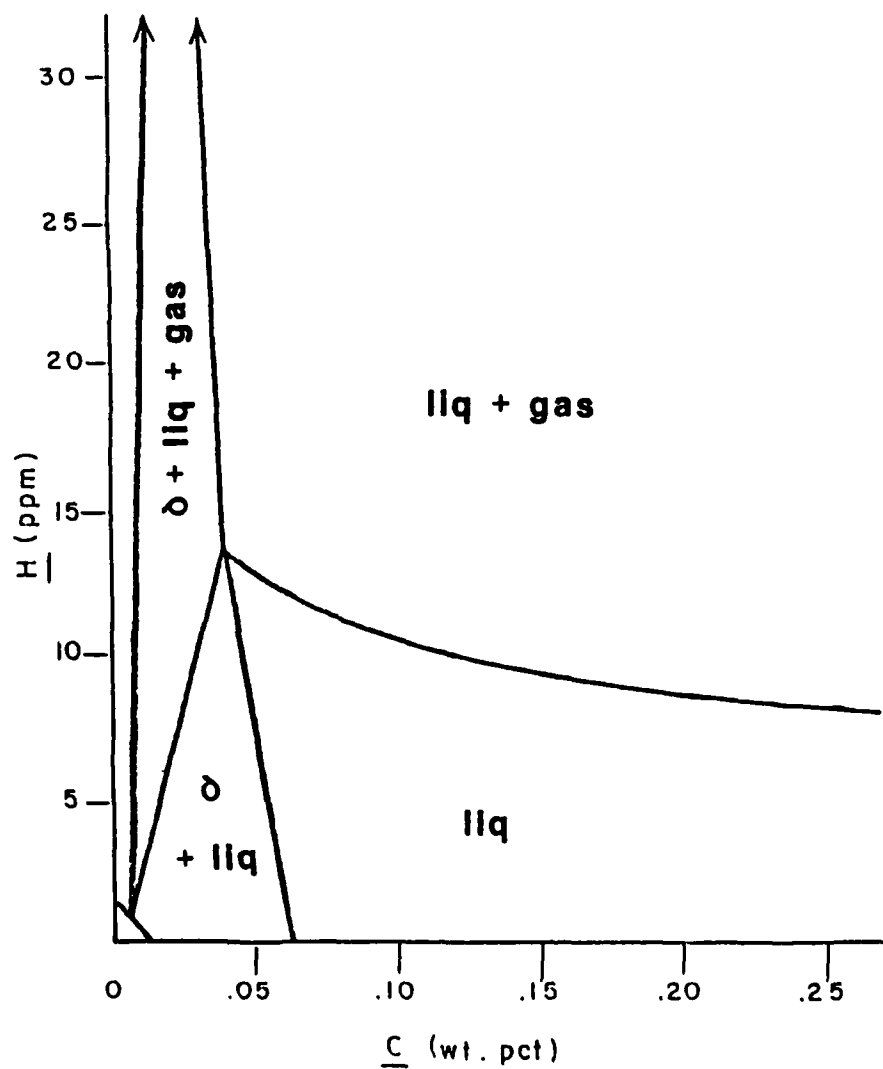
4.11 Isotherm of Fe-H-O at 1528 C and .05 atm moisture. The three phase region touches the H-O binary at a ratio of $P_{H_2O} / P_{H_2} = .64$



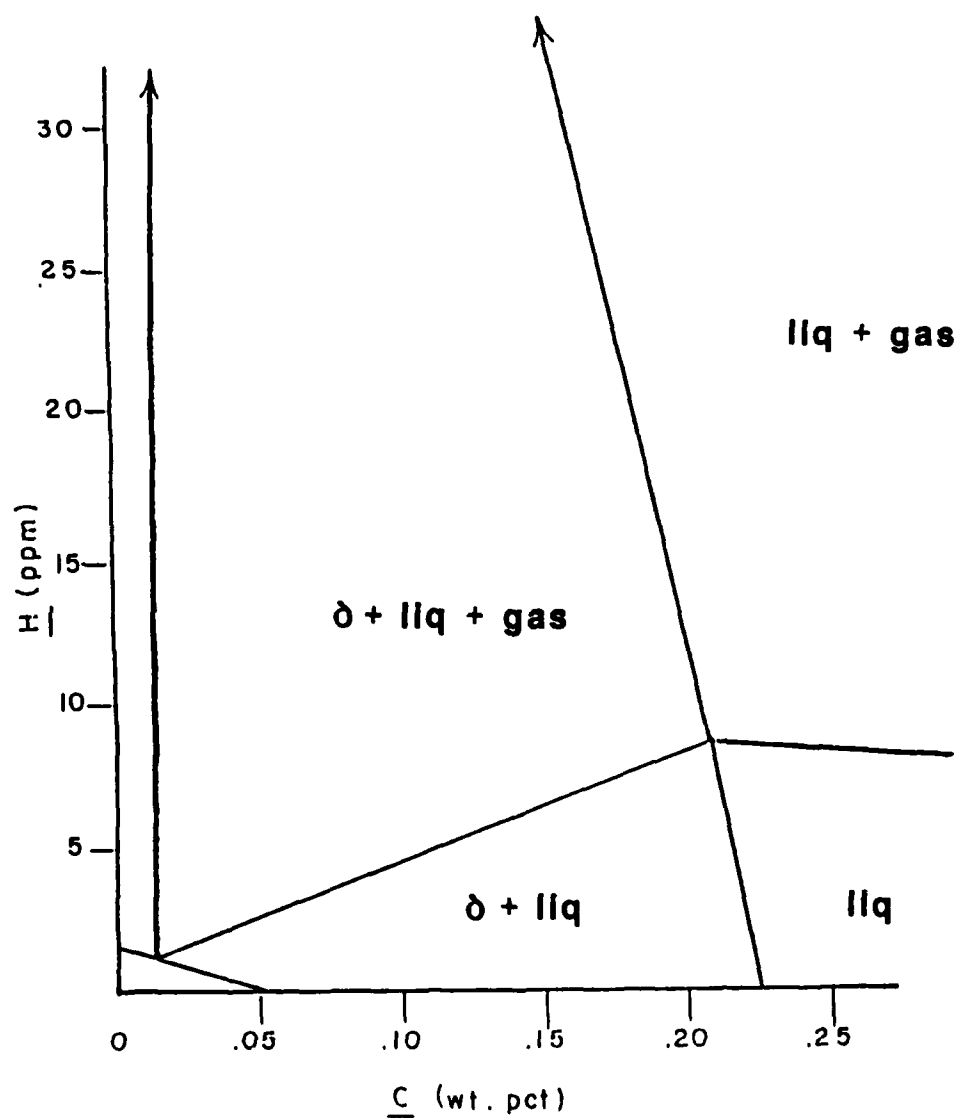
4.12 Isotherm of Fe-H-O at 1533 C and .001 atm moisture. The three phase region touches the H-O binary at a ratio of $P_{H_2O} / P_{H_2} = .28$



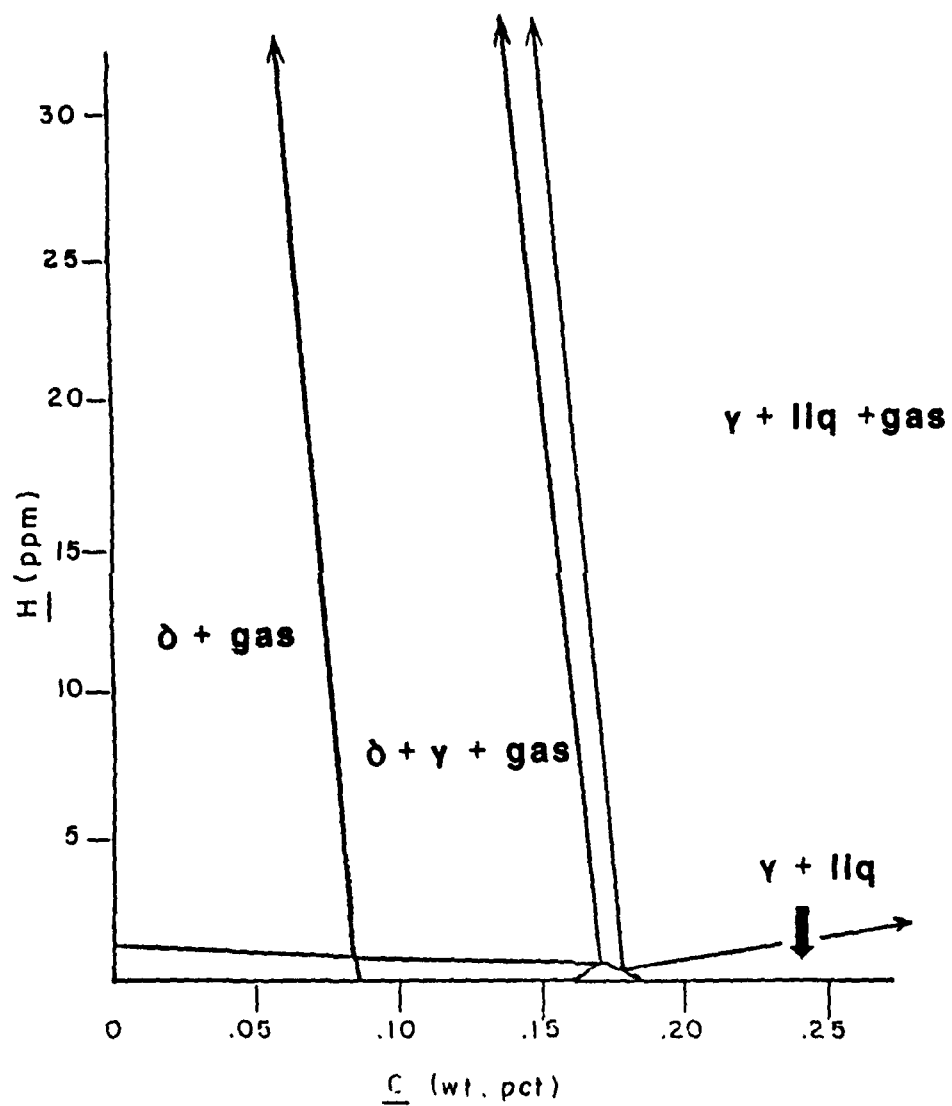
4.13 Isotherm of Fe-C-H at 1538 C. Each line shows the solubility of carbon and hydrogen in liquid iron at a specified pressure of methane.



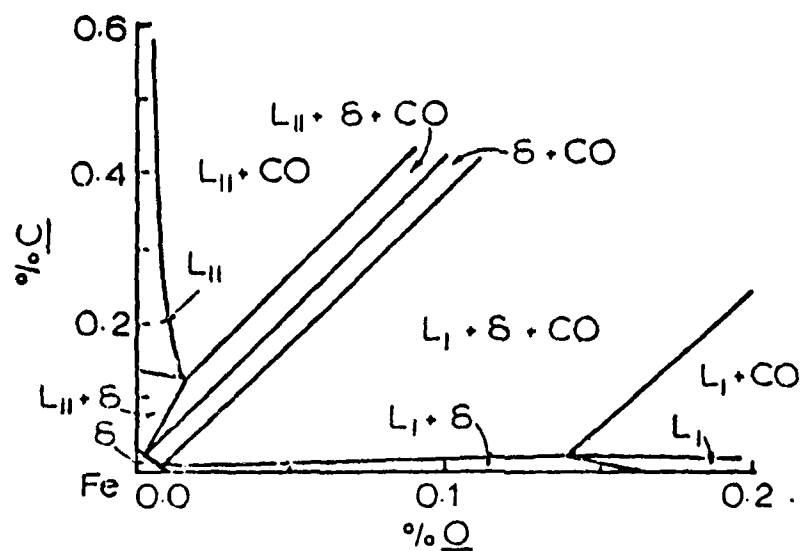
4.14 Isotherm of Fe-C-H at 1533 C and a pressure of 10^{-7} atm methane. The three phase region touches the C-H binary very close to the hydrogen corner.



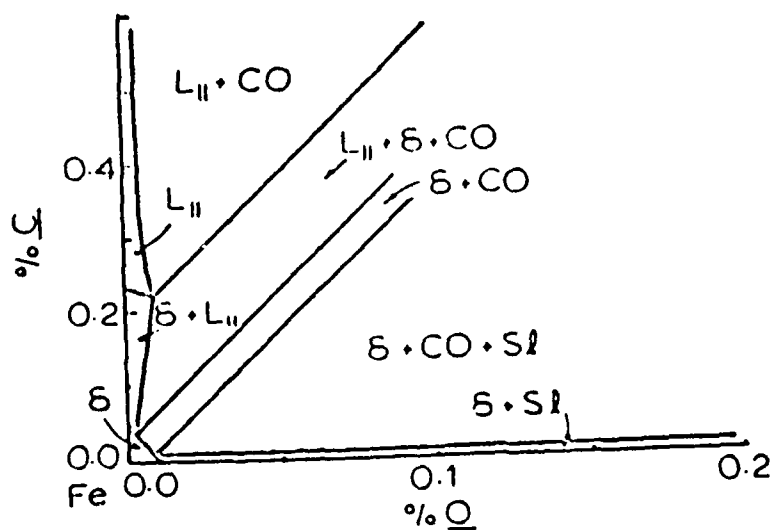
4.15 Isotherm of Fe-C-H at 1520 C and 10^{-7} atm methane. The three phase region still touches the C-H binary near the hydrogen corner.



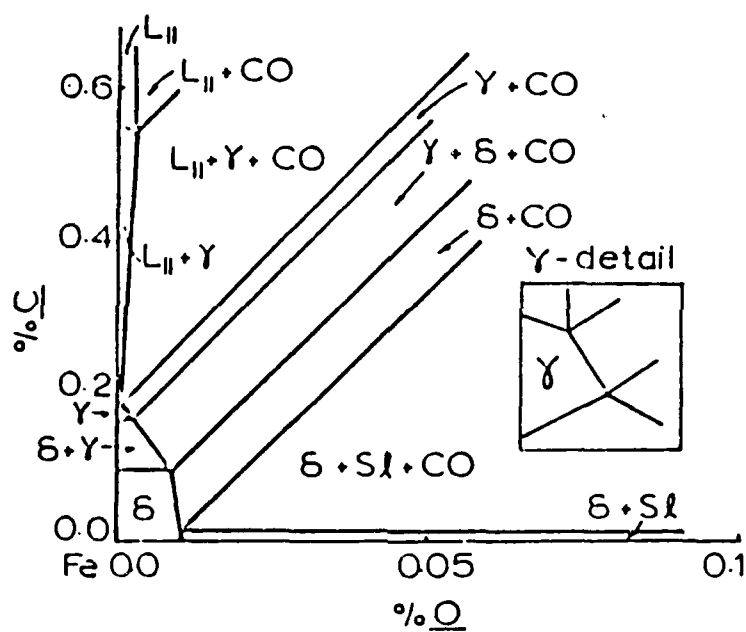
4.16 Isotherm of Fe-C-H at 1490 C and 10^{-6} atm methane. γ iron is now in equilibrium with the liquid phase which is off the diagram. The maximum solubility is 6 ppm hydrogen at .56 % carbon in this liquid.



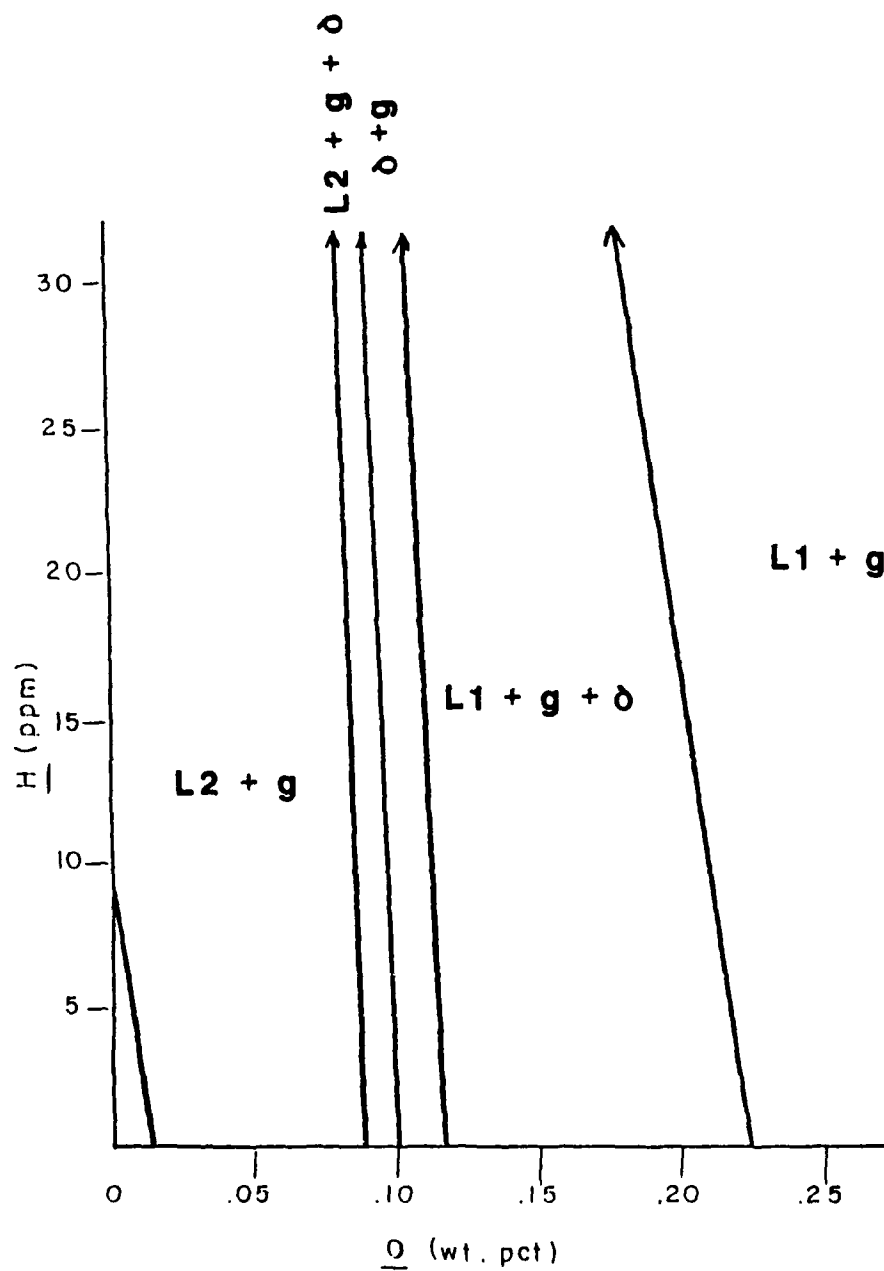
4.17 Isotherm of Fe-C-O at 1528 C and 1 atm CO.
(Ref. W.10)



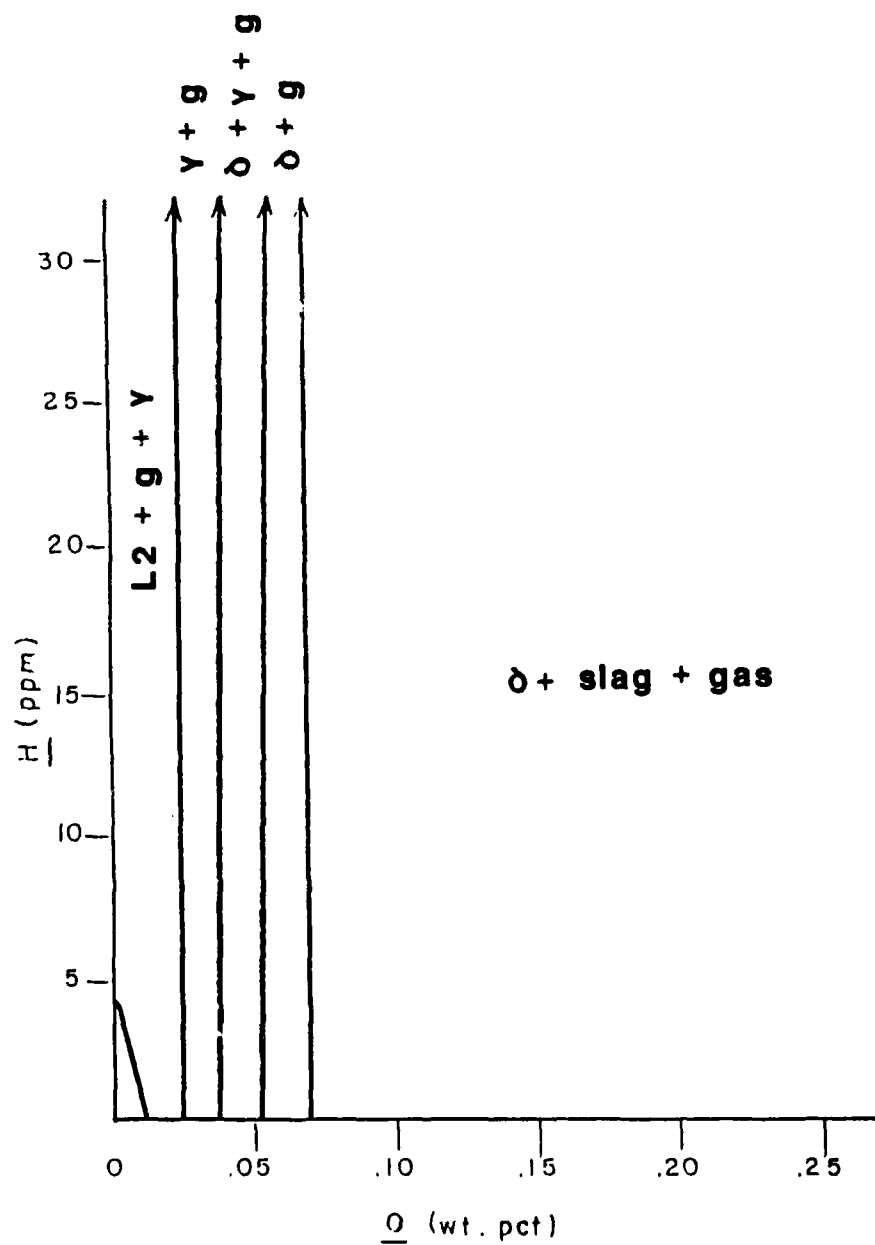
4.18 Isotherm of Fe-C-O at 1520 C and 1 atm CO.
(Ref. W.10)



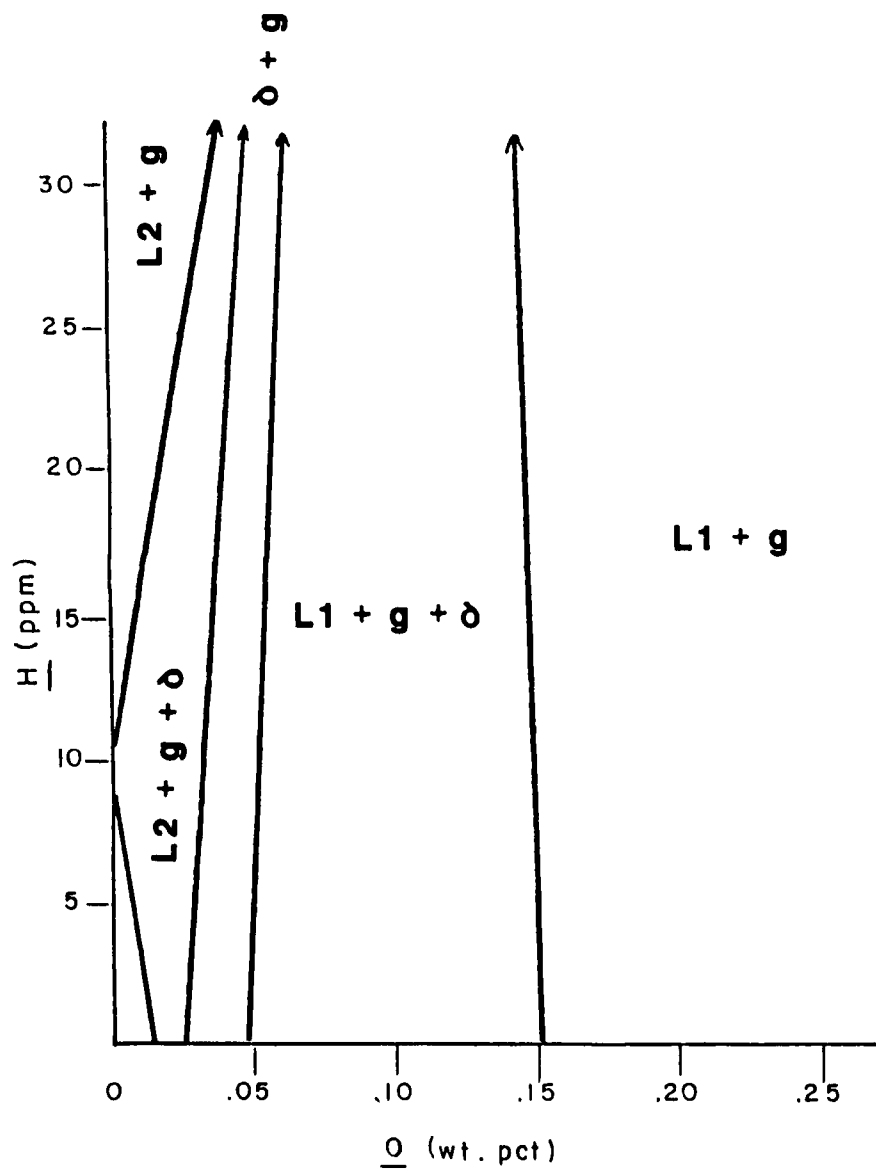
4.19 Isotherm of Fe-C-O at 1490 C and 1 atm CO.
(Ref. W.10)



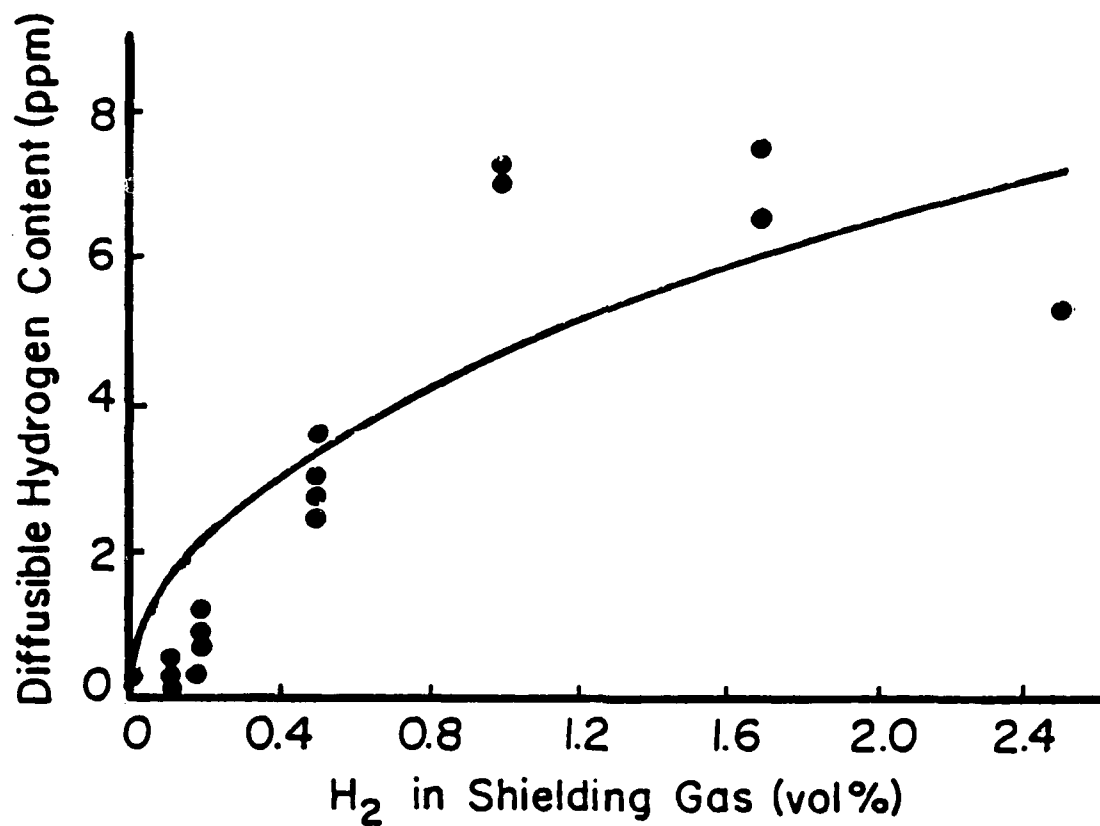
4.20 Slice through the Fe-C-O-H quaternary at 1528 C and .4% carbon.



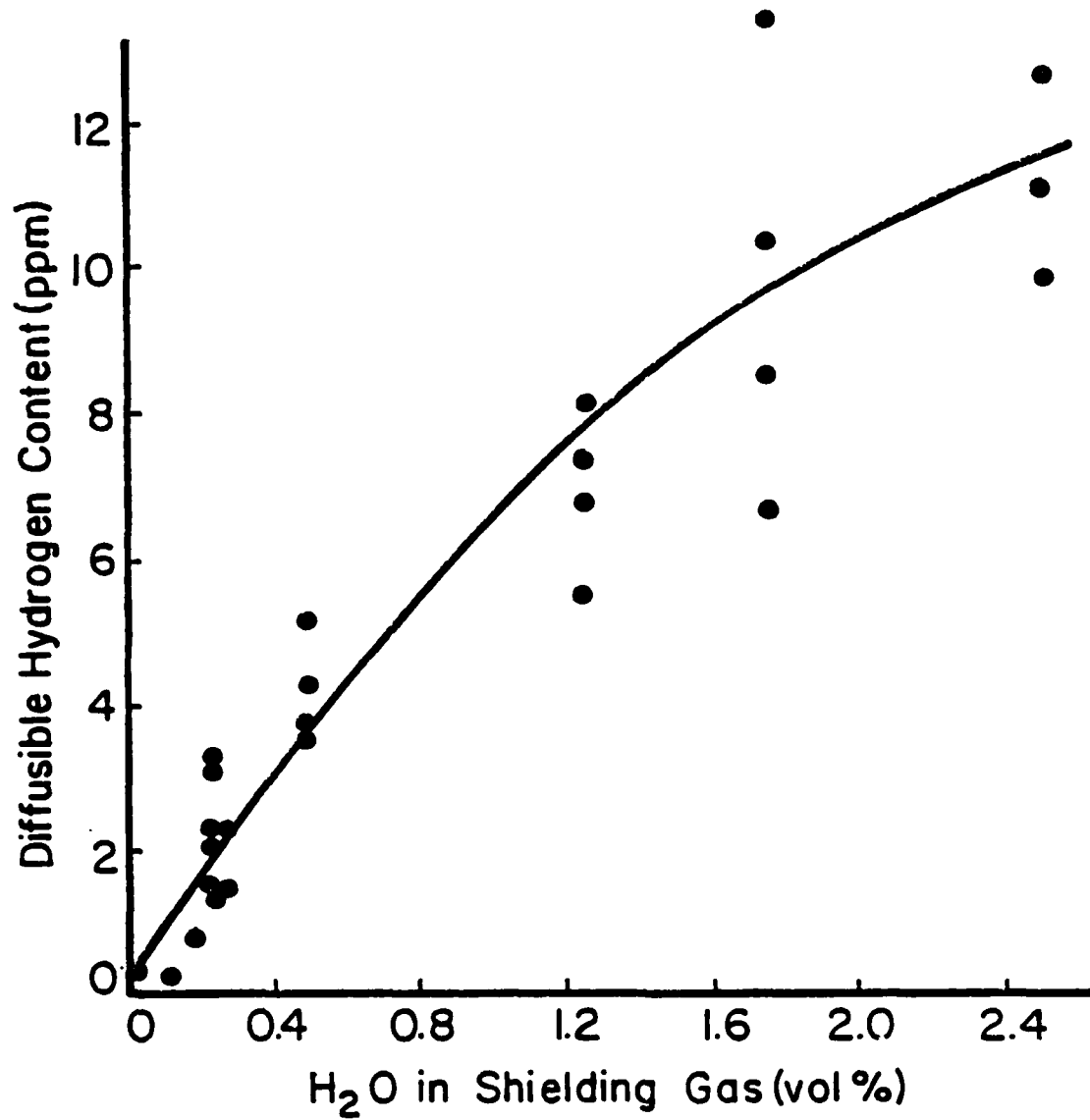
4.21 Slice through the Fe-C-R-O quaternary at 1490 C and .4% carbon.



4.22 Slice through the Fe-C-H-O quaternary at 1528 C and .1% carbon.



4.23 Diffusible hydrogen content in pulsed GMAW welds on metal added basis, hydrogen additions to the shielding gas. (Ref. S.6)



4.24 Diffusible hydrogen content in pulsed GMAW welds on metal added basis, moisture additions to the shielding gas. (Ref. S.6)

ASSESSING HYDROGEN ASSISTED CRACKING OF HIGH STRENGTH STEEL
WELDMENTS USING THE IMPLANT TESTING METHOD

5.0 ABSTRACT

The implant testing method is used to determine the hydrogen crack susceptibility of high strength steel welds. The amount of hydrogen in the weldment is varied to investigate the effect on the fracture strength. The hydrogen distribution model of Coe and Chano is used to determine the fracture strength as a function of the actual hydrogen content of the cracking zone. The results of this study are compared to the predictive methods of other researchers.

Quantitative fractography and fracture mechanics are used to assess the mechanisms of hydrogen cracking. It was found that the microplasticity theory of Beaumont can be used to describe how the stress intensity factor and hydrogen content affect the modes of intergranular, quasi-cleavage, and microvoid coalescence fracture.

The stress intensity factor and hydrogen content responsible for the microvoid coalescence fracture mode have been quantified for the high strength steel used in this study.

5.1 INTRODUCTION AND EXPERIMENTAL PROCEDURE

Among the various testing methods for assessing hydrogen embrittlement, the implant test has become the most popular for scientific investigations of the cracking phenomenon in welds. This is due to the fact that the stress, hydrogen level, and microstructure can be independently varied and controlled.

Although no standard procedure exists for the implant method (B22), the IIW has published a document (I7) containing guidelines for performing this test. These procedures were followed in this study using the I65 notch geometry and a helical notch. A sketch of the specimen geometry is shown in figure 5.1.

The material studied in this investigation is a high strength steel conforming to MIL-A-46100C (M10). Due to its extremely high hardness, its main use in industry is for armor in military applications. It is the main structural steel used in the M1 tank. Chemical composition requirements in MIL-A-46100C are very loose, and the main criteria are good hardenability and ballistic integrity. It is felt that this material is very susceptible to hydrogen embrittlement.

The composition of the heat of 46100 used throughout this investigation is listed in table 5.1. The microstructure of this steel is shown in figures 5.2 and 5.3. It is composed primarily of tempered

martensite with some banding. Due to the high hardness ($53 R_c$), this steel had to be normalized down to $35 R_c$ in order to be machined into implant specimens. The specimens were then austenitized in vacuum, quenched in oil, and tempered in air back to their original condition in accordance with the procedure shown in table 5.2. The resulting microstructure is shown in figures 5.4 and 5.5. The implant specimens were machined longitudinally in the rolling direction.

5.2 EXPERIMENTAL RESULTS

Figures 5.6 through 5.9 show sample implant test results of stress versus time to failure for GMA welds performed with varying shielding gas hydrogen contents, preheat temperatures, and times to loading. The level of crack susceptibility is ranked by determining the Lower Critical Stress (LCS) from these curves. The LCS is the maximum stress at which failure will not occur for an arbitrarily long period of time, usually quoted as 24 to 72 hours. Figure 5.6 demonstrates the fact that preheat will increase the LCS. Figure 5.7 demonstrates the fact that waiting 24 hours before applying the load will allow time for hydrogen to escape, thereby increasing the LCS. Figure 5.8 shows that increasing the amount of hydrogen in the shielding gas will decrease the LCS, but that at high hydrogen contents, the decrease in LCS becomes slight. Figure 5.9 again demonstrates that waiting 24 hours before loading will increase the LCS.

By varying the amount of hydrogen in the GMAW shielding gas, time to loading, and preheat temperature, the amount of hydrogen remaining in the weldment at the time of cracking can be varied. Table 5.3 summarizes the experimental results acquired during this portion of the research program. A matrix of 7 conditions was studied for each shielding gas composition: initially absorbed hydrogen content; hydrogen remaining 24 hours after welding; hydrogen remaining 24 hours after welding with preheat; LCS when loaded 5 minutes after welding; LCS when loaded 24 hours after welding; LCS when loaded 5 minutes after welding with

preheat; and LCS when loaded 24 hours after welding with preheat. Seven different shielding gas compositions were studied (although not every gas was evaluated both with and without preheat). The hydrogen values shown in table 5.3 were determined in chapter 2 (tables 2.3 and 2.9).

A loading time of 5 minutes was chosen based on previous research by Peng (P4) who showed that variations in loading time from 2 to 7 minutes after welding did not effect the LCS. The 24 hour loading time was chosen so that the hydrogen distribution model of Coe and Chano (C13) could be used to determine the amount of hydrogen in the cracking zone. The cracking zone in all of the implant fractures studied was at the weld fusion line. By combining these results, the LCS versus hydrogen content can be determined for various conditions.

Figure 5.10 shows the LCS for welds loaded after 5 minutes versus the diffusible hydrogen content. This is the standard figure used by most researchers for presenting their implant test results. The predictive methods of other researchers will be reviewed in section 5.5 to determine how accurately they assess these results. Although the LCS in figure 5.10 decreases with increasing hydrogen content, it is difficult to interpret the hydrogen values since the amount of hydrogen at the crack location will be changing with time during the test. The amount of hydrogen at the crack location will be more constant and evenly distributed if the weld is not loaded for 24 hours.

Figure 5.11 shows the LCS for welds loaded 24 hours after welding

versus the amount of hydrogen remaining in a diffusible hydrogen specimen 24 hours after welding. Once again, the LCS decreases with increasing hydrogen.

The amount of hydrogen actually present in the cracking zone (for the specimens loaded at 24 hours) can be determined using the hydrogen distribution model developed by Coe and Chano (C13). This model was described in section 2.5.5 and shown in figures 2.15 and 2.16. The ratio Q/Q_0 is approximately equal to the ratio of the hydrogen content at 24 hours divided by the initial hydrogen content. Using the data from table 5.3, this ratio averages .25. From figure 2.16, this corresponds to a r of 0.9, which is very close to the value of 1.0 found if r is calculated directly from the cooling curve and diffusivity versus temperature data.

Based on the experimentally determined r value of 0.9, the amount of hydrogen located at the fusion line ($l = 0.3$ in figure 2.16) will be equal to 12.5% of the initial hydrogen content in the weld. Thus, the LCS as a function of the actual hydrogen at the cracking zone is as shown in figure 5.12.

It has been postulated that dislocation sweeping will dramatically increase the actual amount of hydrogen at the crack tip. This effect has not been evaluated in the present research, and only the bulk hydrogen composition in the entire cracking region has been determined with the aid of the Coe model. The increased solubility of hydrogen under an applied axial tensile stress has been well researched. Louthan, et al.

have estimated that the solubility at the crack tip can be as high as 5 times the normal solubility.

This increase in solubility is evidenced in the present results. A comparison of the LCS of welds loaded after 24 hours versus welds loaded after 5 minutes (with otherwise identical conditions) shows that the LCS is higher for the welds loaded after 24 hours. For welds loaded after 5 minutes, much of the hydrogen is not allowed to escape due to the increase in solubility. The extra locked in hydrogen causes hydrogen cracking even after 24 hours under an applied load. Some hydrogen diffuses completely out of the specimen, but not before it causes some damage. When the weld is allowed to cool without an applied load for 24 hours, the majority of hydrogen leaves the specimen without causing any damage.

Previous authors have postulated that there should be a linear relationship between the LCS and log of the hydrogen content. This was not found to be the case in the present investigation. This non-linear relationship will now be investigated on the postulate that the mechanism of embrittlement may change from one stress or hydrogen level to another.

5.3 FRACTOGRAPHIC ANALYSIS OF IMPLANT SPECIMENS

A Scanning Electron Microscope (SEM) was used to examine the fractured surfaces of the implant specimens. The initial fracture in the

majority of specimens was due to hydrogen embrittlement, with the remaining area failing due to microvoid coalescence. Quantitative fractography was performed to map the various failure zones across the failed surfaces of over 60 implant specimens.

Figure 5.13 shows a typical overall view of the fractured surface of an implant specimen. Figure 5.14 shows the location of each of the magnified photos taken of this surface. Figure 5.15 shows the fracture morphology typical of hydrogen embrittlement as evidenced by intergranular faceting. The fracture morphology associated with microvoid coalescence is shown in figure 5.16 as evidenced by the ductile dimples. The transition region evidencing areas of intergranular faceting below or next to areas of microvoid coalescence is shown in figure 5.17. The shear lip where the final fast fracture occurred in this specimen is shown at the far left of figure 5.18.

The resulting quantitative fracture map developed for this specimen is depicted in figure 5.19. A few specimens also exhibited small regions of quasi-cleavage, an example of which is shown in figures 5.20 and 5.21.

Not all of the specimens exhibited such a clear cut distinction between the different fracture zones. For example, a number of the low hydrogen samples had substantial areas of "fisheyes" as shown in figures 5.22 through 5.24. A fisheye is an inclusion which is locally surrounded by an area of hydrogen embrittlement. Outside this immediate vicinity the fracture type is that of the surrounding matrix.

The local area of hydrogen embrittlement surrounding a "fisheye" is presumed to be due to hydrogen trapping at the inclusion. Numerous investigators have found that hydrogen can be trapped at inclusions (C2, K11, T13). Photographs of a large number of inclusions which have evidenced fisheyes along with EDX determinations of the inclusion composition are included in appendix 5A as a reference for researchers working in this field.

Through an analysis of the fracture maps, the percentage of the fractured specimen surface which failed due to hydrogen embrittlement versus the applied load was determined. As would be expected, the amount of hydrogen embrittlement increased with decreased loads. This is due to the fact that the specimen had more time to embrittle before the final area was overloaded. Also, the amount of embrittled area decreases with decreasing amounts of hydrogen.

Interestingly, the stress at which the final area failed by microvoid coalescence varied dramatically from one specimen to another. This was investigated with the aid of fracture mechanics. Since the helical notch used on the implant specimens is too blunt to use fracture mechanics, no pertinent data can be obtained about the crack initiation process. However, once hydrogen embrittlement occurs, the embrittled region itself will act as a sharp crack tip, and one can use fracture mechanics to investigate the fracture of the remaining area.

Daoud, et al. have determined the stress concentration factor for

an edge cracked circular bar in tension, and have since modified this to include the effect of the crack geometry (D_1 , D_2). Even though their analysis does not include the effect of a restraining weld close to the crack, it can be used to give an approximation of the K_{1C} of the final fractured area.

Figure 5.25 shows the stress concentration factor found by Daoud, et al. as a function of a/D . The crack geometry, a , and D are shown in figures 5.26 and 5.27. The specimen fracture maps which closely approximate this crack geometry were used to determine the fracture toughness (as estimated by K_{1C}) of the final fracture area. Table 5.4 gives a presentation of the results. The hydrogen values shown in table 5.4 were determined by estimating τ from the cooling curve, knowing the time at which fracture occurred, and finding the corresponding hydrogen concentration from figure 2.16.

The implant specimens which were welded with a high hydrogen content in the shielding gas (2% H_2), had a K_{1C} of about 15 kips $in^{1/2}$. This value agrees quite closely with the work of Herman and Campbell (H7), who used fracture toughness samples of this identical type of steel and determined the stress corrosion cracking toughness which they termed K_{sc} . Herman and Campbell found that the fracture toughness of this material was 15 kips $in^{1/2}$ when exposed to distilled water.

At low hydrogen levels (0% H_2 added to the shielding gas), the final fractures had a toughness of approximately 65 kips $in^{1/2}$, which is the

same value found by Herman and Campbell (H7) for the fracture toughness of samples not exposed to a corrosive environment.

At medium levels of hydrogen (.5% H_2 added to the shielding gas), the fracture toughness varied with the applied load and time to failure. At low applied loads, the fracture toughness was almost as low as the K_{SCC} value of 15. At higher loads, the value increased to approximately the nominal K_{IC} value of 65 kips in^{1/2}.

There were a number of specimens which had both high hydrogen contents and high K_{IC} values. These hydrogen values were much higher than in specimens with K_{IC} values of 15 kips in^{1/2}.

It appears as though at very low hydrogen levels, the hydrogen has no significant effect on the failure of the material ahead of the crack tip. The hydrogen was influential in the hydrogen embrittled region only and cracking was probably due to the increased stress state at the crack tip. Once the crack tip moved faster than the diffusion of hydrogen, the remaining material acted as though no hydrogen was present.

At medium hydrogen levels, there is enough hydrogen in the material far ahead of the crack tip that it can affect the fracture once the crack moves faster than the diffusible hydrogen. At high stress levels the remaining hydrogen will act as dislocation pins and artificially strengthen the material above its normal fracture toughness. This added hydrogen is in no way a benefit, however, since the crack tip will simply

move slower (waiting for the diffusible hydrogen) until the strengthened material is overloaded anyway. At lower stress levels there is less dislocation movement, and the effect of pinning will not be noticed. The crack front will move slower due to the lower stress and the excess hydrogen will act to lower the cohesive strength of the remaining material to the fracture toughness of 15 kips in^{1/2}.

White (W8) also noticed some slight strengthening of her implant specimens when welding with .05% hydrogen in the shielding gas. This result agrees well with the postulate just presented. For example, specimen number 17.2 had a K_{1C} in excess of the nominal value of 65 kips in^{1/2}.

The reason for the high K_{1C} values for some of the specimens with very high hydrogen contents may be due to dislocation pinning.

These postulates will now be examined in detail by an analysis of previously proposed hydrogen embrittlement mechanisms.

5.4 HYDROGEN EMBRITTLEMENT MECHANISMS

The results of theoretical studies of hydrogen embrittlement mechanisms proposed by physical metallurgists have rarely been applied to the field of welding. Sawhill (S12) has, however, used these mechanisms in his doctoral study of HY-130 steel weldments. His analysis provides a

good background for the ensuing analysis of the most often proposed hydrogen embrittlement mechanisms. Even though the problem of hydrogen embrittlement has been studied extensively, no one theory has become generally accepted.

The planar pressure theory, proposed by Zapflee, is based on the decrease in solubility of hydrogen as the temperature is lowered (22). The atomic hydrogen is postulated to reassociate into diatomic hydrogen in pores and microvoids. The pressure of diatomic hydrogen then builds to very high values which adds to the applied external stresses. By using Sievert's law, a steel with 5 ppm hydrogen would have over 17,000 atmospheres pressure built up in the voids at 20 C. Several experimental observations conflict with this mechanism, however. Hydrogen embrittlement can be eliminated by degassing even after exposure to room temperature after exposure to hydrogen charging. The low temperature of the degassing would not be high enough to dissociate the diatomic hydrogen into monatomic hydrogen which could diffuse out of the steel. Also, the observation of hydrogen induced cracks growing on a free surface precludes an internal pressure gradient as the driving force for crack growth.

The adsorption theory of Petch and Stables (P5) and further modifications (P6) propose a lowering of the surface free energy by hydrogen so that a crack can grow under a lower applied stress. This theory has been criticized on the basis that the small but finite plastic deformation on hydrogen induced fracture surfaces requires more energy than could be

accounted for by the adsorption theory. In addition, fracture surfaces at low temperatures indicate rapid void formation and coalescence where the rate of surface migration would be negligible.

A theory proposed by Troiano (T11) suggests that hydrogen interacts with dislocation pile-ups in areas of triaxial stress to lower the cohesive strength. It is known that hydrogen will diffuse toward regions of high triaxial stress such as those associated with a stress riser. When the concentration reaches a given level, the interaction of hydrogen with dislocation arrays ahead of the stress riser is postulated to be sufficient to cause fracture. Troiano suggests that this interaction is due to the valence electrons from hydrogen atoms entering the unfilled "d" shells of the iron and modifying the repulsive forces which determine the interatomic spacing in transition metals.

Others have modified the planar pressure theory and the adsorption theory by assuming that hydrogen atoms are transported to the void or crack tip as Cottrell atmospheres. Bastein has proposed that hydrogen atoms are carried along by the movement of dislocations during plastic deformation. Thus, he reasons, dislocation pile-ups at structural defects will produce an oversaturation of hydrogen which will result in an increase in pressure which produces triaxial stresses and embrittlement (B5). Research by Graville supports the hypothesis that hydrogen transport by dislocations to the site of crack initiation is a necessary part of the embrittlement process (G17, G18).

Beachem has proposed a theory of hydrogen assisted cracking which is based on a microplasticity mechanism rather than embrittlement (B7). He suggests that the hydrogen in the lattice ahead of the crack tip assists whatever microscopic deformation processes the microstructure will allow. Thus, intergranular, quasi-cleavage, or microvoid coalescence fracture modes will operate depending on the microstructure, the crack-tip stress intensity, and the concentration of hydrogen. The model unifies several theories but shows that the planar pressure and adsorption theories are unnecessary. He proposes that the basic hydrogen-steel interaction appears to be an easing of dislocation motion or generation, or both.

One of the features of this theory is the classification of fracture modes with respect to stress and hydrogen level. At relatively high stresses, hydrogen assisted cracking can propagate by microvoid coalescence, which is normally thought of as a ductile failure mechanism. Beachem proved that hydrogen can be responsible for microvoid coalescence by partially fracturing a sample in hydrogen, then freezing the sample in liquid nitrogen and sectioning the sample to find evidence of the processes occurring ahead of the crack tip. As the stress intensity decreases, crack propagation proceeds by the lower plastic deformation processes of quasi-cleavage, and finally, intergranular. Increasing hydrogen concentration at the crack tip has the effect of decreasing the stress intensity at which these fracture processes occur.

This model adequately explains the presence of plastic deformation preceding hydrogen cracking in the HAZ of welds (H14) and plastic defor-

mation in other systems as well (B9, B10, H11, O7). Also, the experimental results in Beachem's paper bear a remarkable resemblance to the results of the present investigation. The 4340 steel used in his research is similar to the 46100 used here.

The Beachem model appears to be the most comprehensive model to date, and accounts for most experimental observations of hydrogen cracking. In addition, since his results seem to eloquently describe the fracture modes operative in the present research, this model will be used to explain the results of this investigation.

The interrelationship between stress intensity factor, dissolved hydrogen content, and fracture mode proposed by Beachem is shown in figure 5.28. Beachem goes into detail describing various paths through this map and the resulting fractured surface. He concentrates on decreasing stress intensity factors, whereas the implant test used in the present investigation will result in an increasing stress intensity factor.

Using the results presented in table 5.4, a fracture relationship map similar to that proposed by Beachem can be developed as is shown in figure 5.29. As can be seen, the K_{IC} at which microvoid coalescence occurs lowers with increasing hydrogen in the crack zone. With the exception of the three points at very high hydrogen contents, this relationship is the same as that proposed by Beachem. The present investigation could not quantify the hydrogen concentration which caused intergranular or quasi-cleavage fracture. Before describing the differ-

ences between these two maps, it must be recalled that Beachem used specimens more amenable to fracture mechanical calculations than the implant specimens used here.

The major difference between the fracture map proposed by Beachem and the one proposed in the present investigation, is that this investigation shows that intergranular failure can still occur at much higher values of hydrogen. It makes sense that intergranular failure will occur at high hydrogen contents, but Beachem suggests that microvoid coalescence will occur faster, and thus predominate. The three points at high hydrogen concentrations are beyond the range investigated by Beachem. Thus, figure 5.29 shows a modification to the original work by Beachem, namely, that high hydrogen concentrations can suppress the microvoid coalescence fracture mode, and that intergranular fracture will still be operative.

The current research has attempted to quantify both the stress intensity factor and the amount of hydrogen responsible for causing microvoid coalescence. This is the first time that this has been attempted. Notable discrepancies may arise due to the fact that the implant specimens were not well suited to K_{IC} measurements. Another shortcoming may be that the bulk hydrogen in the cracking zone was determined rather than the hydrogen due to dislocation sweeping or stress concentrations at the crack tip.

5.5 COMPARISON OF CURRENT RESULTS WITH THE PREDICTIONS OF OTHER RESEARCHERS

As was described in section 1.10, a large number of researchers have studied hydrogen cracking with the intent of developing predictive methods for eliminating cracking. This has not been attempted in the present investigation. Instead, currently available methods were examined for the accuracy with which they predict cracking in the material used in this investigation.

Ito, et al. have developed a method which is readily usable (111). As shown in figure 5.30, the implant strength is read off of graph (c) using an equation based on a carbon equivalent formula (P_{CM}) and the as-deposited hydrogen content. The resulting implant strength is then modified by the cooling time to 100 C (found in graphs a and b). Using this method, the predicted implant strength for a weld made with no preheat, and 2.3 ml/100 g deposited, is about 6 ksi. The experimental result in the current study was actually about 50 ksi. This large discrepancy is probably due to the extremely high P_{CM} found for the composition used in this study. Even though this value is covered in the graph, it is probably outside of the accurate range. If any hydrogen is added to the specimen, Ito, et al. predict a negative implant strength. This is obviously outside of the useful range of their analysis.

Coe presented a method of predicting the preheat temperature to pre-

vent cracking for a large variety of material types (C15). If the correct table is chosen, his method very accurately predicts the anticipated HAZ hardness. The resulting range of preheat temperatures required is from 170 C for low restraint welds to 225 C for highly restrained welds. The current study found that preheat temperatures of over 100 C increased the LCS. Unfortunately, the accuracy of their method cannot be directly tested since the Coe results predict HAZ cracking in self restrained welds. However, it is felt that his prediction will prevent cracking, but may be somewhat conservative.

The predictive method of Karppi, et al. (K5) was found to very accurately predict the LCS observed in the present study, but required knowledge of the amount of hydrogen remaining at 100 C, the HAZ hardness, and the stress field parameter. At large hydrogen contents, the prediction method breaks down, but for most anticipated applications, this was found to be a highly accurate method.

Okuda, et al. developed a single equation for all steels with between 109 and 156 ksi yield strength (04). Since the strength of the steel used in the present study is well above this range, the predicted preheat temperature is unreasonably high.

The method of Pavaskar and Kirkaldy (P2) also did not accurately predict the implant rupture strengths found in the present study. This is felt to be due to the relatively narrow range of HAZ hardnesses which they studied.

In general, the material studied in the present investigation was much harder and stronger than those studied by the majority of other reseachers. This inevitably will render most other predictions inaccurate. Extrapolating others' results often can be misleading, especially with the extremely large carbon equivalent studied.

It is not surprising that few predictive methods can be used outside of the scope in which they were formulated. Peng (P4), studying HY-80 steels, found that none of the predictive methods available were suitable for his materials. Thus, caution is well advised when using the predictive formulae of others.

TABLE 5.1

Composition of the Steel Used in This Study

	C	Si	Mn	Cu	P	Ni	S	Al	Cr	Mo
MIL-A-40100	.31	.41	.97	.38	.011	1.21	.008	.044	.51	.50

Table 5.2

Heat Treatment Procedure for Implant Specimens

- Austenitize in vacuum at 1650 F for 1/2 hour
- Drop axially from vacuum into integral oil quench at 110 F
- Deep freeze at -110 F for 1 hour
- Check specimens for hardness of 52 - 54 Rc
- Temper in air at 400 F for 1 hour
- Check specimens for correct hardness of 50 - 52 Rc

Heat treatment performed at C.I. Hayes,
Cranston, Rhode Island. Supervised by
Steven Gedeon.

Table 5.3

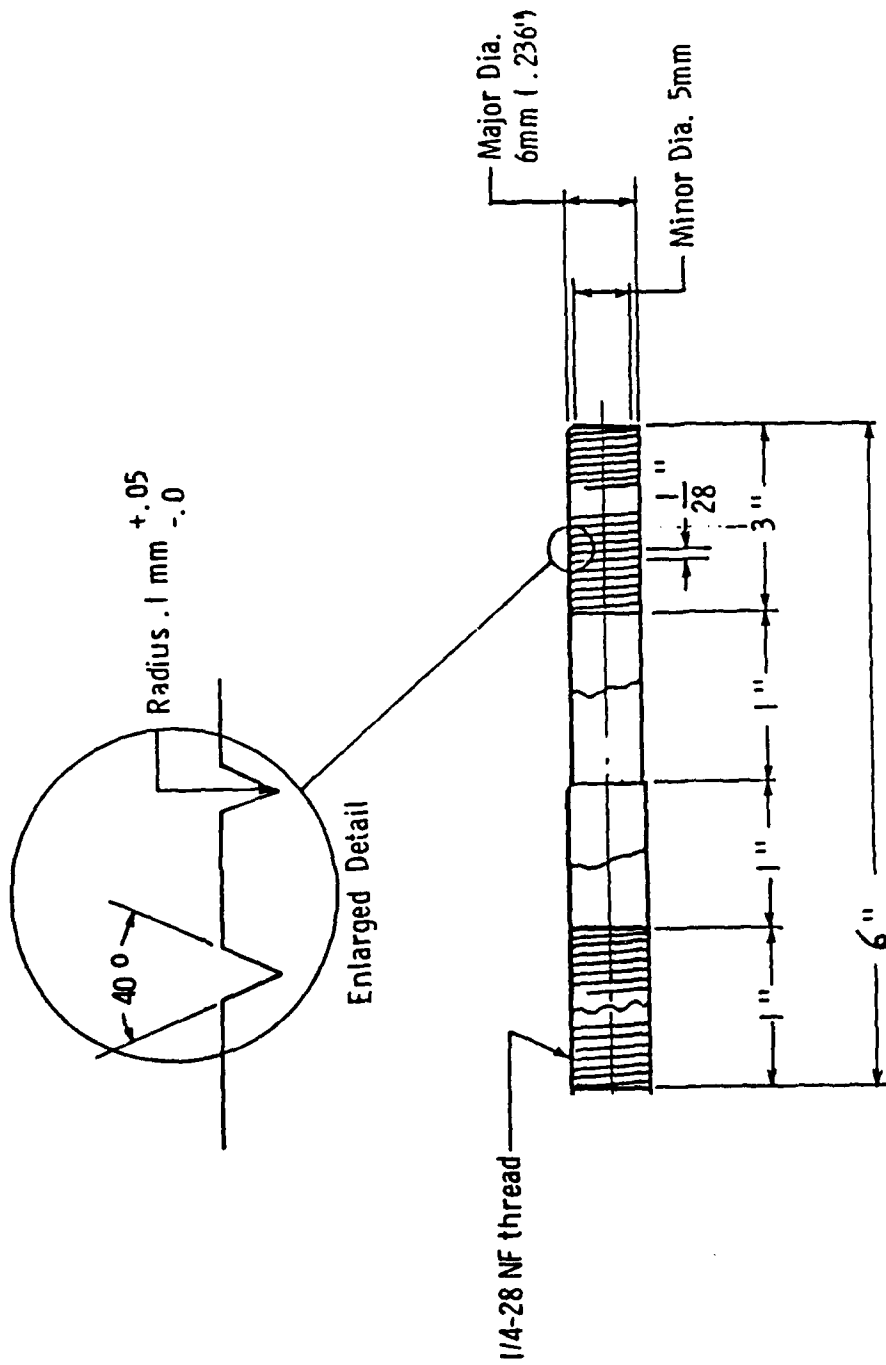
Summary of Experimental Results

% H ₂	% O ₂	Preheat	LCS	LCS	<u>H</u>	<u>H</u>
			5 min.	24 hr.	3 sec.	24 hr.
0	2	NONE	48.5	58	2.14	0.74
0	2	150 F	79	---	XXX	0.29
0	2	250 F	82.5	86	XXX	0.22
.01	2	NONE	56	52.5	4.52	1.09
.1	2	NONE	46	48.5	6.80	1.23
.1	2	250 F	47.5	52	XXX	0.42
.5	2	NONE	28	39	8.28	1.96
.5	1	NONE	---	---	8.42	1.80
.5	1	250 F	45	53	XXX	1.58
2	2	NONE	25	---	14.0	---
2	1	NONE	26.5	34	8.17	2.19
2	1	250 F	45	---	XXX	1.31

Table 5.4

Tabulation of Fracture Toughness Estimates

Sample	Stress (ksi.)	a/D	K_{1C} ksi(in) ^{1/2}	\bar{H} at crack (ppm)
1.3	88.4	.30	46.3	.14
1.4	82.2	.42	65.0	.15
2.18	24.3	.45	17.9	.26
2.20	113.0	.13	32.0	.245
3.6	24.0	.41	14.4	.275
4.1	89.2	.15	31.8	.215
4.6	82.8	.35	57.8	.19
17.2	55.0	.50	70.5	.135
2.1	109.0	.45	116	.75
2.2	82.2	.41	68	.81
16.5	27.0	.60	60.8	.56
20.1	28.0	.60	63.1	.69



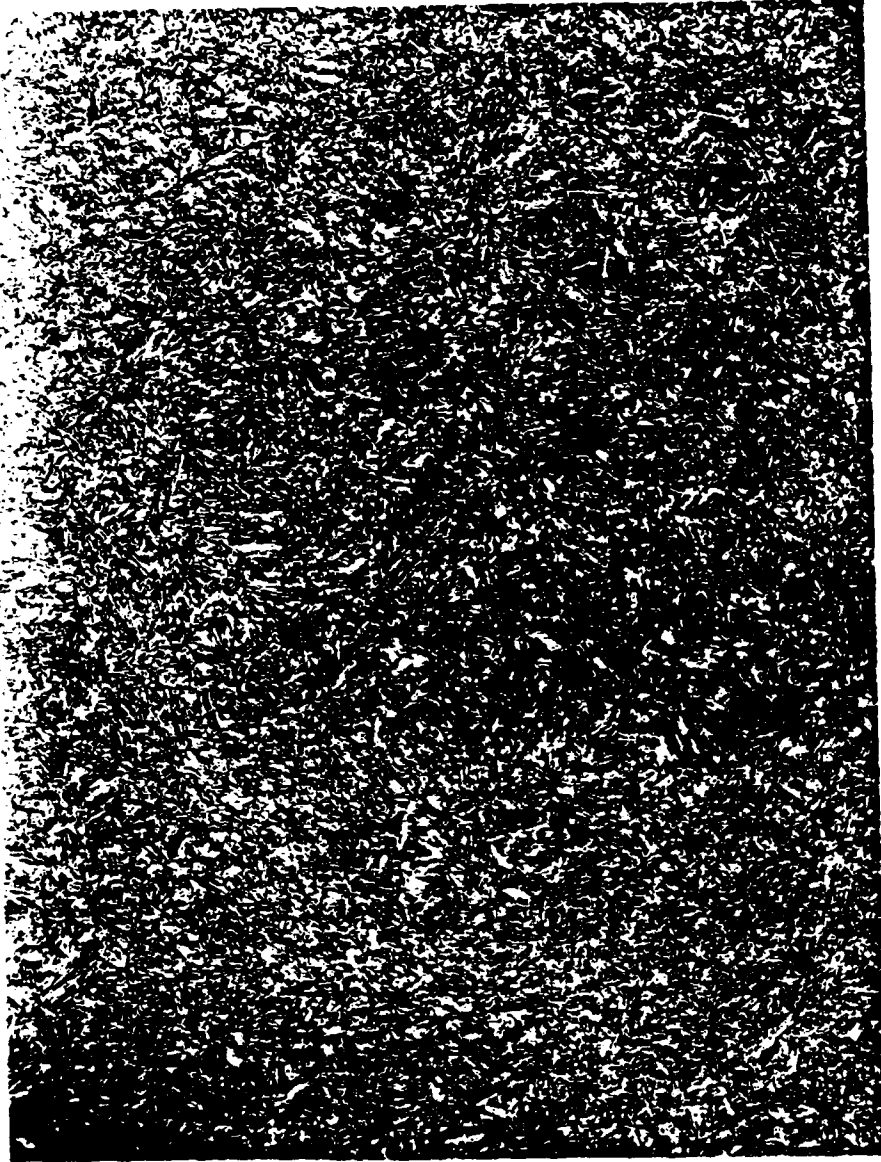
IMPLANT SPECIMEN

Scale - 2/1

5.1 Implant specimen geometry



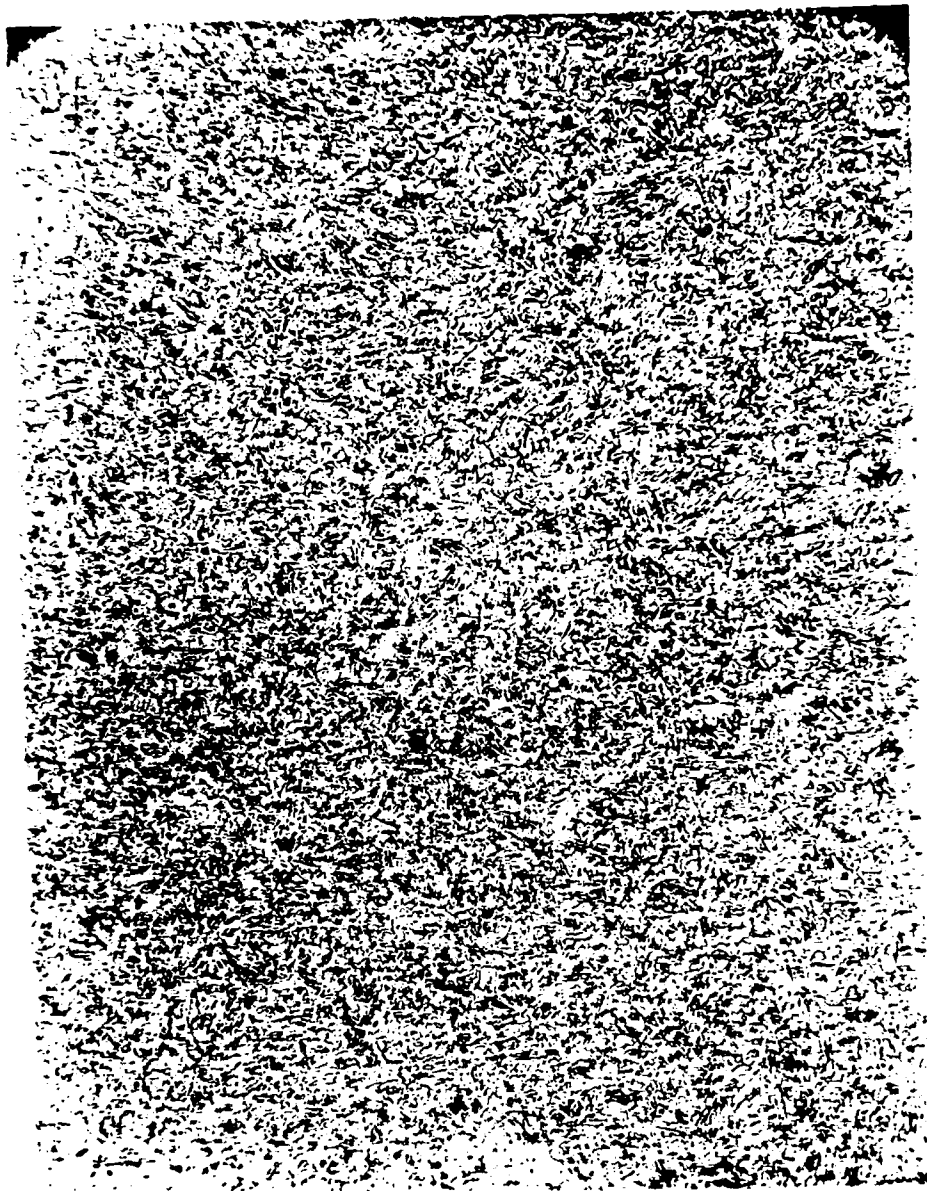
5.2 Microstructure of as-received MIL-A-46100
high strength steel alloy. 100X, Nital etch.



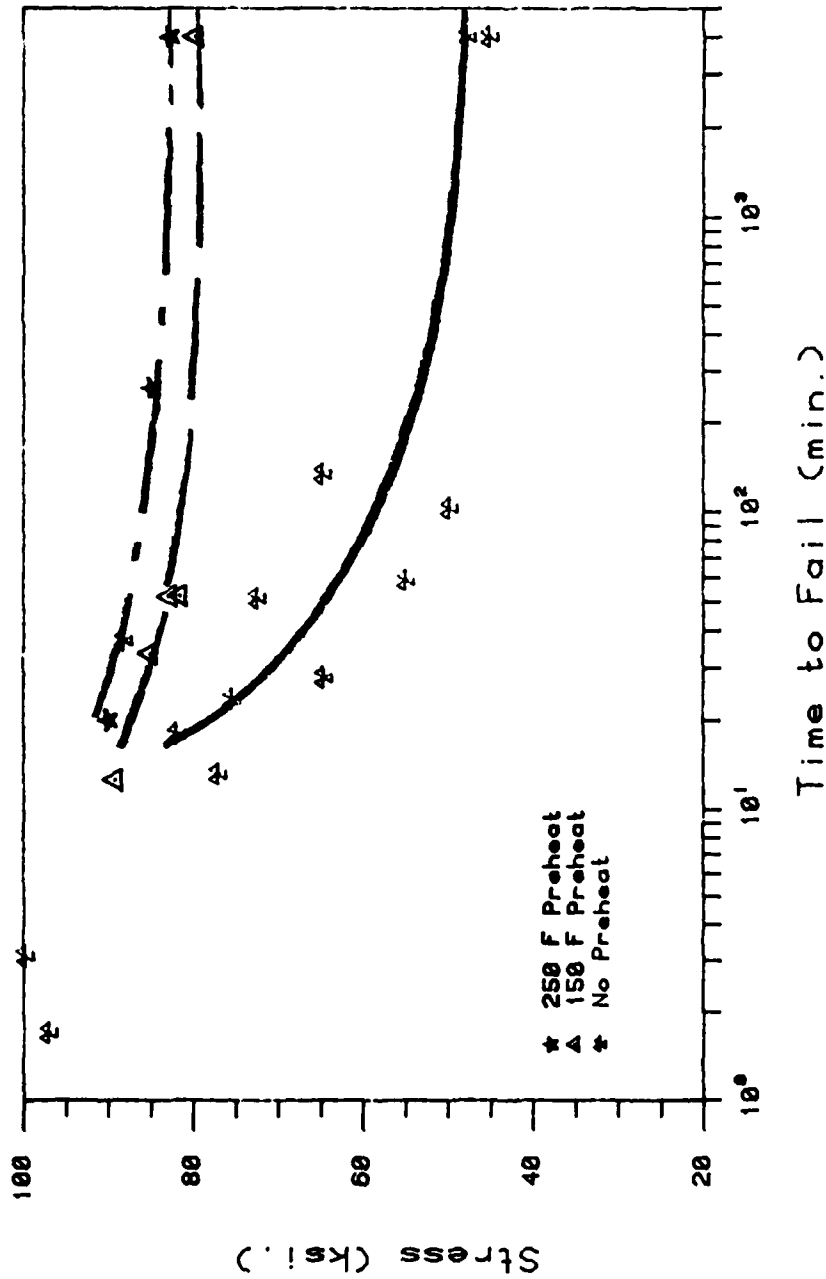
5.3 Microstructure of as-received MIL-A-46100
500X, Nital etch.



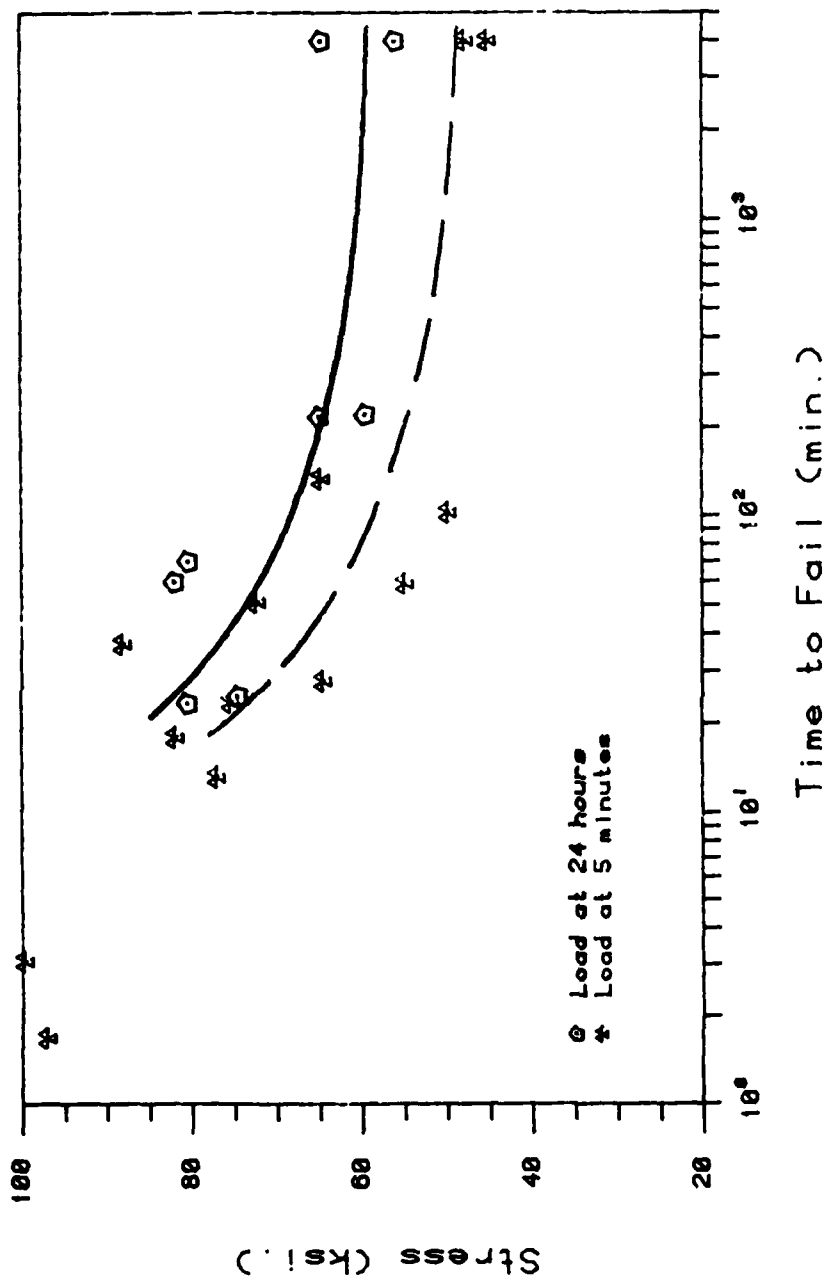
5.4 Microstructure of MIL-A-46100 after heat treatment procedure and machining. 50X, Nital etch.



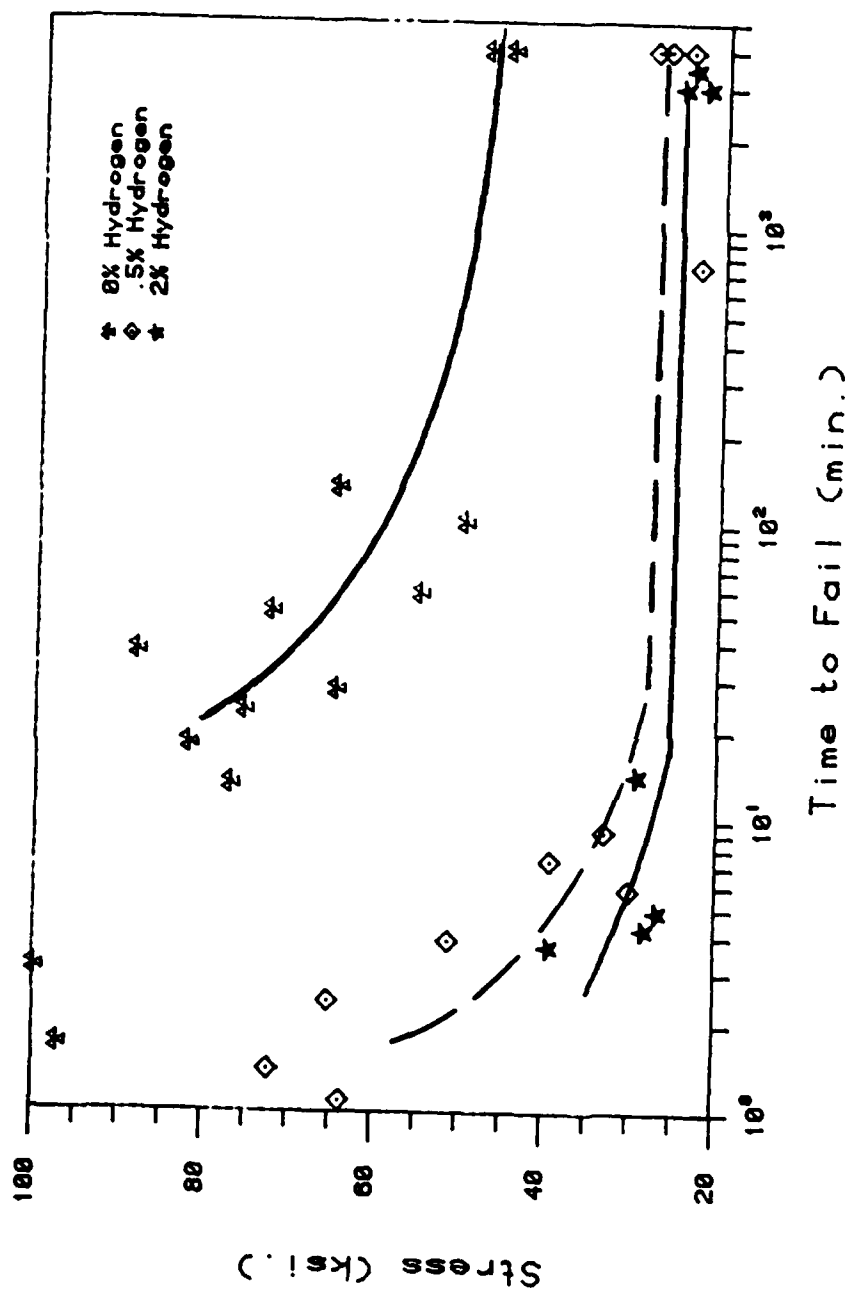
5.5 Microstructure of MIL-A-46100 after heat treatment procedure. 500X, Nital etch.



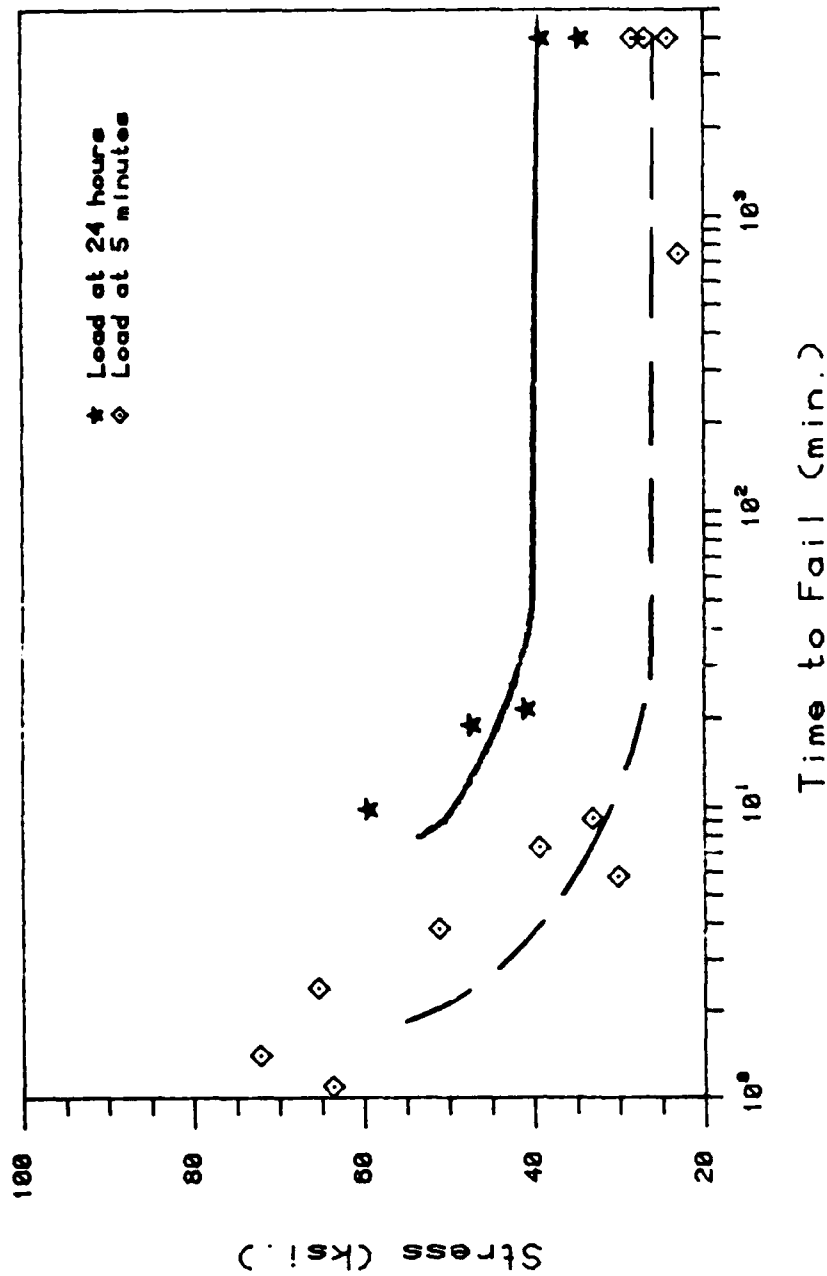
5.6 Implant test results for GMA welds made with 0% H₂ / 2% O₂ / Ar and loaded 5 minutes after welding. Curves depict welds made with 250 F, 150 F, and no preheat.



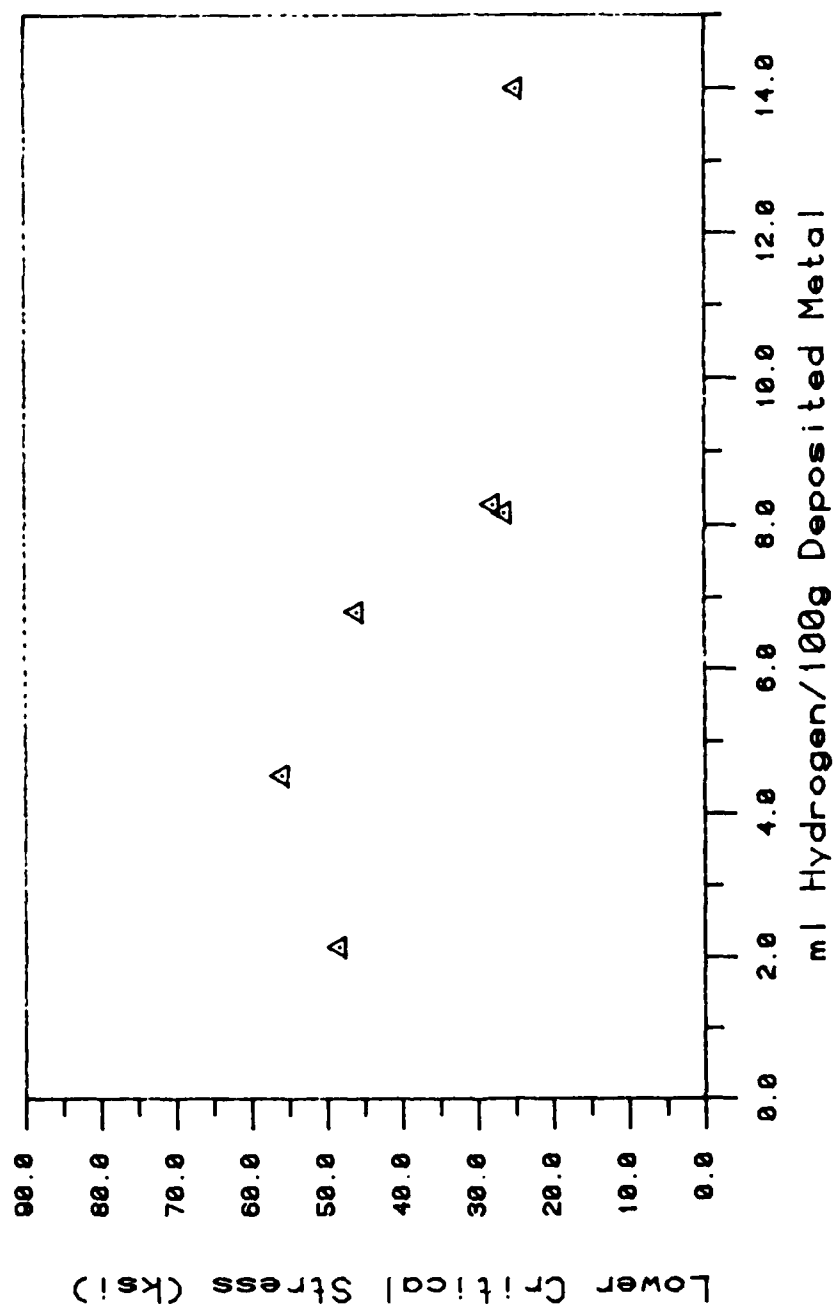
5.7 Implant test results for GMA welds made with 0% H₂ / 2% O₂ / Ar and loaded 5 minutes after welding and 24 hours after welding.



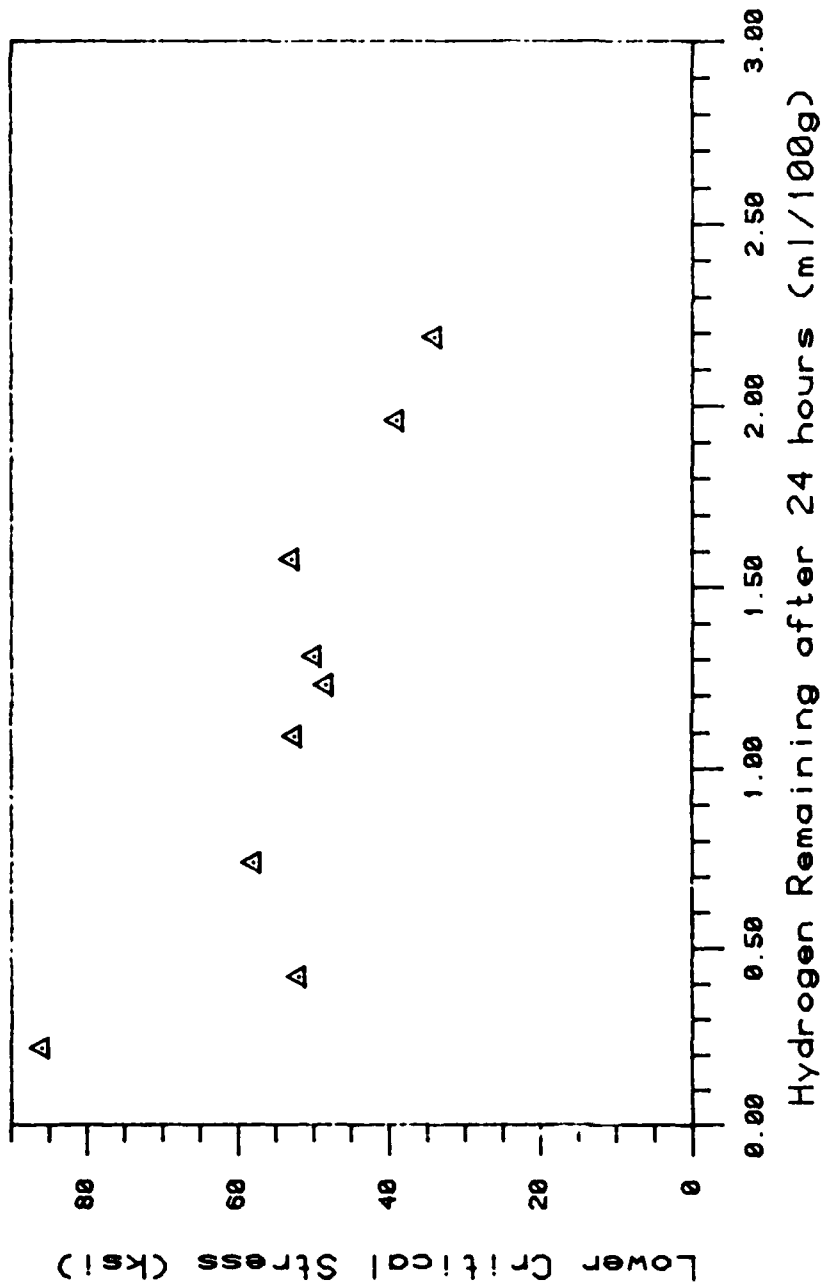
5.8 Implant test results for GMA welds made with 2% O₂ and loaded after 5 minutes. Curves depict 0%, .5%, and 2% H₂ added to the shielding gas.



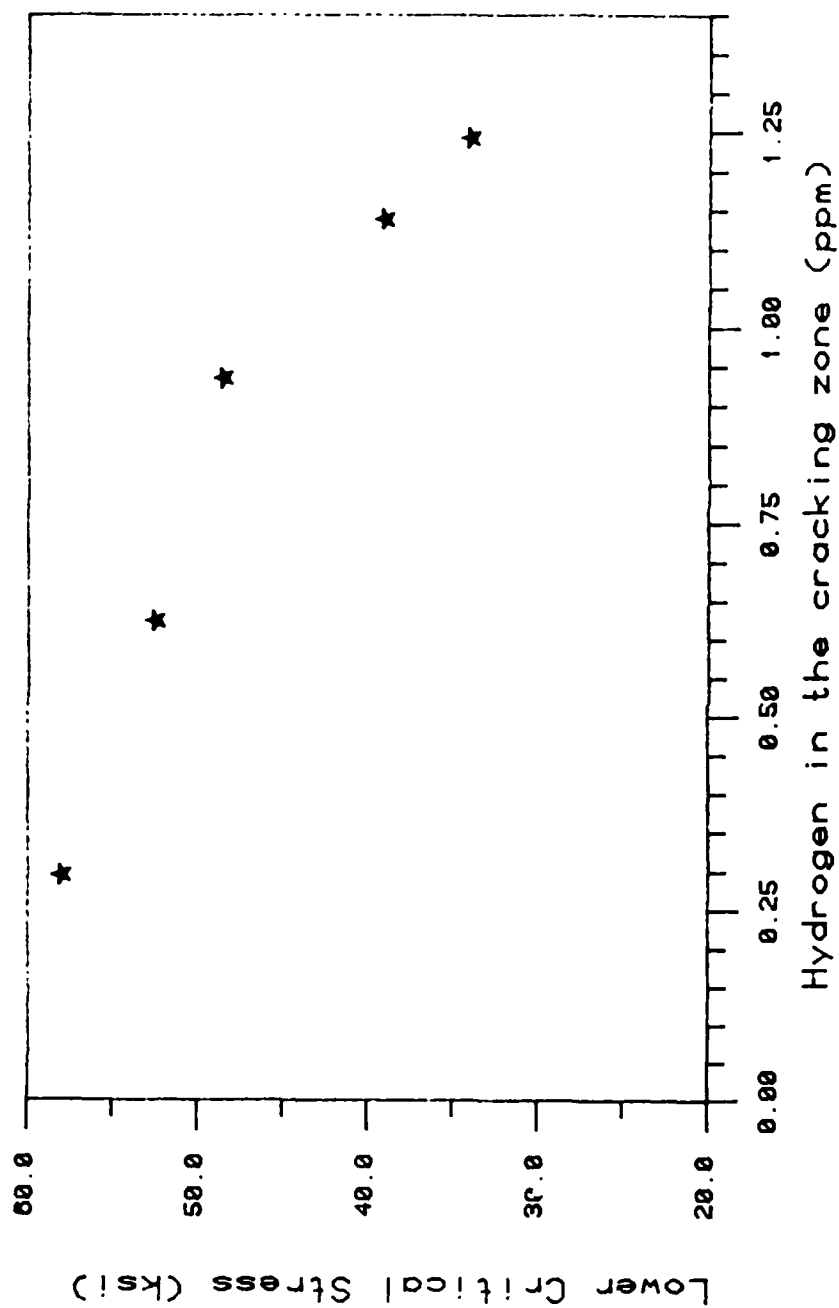
5.9 Implant test results for GMA welds made with
 .5% H₂ / 2% O₂ / Ar and loaded at
 5 minutes and 24 hours.



5.10 Lower Critical Stress for welds loaded at 5 minutes after welding versus the initially absorbed hydrogen content.



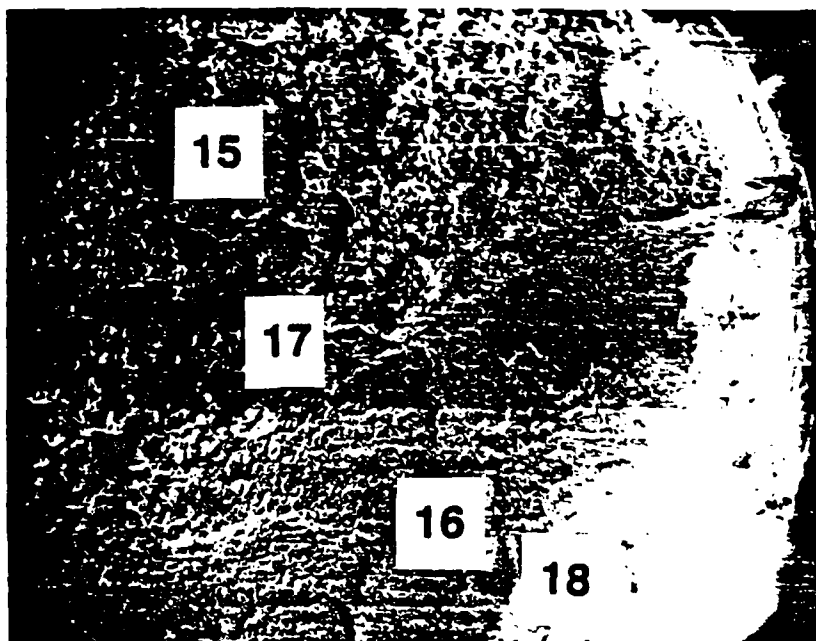
5.11 Lower Critical Stress for welds loaded at 24 hours after welding versus the amount of hydrogen remaining 24 hours after welding.



5.12 Lower Critical Stress for welds loaded at 24 hours after welding versus the amount of hydrogen present in the cracking zone after 24 hours.



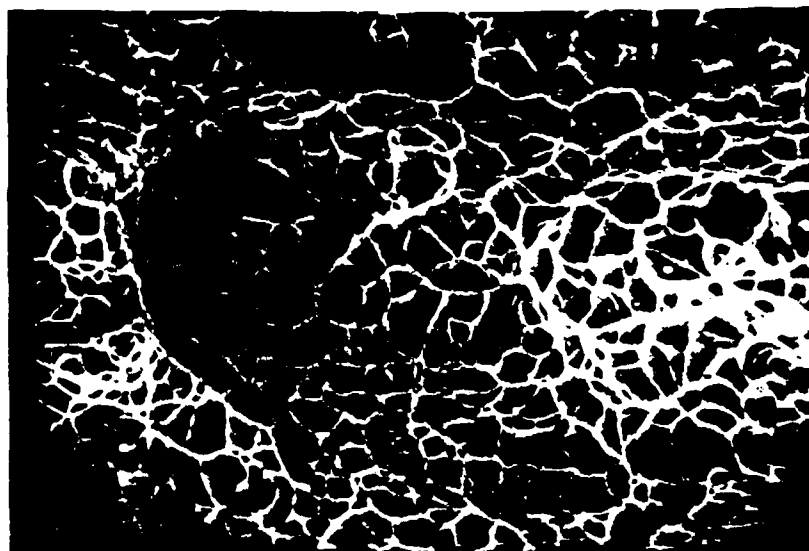
5.13 Overall SEM view of a fractured implant specimen surface. 20X



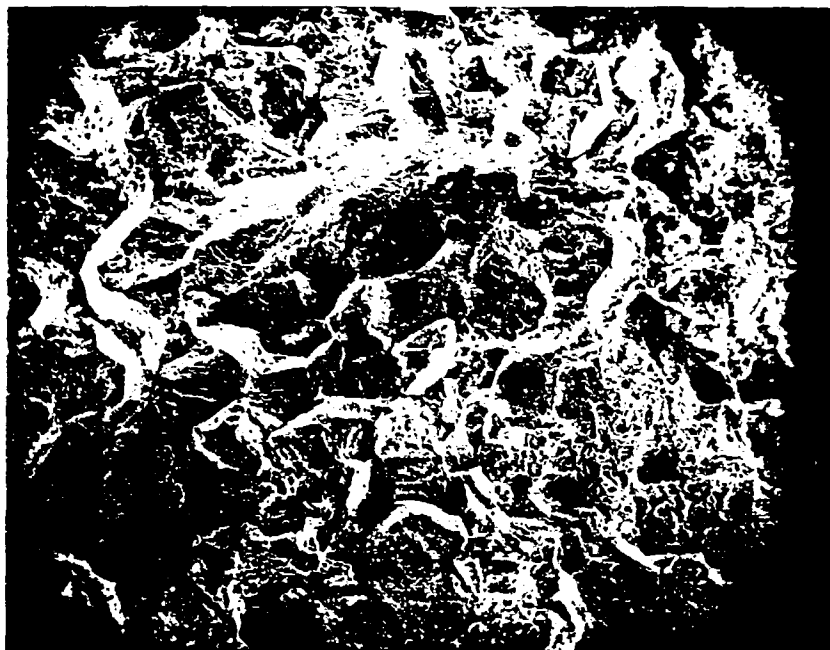
5.14 Schematic showing the regions from which the magnified photos were taken.



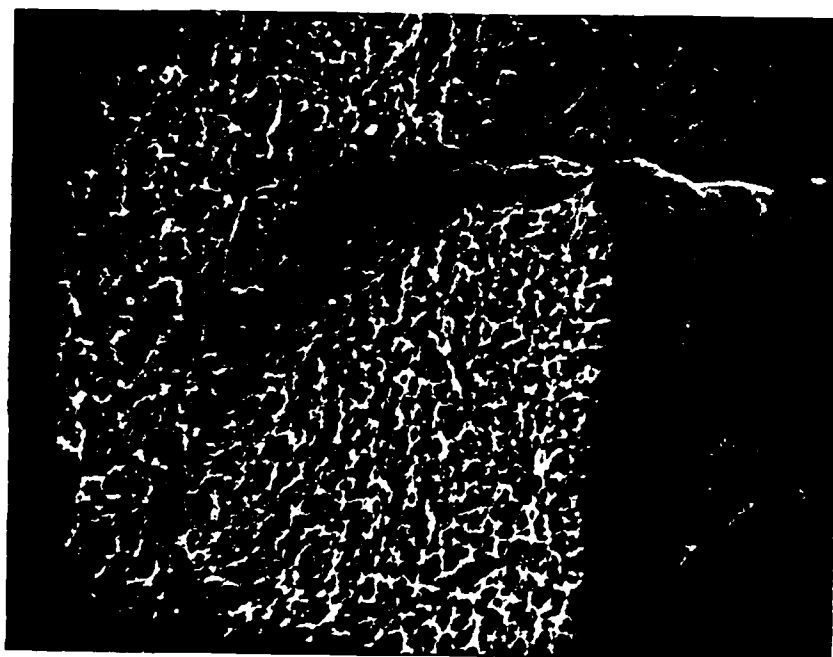
5.15 Region of intergranular fracture characteristic of hydrogen embrittlement. 2000X



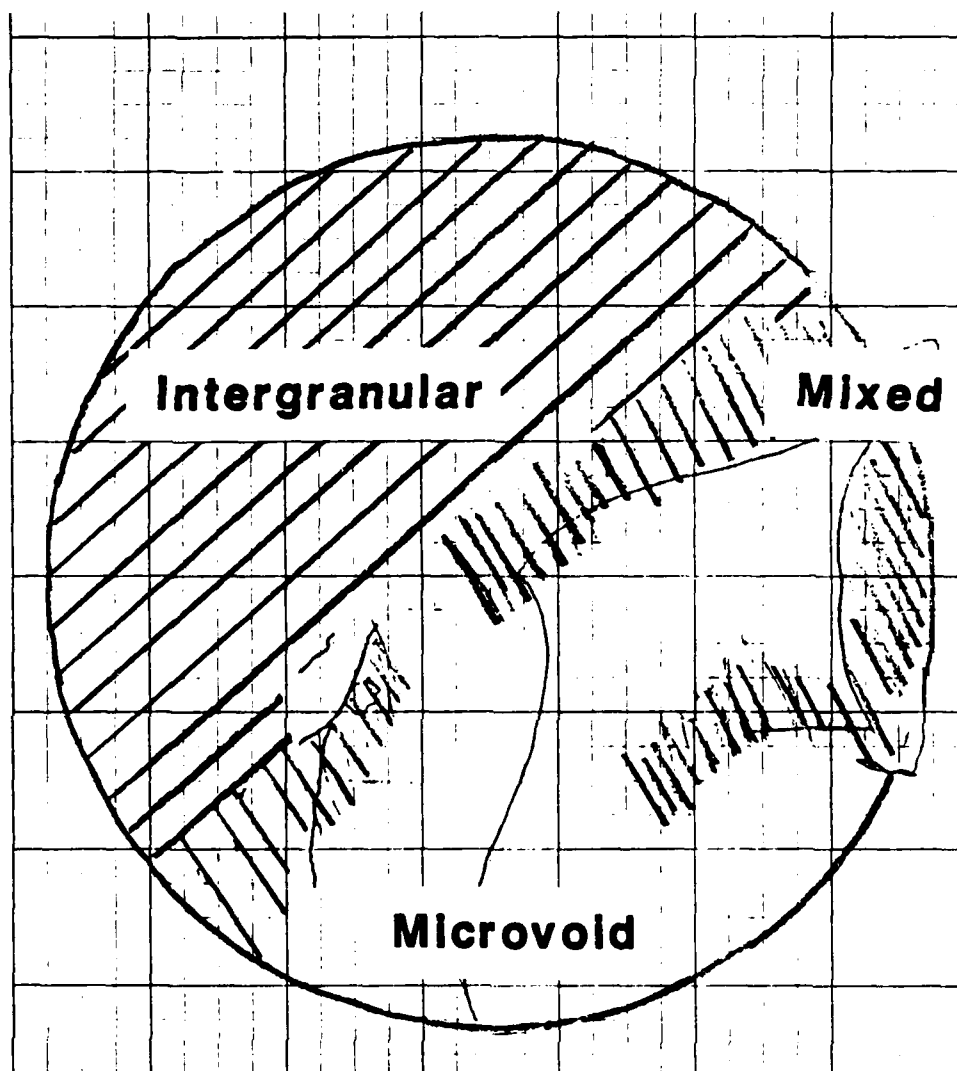
5.16 Region of microvoid coalescence showing ductile dimples. 2000X



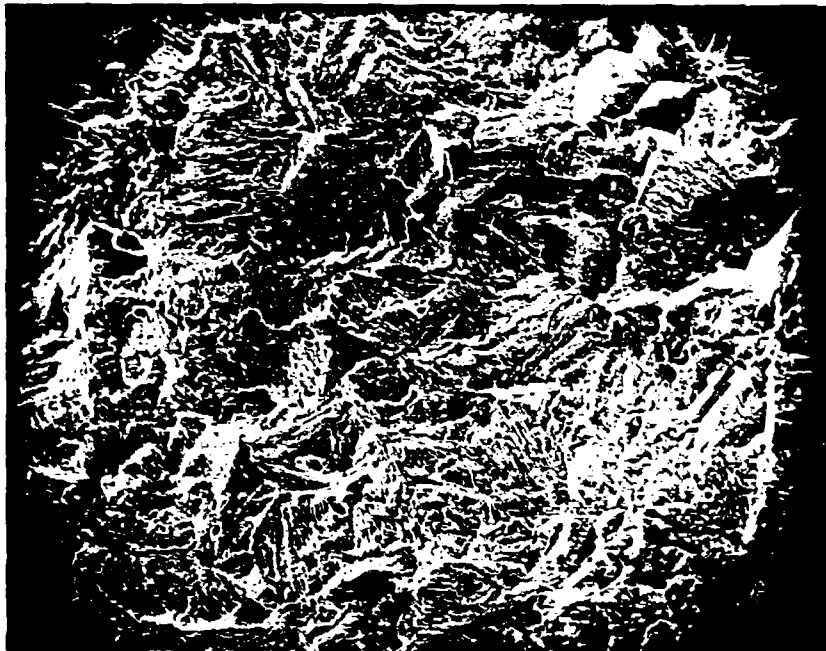
5.17 Transition region where both intergranular fracture and microvoid coalescence are evidenced. 200X



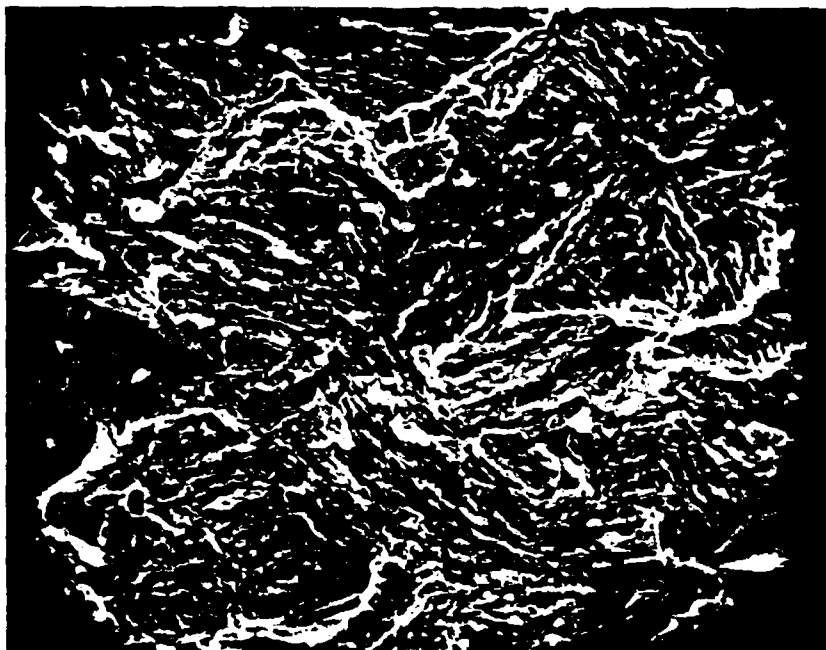
5.18 Region of fast fracture in the shear lip bordered by microvoid coalescence. 2000X



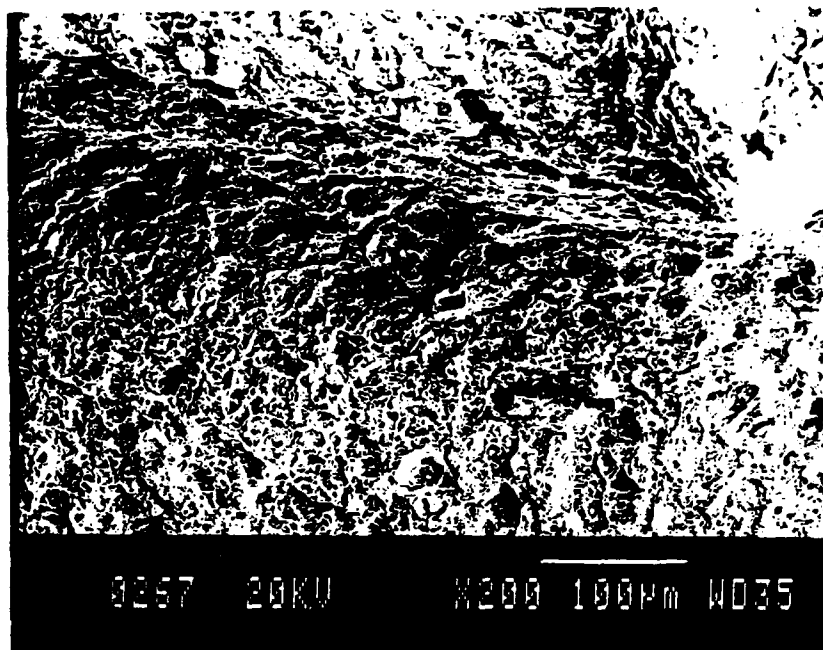
5.19 Quantitative fracture map showing the regions of fracture types.



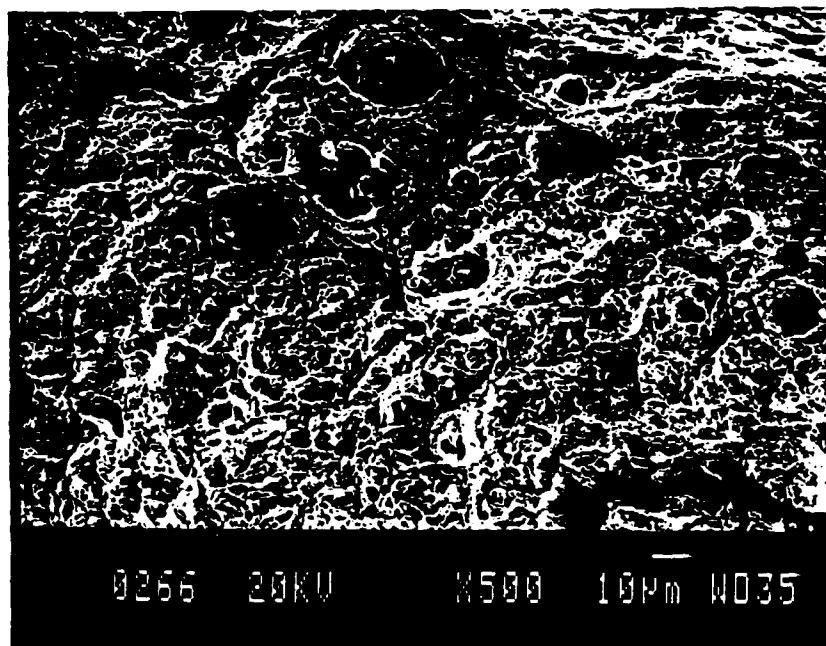
5.20 Area of quasi-cleavage fracture. 200X



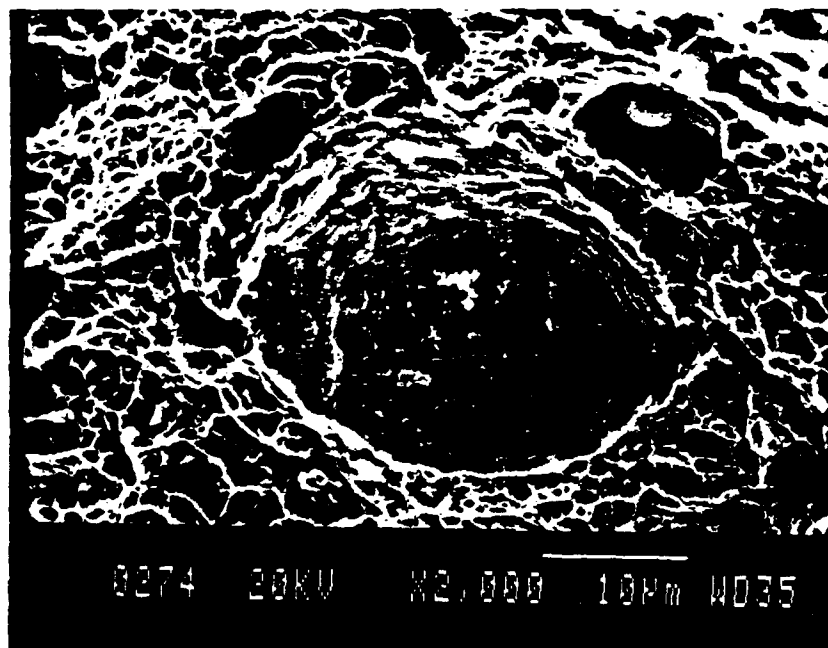
5.21 Magnified area of quasi-cleavage fracture. 1000X



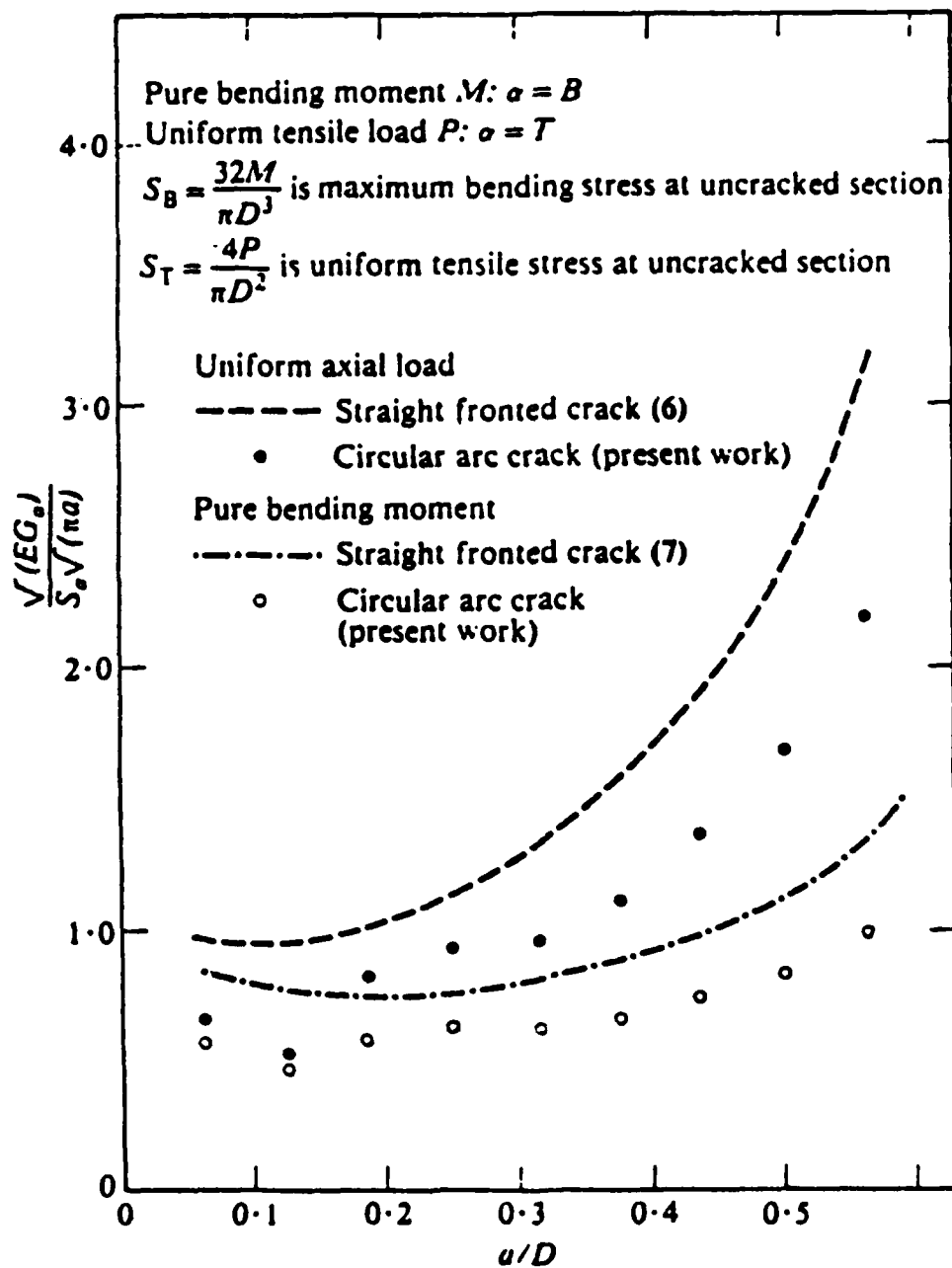
5.22 Area of "fisheyes" evidenced in implant specimens with low hydrogen content. 200X



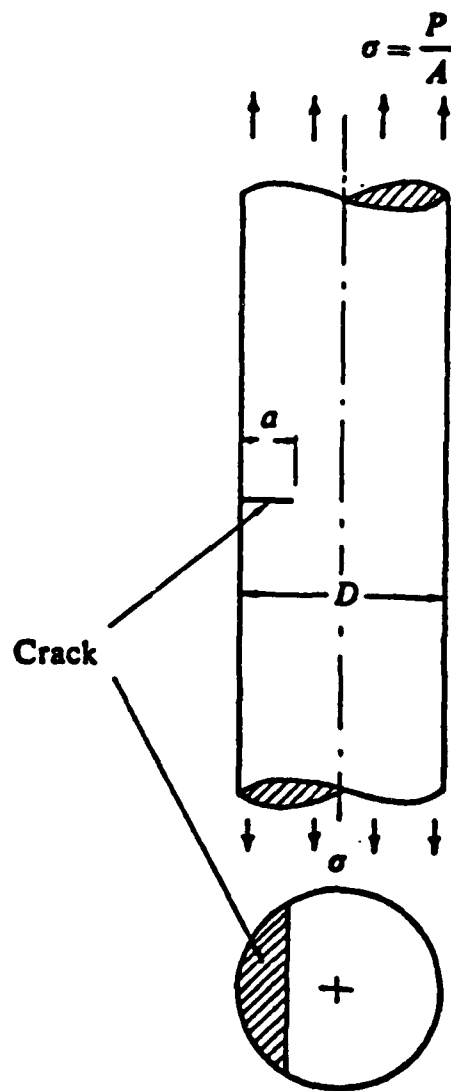
5.23 Magnified area of "fisheyes". 500X



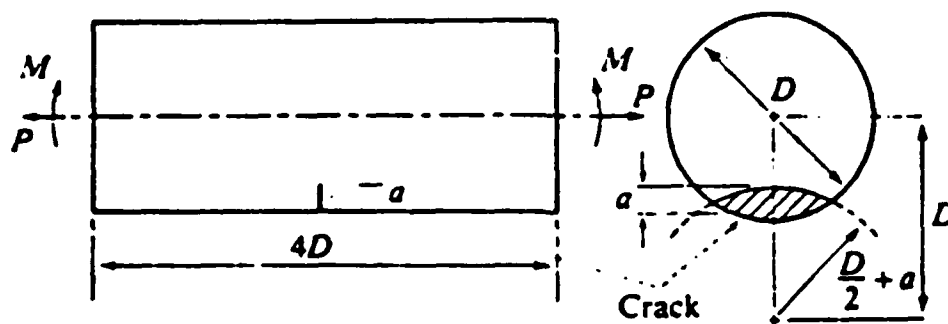
5.24 Magnification of one "fisheye" showing the inclusion at the bottom of the embrittled region. 2000X



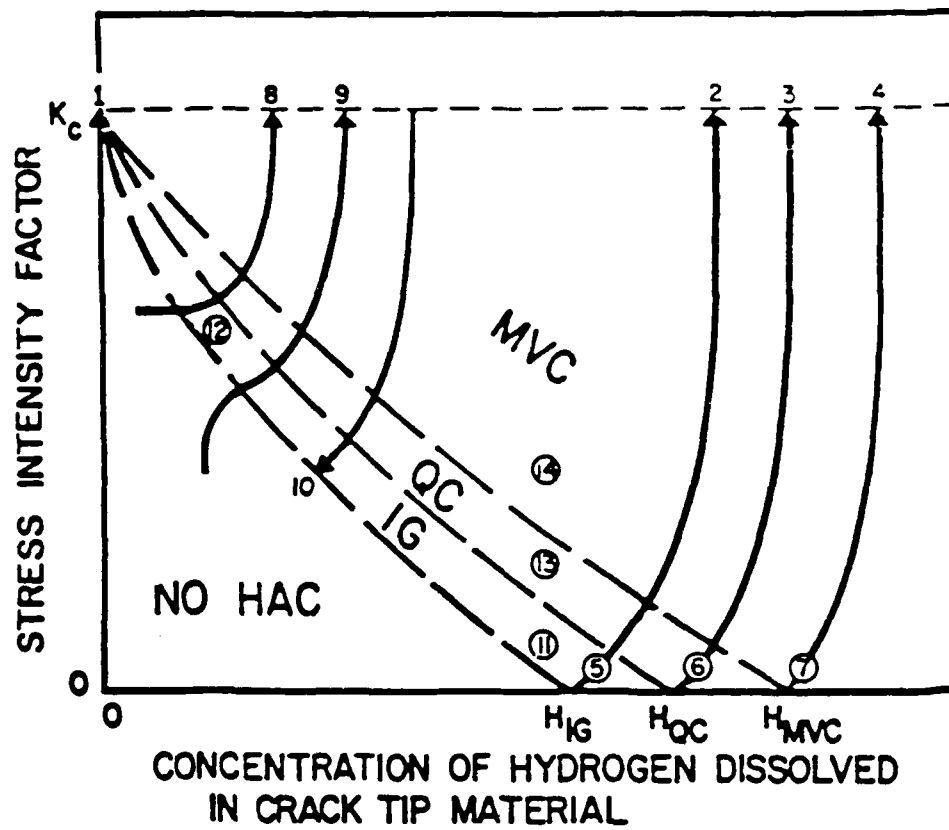
5.25 Strain energy release rates for a circular-arc fronted edge crack and a straight fronted edge crack in a round bar in tension. (Ref D.2)



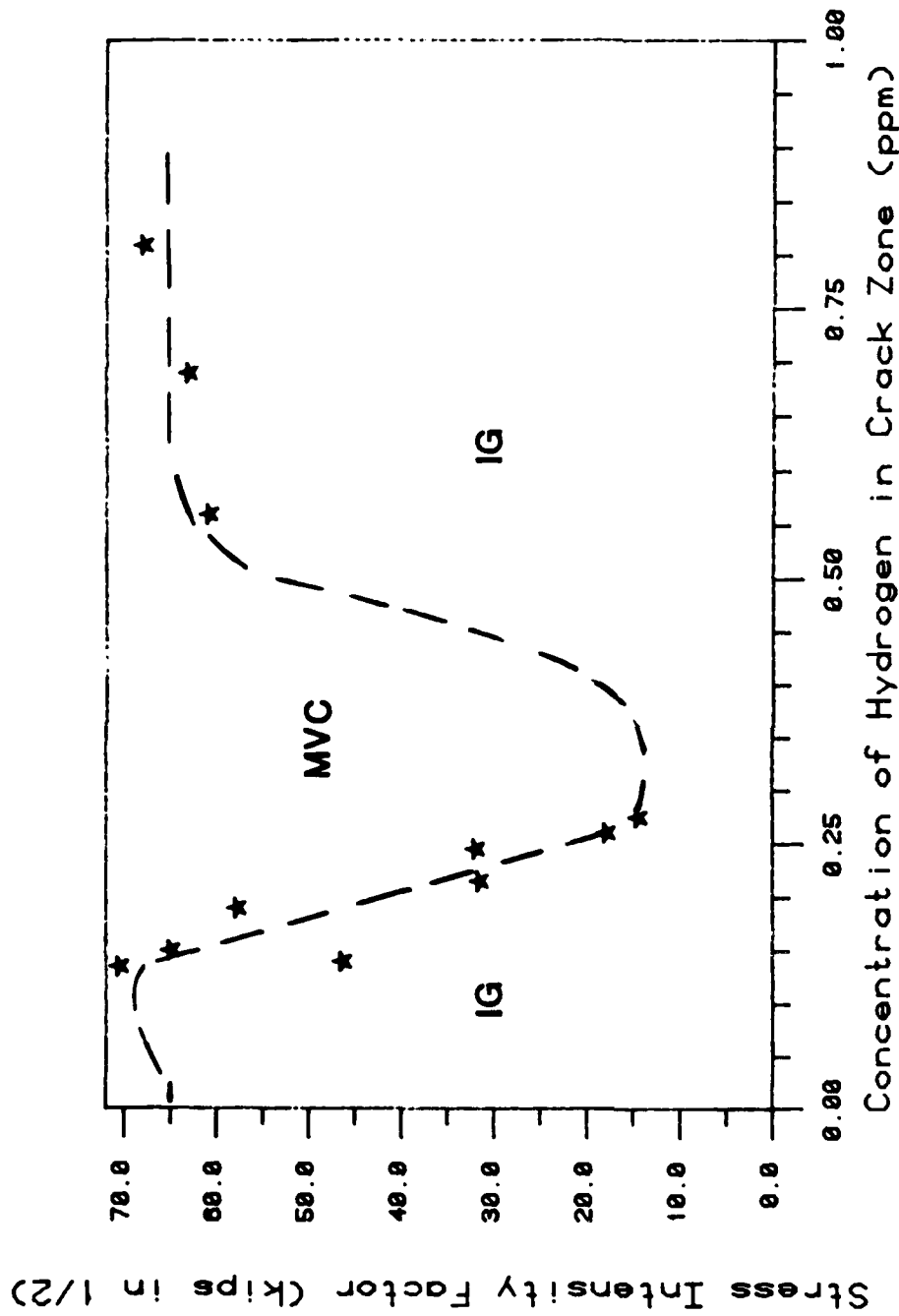
5.26 Crack geometry for a single straight fronted edge cracked round bar in tension. (Ref D.1)



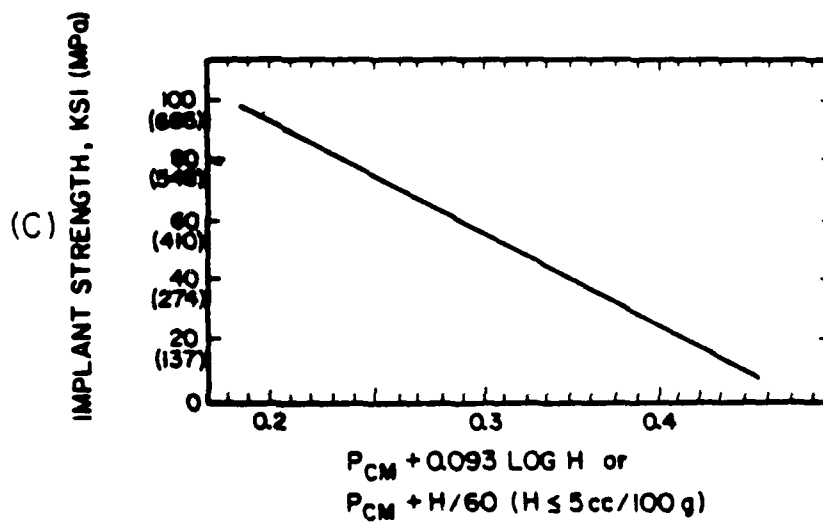
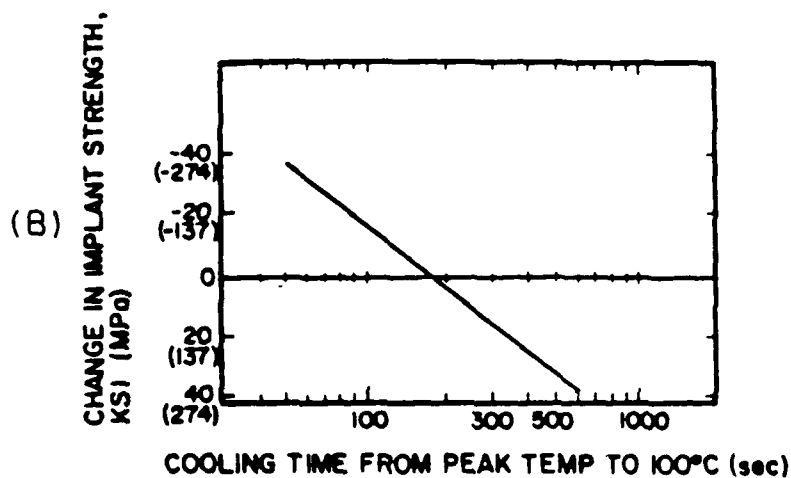
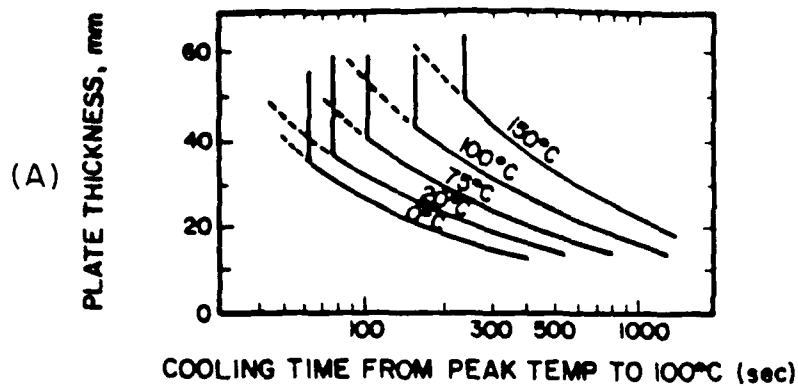
5.27 Crack geometry for a circular-arc fronted edge crack in a round bar in axial tension. (Ref D.2)



- 5.28 Suggested interrelationship by Beachem between stress intensity factor, dissolved hydrogen content, and HAC deformation mode of microscopically small volumes of crack-tip material. (Ref B.7)



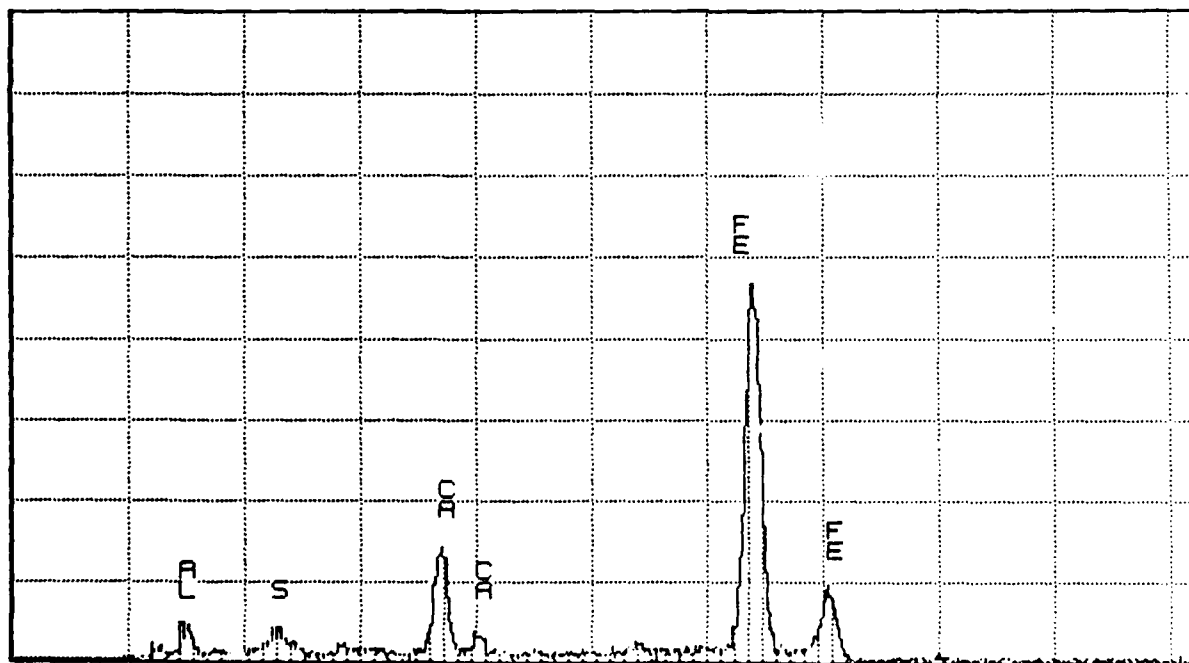
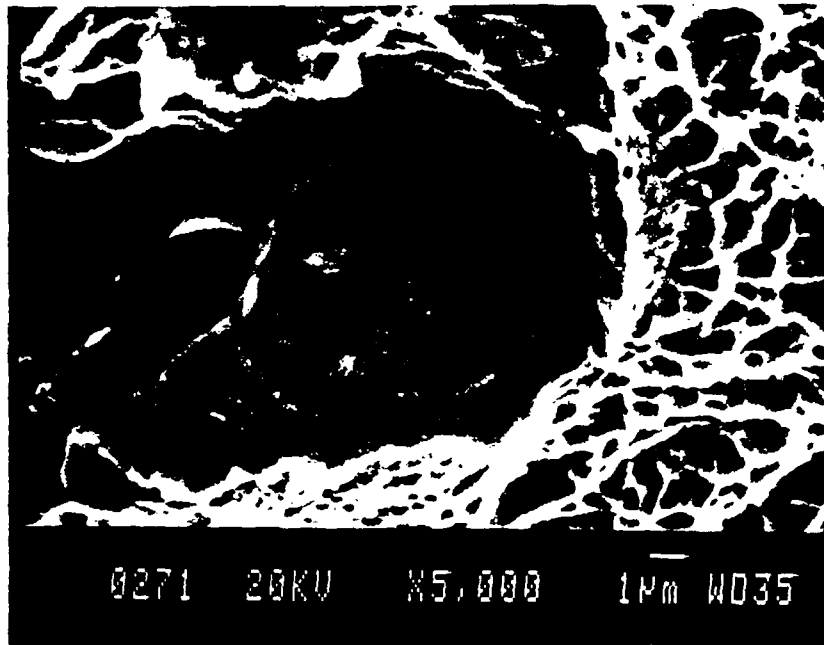
5.29 Interrelationship developed in this study between the stress intensity factor, hydrogen content in the cracking zone, and mode of fracture.



5.30 A method of predicting the LCS developed by Ito, et al. (Ref. I.11)

APPENDIX 5A

Scanning Electron Microscope (SEM) photographs of "fisheyes" along with the corresponding Elemental Dispersive X-ray Analysis (EDX) of the inclusion composition.



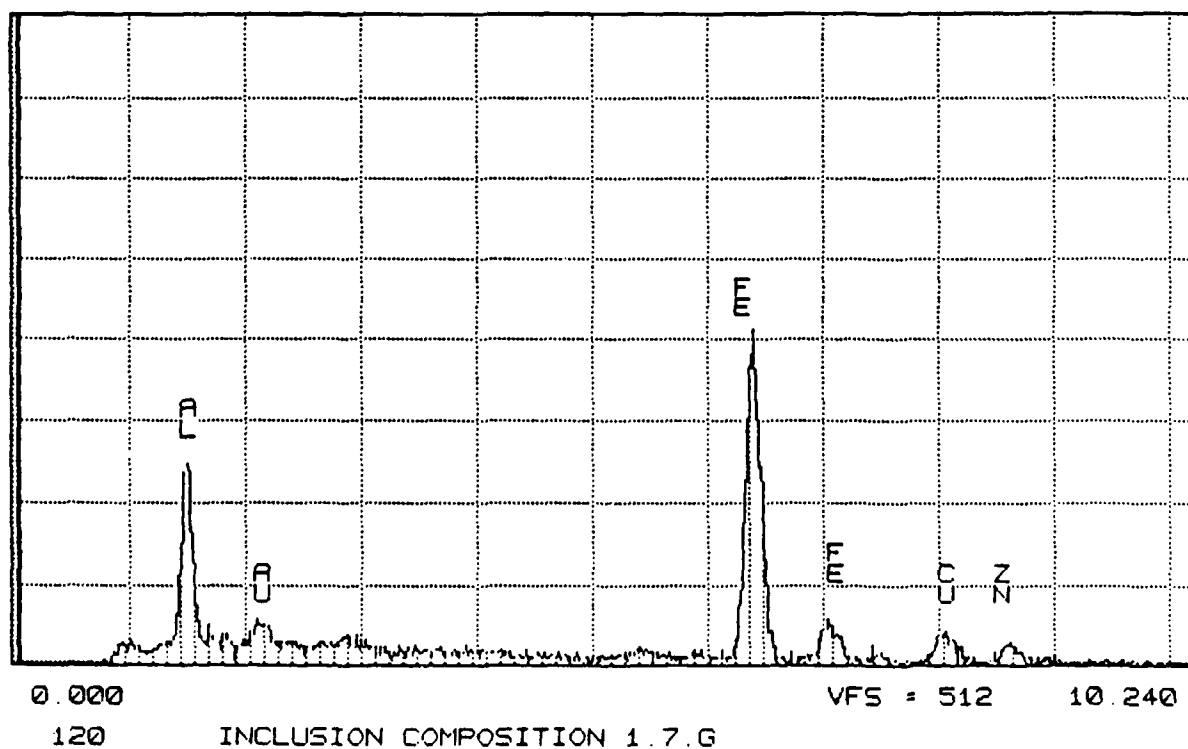
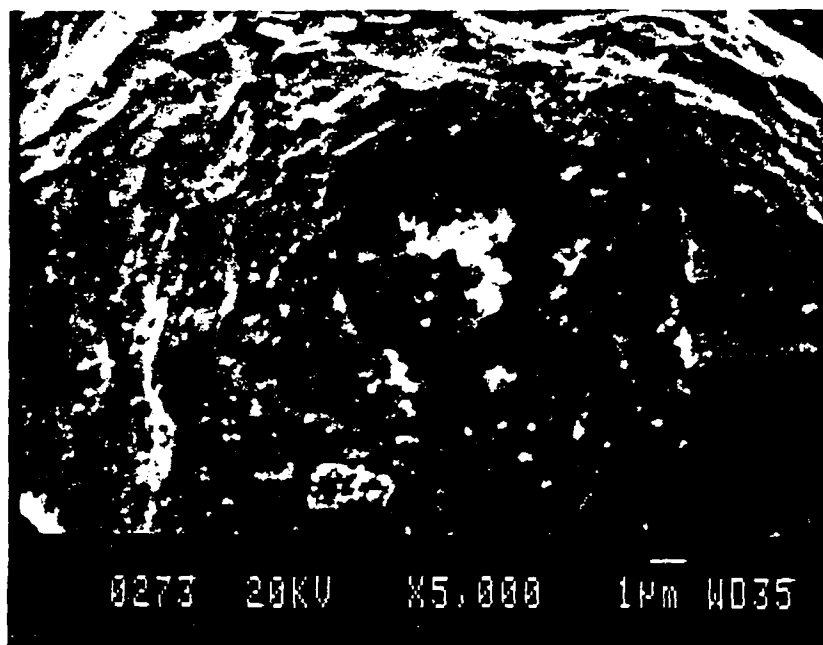
0.000

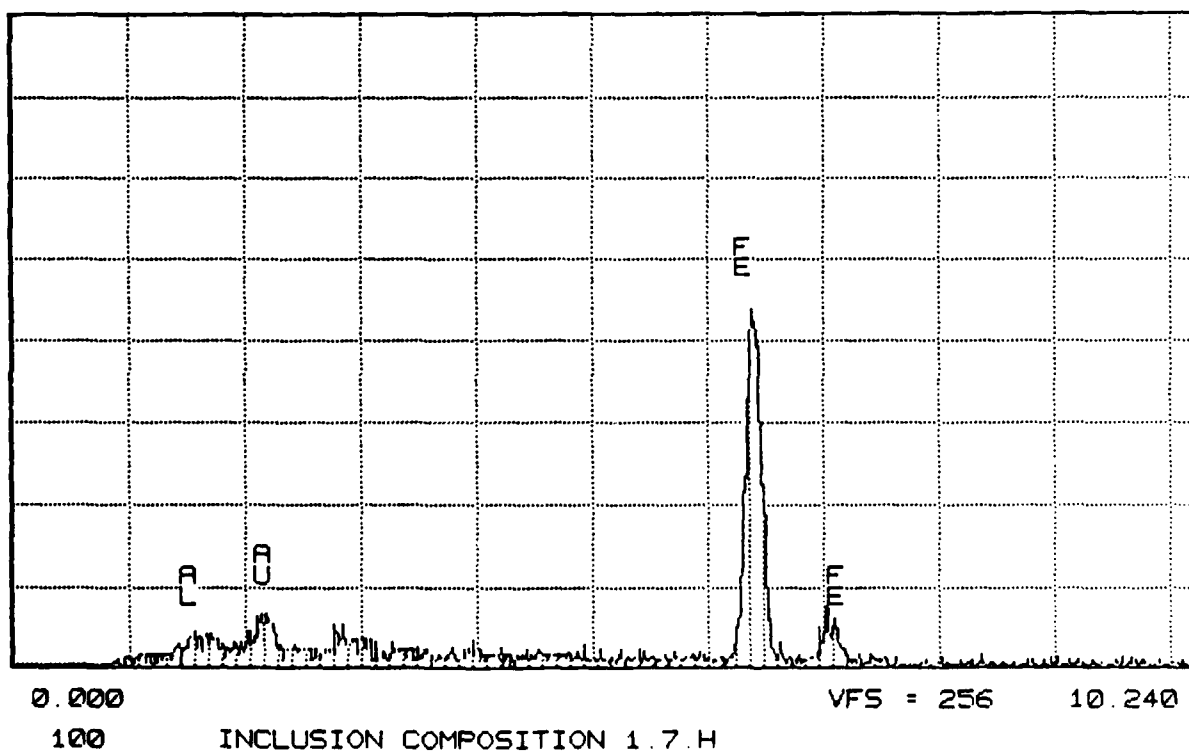
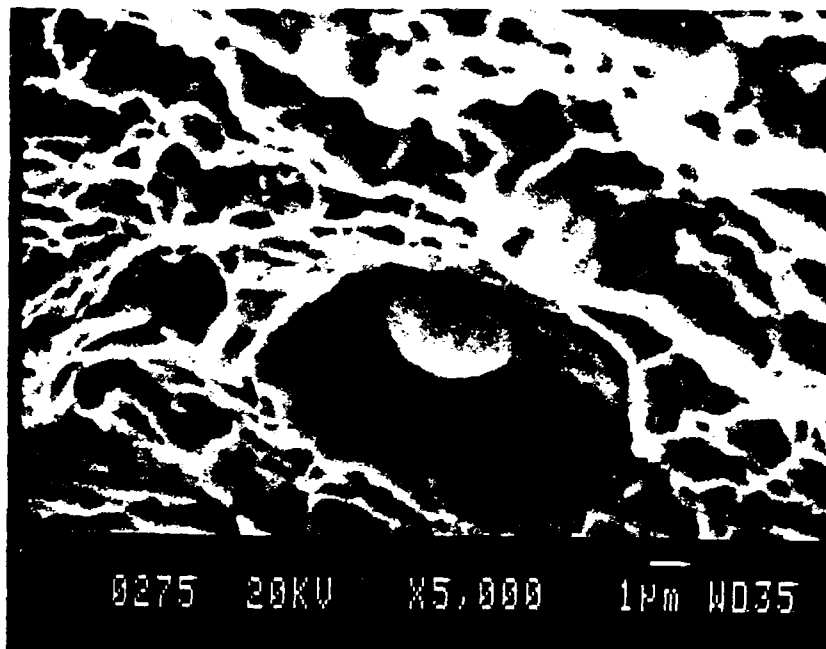
VFS = 512

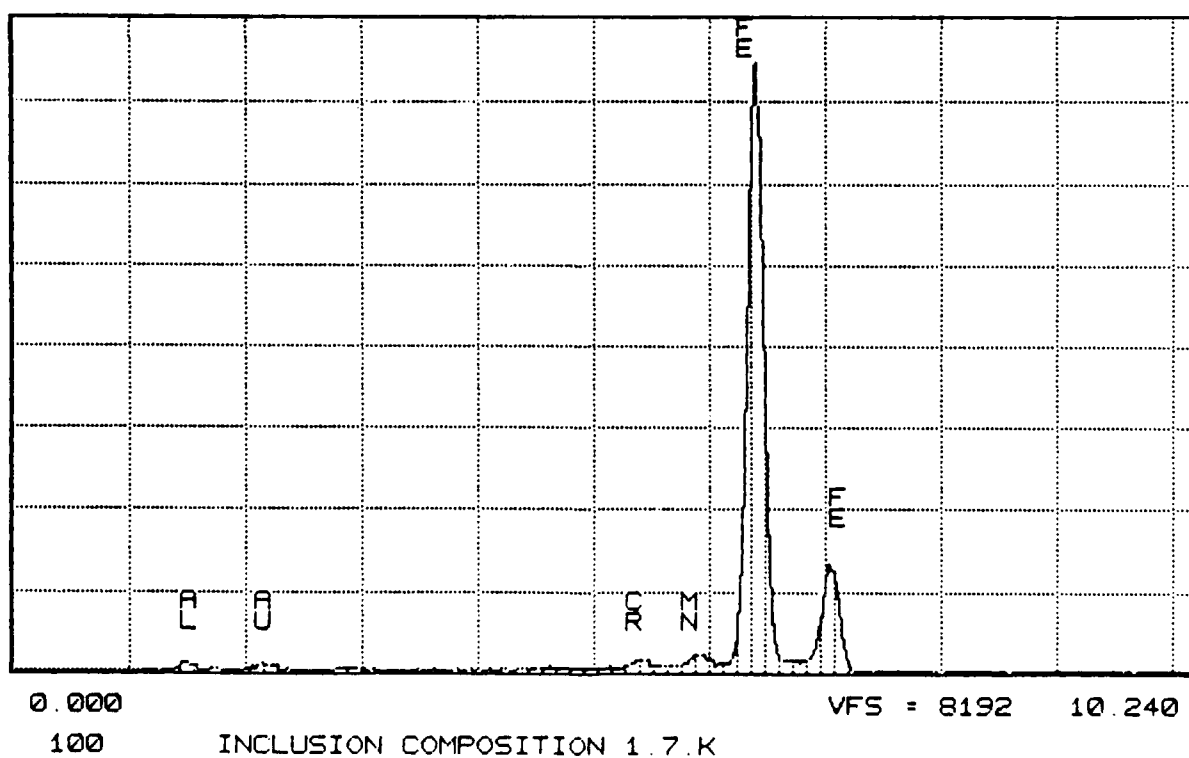
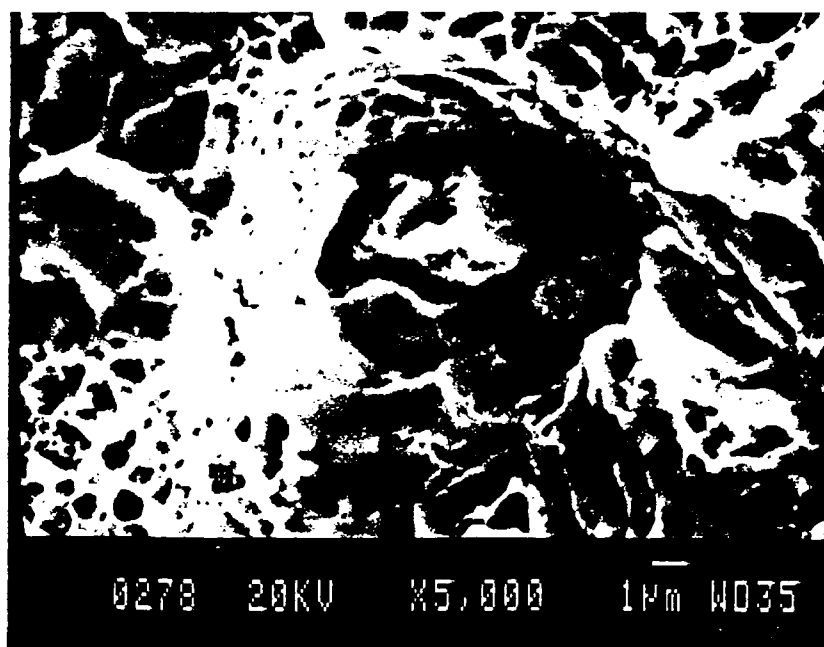
10.240

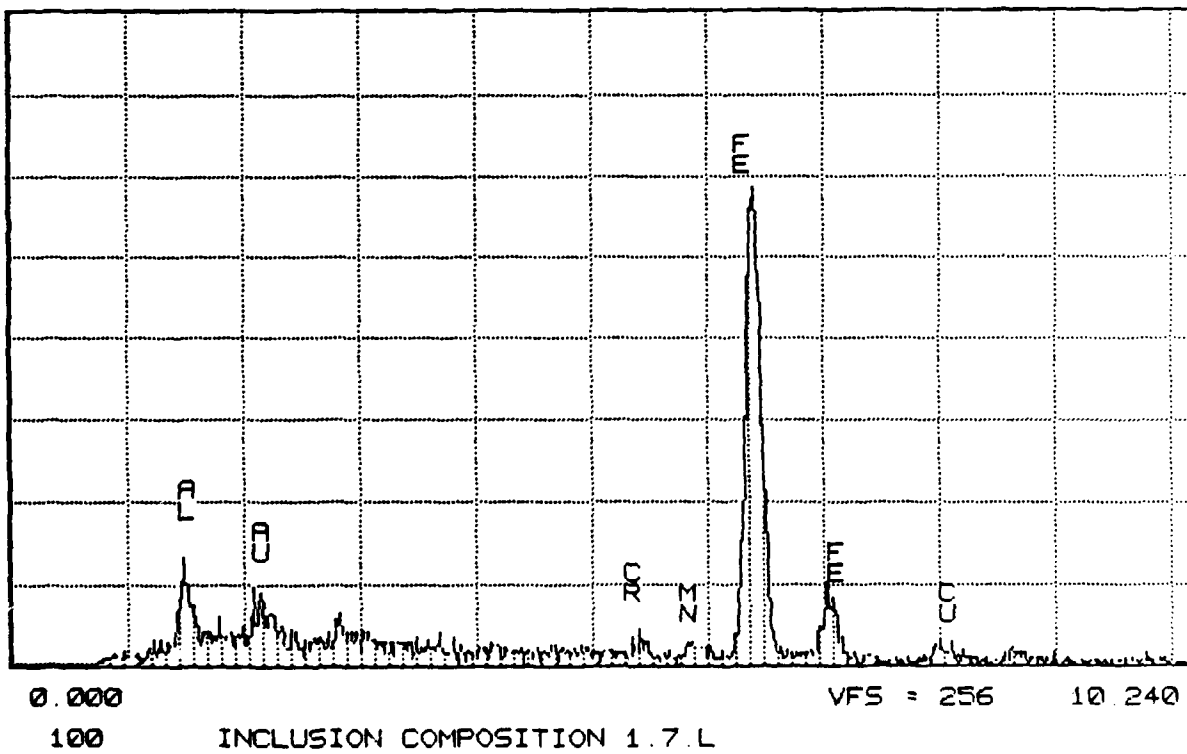
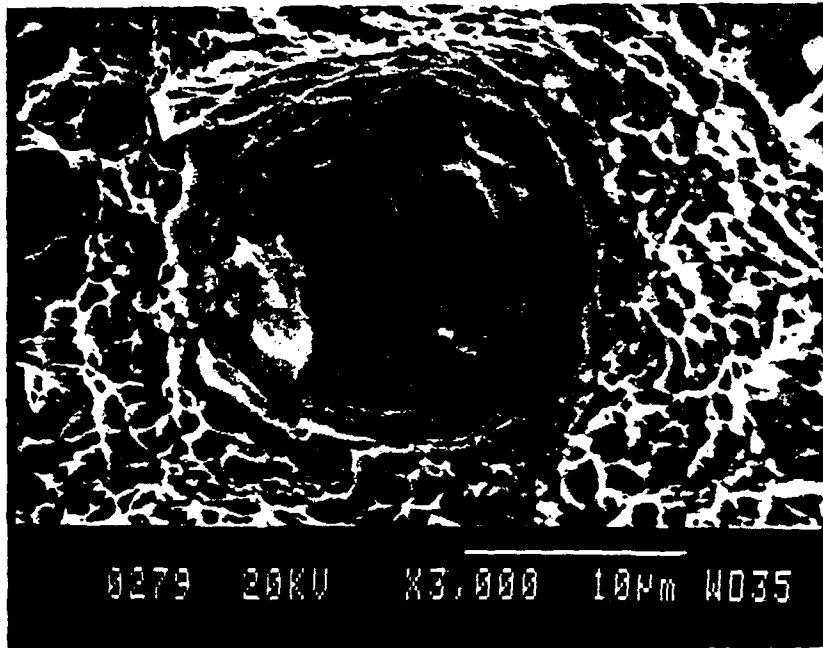
101

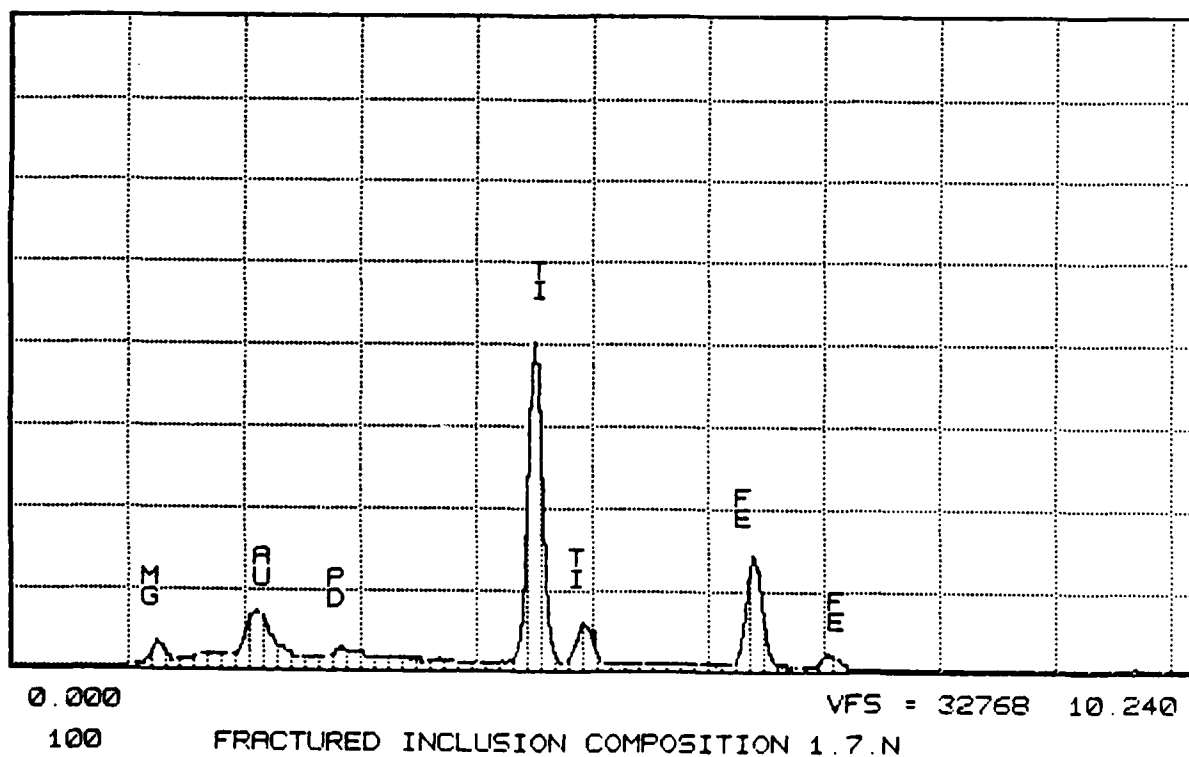
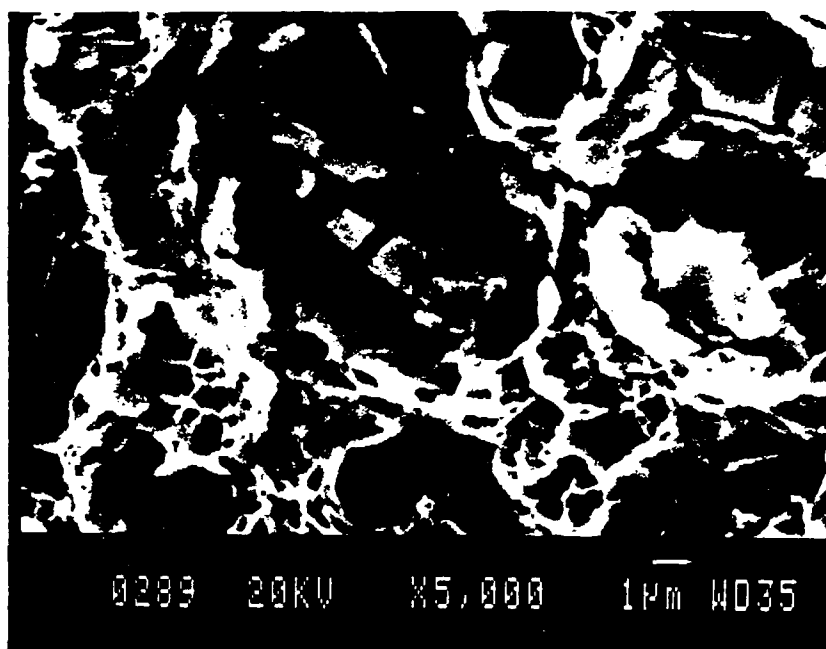
FRACTURED INCLUSION COMPOSITION 1.7.F











6.0 SUMMARY

A thorough literature review was performed in the field of hydrogen assisted cracking of high strength steel welds. This survey showed that: hydrogen measurement methods are incompletely understood and standardized in the welding field, the mechanism of hydrogen absorption into GMA weld pools needs to be researched, the effect of shield gas composition needs to be quantified, and hydrogen cracking mechanisms need to be applied to high strength steel weldments.

In response to these and other needs, chapter 2 investigates the measurement of hydrogen in welds. Results demonstrate that the AWS commission standard A4.3-86, completed in 1986, will result in more accurate measurements than the current IIW standard. The outgassing temperature should be standardized at 45 C, however, in order to eliminate the effect of variations in trapping sites from one steel to another. Gas Chromatography can be more accurate and reliable than outgassing under a eudiometer tube, but the GC must be carefully calibrated and operated or there can be substantial errors.

The hydrogen measurement technique chosen with the above results was then used to study the effect of weld process variations on the weld hydrogen content. It was shown that increasing oxygen in the argon shielding gas (for 0%, 2%, 5%, and 10% O_2) resulted in increased amounts of hydrogen in the weld. It was shown that similar carbon dioxide addi-

tions to argon did not result in as much absorbed hydrogen. Weld voltage, current, and electrode extension were shown not to affect the amount of absorbed hydrogen as much as changing droplet transfer modes from globular to spray.

The hydrogen absorption mechanism was then theoretically modeled with the aid of chemical thermodynamics and arc plasma physics in chapter 3. Results show that Sievert's law is not applicable for modeling hydrogen absorption in weld pools. Previous investigations are reviewed to show how their results are incompatible with using Sievert's law. A new model is postulated based on the hypothesis that diatomic hydrogen will dissociate in the cathode boundary layer at a different reaction temperature than the hydrogen absorption reaction which occurs at the temperature of the weld pool surface. Using this hypothesis it is shown that hydrogen absorption will be controlled by monatomic hydrogen absorption into the cooler outer region of the weld pool. This new model conflicts with the previous theory that hydrogen will absorb primarily into the hot central region of the weld pool.

The effect of oxygen and carbon dioxide in GMAW shielding gases on hydrogen absorption is modeled with the aid of Fe-H-O and Fe-C-H-O phase diagrams developed in chapter 4. The relative stability of H_2O and H_2 in the presence of CO_2 dictate whether hydrogen absorption is governed by the Fe-H or Fe-H-O phase diagram. The experimental results of chapter 2 are thus theoretically explained.

Chapter 5 then investigates the effect of hydrogen on weld cracking. Fracture mechanics are applied to the implant test results assuming that the intergranular area acts as a sharp crack tip, and a fracture mechanism map is developed to show the effect of stress intensity factor and hydrogen level on the fracture type (i.e. microvoid coalescence, quasi-cleavage, or intergranular). The hydrogen assisted cracking theory of Beachem is shown to explain the effect of hydrogen concentration and stress intensity level on the observed fracture mode. This theory postulates that hydrogen will promote cracking by a microplasticity mechanism rather than truly embrittling the lattice. The results of the present investigation are used to postulate a modification to the original Beachem theory.

The prediction equations of other researchers are examined to determine how accurately they assess the fracture stresses found in the present investigation.

Thus, this thesis document has followed a logical investigative procedure from studying how to measure hydrogen, to the effect of welding on how the hydrogen gets into the weld, to the effect of this hydrogen on cracking. This research has drawn heavily on other fields to explain phenomena occurring in welding, and has shed new insights into the very heavily researched area of hydrogen assisted cracking of welds.

REFERENCES

A.1. R.S. Acosta, Inst. Hierro Acero, Vol. 16, 1963. p. 173; through "Chemical Abstracts" Vol. 59, 1963. p.12171d.

A.2. N.A. Alcantara, and J.H. Rogerson, "A Prediction Diagram for Preventing Hydrogen-Assisted Cracking in Weld Metal" Welding Journal, April. 1984, pp. 116s-122s.

A.3. D.J. Allen, B. Chew, and P. Harris, "The Formation of Chevron Cracks in Submerged Arc Weld Metal" Welding Journal, July 1982. pp. 212s-221s.

A.4. Atlas of Isothermal Transformation and Cooling Transformation Diagrams. ASM, 1977.

B.1. J.G. Baillie, "Underbead and Toe Cracks" British Welding Journal, Vol. 14, No. 2, Feb. 1967. pp. 51-61.

B.2. R.G. Baker, "Weld Cracking - A Modern Insight" British Welding Journal, June 1968. pp. 283-295.

B.3. E.A. Barringer, and T.W. Eagar, "Process for Improving Low Moisture Welding Fluxes" U.S. Patent No. 4512822.

B.4. C.F. Barth, and E.A. Steigerwald, "Evaluation of Hydrogen

Embrittlement Mechanisms" Metallurgical Transactions, Vol. 1, No. 12, Dec. 1970. pp. 3451-3455.

B.5. P. Bastien and P. Azou, "Effect of Hydrogen on the Deformation and Fracture of Iron and Steel in Simple Tension" Proc. First World Metallurgical Congress, ASM Cleveland, 1951, pp. 535-552.

B.6. P.G. Bastien, "Hydrogen in Welding - A Comparison Between the Behavior of Welded, Cast, and Wrought Steel" British Welding Journal, Houdremont Lecture, Sept. 1960. pp. 546-557.

B.7. C.D. Beachem, "A New Model for Hydrogen Assisted Cracking (Hydrogen Embrittlement)" Metallurgical Transactions, Vol. 3, No. 2, Feb. 1972, pp. 437-451.

B.8. W. Beck, J.O.M. Bockris, J. McBreen, and L. Naniss, "Hydrogen Permeation in Metals as a Function of Stress, Temperature, and Dissolved Hydrogen Concentration" Proceedings of the Royal Society of London, Series A, Vol. 290, 1965.

B.9. I.M. Bernstein, and G.M. Pressouyre, "The Role of Traps in the Microstructural Control of Hydrogen Embrittlement of Steels" in: "Hydrogen Degradation of Ferrous Alloys" ed: Oriani et. al. Noyes Publications 1985. pp. 641-685.

B.10. Seminar by Prof. H.K. Birnbaum at Worchester Polytechnical

Institute, March 5, 1985.

B.11. P.D. Blake, M.F. Jordan, and W.I. Pumphrey, "The Solubility of Hydrogen in Alpha-Iron of High Purity and in the Laves Phases TiFe_2 and NbFe_2 ," Iron and Steel Institute, Special Report No. 73, London, 1962. pp. 76-82.

B.12. A. Block-Bolten, and T.W. Eagar, "Metal Vaporization from Weld Pools" Met. Trans. Vol. 15B, Sept. 1984. pp. 461-469.

B.13. A. Block-Bolten, and T.W. Eagar, "Selective Evaporation of Metals from Weld Pools" from Trends in Welding Research in the U.S. ASM, Metals Park, Ohio, 1982. pp. 53-73.

B.14. O.W. Blodgett, "Calculating Cooling Rates by Computer Programming" Welding Journal, March 1984. pp. 19-35.

B.15. T. Boniszewski, and R.G. Baker, "Hydrogen Embrittlement in Low Carbon Nickel and Manganese Steels" British Welding Journal, July 1965. pp. 349-362.

B.16. T. Boniszewski, and J. Moreton, "Hydrogen Entrapment in Mild Steel Weld Metal with Micropores" Metal Construction, Vol. 1, No. 6, June 1969. pp. 269-276.

B.17. T. Boniszewski, and A.G.C. Morris, "More Sensitivity Need-

ed, Say Boniszewski and Morris" Welding and Metal Fabrication, July/Aug. 1981. pp. 336-338.

B.18. T. Boniszewski, and A.G.C Morris, "Tests show IIW Mercurey Method Unreliable for Hydrogen Determination" Weld and Metals Fabrication, April 1981. pp. 131-139.

B.19. J.C. Borland, "Cracking Tests for Assessing Weldability" British Welding Journal, Oct. 1960. pp. 623-637.

B.20. J.E.M. Braid, and J.A. Gianetto, "The Effects of PWHT on the Toughness of Shielded Metal Arc Weld Metals of Use in Canadian Offshore Structure Fabrication" IIW Doc. IX-1385-86.

B.21. C.J. Brinker, K.D. Keefer, D.W. Schaefer, and C.S. Ashley, "Sol-Gel Transition in Simple Silicates" Sandia National Labs, under contract DE-AC04-76-DP00789.

B.22. A.J. Bryhan, "The Effect of Testing Procedure on Implant Test Results" Welding Journal, Sept. 1981. pp. 169s-176s.

C.1. J.S. Caplan, and E Landerman, "Preventing Hydrogen-Induced Cracking after Welding of Pressure Vessel Steels by Use of Low Temperature Postweld Heat Treatments" Welding Research Council Bulletin, No. 216, June 1976

C.2. G.R. Caskey, Jr., "Tritium Autoradiography" in "Advanced Techniques for Characterizing Hydrogen in Metals" ed: Fiore and Berkowitz, Conference Proceedings, The Metallurgical Society of AIME, Warrendale, PA 1982. pp. 61-76.

C.3. K.D. Challenger, and B.J. Mason, "Comparison of Hydrogen Assisted Cracking Susceptibility of Cast and Rolled HY-130 Steel Plate" Welding Journal, Feb. 1984. pp. 39s-46s.

C.4. K.D. Challenger, "The Czechoslovakian Welding Research Institute" ESN 39-12, 1985. pp. 561-564.

C.5. B. Chew, "Hydrogen Control of Basic-coated MMA Welding Electrodes-part III: Relationship between Coating Moisture and Weld Hydrogen" Metal Construction, 14 (7), 1982.

C.6. B. Chew, "Prediction of Weld Metal Hydrogen Levels Obtained Under Test Conditions" Welding Journal, 52 (9), 1973. pp. 386s-391s.

C.7. B. Chew, and R.A. Willgoss, "Weld Metal Hydrogen Absorption During TIG-Welding with Argon-Hydrogen Gas Shields" in Weld Pool Chemistry and Metallurgy, International Conference London, April, 1980, pp. 155-165.

C.8. N. Christensen, and T. Simonsen, "Assessment of Weldability by the Implant Method" Scandinavian Journal of Metallurgy, Vol. 10,

1981. pp. 120-126.

C.9. N. Christensen, Lecture Notes, Welding Metallurgy, Massachusetts Institute of Technology, Cambridge, MA, 1981.

C.10. N. Christensen, and J. Chipman, Welding Research Council Bulletin, Jan. 1953, 14pp.

C.11. J.D. Cobine, and E.E. Burger, "Analysis of Electrode Phenomena in the High-Current Arc" Journal of Applied Physics, Vol.26, No.7, July 1955. pp. 895-900.

C.12. F.R. Coe, "Annual Report of Commission II-- Arc Welding" IIW Doc. II-1007-83. 1983.

C.13. F.R. Coe, and Z. Chano, "Hydrogen Distribution and Removal for a Single Bead Weld during Cooling" Welding Research Institute, Vol. 5, 1975. pp. 33-90.

C.14. F.R. Coe, "More on the IIW Mercury Method" Welding and Metal Fabrication, July/Aug. 1981. pp. 335-336.

C.15. F.R. Coe, "Welding Steels Without Hydrogen Cracking". The Welding Institute, Cambridge, England, 1973.

C.16. F.R. Coe, Welding Institute Research Bulletin, 11 (5), 1971,

pp. 133-135.

D.1. O.E.K. Daoud, and D.J. Cartwright, "Strain Energy Release Rate for a Circular-Arc Edge Crack in a Bar Under Tension or Bending" *Journal of Strain Analysis*, Vol 20, NO 1, 1985, pp. 53-58.

D.2. O.E.K. Daoud, D.J. Cartwright, and M. Carney, "Strain Energy Release Rate for a Single-Edge-Cracked Circular Bar in Tension" *Journal of Strain Analysis*, Vol 13, NO 2, 1978, pp. 83-89.

D.3. D.W. Dickinson, and G.D. Ries, "Implant Testing of Medium to High Strength Steel - A Model for Predicting Delayed Cracking Susceptibility" *Welding Journal*, July 1979. pp. 205s-211s.

D.4. H.A. Dinulescu, and E. Pfender, "Analysis of the Anode Boundary Layer of High Intensity Arcs" *Journal of Applied Physics*, 51 (6), June 1980. pp. 3149-3157.

D.5. R.E. Dolby, and M.W.F. Cane, "A New Mechanical Test Approach for Assessing Susceptibility to Hydrogen Induced HAZ Cracking" *Metal Construction and British Welding Journal*, Sept. 1971. pp. 351-354.

D.6. G.J. Dunn, "Metal Vapors in Gas Metal Welding Arcs" *Bachelor's and Master's Thesis at the Massachusetts Institute of Technology*. September 1984.

E.1. L.P. Earvolino, "Evaluation of Moisture-Resistant E70XX Electrodes at Extended Exposure Times" Welding Journal, March 1979. pp. 36-38.

E.2. K. Easterling, "Introduction to the Physical Metallurgy of Welding" Butterworths and Company Ltd., London, England. 1983.

E.3. R. Eborall, "Special Report No. 68" Iron and Steel Institute, London, 1960. p. 192.

E.4. J.F. Elliot, and J.K. Wright, "Equilibrium Phase Relationships during Solidification of Fe-O-C-X Alloys" Canadian Metallurgical Quarterly, Vol. 11, No. 4, 1972. pp. 573-584.

E.5. J.F. Elliot, "Physical Chemistry of Liquid Steel" Chapter 21 of Electric Furnace Steelmaking. American Iron and Steel Institute. pp. 291-319.

E.6. J.F. Elliot, "Physical Chemistry of High Temperature Reactions" Chapter 20 of Electric Furnace Steelmaking. American Iron and Steel Institute. pp. 265-290.

E.7. J.F. Elliot, Private Communications throughout 1985 and 1986.

E.8. J.F. Elliot, M. Gleiser, and V. Ramakrishna, "Thermochemistry for Steelmaking" Vol. II, Addison-Wesley Publishing Company.

Reading, Massachusetts, 1963.

E.9. E. Enjo, T. Kuroda, and N. Mitsui, "Analysis of Fracture Morphology in Hydrogen Embrittlement for Cr-Mo Steel" Transactions of the Welding Research Institute of Japan, Vol. 12, No. 2, 1983. pp. 67-73.

E.10. G.M. Evans, "Committee Correspondence to AWS A5.A, Hydrogen Task Group Members -- Round Robin Test Results".

E.11. G.W. Ewing, "Instrumental Methods of Chemical Analysis" 4th ed. McGraw-Hill Book Company, New York, 1975.

F.1. Fabling and Chew, "The Performance of Collecting Fluids in Diffusible Hydrogen Analysis" Welding Research International, 3 (4), 1973.

F.2. N.F. Fiore, and B.J. Berkowitz, editors: "Advanced Techniques for Characterizing Hydrogen in Metals" Conference Proceedings AIME, Oct. 1981.

F.3. A.E. Flanigan, and U.E. Lee, "On Escape of Dissolved Hydrogen from Weld Metal" Welding Journal, Oct. 1960. pp. 477s-480s.

F.4. S.N. Flengas, and A. Block-Bolten, "Solubilities of Reactive Gases in Molten Salts" In: Advances in Molten Salt Chemistry. edited by E.J. Braunstein, G. Mamontov, and G. Smith. Plenum Press, New York,

1973. pp. 27-81.

F.5. W. Florian and V. Neumann, "Influence of the H_2 -Content in the Shielding Gas (during TIG-Welding) on the Diffusible Hydrogen in the Weld Metal and the Cold Cracking Sensitivity of Implant Specimens" In: Current Solutions to Hydrogen Problems in Steels. ASM, 1982. pp. 119-123.

F.6. M.G. Fontana, and N.D. Greene, "Corrosion Engineering" 2nd ed. 1978, p. 109.

G.1. Private Communication with G.J. Garvey, Postdoctorate, MIT, Cambridge, MA. June, 1984.

G.2. D.R. Gaskell, "Introduction to Metallurgical Thermodynamics" McGraw-Hill Book Company, New York, 1973.

G.3. S.A. Gedeon "Development of Joining and Cutting Processes for Armor" Core Research Program for the U.S. Army Materials and Mechanics Research Center, No. 612105.H84, 6MRR3M365N4, 1985.

G.4. S.A. Gedeon, "A Proposed Study on the Influence of Very Low Weld Hydrogen Contents on Preheat Requirements" Oral Examination for the Doctoral Degree at the Massachusetts Institute of Technology, June 1984.

G.5. S.A. Gedeon, "A Study on the Effect of Shielding Gas Varia-

tions on Diffusible Weld Hydrogen" U.S. Army Materials Technology Laboratory Contract AW-6-DD0045. 1986.

G.6. S.A. Gedeon, "Value Engineering Proposal to Reduce M1 Weld Fabrication Costs" U.S. Army Materials Technology Laboratory Project 7ME00N3P87X12. 1987.

G.7. S.A. Gedeon, "Welding, Cutting, and Joining for Army Applications" Core Research Program for the U.S. Army Materials and Mechanics Research Center, No. 623102.065, 6MRT1M36PN1, 1985.

G.8. S.A. Gedeon, "Welding, Cutting, and Joining for Army Applications" Core Research Program for the U.S. Army Materials Technology Laboratory, DA Project No. 1L263102D071, 1986.

G.9. R. Gibala, and R.F. Hehemann, "Hydrogen Embrittlement and Stress Corrosion Cracking" American Society for Metals, Metals Park, Ohio. 1984.

G.10. R. Gibala, and A.J. Kumnick, "Hydrogen Trapping in Iron and Steels" *ibid.* pp. 61-77.

G.11. H.G. Gillit, "Hyperbaric Welding -- Cold Cracking in SMAW" Welding Research, PR-147-161.

G.12. T. Godai, T. Sugiyama, M. Sugino, and M. Kondoh, "Beha-

viol of Hydrogen in Weld Metal and Welding Consumables" Welding Technology, Vol. 30, No. 3. pp.5-9.

G.13. H. Granjon, "The Implants Method for Studying the Weldability of High Strength Steels" Metal Construction and British Welding Journal, Nov. 1969. pp. 509-515.

G.14. H.P. Granjon, "Studies on Cracking of and Transformation in Steel During Welding" Welding Journal, Jan. 1962. pp. 1s-11s.

G.15. H. Granjon, "Survey of Cracking Tests" Welding in the World, Vol 17 no. 3/4 1979. pp. 81-90.

G.16. B.A. Graville, "Cold Cracking in Welds in HSLA Steels" Welding Design and Fabrication, Feb. 1979. pp. 57-61.

G.17. B.A. Graville, "Effect of Hydrogen Concentration on Hydrogen Embrittlement" British Welding Journal, Vol. 15, No. 4, April 1968, pp. 191-195.

G.18. B.A. Graville, R.G. Baker, and F. Watkinson, "Effect of Temperature and Strain Rate on Hydrogen Embrittlement of Steel" British Welding Journal, Vol.14, No. 6, June 1967. pp. 337-342.

G.19. B. Graville, "A Short Review of Weld Metal Hydrogen Cracking" IIW Doc. IX-1374-85.

G.20. O. Grong, and N. Christensen, "Factors Controlling MIG Weld Metal Chemistry" Scandinavian Journal of Metallurgy, Vol 4, No 12, 1983, pp. 155-165.

G.21. V.G. Guglya, A.G. Urraco, and A.M. Zaitsev, "The Use of the Pyrokatharometer for the Determination of Low Hydrogen Contents in Metals" Russian Journal of Physical Chemistry, 54 (11), 1980. pp. 1677-1679. Translated from Zhurnal Fizicheskoi Khimii, 54, 2928-2932, 1980.

H.1. M. Hansen, K. Anderko, R.P. Elliot, and F.A. Shunk, "Constitution of Binary Alloys" McGraw Hill Book Company, New York, 2nd Supplement, 1969.

H.2. P.H.M. Hart, "Some Limitations of the Implant Cracking Test for Predicting Hydrogen Cracking Behavior in Welds" Int. Conf. Welding of HSLA Structural Steels, ASM, Rome, Italy, 1976. pp. 102-125.

H.3. P.H.M Hart, and E. Watkinson, "Weld Metal Implant Test Ranks Cr-Mo Hydrogen Cracking Resistance" Welding Journal, Sept. 1975. pp. 288s-295s.

H.4. M. Hashimoto, "Hydrogen Transport During Plastic Deformation of Iron" Doctoral Thesis at Massachusetts Institute of Technology, June 1984.

H.5. T. Hayashi, and H. Saito, "Preparation of Ca-SiO₂ Glasses by the Gel Method" Journal of Materials Science 15 (1980) pp. 1971-1977.

H.6. D.O. Haywood, "Gas Adsorption" in: "Chemisorption and Reactions on Metallic Films" ed: J.R. Anderson, Vol. 1, Academic, New York, 1971. p. 231.

H.7. W.A. Herman, and G.M. Campbell, "Environmental Assisted Cracking in High Hardness Armor Steel" U.S. Army Materials and Mechanics Research Center Technical Report TR 85-28. Sept. 1985.

H.8. J. Hewitt "The Study of Hydrogen in Low-Alloy Steels by Internal Friction Techniques" Iron and Steel Institute, Special Report No. 73, London, 1962. pp. 83-89.

H.9. J.P. Hirth, and B. Carnahan, "Hydrogen Adsorption at Dislocations and Cracks in Fe" Acta Metallurgica, Vol. 26, Nov. 1978. pp. 1795-1803.

H.10. J.P. Hirth, "Hydrogen-Defect Interactions" in: Hydrogen Degradation of Ferrous Alloys" ed: Oriani et. al. Noyes Publications 1985. pp. 131-139.

H.11. J.P. Hirth, "Theories of Hydrogen Induced Cracking in Steels" *ibid.*

H.12. J.D. Hobson, "Hydrogen in Steel" BISRA Harrogate Conference, 1961. pp. 62-75.

H.13. H. Hoffmeister, "Concept and Procedure Description of the IRC Test for Assessing Hydrogen Assisted Weld Cracking" IIW Doc. IX-1369-85, 1985.

H.14. H. Homma, "A Study of Delayed Cracking in HY-80 Weldments" Doctoral Thesis, Rensselaer Polytechnic Institute, Troy, New York, 1977.

H.15. D.G. Howden, "Behavior of Hydrogen in Arc Weld Pools" in Weld Pool Chemistry and Metallurgy, International Conference London, April, 1980. pp. 205-215.

H.16. D.G. Howden, Class notes, Welding Engineering 620, The Ohio State University, 1982.

H.17. D.G. Howden, and D.R. Milner, "Gas Absorption in Consumable Electrode Welding" British Welding Journal, Aug. 1963. pp. 395-398.

H.18. D.G. Howden, and D.R. Milner, "Hydrogen Absorption in Arc Melting" British Welding Journal, June 1963. pp. 304-316.

H.19. G. Huismann, H. Hoffmeister, and H.G. Schafstall, "Effect of Ambient Pressure and Shielding Gas Flow on Hydrogen and Nitrogen Contamination of Hyperbaric TIG and GMA Welds" IIW Doc. IX-1371-85, 1985.

I.1. M. Inagaki, "Effects of Testing Parameters and Standardization in Implant Cracking Test in Japan" IIW Doc. IX-1151-80. 1980.

I.2. C.G. Interrante, "Basic Aspects of the Problems of Hydrogen in Steel" In: Current Solutions to Hydrogen Problems in Steels. ASM 1982 pp. 3-17.

I.3. "Current Solutions to Hydrogen Problems in Steel" Proceeding of the first international conference. ed. C.G. Interrante, and G.M. Pressouyre, ASM, Metals Park, Ohio. 1982.

I.4. C.G. Interrante, and R.D. Stout, "Delayed Cracking in Steel Weldments" Welding Journal, April 1964. pp. 145s-161s.

I.5. Annual Report of Commission II "Arc Welding" IIW Doc. II-1054-85. Strasbourg, Sept. 1985.

I.6. "The Anode Boundary Region in Argon Shielded Tungsten Arcs" IIW Doc. 212-640-86.

I.7. "Cold Cracking Test Methods Using Implants" Welding in the World, Vol. 23, No. 1/2, 1985. pp. 8-12. IIS/IIW-802-84 (exdoc. IX-1240-82).

I.8. "The Determination of the Hydrogen Content of Ferritic Arc

Weld Metal" IIW doc. II-1002-83 (revision of II-959-81).

I.9. "The Measurement of Weld Hydrogen Levels" Welding in the World, Vol. 23. No. 3/4, 1985. pp. 50-62. (also IIS/IIW-805-85, ex doc. II-1018-84).

I.10. "Standard Procedures for Determination of the Diffusible Hydrogen Content of Martensitic, Bainitic, and Ferritic Steel Weld Metal Produced by Arc Welding" IIW Doc. II-1051-85, AWS A4.3-86, 1986.

I.11. Y. Ito, M. Ikeda, and M. Nakanishi, IIW Doc. No. IX-969-76.

J.1. C.E. Jackson, Lecture Notes, Welding Fluxes and Slags course, The Ohio State University, Columbus, Ohio, 1981.

J.2. "Method for Measurement of Hydrogen Evolved from Deposited Metal" Japanese standard JISZ3113.

J.3. N. Jenkins, and F.R. Coe, "Extraction and Analysis of Gases from Pores in Weld Metal" Metal Construction and British Welding Journal, Jan. 1970. pp. 27-31.

J.4. H.H. Johnson, "Keynote Lecture: Overview on Hydrogen Degradation Phenomena" in: Hydrogen Embrittlement and Stress Corrosion Cracking, ASM, 1984. pp. 3-27.

K.1. H.I. Kaplan, and D.C. Hill, "Thermodynamics of Air-Operating Flux Cored Electrodes and an Analysis of Weld Toughness" Welding Journal, Jan. 1976. pp. 13s-19s.

K.2. R. Karppi, J. Ruusila, P. Rajamaki, and K. Vartiainen, "Correlation Between Implant Test and Restraint Test" IIW Doc. IX-1215-81. 1981.

K.3. R. Karppi, J. Ruusila, K. Satoh, M. Toyoda, and K. Vartiainen, "Determination of Weld Hydrogen Content" 0358-5077 Tutkimus-Valtion Teknillinen Tutkimuskeskus (The Technical Research Center of Finland--VTT), Report No. 240, Project No. 622010-1, ISBN 951-38-1910-8, Nov. 1983.

K.4. R. Karppi, J. Ruusila, K. Satoh, M. Toyoda, and K. Vartiainen, "Note on Standardization of Implant Test" IIW Doc. IX-1296-83. 1983.

K.5. R.A.J. Karppi, J. Ruusila, M. Toyota, K. Satoh, and K. Vartiainen, "Predicting Safe Welding Conditions with Hydrogen Cracking Parameters" Scandinavian Journal of Metallurgy, Vol. 13, 1984. pp. 66-74.

K.6. P. Kedzierzawski, "Hydrogen Trapping in Iron and Iron Alloys" in: "Hydrogen Degradation of Ferrous Alloys" ed: Oriani et. al. Noyes Publications 1985. pp. 271-288.

K.7. Private Communication with J.I. Kleive, Cylinder Products Manager, Liquid Air Corporation, April 1986.

K.8. Y.A. Klyachko, and O.D. Larina, Stal', Vol. 21, 1961, p. 604; through "Chemical Abstracts" Vol. 55, 1961, p. 25583e.

K.9. D.J. Kotecki, and R.A. LaFava, "AWS A5 Committee Studies of Weld Metal Diffusible Hydrogen" Welding Journal, March 1985, pp. 31-37.

K.10. D.J. Kotecki, private communications August, 1985.

K.11. A.J. Kumnick, and H.H. Johnson, "Deep Trapping States for Hydrogen in Deformed Iron" Acta Metallurgica, Vol. 28, Jan. 1980. pp. 33-39.

K.12. W.S. Kyte, and B. Chew, "Postweld Heat Treatment for Hydrogen Removal" Welding Journal, Feb. 1979. pp. 54s-58s.

L.1. R.M. Latanison, O.H. Gastine, and C.R. Compeau, "Stress Corrosion Cracking and Hydrogen Embrittlement: Differences and Similarities" Conf. Proc. AIME on Environment-Sensitive Fracture of Engineering Materials. Edited by Z.A. Foroulis. Oct. 1977. pp. 48-70.

L.2. S. Lathabai, and R.D. Stout, "Hydrogen-Induced Cracking in Flux-Cored Electrode Welds" Welding Journal, March 1983. pp. 59s-62s.

L.3. Leco Corporation literature, 3000 Lakeview Ave., St. Joseph, MI.

L.4. J.Y. Lee, J.L. Lee, and W.Y. Choo, "Thermal Analysis of Trapped Hydrogen in AISI 4340 Steel" in "Current Solutions to Hydrogen Problems in Steels" ed: Interrante and Pressouyre, 1982. pp. 421-427.

L.5. Lincoln Electric, welding plant tour 1982.

L.6. G.E. Linnert, "Welding Metallurgy, Volume 2" Published by: American welding Society, New York, NY, 1967, pp. 250-276.

L.7. M.R. Louthan, Jr., and R.P. McNitt, "The Role of Test Technique in Evaluating Hydrogen Embrittlement Mechanisms" In: Effect of Hydrogen on Behavior of Materials. Edited: Thompson and Bernstein. AIME, New York, NY, 1976, pp. 496-506.

L.8. M.R. Louthan, R.P. McNitt, and R.D. Sisson, "Importance of Stress State on Hydrogen Embrittlement" In: Advanced Techniques for Characterizing Hydrogen in Metals. Edited: N.F. Fiore, and B.J. Berkowitz. The Metallurgical Society of AIME, New York, 1982. pp. 25-42.

L.9. K. Lyttle, and J. DeVito, "The Effect of Weld Parameters, Material, and Equipment on GMAW Weld Hydrogen" presented at the 1985 AWS convention.

M.1. J.R. Manning, "Theory of Diffusion" in: "Diffusion" ASM, Metals Park, OH, 1973. pp. 1-24.

M.2. J.F. Martin, R.C. Takacs, R. Rapp, and L.M. Melnik, Trans. AIME, Vol. 230, 1964. p. 107.

M.3. G. Masing, "Ternary Systems" Reinhold Publishing Corp, New York, 1944.

M.4. K. Masubuchi, and D.C. Martin, "Mechanisms of Cracking in HY-80 Steel Weldments" Welding Journal, Aug. 1962. pp. 375s-384s.

M.5. F. Matsuda, H. Nakagawa, and K. Shinozaki, "Cold Cracking Susceptibility and its Improvement of Weld Metals in HY-type High Strength Steels" IIW Doc. No. IX-1403-86.

M.6. F. Matsuda, H. Nakagawa, S. Takaba, and H. Kihara, "Effect of Residual Hydrogen Content on Cold Crack Susceptibility in Weld Metal of High Strength Steels" Transactions of JWRI, Oct. 1981. pp. 55-64.

M.7. S. Matsui, and M. Inagaki, "Recent Trend of Research on Cold Cracking with the Implant test in Japan" IIW Doc. IX-970-76.

M.8. C.F. Meitzner, and R.D. Stout, "Microcracking and Delayed Cracking in Welded Quenched and Tempered Steels" Welding Journal, Sept. 1966. pp. 393s-400s.

M.9. L.M. Melnik, L.L. Lewis, and B.D. Holt, "Determination of Gaseous Elements in Metals" John Wiley and Sons, New York. 1974.

M.10. Military Specification, "Armor Plate, Steel, Wrought, High-Hardness" Mil-A-46100, revision C, 13 June 1983.

M.11. Military Specification, "Electrodes, Welding, Mineral Covered, Iron-Powder, Low-Hydrogen Medium, High Tensile and Higher-Strength Low Alloy Steels" Mil-E-0022200/10A(SH), 8 July 1983.

M.12. E.L. Montgomery, "An Improved Method for the Determination of Water in Welding Electrode Coatings" Welding Journal Dec. 1982, pp.39-42.

M.13. R.A. Morris, "An Improved Procedure for Moisture Analysis of Low-Hydrogen Shielded Metal-Arc Welding Electrodes" Naval Ship Research and Development Center, Report 4282, March 1974.

M.14. J.M.F. Mota, and R.L. Apps, "Chevron Cracking - A New Form of Hydrogen Cracking in Steel Weld Metals" Welding Journal, July 1982. pp. 222s-228s.

N.1. "Effective Use of Weld Metal Yield Strength for HY-Steels", National Materials Advisory Board, Report number NMAB-380, Contract MDA-903-82-c-0434, National Academy Press, 1983.

N.2. V. Neumann, W. Florian, and W. Schonherr, "The Hydrogen Influenced Cold Cracking Tendency of Low Alloyed High-Strength Steels - Evaluated by the Implant Test" IIW Doc. IX-1244-82. also in: Current Solutions to Hydrogen Problems in Steels, ed: Interannte and Pressouyre, ASM, Metals Park, OH, 198

N.3. T.H. North, A.B. Rothwell, A.G. Glover, and R.J. Pick, "Weldability of High Strength Line Pipe Steels" Welding Journal, Aug. 1982. pp. 242s-257s.

O.1. Ohno and Uda, "An Examination of Collecting Mediums for Determination of Diffusible Hydrogen in Welded Metals" Trans. National Research Institute for Metals. 22 (2), 1980.

O.2. T. Ohtsubo, S. Goto, and M. Amano, "Development of Apparatus for Determination of Diffusible Hydrogen in Steel" Transactions of the Iron and Steel Institute of Japan, Vol 25, 1985. pp. 21-29.

O.3. N. Ohtsubo, S. Goto, and H. Sato, "Thermal Analysis of Hydrogen in Steel" Proc. 2nd JIM International Symposium on Hydrogen in Metals. also IIW Doc. No. II-1074-86. 1986.

O.4. N. Okuda, Y. Nishikawa, T. Aoki, A. Goto, T. Abe, "Hydrogen Induced Crack Susceptibility of Weld Metal" IIW/IIS Doc. No. II-1072-86. July 1986.

O.5. R.A. Oriani, "The Diffusion and Trapping of Hydrogen in Steel" *Acta Metallurgica*, Vol. 18, Jan. 1970. pp. 147-157.

O.6. R.A. Oriani, J.P. Hirth, and M. Smialowski, "Hydrogen Degradation of Ferrous Alloys" Noyes Publications, Park Ridge, New Jersey, 1985.

O.7. R.A. Oriani, "A Mechanistic Theory of Hydrogen Embrittlement of Steels" *Ber. Bunsenges Phys. Chem.* 76, 1972, pp. 848-857.

P.1. L.S. Palatnik and A.I. Landau, "Phase Equilibria in Multicomponent Systems" Holt, Reinhart, and Winston, Inc., New York, 1964.

P.2. V. Pavaskar, and J.S. Kirkaldy "Assessing Cold-cracking Susceptibility in Low-alloy Steel Welds" *Scandinavian Journal of Metallurgy*, Vol. 11, 1982. pp. 256-262.

P.3. G. Pelley, "Low Hydrogen Electrodes" *Metals Australasia*, Oct. 1977. pp. 234-237.

P.4. J. Peng, "Weldability Studies of High-Strength Steels Using the Implant Test Method" Master's Thesis, The Ohio State University, 1981.

P.5. N.O. Petch and P. Stables, "Delayed Fracture of Metals under Static Load" *Nature*, 169, 1952, pp. 842-843.

P.6. N.O. Petch, "Lowering of the Fracture Stress Due to Surface Adsorption" Philosophical Magazine, Series 8, Vol. 1, 1956. pp. 331-335.

P.7. D.G. Peters, J.M. Hayes, and G.M. Hieftje, "Chemical Separations and Measurements" W.B. Saunders Company, Philadelphia 19105, 1974.

P.8. J. Pielaszek, "Nickel Hydride" in: Hydrogen Degradation of Ferrous Alloys" ed: Oriani et. al. Noyes Publications 1985, pp. 167-179.

P.9. H.H. Podgurski, Transactions AIME, Vol. 221, 1961, p. 389.

P.10. I.K. Pokhodnya and A.P. Pal'tsevich, "Chromatographic Determination of the Amount of Diffusional Hydrogen in Welded Joints" Russian Journal of Physical Chemistry, 54 (11), 1980. pp. 1675-1677.

P.11. G.M. Pressouyre, "Current Solutions to Hydrogen Problems in Steel" In: Current Solutions to Hydrogen Problems in Steel. Edited: Interrante and Pressouyre, ASM, 1982. pp. 18-34.

P.12. G.M. Pressouyre, "Trap Theory of Hydrogen Embrittlement: Experimental Investigation" In: Hydrogen Effects in Metals. Edited: Bernstein and Thompson. Conf. Proc. AIME, 1980, pp. 27-36.

P.13. A. Prince, "Alloy Phase Equilibria" Elsevier Publishing Company, New York, 1966.

Q.1. M.B.C. Quigley, P.H. Richards, D.T. Swift-Hook, and A.E.F. Gick, "Heat Flow to the Workpiece from a TIG Welding Arc" J. Phys. D: Appl. Phys., Vol.6, 1973. pp. 2250-2258.

Q.2. M.B.C. Quigley, "Physics of the Welding Arc" Welding and Metal Fabrication, Dec. 1977. pp. 619-626.

Q.3. M.A. Quintana, "A Critical Evaluation of the Glycerin Test" Welding Journal, May 1984, pp. 141s-149s.

Q.4. Private Communications with M.A Quintana, Electric Boat Division of General Dynamics, Gratin Conn. May, 1984.

R.1. H.F. Reid, "It Still Isn't Mud" Reprinted from Welding Engineer by Teledyne McKay, Bulletin No. 1201A. used in conjunction with Weld Tech '81 Seminar held by Alloy Rods Inc.

R.2. F.N. Rhines, "Phase Diagrams in Metallurgy, Their Development and Application", McGraw-Hill Book Company, New York, 1956.

R.3. W.M. Robertson, "An Improved Model for Hydrogen Trapping in Metals" Scripta Metallurgica, Vol. 15, 1981. pp. 137-139.

R.4. R.R. Robinson, "A Nonhygroscopic Welding Flux Binder Produced by the Sol-Gel Method" Bachelor's Thesis at the Massachusetts Institute of Technology, June 1985.

R.5. S.T. Rolfe, and J.M. Barsom, "Fracture and Fatigue Control in Structures" 1977.

R.6. T.F. Russell, "Some Mathematical Considerations on the Heating and Cooling of Steel" Iron and Steel Institute, Special Report No. 14, 1936. pp. 149-187.

S.1. D. Sadoway, Lecture Notes, Massachusetts Institute of Technology, 3.21, "Kinetic Processes in Materials" 1983.

S.2. S. Sakka, "Gel Method for Making Glass" Treatise on Materials Science and Technology, Vol 22, pp. 129-167.

S.3. G.R. Salter, and D.R. Milner, "Gas Absorption from Arc Atmospheres" British Welding Journal, Feb. 1960. pp. 89-100.

S.4. N.A. Sanders, and E. Pfender, "Measurement of Anode Falls and Anode Heat Transfer in Atmospheric Pressure High Intensity Arcs" Journal of Applied Physics, Vol.55, No.3, Feb. 1984. pp. 714-722.

S.5. K. Satoh, S. Matsui, H. Horikawa, K. Bessyo, and T. Okumura, "JSSC Guidance Report on Determination of Safe Preheating Condi-

tions Without Weld Cracking in Steel Structures" IIW Doc. IX-834-73. 1973.

S.6. W.F. Savage, E.F. Nippes, and E.I. Husa, "Hydrogen-Assisted Cracking in HY-130 Weldments" Final Report to the Office of Naval Research, Contract No. N00014-75-c-0944, NR 031-780. Jan. 1981.

S.7. W.F. Savage, E.F. Nippes, and E.I. Husa, "Hydrogen-Assisted Cracking in HY-130 Weldments" Welding Journal, Aug. 1982. pp. 233s-242s.

S.8. W.F. Savage, E.F. Nippes, and J.M. Sawhill, Jr., "Hydrogen Induced Cracking During Implant Testing of Alloy Steels" Welding Journal, Dec. 1976. pp. 400s-407s.

S.9. W.F. Savage, E.F. Nippes, and H. Homma, "Hydrogen Induced Cracking in HY-80 Steel Weldments" Welding Journal, Nov. 1976. pp. 368s-376s.

S.10. W.F. Savage, E.F. Nippes, and Y Tokunaga, "Hydrogen Induced Cracking in HY-130 Steel Weldments" Welding Journal, April 1978. pp. 118s-126s.

S.11. J.M. Sawhill, Jr., J.C. Baker, and P. Howe, "Hydrogen-Assisted Cracking in High-Strength Pipeling Steels, Part II" Presented at the AWS Annual Convention, May 1985.

S.12. J.M. Sawhill, Jr., "A Modified Implant Test for Studying Delayed Cracking" Doctoral Thesis at Rensselaer Polytechnic Institute, June 1973.

S.13. J.M. Sawhill, A.W. Dix, and W.F. Savage, "Modified Implant Test for Studying Delayed Cracking" Welding Journal Dec. 1974. pp. 554s-560s.

S.14. J.M. Sawhill, Jr., Engineer, Homer Research Lab, Bethlehem Steel, Personal Communications, 1985.

S.15. H Schmalzried "Solid State Reactions" 2nd ed. Verlag Chemie, Weinheim. 1981. p. 59.

S.16. G.C. Schmid, and R.D. Rodabaugh, "A Water Displacement Method for Measuring Diffusible Hydrogen in Welds" Welding Journal, Aug. 1980. pp. 217s-225s.

S.17. J. Searden and H. O'Neill, Trans. Inst. Weld. Vol. 1, 1938, Appendix, pp. 203.

S.18. P.G. Shewmon, "Diffusion in Solids" McGraw-Hill Book Company, New York, 1963.

S.19. R.C. Shutt, and D.A. Fink, "New Considerations for the Measurement and Understanding of Diffusible Hydrogen in Weld Metal" Weld-

ing Journal, Jan. 1985. pp. 19-28.

S.20. W. Siegfried, "A New Approach to the Calculation of Heat-Affected Zone Structures in Welded Joints" Schwiesen Schnieden (Welding and Cutting), 12, 1983. pp. E209-E212.

S.21. E.G. Signes, J.C. Baker, and P. Howe, "Hydrogen-Assisted Cracking in High-Strength Pipeline Steels, Part I" Presented at the AWS Annual Convention, April 1984.

S.22. D.A. Skoog, and D.M. West, "Fundamentals of Analytical Chemistry" 3rd ed. Holt, Rinehart, and Winston, New York, 1976.

S.23. M. Smialowski, "Hydrogen in Steel" Pergamon Press, 1962.

S.24. N. Stenbacka, "Calculation of Soaking Times for Hydrogen Removal in Steel Weldments" Scandinavian Journal of Metallurgy, Vol. 12, No. 1, pp. 40-42.

S.25. H. Suzuki, "Cold Cracking and its Prevention in Steel Welding" Trans. Japan Welding Society, Vol 9, No 2, 1978, pp. 82-91.

S.26. H. Suzuki, "Cold Cracking and its Prevention in Steel Welding (Report 2 Root Cracking)" Trans. Japan Welding Society, Vol 10, No 2, October 1979, pp. 10-19.

S.27. H. Suzuki, "Cold Cracking and its Prevention in Steel Welding (Report 3 Effects of Heat Input and Restraint)" Trans Japan Welding Society, Vol 11, No 2, October 1980, pp. 20-30.

S.28. H. Suzuki, "Comparison of Carbon Equivalents for Steel Weldability" Nippon Steel Corporation, 2-6-3, Oct. 1983.

S.29. H. Suzuki, "Estimation of Weldability of Thick Steel Plate" Nippon Steel Corporation 2-6-3, June 1983.

S.30. H. Suzuki, N. Yurioka, and M. Okumura, "A New Cracking Parameter for Welded Steels Considering Local Accumulation of Hydrogen" Trans. Japan Welding Society, Vol 13, No 1, April 1982, pp. 3-12.

S.31. H. Suzuki, "A New Formula for Estimating HAZ Maximum Hardness in Welded Steel" IIW Doc. IX-1351-85, April 1985.

S.32. H. Suzuki, and N. Yurioka, "Prevention Against Cold Cracking by the Hydrogen Accumulation Cracking Parameter PHA" Trans. Japan Welding Society, Vol. 14, No. 1, 1983.

S.33. H. Suzuki, "Revised Cold Cracking Parameter PHA and Its Applications" Nippon Steel Corporation, 2-6-3, Jan. 1984. (Submitted to IIW Comm. IX).

S.34. E.S. Szekeres, "A Study of Weld-Interface Phenomena and

Associated Crack Initiation of in a Low-Alloy Steel" Doctoral Thesis, Rensselaer Polytechnic Institute, Troy, New York, 1968.

T.1. E. Takahashi, and K. Iwai, "Omission of Intermediate Postweld Heat Treatment (PWHT) by Utilizing Low-Temperature PWHT for Welds in Pressure Vessels" ASTM Special Technical Publication, 755. 1982.

T.2. T. Terasaki, T. Akiyama, S. Hamashima, and K. Kishikawa, "An Analysis on Specimen Size for Determination of Diffusible Hydrogen Content in Weld Metal" Trans. Japan Welding Society, Vol. 17, No. 1, April, 1986. pp. 93-101.

T.3. T. Terasaki, T. Akiyama, K. Ishimoto, and K. Kishikawa, "Experiment on Specimen Size for Determination of Diffusible Hydrogen Content in Weld Metal" IIW Doc. II-1071-86. July 1986.

T.4. T. Terasaki, R. Karppi, and K. Satoh, "Relationship between Critical Stress of HAZ Cracking and Residual Diffusible Hydrogen Content" Trans. Japan Welding Society, Vol 10, No 1, April 1979, pp. 53-57.

T.5. T. Terasaki, and T. Akiyama, "Specimen Size for Determination of Diffusible Hydrogen Content in Weld Metal" IIW Doc. II-1041-85, Sept. 1985.

T.6. A.W. Thompson and I.M. Bernstein, In: Hydrogen Effects in

Metals. Edited: Bernstein and Thompson. Conf. Proc. on effect of hydrogen on behavior of materials, 1980, Publ: Met. Society of AIME. p. 291.

T.7. J.K. Tien, S.V. Nair, and R.R. Jensen, "Dislocation Sweeping of Hydrogen and Hydrogen Embrittlement" In: Hydrogen Effects in Metals. Edited: Bernstein and Thompson. The Met. Soc. of AIME, Warrendale, PA, 1980, pp. 37-56.

T.8. T.E. Torok, and R.D. Stout, "Relation of Dilatometric Characteristics of Steels to Delayed Cracking in Welds" Welding Journal, Dec. 1965. pp. 529s-544s.

T.9. B.M.W. Trapnell, Proceedings of the Royal Society, Series A, Vol. 218, 1953. p. 566.

T.10. Y.S. Trivedi, M. Manohar, and R. Veeraragavan, "Analysis of Weld Thermal Cycles and Generation of Weld-CCT Diagrams by In-Situ Method" Welding Research Institute, 1982. pp. 255-262.

T.11. A.R. Troiano, "The Influence of Hydrogen on the Mechanical Behavior of Steel" Special Report No. 73, The Iron and Steel Institute, 1962.

T.12. A.R. Troiano, "The Role of Hydrogen and Other Interstitials in the Mechanical Behavior of Metals" Trans. ASM 52, 1960, pp. 54-80.

T.13. D.L. Tuyen, and B. Wilde "An Autoradiographic Technique for Studying the Segregation of Hydrogen Absorbed into Carbon and Low-Alloy Steels" in: "Current Solutions to Hydrogen Problems in Steel" ed: Interrante and Pressouyre, ASM, Metals Park, OH 1982. pp. 413-422.

U.1. Y. Ueda, and Y.G. Kim, "Dynamical Aspect of Cold Cracking Parameter" Trans. of JWRI, Vol 13, No. 1, 1984. pp. 77-86. also IIW Doc. IX-1435-86 and X-1109-86.

U.2. Y. Ueda, K. Fukuda, and Y.C. Kim, "Dynamical Characteristics of Oblique Y-Groove Weld Cracking Test Specimen of Arbitrary Thickness" Transactions of JWRI, Vol. 13, No. 2, 1984. pp. 131-138. also IIW Doc. No. X-1107-86.

V.1. V.O. Valanti, "The Formation of Fish-eyes in Weld Metal as a Result of Stressing" IIS/IIW Doc. II-10-59 (ex. Doc. II-21-58).

V.2. R. Vasudevan, R.D. Stout, and A.W. Pense, "Hydrogen-Assisted Cracking in HSLA Pipeline Steels" Welding Journal, Sept. 1981. pp. 155s-168s.

V.3. B. Vialatte, "Inspection of Welding Consumables as a Means of Controlling Hydrogen in Deposited Metal" In: Current Solutions to Hydrogen Problems in Steel. Edited: Interrante and Pressouyre, ASM, 1982. pp. 142-146.

W.1. J.B. Wade, "Implant Testing of Steels" AWRA Contract 74. Australian Welding Research, Dec. 1982. pp. 26-31.

W.2. C. Wagner, "Thermodynamics of Alloys" Addison Wesley Press, Inc., Reading MA. 1952.

W.3. F. Watkinson, "Hydrogen Cracking in High Strength Weld Metals" Welding Journal, Sept. 1969. pp. 417s-424s.

W.4. "Instruction Manual of the Oerlikon-Yanaco Diffusible Hydrogen Analyzer Model G-1006" Welding Industries Oerlikon Buhrle Ltd., Zurich, Switzerland, 1983.

W.5. Weld Tech '81, 3-day seminar held by Alloys Rods Inc. for recipients of their 1981 scholarship grant.

W.6. D.G. Westlake, "A Generalized Model for Hydrogen Embrittlement" Trans. ASM 62, 1969, pp. 1000-1006.

W.7. C.R. Weymueller, "Electrodes and Fluxes- needed: Speed, Quality" Welding Design and Fabrication, June 1981. pp. 56-64.

W.8. D.R. White, "In Process Measurement of Hydrogen in Welding", Doctoral Thesis, University of Illinois, 1986.

W.9. A. Wojcik, Hutnik, Vol. 30, 1963. p. 281; through "Chemi-

cal Abstracts" Vol. 60, 1964. p. 6191h.

W.10. J. Wright, "Phase Relationships During Deoxidation and Solidification of Iron Alloys" Doctoral Thesis, Massachusetts Institute of Technology, June, 1973.

Z.1. T. Zakroczymski, "Entry of Hydrogen into Iron Alloys from the Liquid Phase" in: "Hydrogen Degradation of Ferrous Alloys" ed: Oriani et. al. Noyse Publications 1985. pp. 215-250.

Z.2. C.A. Zapffe and C.E. Sims, "Hydrogen Embrittlement, Internal Stress, and Defects in Steel" Trans. AIME 145, 1941, pp. 225-259.

BIOGRAPHICAL NOTE

The author was born, went to school, and then to work. This hardly constitutes a biographical sketch of myself, however, as all of these experiences were interesting and rewarding in their own fashion. My parents helped tremendously in the earlier portion and instilled in me a profound interest in and desire for knowledge. This and my desire for happiness have influenced every major decision in my life.

In addition to obtaining a B.S. in Welding Engineering at The Ohio State University, I learned a lot about the way people live or fail to live their lives. I also had a great time. My desire for personal fulfillment led me to pursue a doctorate at M.I.T. Fortunately, this dissertation did not prevent me from living my life the way I want to. My scientific methodology and decision making processes have been enriched as has my personal outlook during my stay in Boston. I currently work for an Army research lab, which is quite a learning experience as well.

I am married to a wonderful woman whose desire for knowledge and fulfillment match my own. Her Master's degrees in Philosophy and Information Science make for many interesting conversations at home. Contrary to the popular trend, I feel that our marriage actually works.

I play on about 8 different sports teams and read voraciously. I firmly believe that one can only play hard if one has worked hard enough to deserve it. I probably have too many interests, but the ones I pursue the most are: writing, skiing, sailing, guitar playing, camping, and traveling. My professional interests include private consulting and membership in: the American Welding Society, National Society of Professional Engineers, American Society for Metals, Order of the Engineer, Sigma Xi, Tau Beta Pi, Alpha Lambda Delta, Phi Eta Sigma, and the International Institute of Welding.

DISTRIBUTION LIST

No. of Copies	To
1	Office of the Under Secretary of Defense for Research and Engineering, The Pentagon, Washington, DC 20301
	Commander, U.S. Army Laboratory Command, 2800 Powder Mill Road, Adelphi, MD 20783-1145
1	ATTN: SLCIS-IM-TL
	Commander, Defense Technical Information Center, Cameron Station, Building 5, 5010 Duke Street, Alexandria, VA 22304-6145
2	ATTN: DTIC-FDAC
	Metals and Ceramics Information Center, Battelle Columbus Laboratories, 505 King Avenue, Columbus, OH 43201
1	ATTN: J. H. Brown, Jr.
	Commander, Army Research Office, P.O. Box 12211, Research Triangle Park, NC 27709-2211
1	ATTN: Information Processing Office
	Commander, U.S. Army Materiel Command (AMC), 5001 Eisenhower Avenue, Alexandria, VA 22333
1	ATTN: AMCLD
	Commander, U.S. Army Materiel Systems Analysis Activity, Aberdeen Proving Ground, MD 21005
1	ATTN: AMXS-YP, Director
	Commander, U.S. Army Missile Command, Redstone Scientific Information Center, Redstone Arsenal, AL 35898-5241
1	ATTN: AMSMI-RD-CS-R, (Documents)
1	ATTN: AMSMI-CS, R. B. Clem
	Commander, U.S. Army Armament, Munitions and Chemical Command, Dover, NJ 07801
2	ATTN: Technical Library
	Commander, U.S. Army Tank-Automotive Command, Warren, MI 48090
1	ATTN: AMSTA-ZSK
2	ATTN: AMSTA-TSL, Technical Library
1	ATTN: AMSTA-RCK
	Commander, U.S. Army Foreign Science and Technology Center, 220 7th Street, N.E., Charlottesville, VA 22901
1	ATTN: Military Tech
	Director, Eustis Directorate, U.S. Army Air Mobility Research and Development Laboratory, Fort Eustis, VA 23604
1	ATTN: SAVDL-E-MOS (AVSCOM)
1	ATTN: SAVDL-EU-TAP
	U.S. Army Aviation Training Library, Fort Rucker, AL 36360
1	ATTN: Building 5906--5907
	Commander, U.S. Army Aviation Systems Command, 4300 Goodfellow Boulevard, St. Louis, MO 63120
1	ATTN: AMDAV-EGX
1	ATTN: AMDAV-EX, Mr. R. Lewis
1	ATTN: AMDAV-EQ, Mr. Crawford
1	ATTN: AMCPM-AAH-TM, Mr. R. Hubbard
1	ATTN: AMDAV-OS, Mr. W. McClane
	Naval Research Laboratory, Washington, DC 20375
1	ATTN: Dr. C. I. Chang - Code 5830
1	ATTN: Code 2627
	Chief of Naval Research, Arlington, VA 22217
1	ATTN: Code 471
	Director, Structural Mechanics Research, Office of Naval Research, 800 North Quincy Street, Arlington, VA 22203
1	ATTN: Dr. N. Perrone

No. of Copies	To
	Commander, U.S. Air Force Wright Aeronautical Laboratories, Wright-Patterson Air Force Base, OH 45433
1	ATTN: AFWAL/MLC
1	AFWAL/MLLP, D. M. Forney, Jr.
1	AFWAL/MLBC, Mr. Stanley Schulman
1	AFWAL/MLXE, A. Olevitch
1	Edward J. Morrissey, AFWAL/MLTE, Wright Patterson Air Force Base, OH 45433
	National Aeronautics and Space Administration, Marshall Space Flight Center, Huntsville, AL 35812
1	ATTN: R. J. Schwinghammer, EH01, Dir, M&P Lab
1	Mr. W. A. Wilson, EH41, Bldg. 4612
	Chief of Naval Operations, Washington, DC 20350
1	ATTN: OP-987, Director
	Aeronautical Systems Division (AFSC), Wright-Patterson Air Force Base, OH 45433
1	ATTN: ASD/ENFEF, D. C. Wight
1	ASD/ENFTV, D. J. Wallick
1	ASD/XRHD, G. B. Bennett
	Air Force Armament Laboratory, Eglin Air Force Base, FL 32542
1	ATTN: AFATL/DLYA, V. D. Thornton
	Air Force Flight Dynamics Laboratory, Wright-Patterson Air Force Base, OH 45433
1	ATTN: AFFDL/FES, G. W. Ducker
1	AFFDL/FES, J. Hodges
1	AFFDL/TST, Library
	Air Force Test and Evaluation Center, Kirtland Air Force Base, NM 87115
1	ATTN: AFTEC-JT
	NASA - Ames Research Center, Army Air Mobility Research and Development Laboratory, Mail Stop 207-5, Moffett Field, CA 94035
1	ATTN: SAVDL-AS-X, F. H. Immen
	NASA - Johnson Spacecraft Center, Houston, TX 77058
1	ATTN: JM6
1	ES-5
	Naval Air Development Center, Warminster, PA 18974
1	ATTN: Code 063
	Naval Air System Command, Department of the Navy, Washington, DC 20360
1	ATTN: AIR-03PAF
1	AIR-5203
1	AIR-5204J
1	AIR-530313
	Naval Post Graduate School, Monterey, CA 93948
1	ATTN: Code 57BP, R. E. Ball
	Naval Surface Weapons Center, Dahlgren Laboratory, Dahlgren, VA 22448
1	ATTN: Code G-54, Mr. J. Hall
1	Code G-54, Mr. E. Rowe
	Naval Weapons Center, China Lake, CA 93555
1	ATTN: Code 40701
1	Code 408
	Commander, Rock Island Arsenal, Rock Island, IL 61299
1	ATTN: AMSAR-PPV
	Armament Systems, Inc., 712-F North Valley, Anaheim, CA 92801
1	ATTN: J. Musch

No. of Copies	To
1	Beech Aircraft Corporation, 9709 E. Central Avenue, Wichita, KS 67206 ATTN: Engineering Library
1	Bell Helicopter Company, A Textron Company, P.O. Box 482, Fort Worth, TX 76101 ATTN: J. R. Johnson
1	Boeing Vertol Company, A Division of the Boeing Company, P.O. Box 16858, Philadelphia, Philadelphia, PA 19142 ATTN: J. E. Gonsalves, M/S P32-19
1	Cessna Military, P.O. Box 7704, Wichita, KS 67277-7704
1	Fairchild Industries, Inc., Fairchild Republic Company, Conklin Street, Farmingdale, Long Island, NY 11735 ATTN: Engineering Library, G. A. Mauter
1	FMC Corporation, Central Engineering Labs, 1185 Coleman Avenue, Box 80, Santa Clara, CA 95052 ATTN: Gary L. Boerman
1	FMC Corporation, Ordnance Division, 1105 Coleman Avenue, Box 1201, San Jose, CA 95108 ATTN: William H. Altergott
1	General Dynamics Corporation, Convair Division, P.O. Box 80877, San Diego, CA 92138 ATTN: Research Library, U. J. Sweeney
1	Gruman Aerospace Corporation, South Oyster Bay Road, Bethpage, NY 11714 ATTN: Technical Information Center, J. Davis
1	Hughes Helicopters, A Division of Summa Corporation, Centinela & Teale Street, Culver City, CA 90230 ATTN: Library, 2/T2124, D. K. Goss
1	Mr. A. Hirko
1	Mr. L. Soffa
1	IIT Research Institute, 10 West 35th Street, Chicago, IL 60616 ATTN: K. McKee
1	Kaman Aerospace Corporation, Old Winsor Road, Bloomfield, CT 06002 ATTN: H. E. Showalter
1	Lockheed-California Company, A Division of Lockheed Aircraft Corporation, Burbank, CA 91503 ATTN: Technological Information Center, 84-40, U-35, A-1
1	Vought Corporation, P.O. Box 5907, Dallas, TX 75232 ATTN: D. M. Reedy, 2-30110
1	M. P. Poulos, Jr.
1	Martin Marietta Corporation, Orlando Division, P.O. Box 5837, Orlando, FL 32805 ATTN: Library, M. C. Griffith
1	McDonnell Douglas Corporation, 3855 Lakewood Boulevard, Long Beach, CA 90846 ATTN: Technical Library, C1 290/36-84
1	Northrop Corporation, Aircraft Division, 3901 W. Broadway, Hawthorne, CA 90250 ATTN: Mgr. Library Services, H. W. Jones
1	Parker Hannifin Corporation, Bertea Control Systems Division, 18001 Von Karman Avenue, Irvine, CA 92715 ATTN: C. Beneker
1	Rockwell International Corporation, Los Angeles Aircraft Division, B-1 Division, International Airport, Los Angeles, CA 90009 ATTN: W. L. Jackson

No. of Copies	To
1	Sikorsky Aircraft, A Division of United Aircraft Corporation, Main Street, Stratford, CT 06601
1	ATTN: J. B. Faulk
1	Mel Schwartz, Chief of Metals
1	Teledyne CAE, 1330 Laskey Road, Toledo, OH 43697
1	ATTN: Librarian, M. Dowdell
1	Simonds Steel Division, Guterl Special Steel Corporation, Lockport, NY 14094
1	ATTN: Mr. R. Farrington
1	Atlas Testing Laboratories, Inc., 6929 E. Slauson Avenue, Los Angeles, CA 90040
1	ATTN: Mr. P. S. Horvath
1	Georgia Institute of Technology, School of Mechanical Engineering, Atlanta, GA 30332
1	ATTN: Dr. J. T. Berry
1	Lukens Steel Company, Coatesville, PA 19320
1	ATTN: Dr. E. Hamburg
1	Republic Steel Corporation, 410 Oberlin Avenue SW, Massillon, OH 44646
1	ATTN: Mr. R. Sweeney
1	Mr. W. H. Brechtel
1	Mr. T. M. Costello
1	Boeing Commercial Airplane Company, P.O. Box 3707, MS73-43, Seattle, WA 98124
1	ATTN: Dr. K. White
1	United States Steel Corporation, Research Laboratory, Monroeville, PA 15146
1	ATTN: Dr. Hsun Hu
1	METTEC, 1805 E. Carnegie Avenue, Santa Ana, CA 92705
1	ATTN: Dr. L. Raymond
1	Ingersoll Rand Oilfield Products Division, P.O. Box 1101, Pampa, TX 79065
1	ATTN: Mr. W. L. Hallerberg
1	Brown University, Division of Engineering, Providence, RI 02912
1	ATTN: Prof. J. Duffy
1	Illinois Institute of Technology, Metallurgical and Materials Engineering Department, Chicago, IL 60616
1	ATTN: Dr. Norman Breyer
2	Director, U.S. Army Materials Technology Laboratory, Watertown, MA 02172-0001
1	ATTN: SLCMT-IML
1	Author

<p>U.S. Army Materials Technology Laboratory, Watertown, Massachusetts 02172-0001 HYDROGEN ASSISTED CRACKING OF HIGH STEEL WELDS - Steven A. Gedeon</p> <p>Technical Report, MTL TR 88-12, May 1988, 363 pp - illus-tables, D/A Project 11162105.AH84, AMCMS Code 612105.H84</p> <p>AD UNCLASSIFIED UNLIMITED DISTRIBUTION</p> <p>Key Words High strength steels Gas metal arc welds Welds</p> <p>Methods of measuring the hydrogen content of Gas Metal Arc Welds (GMAW) are evaluated. The recently developed American Welding Society standard A4.3-86 using gas chromatography was found to measure the relevant content with reasonable reproducibility, whereas the IIM specification does not. The amount of hydrogen absorbed by Gas Metal Arc Welds as a function of percent H₂, O₂, and CO₂ added to the argon weld shielding gas is quantified. Sievert's law is shown to be invalid for modeling the amount of hydrogen initially absorbed by the molten weld pool. A new model is postulated based on the hypothesis that diatomic hydrogen will dissociate in the cathode boundary layer at a different reaction temperature than the hydrogen absorption reaction which occurs at the temperature of the weld pool surface. Using this hypothesis, it is shown that hydrogen absorption will be controlled by monatomic hydrogen absorption into the cooler outer region of the weld pool rather than diatomic hydrogen absorption into the hotter central portion as was previously believed. When oxygen is added to the shielding gas, the amount of hydrogen absorbed by the weld pool increases. It is shown that the hydrogen will be bound to the more thermodynamically stable H₂O. It is believed that the water molecule is more strongly absorbed than the H₂ molecule. The resulting effect on hydrogen solubility is explained by a consideration of the Fe-H-O phase diagram which was calculated in this study. The effect of CO₂ on hydrogen absorption is explained by its effect on the stability of H₂O and H₂ at high temperature. Implant testing is used to quantify the effect of hydrogen on cracking of high strength steel welds. The microplasticity theory originally proposed by Beachem is used to explain the effect of hydrogen on the various fracture modes observed.</p>	<p>U.S. Army Materials Technology Laboratory, Watertown, Massachusetts 02172-0001 HYDROGEN ASSISTED CRACKING OF HIGH STEEL WELDS - Steven A. Gedeon</p> <p>Technical Report, MTL TR 88-12, May 1988, 363 pp - illus-tables, D/A Project 11162105.AH84, AMCMS Code 612105.H84</p> <p>AD UNCLASSIFIED UNLIMITED DISTRIBUTION</p> <p>Key Words High strength steels Gas metal arc welds Welds</p> <p>Methods of measuring the hydrogen content of Gas Metal Arc Welds (GMAW) are evaluated. The recently developed American Welding Society standard A4.3-86 using gas chromatography was found to measure the relevant content with reasonable reproducibility, whereas the IIM specification does not. The amount of hydrogen absorbed by Gas Metal Arc Welds as a function of percent H₂, O₂, and CO₂ added to the argon weld shielding gas is quantified. Sievert's law is shown to be invalid for modeling the amount of hydrogen initially absorbed by the molten weld pool. A new model is postulated based on the hypothesis that diatomic hydrogen will dissociate in the cathode boundary layer at a different reaction temperature than the hydrogen absorption reaction which occurs at the temperature of the weld pool surface. Using this hypothesis, it is shown that hydrogen absorption will be controlled by monatomic hydrogen absorption into the cooler outer region of the weld pool rather than diatomic hydrogen absorption into the hotter central portion as was previously believed. When oxygen is added to the shielding gas, the amount of hydrogen absorbed by the weld pool increases. It is shown that the hydrogen will be bound to the more thermodynamically stable H₂O. It is believed that the water molecule is more strongly absorbed than the H₂ molecule. The resulting effect on hydrogen solubility is explained by a consideration of the Fe-H-O phase diagram which was calculated in this study. The effect of CO₂ on hydrogen absorption is explained by its effect on the stability of H₂O and H₂ at high temperature. Implant testing is used to quantify the effect of hydrogen on cracking of high strength steel welds. The microplasticity theory originally proposed by Beachem is used to explain the effect of hydrogen on the various fracture modes observed.</p>
<p>U.S. Army Materials Technology Laboratory, Watertown, Massachusetts 02172-0001 HYDROGEN ASSISTED CRACKING OF HIGH STEEL WELDS - Steven A. Gedeon</p> <p>Technical Report, MTL TR 88-12, May 1988, 363 pp - illus-tables, D/A Project 11162105.AH84, AMCMS Code 612105.H84</p> <p>AD UNCLASSIFIED UNLIMITED DISTRIBUTION</p> <p>Key Words High strength steels Gas metal arc welds Welds</p> <p>Methods of measuring the hydrogen content of Gas Metal Arc Welds (GMAW) are evaluated. The recently developed American Welding Society standard A4.3-86 using gas chromatography was found to measure the relevant content with reasonable reproducibility, whereas the IIM specification does not. The amount of hydrogen absorbed by Gas Metal Arc Welds as a function of percent H₂, O₂, and CO₂ added to the argon weld shielding gas is quantified. Sievert's law is shown to be invalid for modeling the amount of hydrogen initially absorbed by the molten weld pool. A new model is postulated based on the hypothesis that diatomic hydrogen will dissociate in the cathode boundary layer at a different reaction temperature than the hydrogen absorption reaction which occurs at the temperature of the weld pool surface. Using this hypothesis, it is shown that hydrogen absorption will be controlled by monatomic hydrogen absorption into the cooler outer region of the weld pool rather than diatomic hydrogen absorption into the hotter central portion as was previously believed. When oxygen is added to the shielding gas, the amount of hydrogen absorbed by the weld pool increases. It is shown that the hydrogen will be bound to the more thermodynamically stable H₂O. It is believed that the water molecule is more strongly absorbed than the H₂ molecule. The resulting effect on hydrogen solubility is explained by a consideration of the Fe-H-O phase diagram which was calculated in this study. The effect of CO₂ on hydrogen absorption is explained by its effect on the stability of H₂O and H₂ at high temperature. Implant testing is used to quantify the effect of hydrogen on cracking of high strength steel welds. The microplasticity theory originally proposed by Beachem is used to explain the effect of hydrogen on the various fracture modes observed.</p>	<p>U.S. Army Materials Technology Laboratory, Watertown, Massachusetts 02172-0001 HYDROGEN ASSISTED CRACKING OF HIGH STEEL WELDS - Steven A. Gedeon</p> <p>Technical Report, MTL TR 88-12, May 1988, 363 pp - illus-tables, D/A Project 11162105.AH84, AMCMS Code 612105.H84</p> <p>AD UNCLASSIFIED UNLIMITED DISTRIBUTION</p> <p>Key Words High strength steels Gas metal arc welds Welds</p> <p>Methods of measuring the hydrogen content of Gas Metal Arc Welds (GMAW) are evaluated. The recently developed American Welding Society standard A4.3-86 using gas chromatography was found to measure the relevant content with reasonable reproducibility, whereas the IIM specification does not. The amount of hydrogen absorbed by Gas Metal Arc Welds as a function of percent H₂, O₂, and CO₂ added to the argon weld shielding gas is quantified. Sievert's law is shown to be invalid for modeling the amount of hydrogen initially absorbed by the molten weld pool. A new model is postulated based on the hypothesis that diatomic hydrogen will dissociate in the cathode boundary layer at a different reaction temperature than the hydrogen absorption reaction which occurs at the temperature of the weld pool surface. Using this hypothesis, it is shown that hydrogen absorption will be controlled by monatomic hydrogen absorption into the cooler outer region of the weld pool rather than diatomic hydrogen absorption into the hotter central portion as was previously believed. When oxygen is added to the shielding gas, the amount of hydrogen absorbed by the weld pool increases. It is shown that the hydrogen will be bound to the more thermodynamically stable H₂O. It is believed that the water molecule is more strongly absorbed than the H₂ molecule. The resulting effect on hydrogen solubility is explained by a consideration of the Fe-H-O phase diagram which was calculated in this study. The effect of CO₂ on hydrogen absorption is explained by its effect on the stability of H₂O and H₂ at high temperature. Implant testing is used to quantify the effect of hydrogen on cracking of high strength steel welds. The microplasticity theory originally proposed by Beachem is used to explain the effect of hydrogen on the various fracture modes observed.</p>